New technologies for the conservation of written paper heritage damaged by fire

Melania Zanetti

MUSEUM NATIONAL D'HISTOIRE NATURELLE

Ecole Doctorale Sciences de la Nature et de l'Homme – ED 227

UNIVERSITÀ DEGLI STUDI DI PADOVA

Year 2022 **N°attribué par la bibliothèque**

|_|_|_|_|_|_|_|_|_|_|_|_|

THESIS SUBMITTED FOR THE DEGREE OF DOCTOR OF PHILOSOPHY

from

MUSEUM NATIONAL D'HISTOIRE NATURELLE

Science des matériaux

and

UNIVERSITY OF PADOVA

Scienza e ingegneria dei materiali e delle nanostrutture

Public defense by

Melania ZANETTI

8 July 2022

New technologies for the conservation of written paper heritage damaged by fire

Ph.D. joint supervision by **Anne-Laurence DUPONT** & **Alfonso ZOLEO**

COMMITTEE

Nathalie MARLIN	**Maîtresse de conférences, Grenoble INP - PAGORA**	**Rapporteur, President of the commitee**
Giovanna POGGI	**Assistant Professor, University of Florence**	**Rapporteur**
Pierre CHASTANG	**Professeur des universités, Université Versailles St-Quentin-en-Yvelines**	**Examiner**
François BOUGARD	**Directeur de recherche, IRHT, CNRS**	**Co-supervisor**
Alfonso ZOLEO	**Assistant Professor, University of Padova**	**Supervisor**
Anne-Laurence DUPONT	**Directrice de recherche, CRC, Muséum national d'Histoire naturelle, CNRS**	**Supervisor**

MUSEUM NATIONAL D'HISTOIRE NATURELLE

Ecole Doctorale Sciences de la Nature et de l'Homme – ED 227

UNIVERSITÀ DEGLI STUDI DI PADOVA

Année 2022 **N°attribué par la bibliothèque**

|_|_|_|_|_|_|_|_|_|_|_|_|_|

THESE EN CO-TUTELLE

Pour obtenir le grade de DOCTEUR

DU MUSEUM NATIONAL D'HISTOIRE NATURELLE

Spécialité : Science des matériaux

ET

DE L'UNIVERSITÉ DE PADOUE

Spécialité : Scienza e ingegneria dei materiali e delle nanostrutture

Présentée et soutenue publiquement par

Melania ZANETTI

Le 8 juillet 2022

Nouvelles technologies de conservation-restauration du patrimoine écrit sur papier endommagé par le feu

---

Sous la direction de **: Anne-Laurence DUPONT et Alfonso ZOLEO**

JURY :

Nathalie MARLIN	**Maîtresse de conférences, Grenoble INP - PAGORA**	**Rapporteur, Présidente**
Giovanna POGGI	**Assistant Professor, Université de Florence (Italie)**	**Rapporteur**
Pierre CHASTANG	**Professeur des universités, Université Versailles St-Quentin-en-Yvelines**	**Examinateur**
François BOUGARD	**Directeur de recherche, IRHT, CNRS**	**Co-directeur de thèse**
Alfonso ZOLEO	**Assistant Professor, Université de Padoue (Italie)**	**Directeur de thèse**
Anne-Laurence DUPONT	**Directrice de recherche, CRC, Muséum national d'Histoire naturelle, CNRS**	**Directrice de thèse**

MUSEUM NATIONAL D'HISTOIRE NATURELLE

Ecole Doctorale Sciences de la Nature et de l'Homme – ED 227

UNIVERSITÀ DEGLI STUDI DI PADOVA

Sede Amministrativa: Università degli Studi di Padova

Dipartimento di Scienze Chimiche

CORSO DI DOTTORATO DI RICERCA IN:

Scienza e ingegneria dei materiali e delle nanostrutture

CICLO 34

New technologies for the conservation of written paper heritage damaged by fire

Tesi redatta in co-tutela con

Muséum National d'Histoire Naturelle, Ecole Doctorale 227 in: Science des matériaux

Coordinatore: Ch.mo Prof. Giovanni Mattei

Supervisore italiano: Ch.mo Prof. Alfonso Zoleo

Supervisore francese: Ch.mo Prof. Anne-Laurence Dupont

Co-Supervisore francese: Ch.mo Prof. François Bougard

Dottoranda: Melania Zanetti

Summary

General introduction

Fires in buildings housing historical collections of books and papers have occurred throughout history and all over the world. Such blazes have been caused by incidental events resulting from poor safety precautions and by the presence of readily flammable materials, such as paper-based collections, as well as by armed conflicts, whose impact on written cultural heritage has frequently been disastrous. Libraries and archives have been the victims of armed conflicts since the First World War and were especially at risk in the Second World War, since the German power considered libraries and archives among the symbols of national and cultural identity and as such had to be erased. Allies' raids were not less destructive by totally destroying or partially damaging the cultural heritage held in numerous libraries and archives on European soil.

Broadening the scope, what happened in the course of the more recent Yugoslav war cannot be overlooked when, in August 1992, incendiary shells of the Bosnian Serb army were fired at the historical library of Sarajevo. Among the ancient books that were totally or partially burnt were, once again, several hundred manuscripts and incunabula (heritage volumes printed in the second half of the fifteenth century). Finally, what is presently happening to cultural heritage due to the unprovoked attack on Ukraine can be added to the long and sad history of World Heritage loss.

A large part of these books and documents on paper harmed by fire in libraries and archives have often been left untouched since the devastations, in very poor condition, as a consequence of routine access and sometimes even from simple handling.

Priority has always been given to the recovery of written parchments, probably due to at least two factors.

On the one hand, parchment has been used as a writing support in the Western Latin world for over a thousand years; it began to replace papyrus as early as the 3^{rd}-4^{th} centuries and was then progressively replaced by paper from the 14^{th} century onwards. As a consequence, parchment manuscripts and documents have usually been considered the most valuable artifacts. On the contrary, the conservation of written paper heritage damaged by fire is still an unsolved problem.

Burnt paper conservation treatments are usually carried out with traditional materials and techniques, which has so far yielded unsatisfactory results and the carbonized areas of fire damaged papers have usually been considered irrecoverable. To the best of our knowledge, in recent years very few research initiatives have been devoted to the development of

methodologies, materials and techniques suitable for the conservation treatment of charred paper in historical collections. One of them has focused on the books belonging to the Duchess Anna Amalia Library in Weimar, which were badly damaged in a devasting blaze in 2004: 50,000 volumes were lost and more than 118,000 were severely damaged [Weber 2009; Weber and Hähner 2014]. Another such project is the present research, whose focus is on manuscripts and incunabula and which has benefitted from a collaboration with the Médiathèque L'Apostrophe in Chartres and with the Library of the Episcopal Seminary in Padua, both damaged by a fire in 1944.

The Municipal Library of Chartres and the Library of the Episcopal Seminary in Padua were both struck by American bombs in the spring of 1944. The former, housing hundreds of important manuscripts, cartulary and archival documents dating from the early Middle Ages to the 19th century, was completely destroyed and more than a half of its written patrimony was lost in the fire caused by the raid. From over 500 codices originally held in the Municipal Library, about 200 have survived, in most cases unbound and in a wide range of fragmentary states.

Over the past decades, a number of the damaged parchment leaves have gradually been recovered and subsequently have undergone a conservation treatment at the conservation department (*Atelier Restauration*) of the Bibliothèque nationale de France. The interdisciplinary project called "*Renaissance virtuelle des manuscrits sinistrés de Chartres"* started in 2005. It involves the Médiatèque L'Apostrophe in Chartres and is overseen by the Institut de Recherche et d'Histoire des Textes (IRHT, CNRS). The project's stated goal is to enhance the conservation, digital reproduction, identification, and virtual rearrangement of the fragments into their correct configuration and order [Poirel 1991; Poirel and Rabel 2018; Rabel 2018].

To date, about thirty of the oldest and most important parchment codices have been recomposed virtually and made available online to the international scientific community in the BVMM virtual library (Bibliotheque virtuelle des manuscrits médiévaux, https://www.manuscrits-de-chartres.fr) created and updated regularly by scholars from the IRHT. Of the many paper manuscripts and paper documents damaged by the fire, only four were included in the project due to their great fragility, since scorched paper material is prone to fragmentation when subjected to the slightest mechanical stress.

Always in Spring 1944 at the Library of the Episcopal Seminary in Padua, serious damage was caused by the fire to the institute's incunabula. These were transformed into solid blocks which

are particularly subject to fragmentation, hence they have become inaccessible and have been set aside pending the formulation of an appropriate interventive procedure.

In an attempt to contribute to the rescue of this heritage and to much more held in libraries and archives around the world, this research is dedicated to the development of an innovative conservation treatment for strengthening burnt paper, with a specific focus on traditional handmade rag paper, which was the support for writing and printing from the 13th to the 19th century in the Western Latin world.

To this end, a research project called CREMIB (*Conservation et REstauration des Manuscrits et des Incunables Brulés*) was set up. This project was coordinated by the IRHT and financially supported by DIM "Domaine d'intérêt majeur", Matériaux anciens et patrimoniaux, a research network of the Ile-de-France Regional Council (2017-2022) for a PhD research co-tutored by the Ecole Doctorale 227 (Muséum Nationale d'Histoire Naturelle, MNHN) and the University of Padua. The experimental work was carried out partly at the Department of Chemical Sciences of Padua's University and partly at the Centre de Recherche sur la Conservation (MNHN).

This thesis is structured in seven chapters. In **Chapter 1**, the importance of cultural heritage as cultural evidence and its close relationship with conservation is highlighted. It also deals with both the theory of restoration and the role played by the humanities and the natural sciences in the formulation of conservation problems and solution seeking. **Chapter 2** is dedicated to the history of papermaking, the degradation produced in paper by heat and fire, and the analytical study and characterization of the burnt papers of the Chartres manuscript and the Padua incunabulum. **Chapter 3** describes the preparation of burnt paper samples used to investigate the physical and chemical processes involved in fire damage. Once the artificial burning technique had been developed, a wide range of analytical investigations were applied to the samples obtained from this process. **Chapter 4** is dedicated to the chemical and physical characteristics of microfibrillated cellulose (MFC) and nanocrystalline cellulose (CNC) on one side, and aminoalkyalkoxysilanes and alkoxysilanes on the other side, since these materials will be used in the following chapters for the conservation interventions on the Chartres manuscript and the Padua incunabulum. **Chapter 5** deals with the experimentation of nanocelluloses on samples obtained from the artificial burning of paper in order to assess which composition and which application technique offer the best guarantee of reinforcement of charred paper. Likewise in **Chapter 6**, the application of different polysiloxanes to burnt papers is experimented with the best result obtained using functionalized tetraethoxysilane (TEOS). Specifically, SIOX-5TO, a commercial formulation of polysiloxane based

on TEOS functionalized with octyl-triethoxymethylsilane, OTES, in isopropanol provided unprecedented results by systematically enhancing the mechanical properties of the damaged paper, allowing an improvement of its fold resistance with no unwanted side-effects such as some of the other polysiloxanes used. Finally, **Chapter 7** describes the final formulation of the product applied to strengthen charred papers. It is composed of a mix of cellulose nanocrystals (CNC) and microfibrillated nanocellulose (MFC) dispersed in SIOX-5TO. A general conclusion summarizes the results and opens the perspective for future research.

General introduction|References

Weber, J. (2009). «Risikominimierung-Vernetzung-Mengenrestaurierung. Organisatorische und konservatorische Herausforderungen nach dem Brand der Herzogin Anna Amalia Bibliothek». *Zeitschrift fur Bibliothekswesen und Bibliographie,* 56, 167–173. https://doi.org/http://dx.doi.org/10.3196/1864295009563457

Weber, J., Hähner, U. (2014). *Restaurieren nach dem Brand: Die Rettung der Bücher der Herzogin Anna Amalia Bibliothek.* Petersberg: Imhof.

Poirel, D. (1991). «Les manuscrits sinistrés de la Bibliothèque municipale de Chartres». Gazette du livre médiéval, 18, 30-32. https://www.persee.fr/doc/galim_0753-5015_1991_num_18_1_1163

Poirel, D., Rabel, C. (2018). «Les manuscrits sinistrés de Chartres de l'incendie à l'hyperspectral. Histoire d'un projet». In: Michelin A., Robinet L. (eds) *Les rescapés du feu. L'imagerie scientifique au service des manuscrits de Chartres.* Chartres: Société archéologique d'Eure-et Loir (SAEL), 29-49.

Rabel, C. (2018). «Des flammes à l'écran. Conservation, numérisation et étude des manuscrits sinistrés de Chartres». In: Zanetti, M. (ed) *Dalla tutela al restauro del patrimonio librario e archivistico. Storia, esperienze, interdisciplinarietà.* Venezia : Edizioni Ca' Foscari, 145-161. http://edizionicafoscari.unive.it/it/edizioni/libri/978-88-6969-216-1/

Chapter 1

Cultural heritage as material evidence

1. Cultural heritage and its conservation

When we talk about 'cultural heritage' and in particular 'tangible cultural heritage', our focus is directed on physical objects produced and used by human societies in earlier eras which have now been superseded by inevitable social and technological developments. They may be immovable monuments and buildings or movable artworks, archaeological collections, written records, books, scientific equipment, music instruments, etc.; indeed, objects of the most diverse nature produced by human ingenuity, skill and creativity. Through the materials, techniques and structures used in their production, they reflect the wealth of knowledge, technological progress and craftsmanship of the society that manufactured them. They are no longer understood merely as tools serving a contingent purpose, and the relationship we establish with them is no longer based on their original purpose, but instead on their cultural significance, with the aim of understanding and preserving the memory of human civilisation and evolution. These artefacts are recognised by humanity to be 'material evidence of the value of civilisation', a notion effectively expressed for the first time in Italy by the Commissione Franceschini in the 1960s [Atti della Commissione Franceschini, 1967].

Although the survival of most of the pieces of material evidence available to us has largely occurred by chance, by becoming components of our overall cultural heritage, they are subject to the important obligations implied by conservation: we should all feel grateful for the privilege of enjoying heritage, but we should also understand our duty to preserve it and to pass it from one generation to the next in the best possible condition, in terms of absolute respect for its historical authenticity.

The protection of cultural objects from damage is a very onerous task. Natural ageing (the passage of time) and use (anthropic effects) induce physico-chemical alterations which usually lead to their material deterioration. Many of the decay processes can be counteracted and limited by well-balanced preservation activities and conservation practices, but these must be properly designed

in order to be effective in slowing down degradation, whilst also respecting the historical value and material features of the objects.

Preservation and conservation treatments have been traditionally understood as empirical practices based on experience and hence verifiable through observation rather than theoretically structured academic disciplines. It is true that they do not belong to any single branch of knowledge but rather integrate multifarious aspects which are the object of study in other specific fields, in a multidisciplinary approach to the acquisition of cultural heritage knowledge and its ultimate preservation and conservation.

2. Theoretical premises in conservation

The words 'preservation', 'conservation' and 'restoration' may have different meanings in different languages and places. For this reason, around twenty years ago the International Council of Museums – Committee for Conservation (ICOM-CC) published a resolution aimed at proposing an internationally shared language in the conservation field. In the ICOM-CC Resolution, the terms "preventive conservation", "remedial conservation", and "restoration" are distinguished according to the aims of the actions involved and, taken as a whole, constitute the wider field which encompasses the "conservation" of the tangible cultural heritage. It follows that conservation includes «all measures and actions aimed at safeguarding tangible cultural heritage while ensuring its accessibility to present and future generations» and that «all measures and actions should respect the significance and the physical properties of the cultural heritage item» [ICOM-CC Resolution 2008].

Because of the importance given to the material features of the historical papers involved in the present study, it is imperative to refer to the origin of the concept of conservation/restoration and to some of the fundamental principles identified by Cesare Brandi. Brandi was the founder and director of the Italian Istituto Centrale per il Restauro (ICR) for twenty years (1939-1959) and played a leading international role in the development of theories and practices for application in the conservation of works of art. In his main work, *Theory of Restoration,* he defined restoration as «the methodological moment of recognising a work of art […]» and he pointed out a fundamental axiom in restoration, stating that «only the material component of a work of art can be restored» [Brandi 1963, 34; Brandi (transl.) 2005, 48].

Brandi's definition was formulated more than half a century ago and was addressed solely to works of art. However, today it can be updated and extended to our entire body of cultural heritage: conservation represents the methodological moment of properly recognising cultural heritage. In other words, when a community decides that an object must be conserved, this fundamental choice results in the recognition of the item as being a part of the overall body of cultural heritage.

As already mentioned, cultural heritage assets and conservation make sense only if considered in a historical perspective. Understanding the cultural role of the object, as material evidence of the society that produced, used and valued it, is a critical step in which the humanities play a key role.

As conservation is the product of several activities, the first and fundamental axiom, as stated by Brandi, should not only concern restoration but conservation in general. It follows that only the material component of objects constituting cultural heritage can be conserved and therefore the contribution of the natural sciences (mainly biology, chemistry and physics) is pivotal.

Their application to understanding and acquiring knowledge of cultural heritage objects has multiple implications. The first, and most important, is that of recognising the content of material information that confers originality and authenticity on the object in question. This is far from being obvious in the case of a book or of an archival document, whose uniqueness frequently risks being neglected. It is true that a manuscript is perceived as *unicum* by definition, but printed books exist in multiple exemplars and the different exemplars of the same text appear identical to anyone interested in the textual content. A good quality digital reproduction of the text can fully meet the study and research needs of the majority of the scholars, even those of manuscript text scholars. Digitisation is often referred to as a "dematerialisation process" and what is reproduced by that process is obviously the immaterial component of the object [Federici 2012; Manžuch 2017], so that the digital reproduction of a document (i.e., its intangible component) can be reproduced in an infinite number of copies, indistinguishable from the first and from one another.

What continues to make these historical artefacts irreplaceable are the testimonies contained in the material from which they are made, and only by directing our interest towards their material composition is it possible to understand their uniqueness.

The investigation of the cellulose fibres that compose a sheet of paper led to the realization that no two sheets of paper are identical, just as no two cellulose fibres are identical.

The natural sciences are therefore central to understanding the irreproducible material essence of books and documents as cultural objects, since they bring out the (often immense) quantity of material information conferring 'historic truth' on the object.

The second important role played by the natural sciences in the study of cultural heritage is that of conservation. Physics, chemistry and biology can apply a wide range of analytical methods to study of constituent materials and their inherent decay processes, as a means of steering the conservation intervention towards appropriate methodologies. A dialectical relationship between the humanities and natural sciences was a goal of this research work, with an intertwining of the history of the historic papers and of the libraries they belong to.

3. Interdisciplinarity in cultural heritage conservation

The terms *multi-* and *inter-*disciplinarity have been under discussion for several decades and have been assigned meanings that are not perfectly interchangeable. According to David Alvarogonzález, multidisciplinarity is «an activity associated with many, multiple or more than one existing discipline» (Alvarogonzález, 2011, 388). The author recalls the work of Bernard C.K. Choi and Anita W.P. Pak, who expressed how multidisciplinarity «draws on knowledge from multiple disciplines but stays within their boundaries» (Choi and Pak 2006, 351).

On the other hand, «interdisciplinarity analyses, synthesizes and harmonizes links between disciplines into a coordinated and coherent whole» (Choi and Pak 2006, 351).

Only a real transition from multidisciplinarity to interdisciplinarity could make conservation a complete discipline and, seen from this perspective, establishing an effective, dialectical relationship between the humanities and the natural sciences would constitute an important step.

In fact, despite its unquestionable relevance, the scientific investigation involved in conservation runs the risk of being somehow merely instrumental. It is aimed at the acquisition of analytical results in order to provide answers to questions posed by the humanistic disciplines (i.e. history, history of art, of architecture, archaeology, philology, history of books, palaeography etc.) related to the identification of, say, a pigment's composition or a lithological fragment and so on. Sometimes scientists are asked to analyse some materials without any idea of the context they come from, or of the purpose their analyses should have for the conservation of the object. Frequently it also occurs that once the results of the analyses are available, the relationship between the natural sciences and the humanities is interrupted and only resumes when new

analytical outcomes are requested, and therefore lacks the coordination and the coherence that should characterise an effective and sufficiently aware level of interdisciplinarity.

It is worthwhile stressing that the different disciplines concerned employ different investigative methods. Intuition and qualitative research are important in the humanistic field, since they focus on understanding individual aspects of the particular phenomena. On the other hand, experimentation is at the core of the scientific method: through an inductive process moving from the specific to the general, researchers integrate information to develop a theory or provide a description that can explain the phenomena under observation. Every aspect of science is informed by its reliance on objectivity, evidence, and experiments aimed at demonstrating its validity.

The analogy drawn between conservation and medicine is quite frequent and widely used: it is said that through conservation one 'prolongs the life' of a work of art and, in general, of cultural heritage artefacts. It is worth reflecting that cultural heritage conservation is concerned with inanimate objects while medicine (human, veterinary or botanical) deals with living organisms. Cultural items can decay more or less rapidly depending on their constituent materials and on the environmental conditions in which they are held, but in any event, they do not die. Moreover, biological organisms are often capable of repairing any damage that may occur to them: a small wound can heal itself without any medical help, whereas a tear in a sheet of paper must always be repaired by a human intervention: it does not heal by itself. Apart from this distinction, the analogy between medicine and conservation is functional in explaining the importance of interdisciplinarity in allowing conservation to emerge from empiricism.

Because of the fundamental role it plays in human society, medicine became familiar with the scientific method well before conservation. For a long time now, its relationship with biology, chemistry and physics has ceased to be merely instrumental, aimed only at the acquisition of analytical results. This demonstrates an understanding of the importance of a continuous and dialectical relationship between the natural sciences and medical practices. Moreover, it is an accepted concept in medicine that, even when a general protocol derived from historical experience is established, therapeutic intervention must be tailored on a case-by-case basis, because no two patients are identical, and the same holds true for objects of cultural heritage.

The importance in conservation of the study of the materials and techniques used in the manufacture of historical objects has been already mentioned, as well as the fundamental contribution provided by the natural sciences. Similarly, the study of anatomy would not have

travelled its long path without the contribution of biology, and the same would not have happened to physiology without the contribution of chemistry. And aren't genetics, the anamnestic reconstruction of each patient's past, analogous to the reconstruction of the history of the objects to be preserved? So history – which also acts as a guide for medicine – is closely related to what might appear to a superficial observer to be a purely factual 'science'. The use of inverted commas for the word science is not accidental.

Carlo Ginzburg [Ginzburg 1986] remarks on the subject of medicine:

«The group of disciplines that we have called circumstantial (including medicine) does not fall within the criteria of scientificity inferable from the Galilean paradigm. They are eminently qualitative disciplines, which have as their object individual cases, situations and documents, and for this very reason they achieve results that have an ineliminable margin of randomness. Only by carefully observing and recording with extreme precision all the symptoms - the Hippocratic approach affirmed - it is possible to construct precise "histories" of individual diseases.» (Ginzburg 1986, 170-171, translated by M. Zanetti).

Therefore medicine, like conservation, cannot be considered an 'exact science', assuming that this expression can have real and constant application. They are both better suited to the definition of "experimental discipline", since no doctor or conservator, despite acting in accordance with pre-established protocols, can be sure of the effect that the intervention will produce in the individual case. For the fundamental role it plays in human society, medicine already possesses a solid epistemological paradigm in which the relationship between the humanities and the natural sciences appears to be successfully recomposed.

In the realm of conservation this has not yet happened; this is due to its relative youth, which means its development as a discipline is somewhat delayed, although I believe this developmental delay can and should be rectified, in particular by the conservator. In fact, the humanities as well as biology, chemistry and physics need to free themselves from instrumentalist temptations in order to work together towards the objective of slowing down the deterioration of cultural heritage, so as to guarantee its transmission to future generations in the best possible way.

The conservator should play a key role in this process, proceeding from the anamnesis and providing a diagnosis, and subsequently carrying out the intervention, which is invasive and alters the physical and/or chemical state of the cultural materials, to a greater or lesser extent depending on the level of invasiveness of the intervention. The conservator is expected to

integrate historical and scientific information by means of an examination of the cultural object to tailor the most appropriate conservation treatment.

4. Ethical considerations: reversibility and removability of conservation treatments

In recent decades, in particular post-1980 or so, theoretical and methodological reflections in the field of book and paper conservation have begun to develop [Federici 1982]. Increasing emphasis has been placed on the importance of safeguarding the original physico-chemical as well as the compositional structures and aesthetic features of artefacts. These issues are the focus of book archaeology, which studies the history of the techniques and materials used in historical book production, in an effort to piece together the material background from which the 'book object' originates [Szirmai 1999]. A strong link has also been established between book archaeology and conservation [Federici 1981], the key goal being for book conservation to evolve from being an intervention aimed at restoring volumes to their previous functional state, to the priority of slowing down the decay process, showing the utmost respect for their original structural elements.

This perspective gave rise to the development of new, progressively less invasive intervention modalities, keeping them as minimal as possible, since only minimally-invasive methods can avoid or at least minimize the alteration of the precious material information – often invisible to the naked eye – harboured by the historical object. It also encouraged the development of less extensive treatments and above all of *in situ* interventions, avoiding as far as possible the unsewing and unbinding of volumes [Clarkson 1999].

Clearly, these basic principles need to be re-examined in the case of written heritage seriously damaged by fire, since the alteration induced by radiant heat and flames to the original materials is so drastic that respect for the artefact's structure necessarily takes second place.

In such a profoundly compromised circumstance, the goal has to be the recovery of the textual elements directly affected by fire, so the removability of added conservation materials and products is carefully assessed on case-by-case base. Removability in cultural heritage conservation is understood as the possibility of separating the materials added by the intervention from the historic artefact without placing it in jeopardy. In paper consolidation and coating, which was the aim of the present work, the applied nanocomposite formulations penetrate the fragile burnt

paper matrix and establish chemical interactions with its fire-damaged but still extant cellulose fibres, partly restoring their flexibility and ability to better resist mechanical stress. Such a process and associated materials cannot really be expected to be removable, primarily because of the extremely weakened condition of the original paper matrix. On the other hand, the tendency towards fragmentation of carbonized paper is such that only an intervention aimed at re-establishing its chemical-physical consistency as far as possible can secure its preservation and allow cautious access to historic written/printed heritage which has up till now been in such a poor state so as to exclude it from even simple handling.

A final consideration should be addressed to reversibility in conservation treatments. The question «Reversibility: does it exist?» was posed more than twenty years ago at a conference organized by the British Museum [Oddy and Carroll 1999] and the issue has recently been taken up again [Udina 2021]. One of the most important notions of thermodynamics is in fact that of *reversible* and *irreversible* processes. According to it, a process is *reversible* if, after it has taken place, can be reversed and, when reversed, the system returns into its initial state.
Although in literature, mass media and even in scientific production the reversibility of restoration interventions is often highlighted, the real answer to the question can only be negative: the object cannot be returned to its pretreatment state; that is, alterations induced by treatment on its chemical composition and physical structure cannot be undone.

Precisely because of these considerations on removability and reversibility, the principle of developing minimally invasive treatments is earnestly recommended – and it has also been the basis of the present research work – so as to devise conservation treatments in which the quantity of materials and products added to the historic artefact can be reduced, thereby retaining as much as possible of the object's original features, whilst at the same time effectively countering its decay.

Chapter 1 | References

Alvarogonzález, D. (2011). «Multidisciplinarity, Interdisciplinatity, Transdisciplinarity, and the Sciences». *International Studies in the Philosophy of the Science,* 25(4), 387-403.

Brandi, C. (1963). *Teoria del restauro.* Roma: Edizioni di Storia e Letteratura.

Brandi, C. (2005). *Theory of restoration*. Basile, G. (ed.), (trans. By Rockwell, C.). Florence: Nardini Editore-Istituto Centrale per il Restauro.

Choi, B.C.K and Pak, A. W. P (2006). «Multidisciplinarity, interdisciplinatity and transdisciplinarity in health research, services, education and policy: 1. Definitions, objectives, and evidence of efectiveness». *Clinical and investigative Medicine,* 29, 351-364.

Federici, C (1981). «Archeologia del libro, conservazione, restauro ed altro. Appunti per un dibattito». In: *Oltre il testo*, a cura di R. Campioni, Bologna: Istituto per i beni artistici culturali naturali della Regione Emilia-Romagna, 13-20.

Federici, C (1982). «Le passage du Nord-Ouest». *Gazette du livre médiéval*, 1, 5-7.

Federici, C. (2012). «Digitale: toccasana o veleno?». *La Fabbrica del Libro*, 18, 1.

Clarkson, C. (1999). «Minimum intervention in treatment of books». Preprint from the 9th International Congress of IADA. Copenhagen, 15-21 August, 1999.

Commissione Franceschini (1967). *Per la salvezza dei beni culturali in Italia. Atti e documenti della Commissione di indagine per la tutela e la valorizzazione del patrimonio storico, archeologico, artistico e del paesaggio*. Roma: Casa Editrice Colombo.
https://www.icar.beniculturali.it/biblio/pdf/Studi/franceschini.pdf

Ginzburg, C. (1986). *Miti, emblemi, spie. Morfologia e storia*. Torino: Einaudi.

ICCOM-CC Resolution. International Council of Museum - Committee for Conservation (2008). *Terminology to characterize the conservation of tangible cultural heritage,* adopted by the ICOM-CC membership at the 15th Triennial Conference, New Delhi, 22-26 September 2008. https://www.icom-italia.org/wp-content/uploads/2018/02/ICOMItalia.CommissioneConservazione.ICOM-CCResolutiononTerminologyEnglish.Relazioni.2008.pdf

Manžuch Z. (2017). «Ethical Issues in Digitization of Cultural Heritage». Journ*al of Contemporary Archival Studies*, 4, 4.https://elischolar.library.yale.edu/jcas/vol4/iss2/4

Oddy, A., Carroll, S. (eds). (1999). «Reversibility: does it exist?». *British Museum occasional papers,* 135. London: British Museum.

Szirmai, J. A. (1999). *The Archaeology of Medieval Bookbinding*. Aldershot: Ashgate.

Udina, R. (2021). «Reversibility and the right conservation treatment». *INTACH Heritage India - Conservation Insights 2020' Lectures,* 201-210. https://doi.org/10.13140/RG.2.2.26130.58560

Chapter 2

Investigation of the physicochemical changes incurred in historical paper upon burning

1. Traditional papermaking technology

Papermaking has a long history of technological development. It spreads from China in the 1st century BC to Korea, Japan, Tibet, Nepal, reaching Samarkand in Central Asia along the silk road in the 6th century, the Islamic lands in the 8th century (Iran, Iraq, Syria, Egypt, Maghreb), from there the Muslim Iberian Peninsula (10th century) and the Christian Europe, where autochthonous productions were attested in Italy by the second half of the 13th century [Bloom 2001]. Some centuries later, paper entered the British America too, with the first mill setup in Pennsylvania in the last years of the 17th century [Hunter 1978, 247].

The long journey of paper through time and places has led to important evolutions in materials, techniques, and know-how for the manufacture of a product that has been used – and still is – for a multitude of different purposes.

Traditional paper was handmade in European mills from the second half of the 13th until at least the middle 19th century, when the first papermaking machine was introduced[1]. Handmade paper is mainly composed of fibres of pure cellulose obtained from light-coloured recycled rags, often hemp and linen or a mixture of both [Collings and Milner 1984; Barrett 2021]. Despite differences in the work organization of the single mills, some key steps were of primary importance in paper manufacture everywhere in Europe. Fabrics were cut, put for fermentation in water under the enzymatic action of the microorganisms, and often calcium compounds such as lime were added to induce chemical swelling of the fabrics. After fermentation, the rags were transferred into vats, constantly keep wet and beaten for a long time by wooden mallets (also called stampers), powered by water wheel and disposed in three sets depending on their function.

The mallets of the first battery were equipped with nails provided with sharp points for cutting rags. In the second battery, the mallets were fitted with rounded nails to separate the fibres from

[1]The first paper machine was patented in France by Louis Nicolas Robert in 1799 and its improvement and

each other and the mallets in the last battery had no nails at all, as they had to beat the fibres, which were disintegrated, defibrated and reduced to pulp consisting of cellulose.

In the second half of the 17th century, a machine was introduced to speed up the process: the Hollander beater could perform all the steps, from cutting rags to obtaining fibre pulp, and replace the action of several hammers. Production time and costs were reduced, but the length (and consequent quality) of the cellulose fibres obtained from the rags began to decrease.

For the manufacture of the paper sheets, a special paper mould was used, composed of a woven metal-wire fastened to a rectangular, rigid wooden frame. The papermaker dipped the mould into a vat where pulp was dispersed in water, and caught enough pulp to cover the surface of the woven metal-wire; the mould was then brought to surface and skilfully shaken to allow the pulp to arrange and intertwine the fibres into a network. Water in excess dripped off the interlocking wires of the frame and the newly formed sheet, still very wet and soft, was put on felts, pressed and progressively brought to dryness. The frame could be used again after removing the newly formed sheet. [de Lalande, 1761; Hunter 1947, 172-173].

Apart from cellulose and water, other "ingredients" were commonly added to provide the paper with suitable properties. As cellulose is highly hygroscopic, sheets intended for writing and painting were sized to limit their permeability to moisture and water and to prevent liquid inks and colours from bleeding. To this aim, gelatine, a protein glue derived from collagen, was extracted from animal connective tissue or bone in boiling water, filtered, further diluted, put in vats and kept heated. Sheets were then immersed into the warm sizing solution, finally hang up and allowed to dry. Moreover, gelatine enhanced paper resistance to mechanical stress, in particular tearing and wrinkling [Barrett and Mosier 1995; Kolbe 2002; Kolbe 2004]. It is also well demonstrated that, in addition to these immediate effects of partial waterproofing and mechanical reinforcement of the paper material, gelatin plays an important protective role for the paper during the degradation processes that occur with aging [Dupont 2003].

Alum (a double salt aluminum potassium sulfate) was usually mixed to gelatin as a mordant to increase its viscosity and the sizing performance, to decrease the fast spoiling of the gelatin by microorganisms and to reduce the costs of production at least from the second half of the 16th century [Brückle 1993] or early in the 17th century [Marini Bettolo et al. 2007].

2. Cellulose and its thermal degradation

Paper resulting from the traditional papermaking process is a complex, organic material mainly constituted by a network of cellulose fibres. Cellulose is a polymer, a polysaccharide made of a variable number of glucose monomers linked by β-(1-4) glucosidic bonds. Cellulose macromolecules are linear and tend to align side by side. Intramolecular and intermolecular hydrogen bonding between the hydroxyl groups of the monomers keep them firmly linked, giving form to **microfibrils**, which are organized in **fibres** (Fig. 2.1).

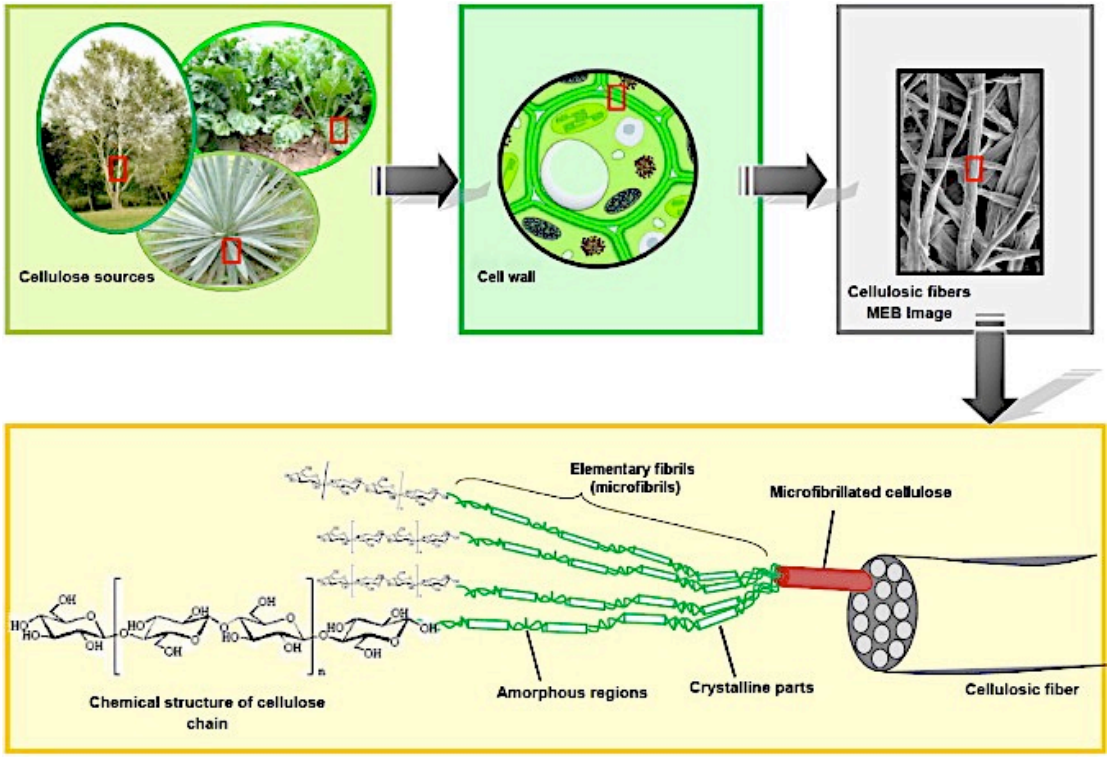

Figure 2.1. From the cellulose sources to the cellulose molecules: hierarchical structure of cellulose fibers [Lavoine et al. 2012].

The number of monomers in a cellulose macromolecule is indicated as the degree of polymerization (DP) and can vary from several hundreds to tens of thousands of units depending on the quality of the cellulose, on the plant source, on the methods used to isolate cellulose from the source material to make paper pulp and on the degradation degree of the paper.

The physical and chemical characteristics of each cellulose fibre are determined by the coexistence of crystalline and amorphous domains. The crystalline areas are rigidly structured and considerably resistant to degradation processes as they present a maximum level of intra and

intermolecular bonding and oppose a good resistance to water penetration. The amorphous areas have a low level of order and therefore are more flexible and elastic.

Water is inseparable from cellulose and is present in higher quantities in the amorphous domains. It acts as a sort of lubricant in the microfibrils and fibres, allows their movement respective to one another and strongly affects the fibre mechanical properties.

In the amorphous areas, water molecules intercalate between the cellulose chains. In large amount, water increases the distance between cellulose macromolecules and weakens the intermolecular hydrogen bonds that usually guarantee the fibre cohesion, which increases the flaccidity of paper. Water also is the reactant in the acid-catalyzed hydrolytic cleavage of β-glycosidic bonds, with a consequent lowering of the degree of polymerization of cellulose and a progressive loss of its physical properties. On the other hand, a water deficit in the fibres leads to stiffness and brittleness of paper.

Changes in water content and in the cellulose structure during heating have been studied and discussed in the scientific literature [Suzuki et al. 1992; Wertz et al. 2014; Hassan 2016; Brillard et al. 2017; Ahn et al. 2018] and effectively delineated by Scheirs, Camino and Tumiatti (2001). According to the authors, the first reaction of the cellulose to heating is a physical desorption of the moisture adsorbed (until 150°C) and chain cleavage, with a progressive depolymerization (until 220°C). At higher temperatures (220-550°C), water is eliminated from the cellulose molecule through direct chemical reactions of dehydration involving the OH and H groups. These reactions could be condensation of OH groups to form ester groups C-O-C or elimination of H to form C-C double bonds (Scheme 2.1).

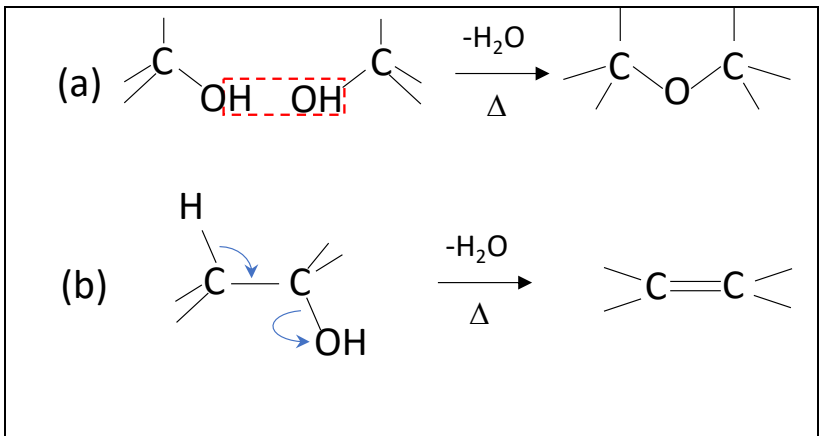

Scheme 2.1. (a) Condensation reaction; (b) elimination of water.

The progressive removal of OH groups causes paper weakening, due to the loss of hydrogen bonds, the formation of various by-products and semi-carbonaceous compounds, more or less dark brown in colour. Such a thermal dehydration usually occurs in the range 150-240°C with 200°C being the minimum temperature at which the newly formed water can evolve from the amorphous domain of cellulose due to chemical processes. Finally, when temperature rises further (500°C and over), combustion occurs, resulting in cellulose decay by oxidation. A partial combustion process leads to the formation of carbonaceous residues; when it is complete, in the transformation of cellulose into carbon dioxide and water and the fragmentation and loss of the burned areas.

3. Historical papers involved in the present research

What happens when a traditional rag paper sheet is exposed to a blaze and what are the remaining residues of the combustion process? Studies carried out on pyrolysis/combustion of paper samples are important to understand the modifications occurring on paper exposed to heat and to fire. On the other hand, one must also consider that laboratory samples can never fully reproduce real materials and their natural decay, which is essential to know in order to develop intervention methodologies.

Based on these considerations, historical burnt papers belonging to the Municipal Library of Chartres – nowadays held in the Médiathèque L'Apostrophe in Chartres – and to the Library of the Episcopal Seminary in Padua have been involved from the very beginning in the experimental part of this research in order to characterize their composition, to investigate degradation induced by flames, and to understand if and to what extent the presence of sizing, minerals and other components in the paper could eventually affect the burning process.

The material from the Chartres Médiathèque is an ink-free leaf belonging to the manuscript Chartres BM ms 1047, *Histoire de l'ancienne cité des Carnute,* a work by Honoré-Félix-André Lejeune written in the 1830s (Omont et al. 1890].

The manuscript is in very poor conservation condition, severely damaged by fire during bombing in 1944 and the leaf involved in the investigation presented residual darkened and carbonized areas all along the margins (Fig. 2.2).

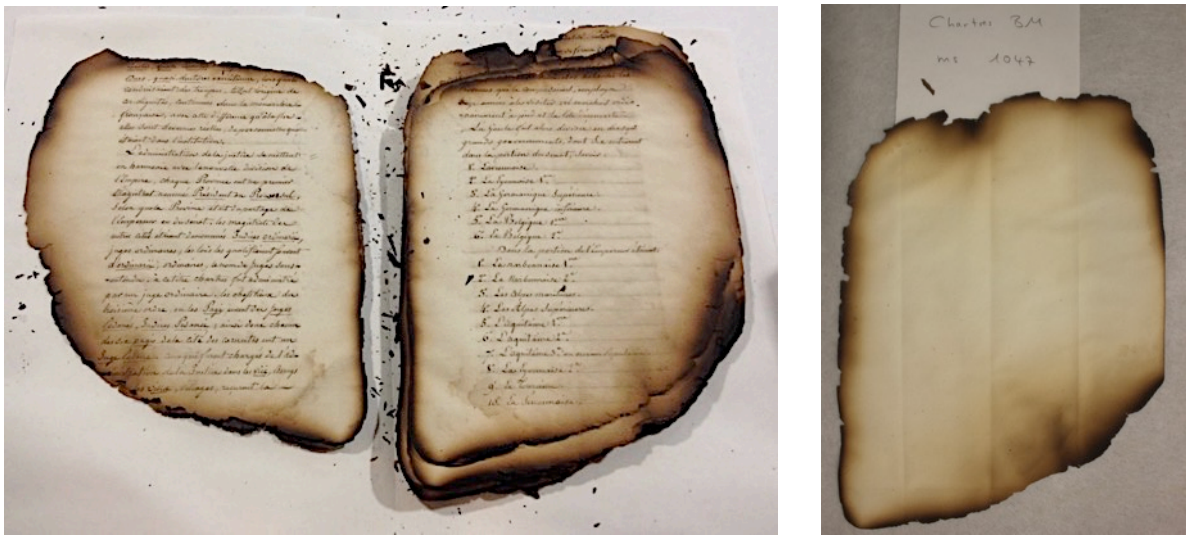

Figure 2.2. The manuscript ms 1047 held at the Médiathèque L'Apostrophe in Chartres, surviving the fire in very poor condition; on the right, the ink-free leaf involved in the present research.

The sheets from the Library of the Episcopal Seminary in Padua are part of the incunabulum *Lectio super secundo Decretalium. Pars prima*, a text by Nicolaus de Tudeschis (Panormitanus), printed by Bernardino Stagnino in Venice in 1487 (Armstrong L. et al. 2008). Struck by bombs in 1944, the flames affected the central area and the upper margins of the book, and water was used to extinguish the fire, as evident from the presence of tidelines on the paper. The volume is still partially sewn, although deprived of its cover (Fig. 2.3 and 2.4).

Figure 2.3. The incunabulum *Lectio super secundo Decretalium* held at the Library of the Episcopal Seminary in Padua, partially burnt but still retaining one of the original sewing supports and the tail endband.

Figure 2.4. Partially burnt sheets of the incunabulum *Lectio super secundo Decretalium,* 1487. The tidelines were produced by the water used to extinguish the fire.

4. Physico-chemical characterization of the historical papers

4.1 Acidity of the burnt paper

pH is a measure of the activity of hydrogen ions (H^+) in solution and its estimation in historical paper is a significant task to better understand the degradation phenomena [Strlic et al. 2004; Wertz et al. 2014]. The pH was tested on ten leaves of the incunabulum using surface measurement, 3 points per leaf: point 1 located in the unburnt area, point 2 located in the area affected by water and tidelines formation, point 3 in the darkest, burnt area (Fig. 2.5).

On the single leaf belonging to the manuscript Chartres BM ms 1047 the pH was measured in 8 location points: 5 points in the unburnt, white area and 3 points in the burnt, marginal area (Fig. 2.6).

Surface pH was measured by non-destructive method using a pHmeter Hanna HI 83141 with a flat electrode, following the protocol described in Strlic et al. 2004: the paper was wetted with a drop of double-distilled water, and the pH was measured by pressing the electrode on the surface after the drop entered inside and waiting 30 sec. for stabilization of the pH value.

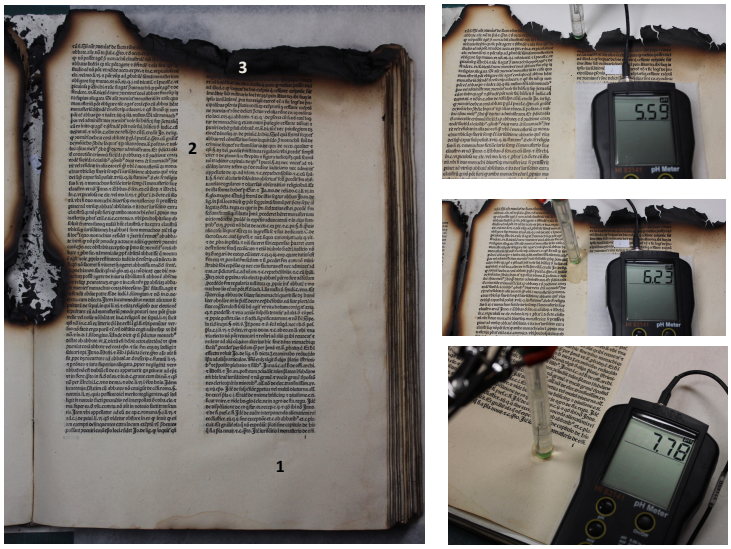

Figure 2.5. Padua incunabulum, pH location and measurements.

Incunabulum pH values (10 leaves)

Leaf	point 1 (white area)	point 2 (slightly brown area)	point 3 (burnt area)
f	8.1	7.0	6.2
g_2	7.5	7.1	6.5
h	7.5	6.9	5.9
i	7.8	6.4	5.6
m_3	8.0	6.4	6.0
o_4	7.7	7.1	6.9
p_2	6.9	6.3	5.9
r_3	7.8	6.6	6.2
s_4	8.0	6.4	6.4
z_4	8.4	7.5	6.2
Av.	7.8 ± 0.4	6.8 ± 0.4	6.2 ± 0.4

Table 2.1. Padua incunabulum, pH values.

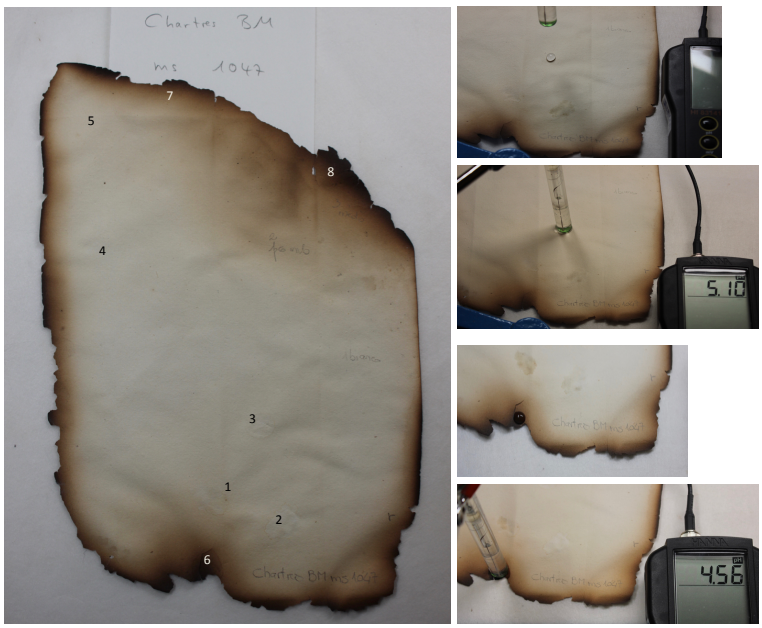

Chartres BM ms 1047 pH values

unburnt area	point 1	5.2
	point 2	5.2
	point 3	5.1
	point 4	5.0
	point 5	5.1
Average		5.1 ± 0.1
burnt area	point 6	4.6
	point 7	4.5
	point 8	4.6
Average		4.6 ± 0.1

Figure 2.6. Chartres BM, ms 1047, pH location on the leaf and measures. **Table 2.2** Chartres BM, ms 1047, pH values.

As clear from the values in Table 2.1, the pH of the papers from the incunabulum is moderately alkaline in the unburnt areas (average pH 7.8 ±0.4), decreases somewhat in areas affected by water (average pH 6.8 ±0.4) and decreases further in the black areas (average pH 6.2 ±0.4). Such alkaline to slightly acidic pH values are expected for a quality medieval paper, produced with pulp of pure rag cellulose and rich in calcium carbonate ($CaCO_3$) as detected by SEM-EDS analysis and by XRPD (which detected $CaCO_3$ in form of calcite, see § 4.2.2 and 5).

Calcium carbonate is in fact usually the result of the lime (Calcium hydroxide, $Ca(OH)_2$), a very alkaline mineral compound dispersed in the water of the basins, where rags were put to ferment, to enhance fiber swelling and help the maceration effects (de Lalande 1761; Barret 2021). Over drying, carbon dioxide is gradually re-absorbed in the paper fibers and this precipitates the lime into calcium carbonate. Calcium carbonate has a positive impact on paper stability, acting as a buffer to prevent, or at least to counteract, the acidity that arises over time, due to both intrinsic causes (unstable elements in paper composition) or induced by external environmental factors.

The pH values presented in Table 2.2 refer to the leaf from Chartres BM ms 1047 and are acidic: average pH is 5.1 ±0.1 in the undamaged areas, and 4.6 ±0.1 in the burnt carbonised edges. Such slightly acidic values may be explained by the degradation level and by the presence of alum, as indicated by aluminium (Al), potassium (K) and sulphur (S) in the fibres, detected by SEM-EDS analysis (see § 4.2.2). Al, K and S are the essential elements in the composition of alum, a double sulphate of potassium and aluminium which was often added to gelatin. Alum is a compound which hydrolyses producing protons and induces acidic degradation which is deleterious to the cellulose stability [Dupont 2003]. Barrett, Ormsby, and Lang [Barrett et al. 2016; Barrett et al. 2021] made a quantitative estimate of the content of elements like Ca, K, Al, and S by XRF in a significant number of historical specimens, converting the XRF peaks to ppm using calibration curves built using ICP-OES. According to the authors, the decline in paper pH over the centuries should not be attributed to greater amounts of alum used in papermaking, but rather be related to less calcium carbonate and to a lower amount of gelatin used for sizing, with a significant and progressive decline of the latter between the 15^{th} and 19^{th} centuries. In their research, the quantity of proteinic glue was inferred from the concentration of amino acids in the historical samples using gas chromatography-mass spectrometry (GC-MS) combined with near-infrared (NIR) spectroscopy.

Actually, the paper from the Chartres manuscript is quite well-sized as the water droplet used in the pH tests struggles to penetrate, but the calcium amount is undoubtedly lower than in the paper from the Padua incunabulum and often in form of gypsum (calcium sulphate) rather than calcium carbonate, as indicated by XRD analysis (see § 5), while K, Al, and S are widely detected among the fibres by SEM (see § 4.2.2).

Overall, the fire-induced effects on the paper from the manuscript and from the incunabulum did not produce a too significant drop in the pH, just a mild acidification probably resulting from the

formation of conjugated carboxyl groups during the combustion process, as confirmed by ATR-FTIR analyses (see § 4.3.1).

4.2 Morphological analysis of burnt paper fibers

4.2.1 Optical microscope examination

The surface and cross section of the samples were examined and photographed at 100x and 200x magnification in visible light. As burnt paper is opaque, reflected light and brightfield illumination modes (in which sample contrast comes from absorbance of light in the sample) were employed, as well as darkfield (sample contrast comes from light scattered by the sample) and interference contrast (sample contrast comes from interference of different path lengths of light through the sample) to obtain a three-dimensional representation of the cellulose fibres. A cellulose fiber structure was clearly seen both in the fragment belonging to the manuscript (Fig. 2.7) and in that from the incunabulum (Fig. 2.8), despite the fact that XRD did not detect any crystalline cellulose peak in this latter case. In the paper from the manuscript, most fibres are smooth with cross marking nodes, no lengthwise striations, and a narrow lumen typical of flax, some others look like hemp fibres and have a more accentuated cylindrical shape and longitudinal striations less regular than those in flax, from which it is difficult to distinguish.

Linen and hemp fibres are clearly detected also in the sample from the incunabulum, whose advanced combustion, as shown by the spectroscopic examinations, make it harder to discern fibrous structures (Fig. 2.9).

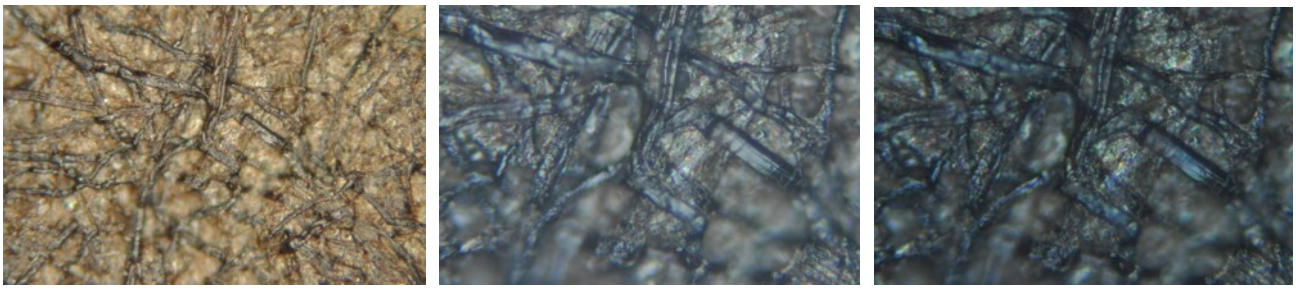

Figure 2.7. Chartres BM ms 1047, burnt area. Surface microscopic observation in reflected-light brightfield illumination, 100x (left); reflected-light dark field, 200x (middle); reflected-light interference contrast, 200x (right).

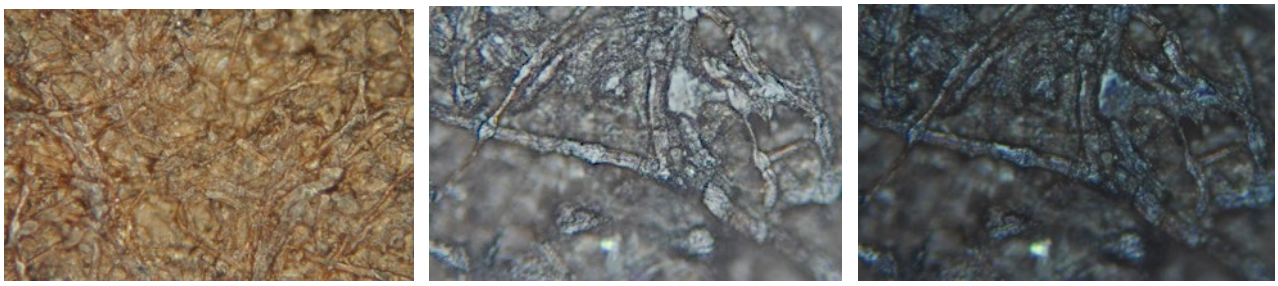

Figure 2.8. Padua incunabulum, burnt area. Surface microscopic observation in reflected-light brightfield illumination, 100x (left); reflected-light dark field, 200x (middle); reflected-light interference contrast, 200x (right).

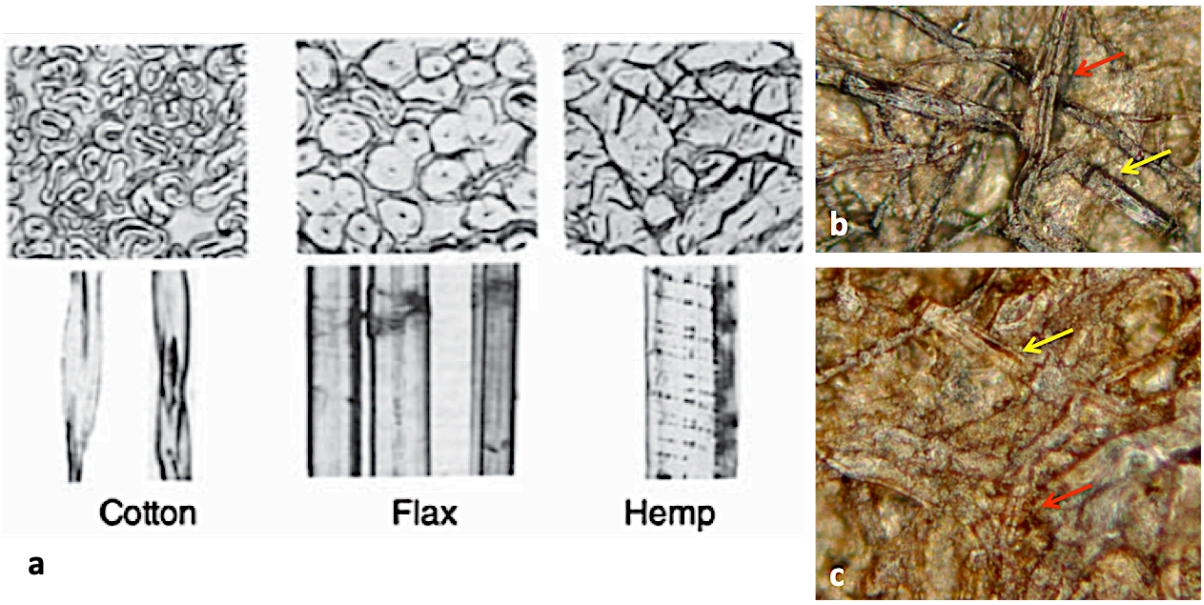

Figure 2.9. (a) Microscopic images of natural fibres from different vegetal species adapted from Hu 2020, p. 9; (b) Chartres BM ms 1047 and (c) Padua incunable, focus on fibres comparable with flax (yellow arrow) and hemp (red arrow).

4.2.2 Scanning electronic microscopy (SEM) investigation

SEM contributed significantly to the study of cellulose fibres and of the other substances present in paper material due to manufacture or to some accidental event and showed in detail the characteristics and the morphology of the samples.

Impurities can enter the paper from the processing water or the sizing agent or can even have been deposited on the surface of the sheet during consultation or storage in a library or archive. According to recent studies, SEM observations can highlight the position of mineral inclusions with respect to the fibres, also contributing to understand if they were added to the cellulose pulp or deposited on the sheet later, evenly distributes or concentrated in single areas (Bicchieri et al. 2019). Fig. 2.10 is the SEM surface image of a burnt fragment from Chartres BM ms 1047, where 6

points were investigated, both on the cellulose fibres and on the white cluster and heterogeneous inclusions. The most significative analyses of the several points investigated are here proposed, complete data are in Appendix Chapter 2.

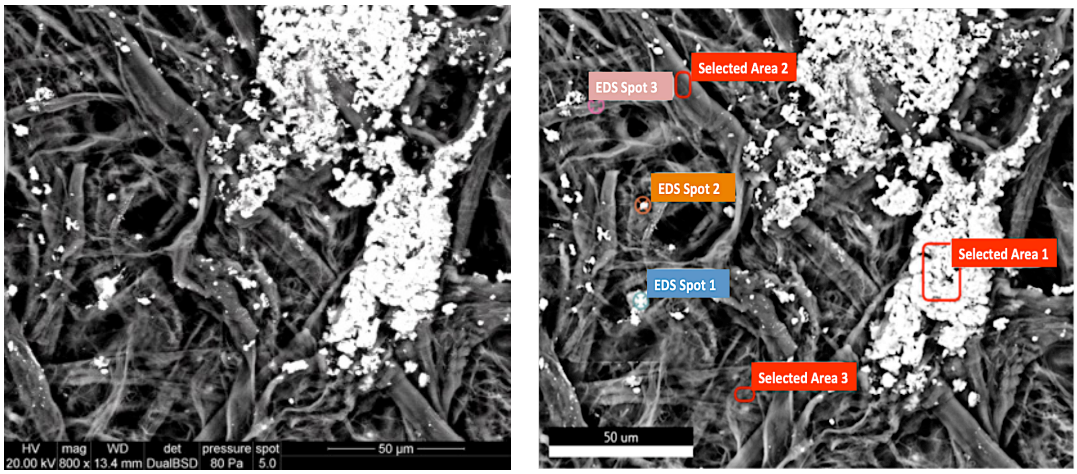

Figure 2.10. Chartres BM ms 1047, surface, burnt area. SEM image (left) and areas investigated (right).

In all the examined areas, C and O characterizing cellulose were always detected and constitute the main part in weight% (average C=43.1% and O=43.7%); the total average amount of C and O is 94.8% in weight in the investigation of cellulose areas of the sample and 72.7 % in weight in areas corresponding to clusters and inclusions.

Other elements were observed in lower amounts. The cluster in the Selected Area 1 consisted mainly of calcium (Ca) and sulfur (S), which are the basic components of gypsum ($CaSO_4 \cdot 2H_2O$), in accordance with the results of X-ray diffraction (§ 5) (Fig. 2.11, Table 2.3).

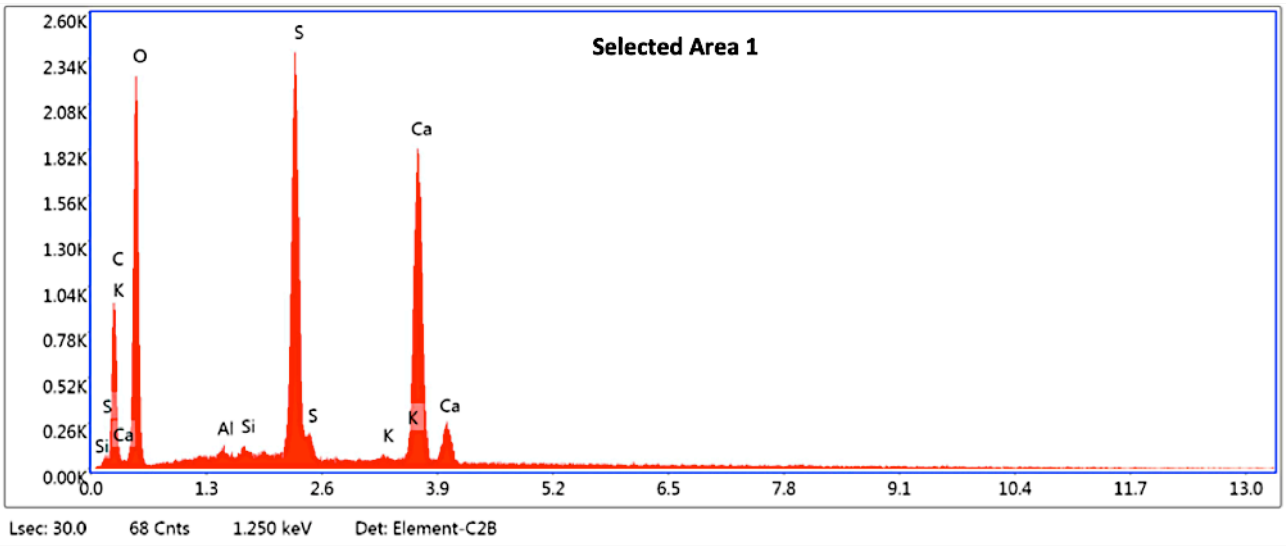

Figure 2.11. Chartres BM ms 1047, burnt area, surface, cluster, EDX spectrum.

Table 2.3. Chartres BM ms 1047, burnt area, surface. Elements weight percentages in the Selected Area 1, on a cluster. Apart from C and O, elements that characterise cellulose fibre, calcium and sulfur are present in high amounts, identifying the cluster as gypsum (Calcium sulfate).

Selected Area 1 eZAF Smart Quant Results

Element	Weight %	Atomic %	Net Int.	Error %	Kratio	Z	A	F
C K	**19.0**	29.6	166.6	11.1	0.0451	1.0800	0.2195	1.0000
O K	**44.2**	51.6	497.7	10.3	0.0781	1.0347	0.1707	1.0000
AlK	0.1	0.1	6.4	63.6	0.0008	0.9219	0.6946	1.0055
SiK	0.2	0.1	9.3	37.8	0.0012	0.9423	0.8077	1.0093
S K	**14.5**	8.5	752.4	2.5	0.1276	0.9231	0.9409	1.0111
K K	0.4	0.2	14.6	26.2	0.0034	0.8742	0.9554	1.0416
CaK	**21.5**	10.0	684.8	2.4	0.1879	0.8903	0.9743	1.0057

Calcium, sulphur and silicon are detected in all the analysed points. These elements are in the composition of some minerals previously identified by XRD as talc (hydrated magnesium silicate $Mg_3Si_4O_{10}(OH)_2$) and gypsum. Also, aluminum and potassium were present in the paper sample from Chartres; the average amount is 0.7% for Al and 1.1% for K, determined as average of the values for Al and K of the three Selected Areas, expressed as weight% (second column in the Table 2.3 and Table 2.4). As these elements were not found by X-ray diffraction – i.e., they have not a crystalline structure – it is reasonable to assume that they have originated from the alum (the metal sulfate composed of potassium, aluminum and sulphate, usually with the ratio 1:1:2) dissolved in the gelatin of the sizing (Fig. 2.12, Table 2.4). This assumption takes a strong basis, if we consider the atomic percentage of Al and K in the examined points (see Appendix Chapter 2), which is always in a ratio close to 1:1, as expected for rock alum: when Al increases, K increases, and vice versa.

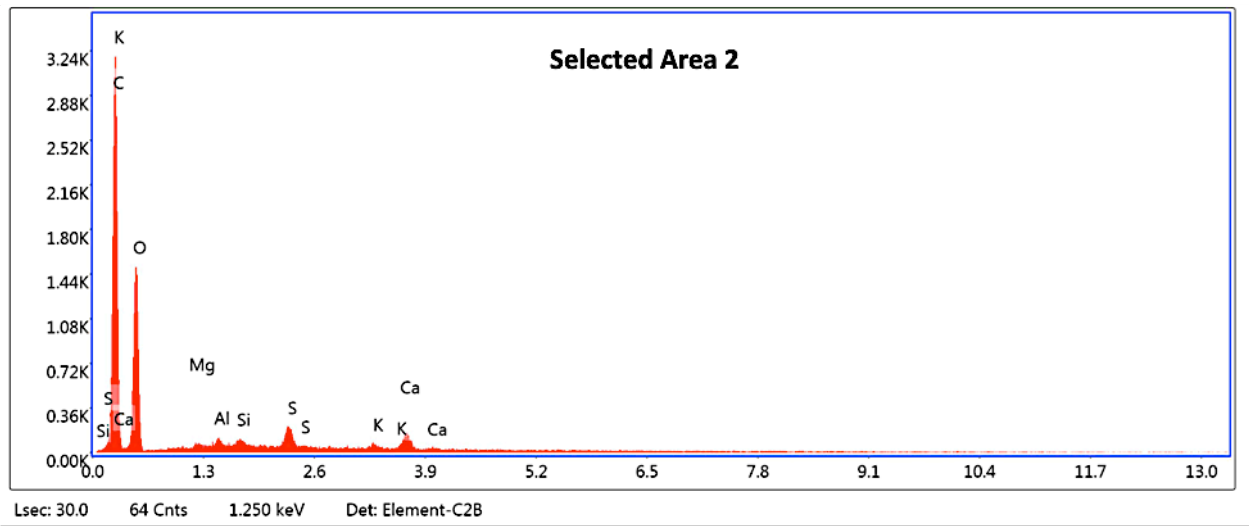

Figure 2.12. Chartres BM ms 1047, burnt area, surface. Cellulose fibre, EDX spectrum.

Table 2.4. Chartres BM ms 1047, burnt area, surface. Semi-quantitative estimation of elements weight percentages in the Selected Area 2, located on a fibre. Apart from the expected elements C and O, Ca and S (gypsum), Mg and Si (talc) and Al and K, basic ingredients of alum, were detected.

		Selected Area 2	**eZAF Smart Quant Results**					
Element	Weight %	Atomic %	Net Int.	Error %	Kratio	Z	A	F
C K	52.0	60.8	623.7	7.0	0.2668	1.0275	0.4991	1.0000
O K	41.9	36.7	328.6	10.4	0.0814	0.9821	0.1980	1.0000
MgK	0.3	0.2	8.6	28.7	0.0017	0.9058	0.6044	1.0026
AlK	0.6	0.3	17.8	18.8	0.0036	0.8720	0.7483	1.0044
SiK	0.5	0.3	18.9	20.0	0.0039	0.8909	0.8496	1.0069
S K	1.8	0.8	57.8	9.2	0.0155	0.8721	0.9645	1.0128
K K	0.6	0.2	14.7	20.0	0.0053	0.8252	1.0124	1.0385
CaK	2.3	0.8	46.9	11.0	0.0203	0.8401	1.0166	1.0270

Finally, it should be noted that the cluster and the inclusions are not embedded in the cellulose matrix, they overlap the fibres and have evidently superimposed on the sheet over time rather than already being part of the pulp used for its manufacture.

In the cross section, five points from the Chartres manuscript were also investigated with SEM. It is clear from the SEM images that the quantity of impurities in the inner layers of the sheet is considerably less than those deposited on the surface, as expected for surface “dust” (Fig. 2.13).

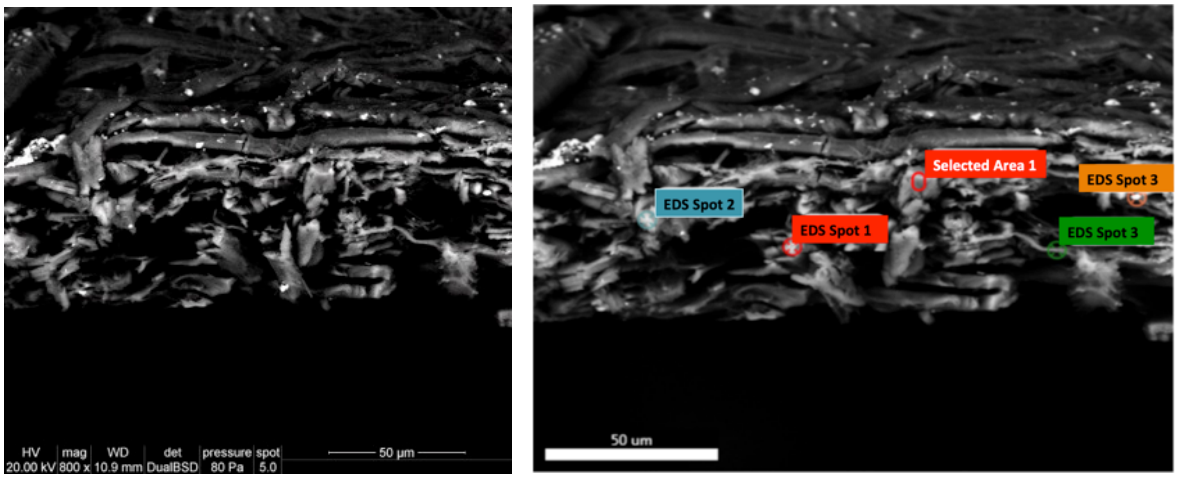

Figure 2.13. Chartres BM ms 1047, burnt, cross section. SEM image (left) and investigated areas (right).

C and O were of course detected everywhere: the average amount in weight% of C is 53.9% and that of O is 41.9%, C and O represent 95.8% of the matter analysed, while other elements are present in minimal amounts (< 1%), usually aluminium, sulphur, magnesium, silicon, potassium and calcium; the spectrum of the Selected Area 1 is exemplary of a burnt cellulose area (Fig. 2.14, Table 2.5).

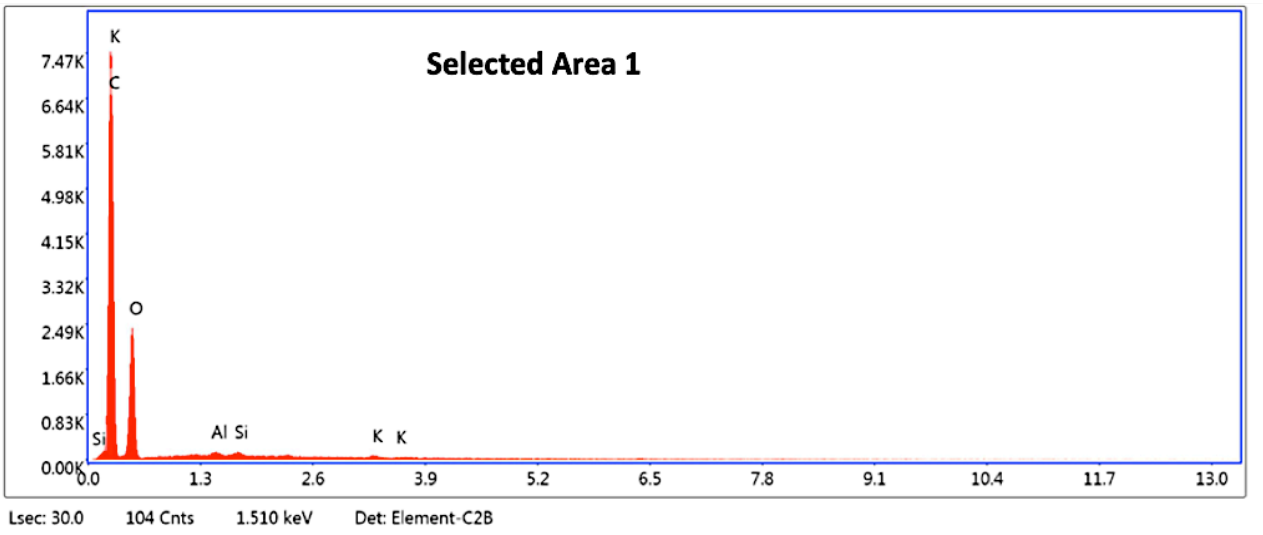

Figure 2.14. Chartres BM ms 1047, burnt cellulose area, EDX spectrum.

Table 2.5. Chartres BM ms 1047, burnt, cross section. Semi-quantitative estimation of elements weight percentages in the Selected Area 1 (cellulose). Apart from C and O mainly referred to cellulose, other elements are present in minimum amount.

Selected Area 1 **eZAF Smart Quant Results**

Element	Weight %	Atomic %	Net Int.	Error %	Kratio	Z	A	F
C K	59.8	66.7	1618.0	5.3	0.3851	1.0186	0.6317	1.0000
O K	39.3	32.9	514.3	10.6	0.0675	0.9731	0.1766	1.0000
AlK	0.3	0.2	21.1	15.4	0.0022	0.8635	0.7390	1.0034
SiK	0.3	0.1	18.9	19.1	0.0019	0.8821	0.8489	1.0052
K K	0.3	0.1	14.0	29.5	0.0025	0.8168	1.0277	1.0366

It is to notice that both in surface and in section, the atomic ratio C:O in burnt cellulose areas is close to 2:1, higher than expected for pure cellulose (about 1:1), and indicative of water loss by chemical reactions as shown, e.g., in Scheme 2.1, § 2.

Spot 3 is one of the few particles included in the cross section of the sample: the presence of high calcium and sulphur peaks suggests that it is gypsum (Fig. 2.15). Apart from Selected Area 1 discussed above, sulphur is always found (average amount 0.5% in weight) as well as aluminum (average amount 0.5%) and potassium (average amount 0.4%), probably confirming the presence of alum most likely related to the size and the historical practice to treat the sheets by dipping them in the liquid gelatin (Table 2.6)

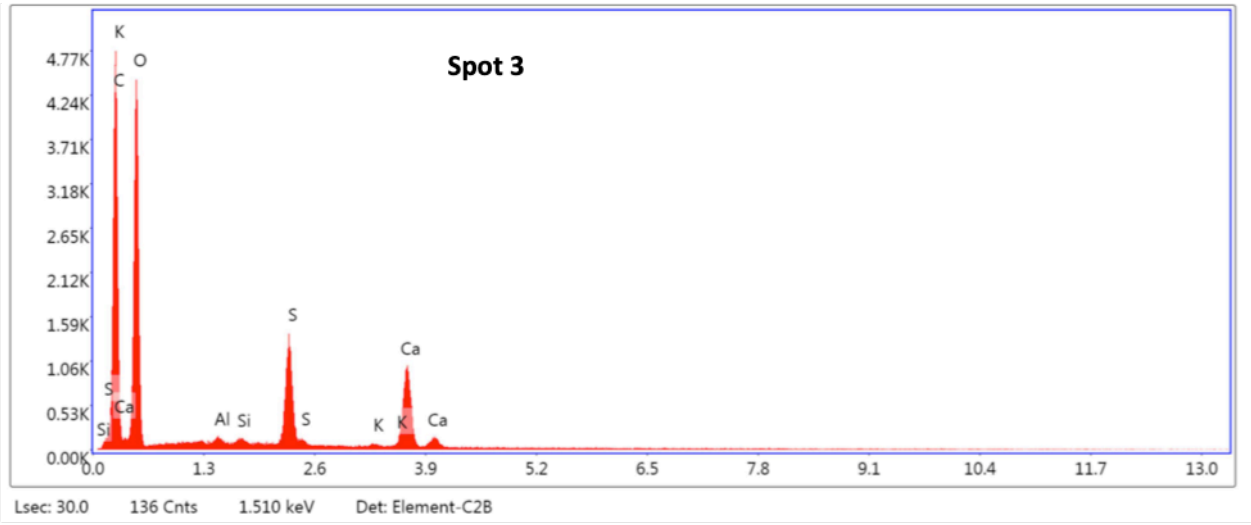

Figure 2.15. Chartres BM ms 1047, burnt, cross section. Inclusion, EDX spectrum.

Table 2.6. Chartres BM ms 1047, burnt, cross section. Semi-quantitative estimation of weight percentages in the area Spot 3, an inclusion. Ca and S (gypsum) are present in significant amount.

Spot 3 eZAF Smart Quant Results

Element	Weight %	Atomic %	Net Int.	Error %	Kratio	Z	A	F
C K	40.7	50.6	948.5	8.1	0.1596	1.0392	0.3778	1.0000
O K	47.6	44.5	965.9	9.8	0.0896	0.9938	0.1894	1.0000
AlK	0.3	0.1	21.1	17.8	0.0015	0.8831	0.6949	1.0048
SiK	0.2	0.1	16.5	21.9	0.0012	0.9023	0.8128	1.0080
S K	4.6	2.1	414.6	2.9	0.0391	0.8834	0.9519	1.0124
K K	0.2	0.1	14.8	23.5	0.0019	0.8360	0.9990	1.0432
CaK	6.5	2.41	375.3	2.8	0.0568	0.8512	1.0096	1.0163

A surface SEM image of a burnt fragment from the incunabulum held in the Episcopal Seminary in Padua is presented in Fig. 2.16. As it was observed in the Chartres manuscript, there are countless white clusters and inclusions on the surface, overlapping the fibres. Several areas were tested by SEM, both cellulose and clusters and heterogeneous particles.

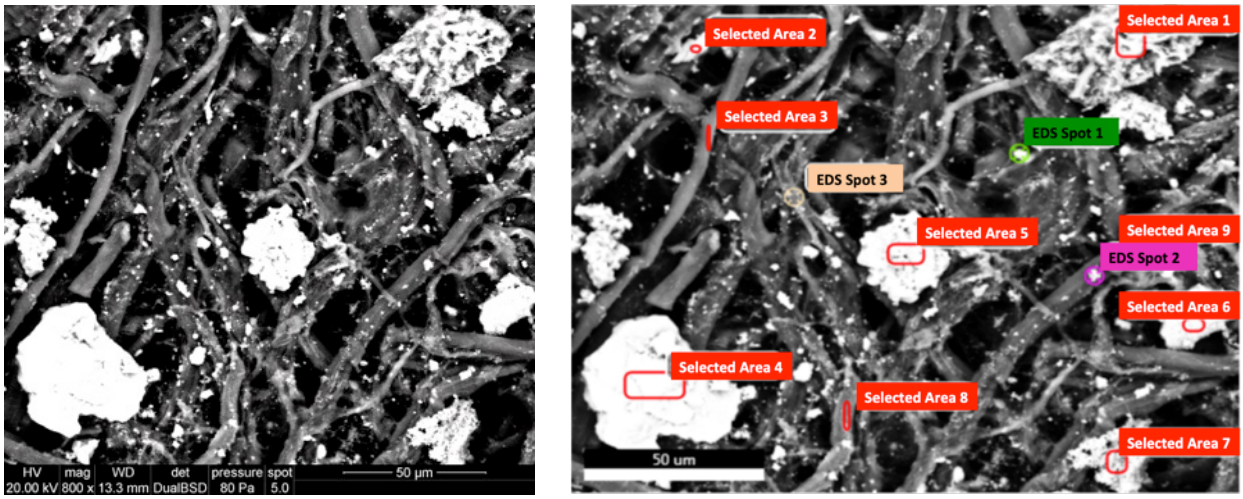

Figure 2.16. Padua incunabulum, burnt, surface. SEM image (left) and areas investigated (right).

Also in this case, C and O are the main elements detected: the average amount of C is 43.9% in weight, O is 37.0%, C and O average amount is 80.9%, a bit lower than in the paper of Chartres BM ms 1047. The percentage of other elements in the samples is in fact higher and in line with the data obtained by XRPD, which found calcite, gypsum, talc, hydrotalcite (a hydrated magnesium aluminate often associated with talc) bassanite (calcium sulphate hemihydrate), quartz (silicon dioxide SiO_2) and feldspar albite ($NaAlSi_3O_8$) in the Padua fragment.

Selected Area 1 (Fig. 2.17, Table 2.7) and Selected Area 4 contain large amounts of aluminum and silicon and consist probably in clusters of feldspar albite. Calcium is also present in large

percentage in these areas (15%) and in all the white particles examined, with an average Ca content of 20.4% (analyses spectra and data in Appendix Chapter 2).

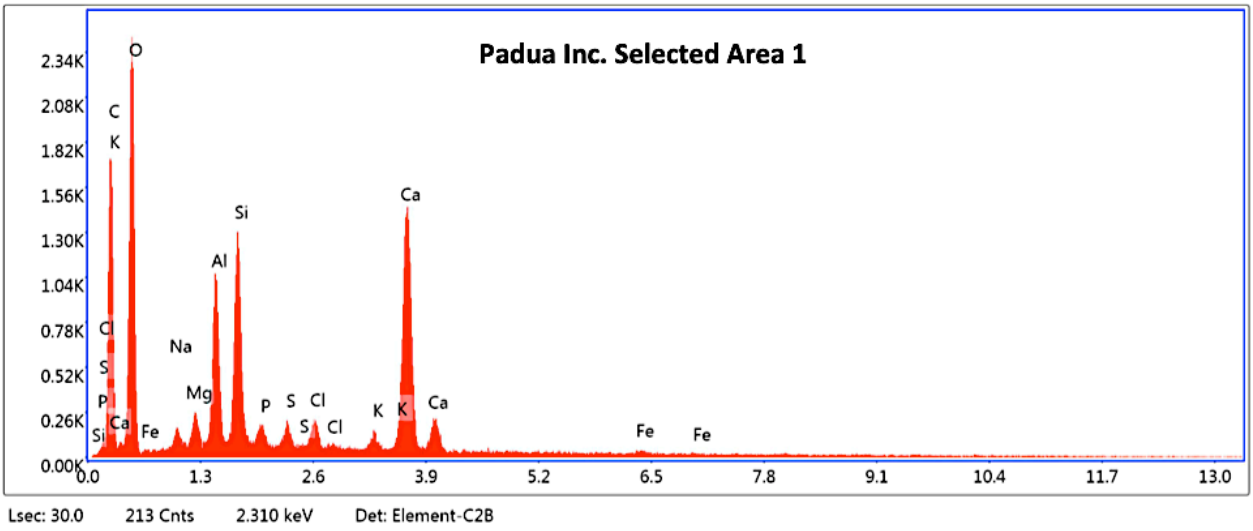

Figure 2.17. Padua incunabulum, burnt, surface. Cluster, EDX spectrum.

Table 2.7. Padua incunabulum, burnt, surface. Semi-quantitative estimation of elements weight percentages in the Selected Area 1. C and O are the main elements detected, but Ca is present in large amount. Na, Mg and particularly Al and Si are also relevant, possibly associated in various compounds such as feldspar albite ($NaAlSi_3O_8$), talc (MgO_3Si) and hydrotalcite.

Selected Area 1 eZAF Smart Quant Results

Element	Weight %	Atomic %	Net Int.	Error %	Kratio	Z	A	F
C K	27.5	40.0	340.4	9.6	0.0821	1.0695	0.2796	1.0000
O K	40.1	43.4	541.6	10.1	0.0756	1.0241	0.1841	1.0000
NaK	1.0	0.8	27.8	16.6	0.0039	0.9306	0.4082	1.0018
MgK	1.2	0.8	55.5	10.2	0.0064	0.9466	0.5693	1.0032
AlK	5.1	3.3	286.9	5.6	0.0331	0.9116	0.7042	1.0045
SiK	5.8	3.5	360.1	4.9	0.0415	0.9317	0.7715	1.0053
P K	0.6	0.3	30.6	18.1	0.0044	0.8950	0.8118	1.0088
S K	0.7	0.4	38.1	14.3	0.0057	0.9126	0.8771	1.0134
ClK	1.2	0.6	57.1	11.2	0.0094	0.8682	0.9225	1.0198
K K	0.7	0.3	29.1	16.6	0.0059	0.8640	0.9753	1.0433
CaK	15.8	6.8	567.6	2.4	0.1383	0.8798	0.9885	1.0087
FeK	0.5	0.1	8.9	40.0	0.0038	0.7845	0.9984	1.0567

The spectrum EDS in Fig. 2.18 refers to Spot 3 on the cellulose fibers and the Ca content is lower than in the cluster, but in any case, higher than anywhere in the analyzed Chartres manuscript sample. It is worth noting that, unlike the Chartres sample, gypsum was not detected by XRPD here and the amount of Ca is so relevant as to confirm its presence as calcite, rather than calcium sulfate (Table 2.8).

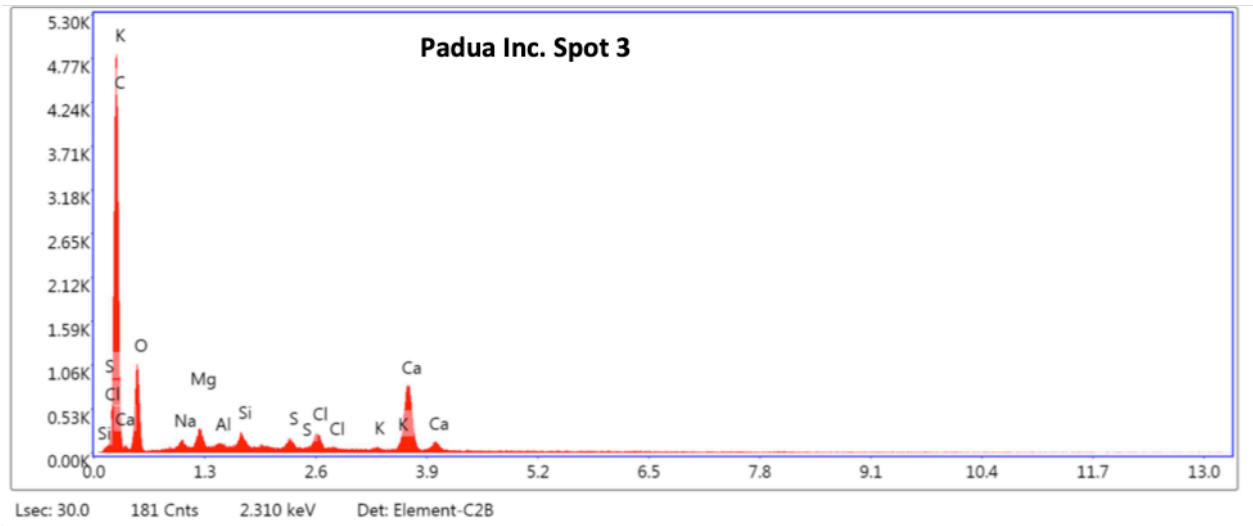

Figure 2.18. Padua incunabulum, burnt cellulose fibre, EDX spectrum.

Table 2.8. Padua incunabulum, surface, burnt. Semi-quantitative estimation of elements weight percentages in the Spot 3, a cellulose area. Apart from C and O, Ca is the element present in the largest amount.

EDS Spot 3 - Det 1 eZAF Smart Quant Results

Element	Weight %	Atomic %	Net Int.	Error %	Kratio	Z	A	F
C K	58.6	70.5	988.7	7.1	0.2859	1.0361	0.4714	1.0000
O K	24.9	22.6	214.1	11.8	0.0358	0.9909	0.1449	1.0000
NaK	1.1	0.7	26.7	16.2	0.0044	0.8995	0.4558	1.0016
MgK	1.5	0.9	61.0	9.9	0.0084	0.9147	0.6201	1.0027
AlK	0.3	0.1	12.7	27.2	0.0018	0.8807	0.7470	1.0048
SiK	0.8	0.4	47.0	10.5	0.0065	0.8999	0.8500	1.0074
S K	0.7	0.3	32.2	12.0	0.0058	0.8811	0.9612	1.0182
ClK	1.5	0.6	64.0	9.3	0.0126	0.8381	0.9856	1.0244
K K	0.2	0.1	7.5	49.4	0.0018	0.8339	1.0084	1.0536
CaK	10.5	3.8	313.3	3.1	0.0914	0.8491	1.0152	1.0125

The cross section of the sample from the Padua incunabulum was investigated in 5 points (Fig. 2.19)

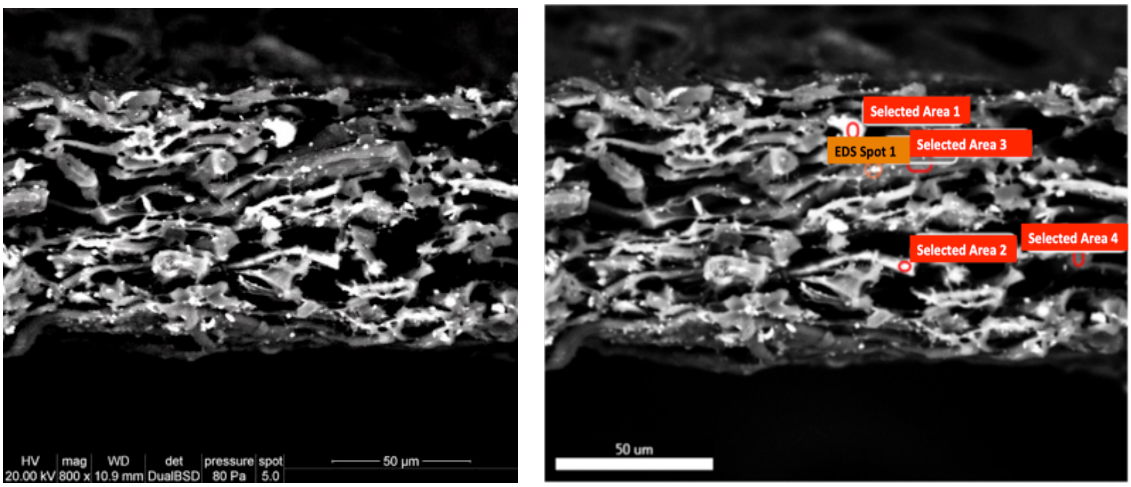

Figure 2.19. Padua incunabulum, cross section. SEM image (left) and areas investigated (right).

C and O are respectively present in the amount of 60.3% and 28.9% in weight; the two elements compose the most part of the sample (89.2%), a higher amount when compared with the sample surface area, where the majority of the heterogenous accidental particles were found. Some calcium inclusions were also in the cross section (Fig. 2.20, Table 2.9) (completed spectra and data in Appendix, Chapter 2).

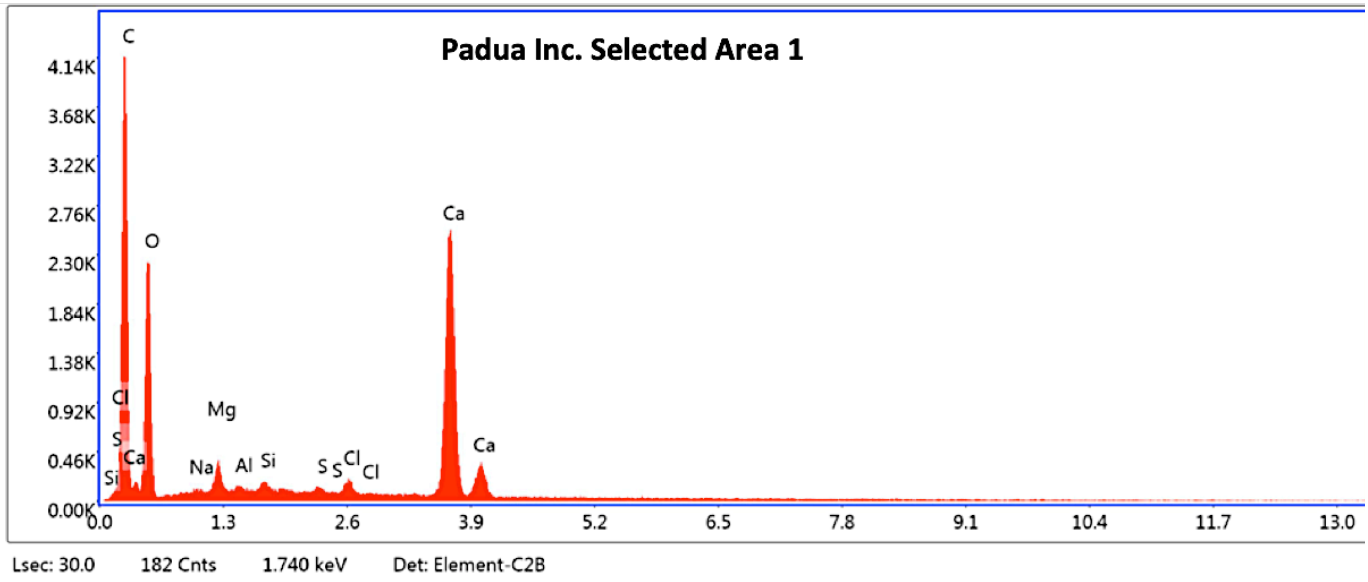

Figure 2.20. Padua incunabulum, burnt area, cross section. Inclusion, EDX spectrum.

Table 2.9. Padua incunabulum, burnt, cross section. Semi-quantitative estimation of elements weight percentages in the Selected Area 1, inclusion. Apart from C and O, Ca is the element present in this particle.

Selected Area 1 eZAF Smart Quant Results

Element	Weight %	Atomic %	Net Int.	Error %	Kratio	Z	A	F
C K	36.8	49.8	850.7	7.0	0.1821	1.0567	0.4688	1.0000
O K	39.2	39.9	482.5	10.7	0.0570	1.0115	0.1435	1.0000
NaK	0.3	0.2	9.8	35.8	0.0011	0.9190	0.3564	1.0014
MgK	1.3	0.9	69.3	10.5	0.0064	0.9347	0.5216	1.0024
AlK	0.2	0.1	9.7	41.7	0.0009	0.9002	0.6629	1.0044
SiK	0.3	0.2	23.0	20.3	0.0021	0.9200	0.7851	1.0073
S K	0.3	0.1	17.6	23.1	0.0021	0.9010	0.9332	1.0189
ClK	0.7	0.3	45.6	11.1	0.0060	0.8571	0.9699	1.0284
CaK	21.0	8.5	969.4	2.1	0.1866	0.8686	1.0158	1.0072

4.3 Investigations into chemical modifications in burnt paper

Spectroscopy is widely used in the field of cultural heritage. It allows often for non-invasive investigation, does not require to destroy any part or fragment of the originals, and in many cases portable instruments exist which can be used *in situ* directly on the cultural objects. The investigation of the artifacts is based on their interaction with electromagnetic radiation as a function of wavelength or frequency of radiation. Data resulting from analytical spectroscopic techniques allow one to characterize the structure of the single materials constituting the objects – a fundamental step in retracing the historical manufacturing techniques –, to detect the presence of products of alteration and to investigate the phenomena of degradation (Bitossi et al. 2005). Their contribution is therefore important also in the evaluation of the most appropriate conservation treatments of cultural objects in critical condition.

In particular, ATR-FTIR (Attenuated Total Reflectance Fourier-Transform Infrared Spectroscopy), FORS (Fiber Optics Reflectance Spectroscopy) and Raman spectroscopy are widely used in the study of paper (Bicchieri et al. 2006; Barrett et al. 2016; Preston 2018).

4.3.1 Infrared spectroscopic analyses (ATR-FTIR)

The Attenuated Total Reflectance Fourier-Transform Infrared Spectroscopy (ATR-FTIR) is largely applied in paper investigation for its high performance in recognizing characteristic organic chemical groups (Mossini et al. 1990; Calvini and Gorassini 2002; Manso and Carvalho 2009). This technique employs infrared (IR) electromagnetic radiation whose wavelength (λ) is between 2.5 μm and 25 μm. Infrared radiation causes oscillations and vibrations of the atoms in the material

occurring at specific frequencies and characteristic for each type of molecule, so that the resulting spectrum is distinctive and constitutes a sort of “fingerprint” for each type of organic molecule.

According to the visual inspection, three areas were analysed on the manuscript and incunabulum leaves: strongly burnt (point 1), burnt (point 2), weakly burnt (point 3) and blank/unburnt (point 4) (Fig. 2.21).

Figure 2.21. The historical sheet belonging to the manuscript from Chartres and a triangular-shape fragment from the Padua incunabulum (left, in evidence the different bunt areas numbered 1,2,3 and the unburnt area 4).

The spectrum in Fig. 2.22 is related to an unburnt (blank) area of the Padua incunabulum and is representative of paper in good condition. For sake of clarity, the region between 1900 and 2500 cm^{-1} has been removed, since in this region no IR peaks of interest were present. Between 700 and 1250 cm^{-1} a structured band, with maxima at 993, 1030 and 1053 cm^{-1}, is present, which is a well-known marker of cellulosic compounds. The band is due to the overlap of peaks at 993, 1030, 1054 cm^{-1}, related to C-O and C-C vibrations of the glucose ring, and peaks at 1109 and 1157 cm^{-1}, due to skeleton deformations of the glucose ring (Makarem et al. 2019). The second region between 1250 and 1500 cm^{-1} is characterized by a band resulting from the overlap of peaks related to CH_2 and CH bending (peaks at 1315, 1369 and 1427 cm^{-1}). Specifically, peaks at about 1430, 1470 and 1490 cm^{-1} are usually attributed to the CH_2 bending of the glucose C6 atom [Lee at al. 2013] in the crystalline cellulose. The third significant region is between 1500 and 1750 cm^{-1}, indicative of the presence of proteinic sizing agents. In fact, in the IR of unsized paper, only a minor component around 1640 cm^{-1} is observed, while the presence of gelatin is easily identified by two strong signals at 1630-1640 and

1530-1540 cm^{-1}, called “Amide I” and “Amide II”, typical markers of proteins, where Amide I is usually stronger than Amide II. The paper of the incunabulum contains gelatin as two signals at 1546 and 1643 cm^{-1} are clearly shown in the spectra.

Finally, the high frequency region between 2500 and 4000 cm^{-1}, is dominated by the strong, broad band due to the stretching of the OH groups in the cellulose and in the water inside the paper leaf. The maximum of the band is around 3322 cm^{-1}, although the band is actually the overlap of various OH peaks corresponding to OH groups with different networks of hydrogen bonds. In gelatin-sized paper, this band gets contributions also from the NH stretching which derives from the amino acids constituting the gelatin.

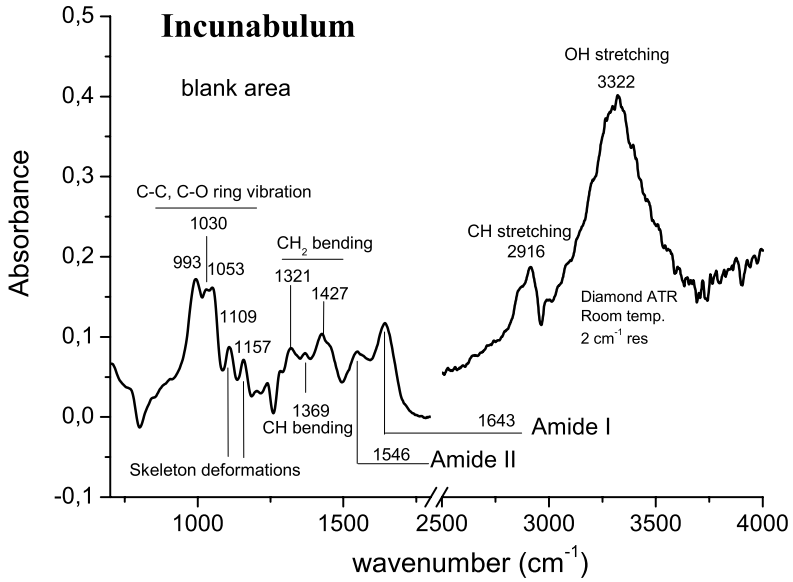

Figure 2.22. Padua incunabulum, ATR-IR spectrum of an unburnt, blank area.

In Fig. 2.23 is the ATR-FTIR spectrum of a slightly burnt area of the same fragment (Padua incunabulum), where paper was weakly affected by fire effects and started to darken.

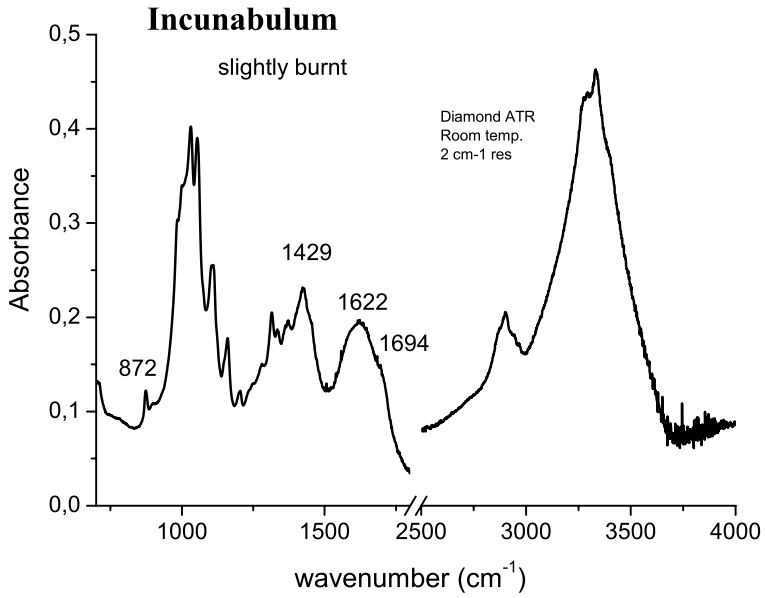

Figure 2.23. Padua incunabulum, ATR-IR spectrum of a slightly burnt area.

A comparison with Fig. 2.22 shows that most of the peaks related to cellulose are still present and well-defined. The only difference is in the region between 1500-1800 cm^{-1}, where the two Amide I and II peaks are replaced by a single band with broad maxima at 1622 and 1694 cm^{-1}. In the IR spectra, the degradation of cellulose can be observed essentially in the region 1500-1800 cm^{-1}, where peaks due to carbonylic and carboxylic compounds occur. Oxidative degradation of cellulose brings about the oxidation of the primary and secondary alcohol groups (C-O-H): in Scheme 2.2, the reaction (a) shows an example of oxidation of the secondary alcohol group at the carbon C2 in a cellulose chain. Primary alcohol groups, like on the C6, are oxidized to an aldehydic and then to a carboxylic group as shown in the reaction (d), this latter being an acidic group which causes lowering of the pH of the degraded areas.

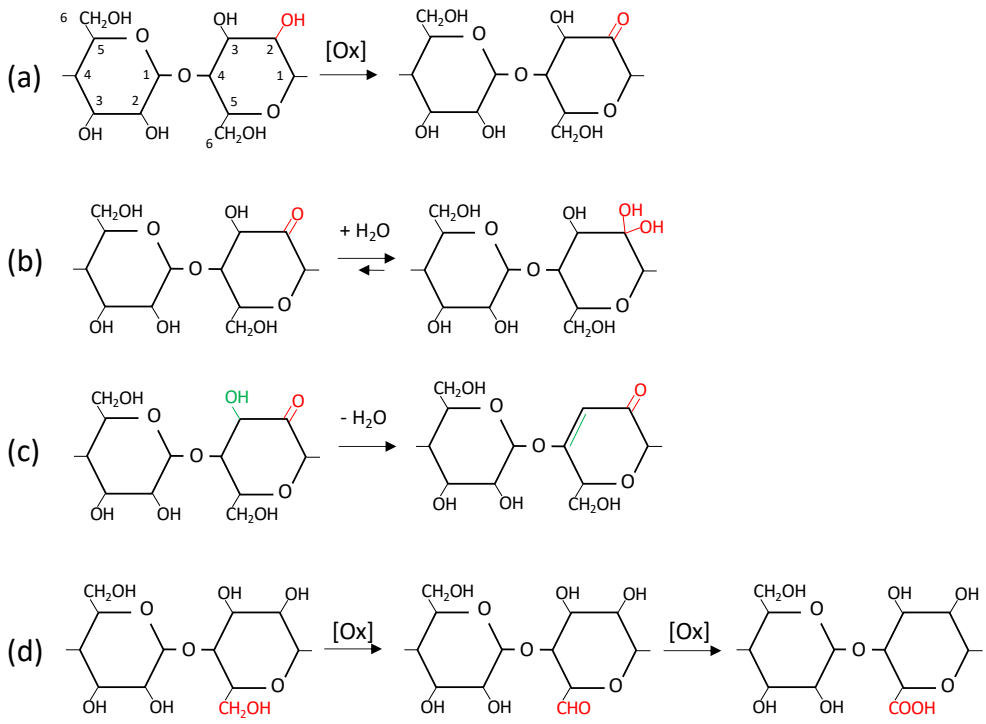

Scheme 2.2. Oxidation reactions occurring on the cellulose moiety.

In the IR spectra of organic compounds, carbonyl stretching is observed between 1680 and 1750 cm^{-1}, but in cellulose it is difficult to detect the signal of the carbonyl group alone, because this group is often hydrated to a geminal diol, which is stabilized by the rich network of hydrogen bonds present in cellulose (Scheme 2.2, reaction (b)). Heating the paper in presence of air (oxygen) should trigger some of the previous reactions, and specifically it should make easier the oxidation of the main alcohol groups, with the formation of carbonylic and carboxylic compounds, and make it easier dehydration, since water is removed upon heating. As conjugation of double bonds stabilizes, by resonance effect, the by-products, dehydration occurs easily if it can generate conjugated carbonylic compounds, as shown in the example of reaction (c), Scheme 2.2.

Several analyses of degradation by-products of cellulose have been carried out (Calvini and Gorassini 2002; Lojewska 2005; Calvini 2006a; Calvini 2006b; Lojewska 2007; Lojewski 2010a, Lojewski 2010b) and it has been shown that these compounds derive from a synergistic effect of oxidation and dehydration of the cellulose molecules (reaction (c), Scheme 2.2), resulting in conjugated carbonylic and carboxylic compounds. Usually, a broad band around 1630 cm^{-1} is observed in the IR spectra of degraded paper/cellulose (Lojewska 2005), deriving from the overlap of signals related to various functional groups:

- Carbonylic and carboxylic groups (1700 - 1730 cm^{-1}), which are usually ionized, at neutral or slightly acidic pH, to carboxylates (1550 - 1610 cm^{-1}) [Calvini and Gorassini 2002; Calvini 2006a; Calvini 2006b]
- Conjugated carbonylic groups of a-diketones, which are usually in the enolic form, and α-β unsaturated carbonylic compounds (symmetrical stretching at 1640 cm^{-1}, asymmetrical stretching at 1681 cm^{-1}) [Calvini 2006b]
- Double C-C bonds (1640 cm^{-1}) [Calvini 2006b]

Based on the literature assignments and chemical considerations on the burning reactions, we can deduce that the two maxima at 1622 and 1694 cm^{-1} observed in the ATR-IR spectrum of the slightly burnt area in the fragment are likely related to conjugated carbonylic and carboxylic compounds, although contributions from carboxylates (usually occurring around 1580 cm^{-1}) cannot be ruled out. On the other side, most of the leaf, in the slightly burnt areas, is well preserved, since the OH band is strong and well structured, which is an indication that most of the OH groups participate to the hydrogen bond network of the cellulose chain.

The IR spectrum of a burnt area of the fragment from the incunabulum, characterized by a completely blackened surface and prone to fragmentation at the minimum touch is in Fig. 2.24, where the main peaks of C-O stretching are almost lost, with just a weak band around 1000 cm^{-1}. Two main, broad bands are observed, at 1419 and 1582 cm^{-1}.

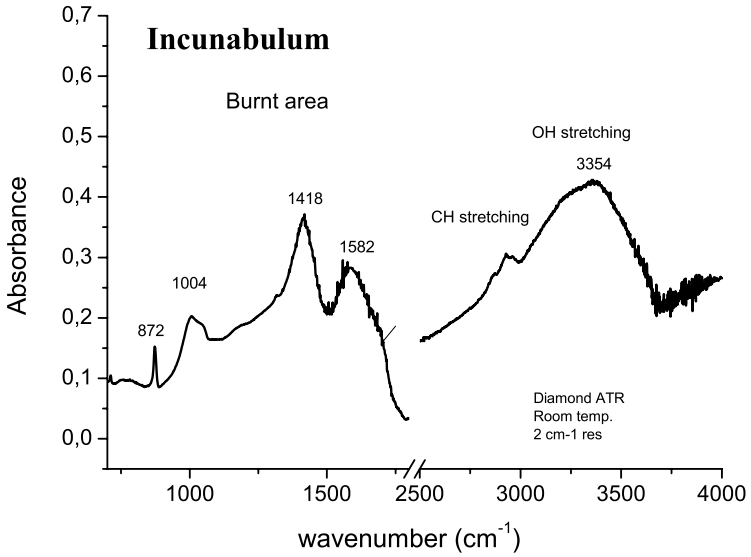

Figure 2.24. Padua incunabulum, ATR-IR spectrum of a burnt, black and fragile area.

The band at 1419 cm^{-1} is about of the same intensity of the band observed in the blank areas. We know that this band is related to CH and CH_2 bending, and if we cross this indication with the strong diminishing of the C-O peaks, we can deduce that the cellulose has lost many C-O groups, keeping CH groups, as expected from dehydration reactions. The second band, at 1582 cm^{-1}, is related to conjugated carbonylic compounds: in the slightly burnt area, the maximum was at 1622 cm^{-1}, and therefore a shift to lower wavenumber is observed with increased burning. This can be explained, considering that the carbonyl stretching frequency gets lower and lower increasing the number of conjugated C=C groups coupled to the carbonyl. The shift is therefore an indication that burning causes an increase in the number of conjugated C=C groups. The carbonylic compounds with many conjugated C=C groups are also strong chromophores in the visible region, because conjugation shifts the absorbance of the carbonyl groups, normally in the UV region, down to the visible region: these compounds are therefore responsible for the progressive blackening of the burnt areas. If we consider the high wavenumber IR region, we observe that the OH band gets broader, and the maximum shifts to higher wavenumbers. The broadening is related to the loss of the hydrogen bond network around the OH groups, due to the disorder that the cellulose chains undergo when the paper is heated. The OH band is weaker than observed in the slightly burnt area, consistently with some loss in OH groups due to dehydration.

The spectrum in Fig. 2.25 considers a completely burnt area.

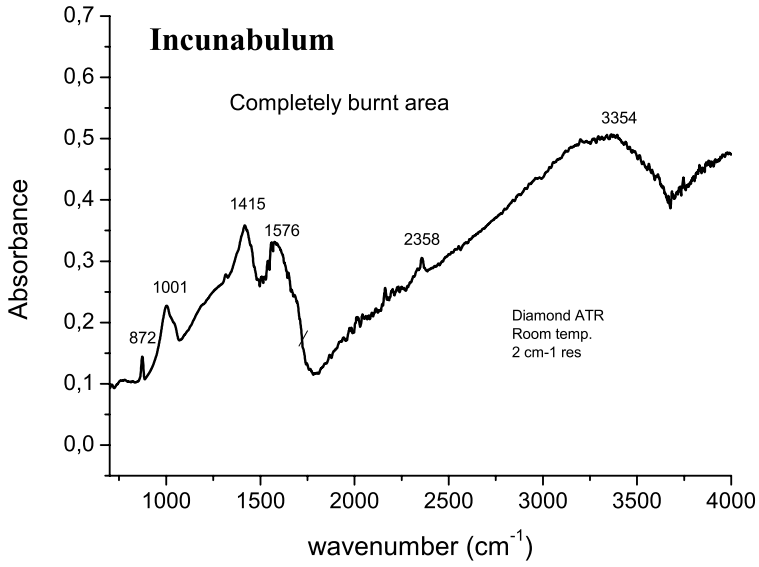

Figure 2.25. Padua incunabulum, ATR-IR spectrum of a completely burnt area.

The C-O peak is almost disappeared, as well as the other main peaks of cellulose. The OH band is shallow, and around 2350 cm^{-1}, in a region usually without signals, a small peak appears, due to C-C triple bond stretching, indicative of alkyne formation. Finally, in Fig. 2.26, the spectra of blank, slightly burnt, burnt, and completely burnt areas are compared. The arrows mark the main transformations, which can be observed in the spectra with increased burning: the progressive reduction of the C-O, C-C peaks of the cellulose, the broadening and the following reduction of the OH band, the shift to lower wavenumber of the conjugated carbonyl peak, from 1624 down to 1580 cm^{-1}, and the increasing slope of the spectral profile between 2000 and 3000 cm^{-1}, which is due to the formation of carbonaceous compounds, whose IR spectrum is characterized by a steady, seeming increase of absorbance from low to high wavenumbers. It is to notice that in the burnt areas a peak at 872 cm^{-1} is observed, related to calcium carbonate.

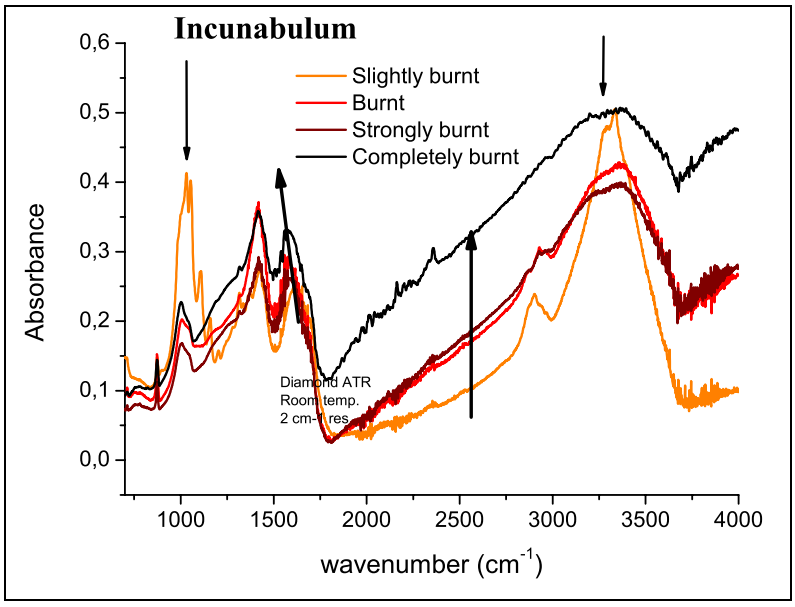

Figure 2.26. Comparison among ATR-IR acquired on differently burnt areas of the Padua incunabulum.

Fig. 2.27 relates to the leaf from Chartres BM ms 1047 and it compares the spectra of unburnt, weakly (slightly) burnt, burnt, and strongly burnt area. As already mentioned, the peaks around 1000 cm^{-1} (993-1053 cm^{-1}) are peculiar of the C-C and C-O ring vibration in cellulosic compounds; the region between 1250 and 1500 cm^{-1} is characterized by a band resulting from the overlap of peaks related to CH_2 and CH bending with peaks at about 1430, 1470 and 1490 cm^{-1} usually attributed to the CH_2 bending of the glucose C6 atom in the crystalline cellulose.

Two more peaks are in the region between 1520 and 1670 cm^{-1} where Amide I and Amide II are detected and highlight the presence of proteins from animal sizing (gelatin) also in this sample.

The high frequency region between 2500 and 4000 cm^{-1} is also well detected, with the band due to the stretching of the OH groups of the cellulose and of the water contained in the paper. As mentioned for the incunabulum, the band is composed by the overlapping of the many OH peaks corresponding to OH groups with different networks of hydrogen bonds, with the contributions of the NH stretching from the amino acids in the proteinic sizing.

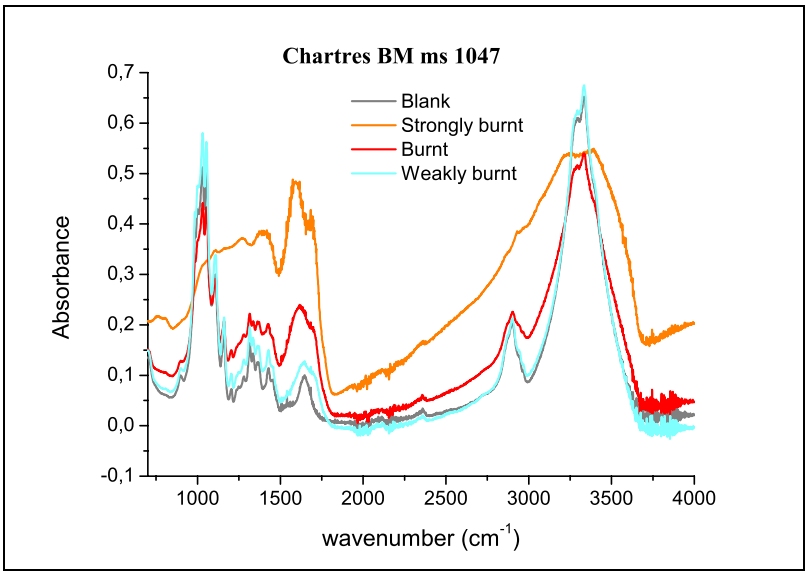

Figure 2.27. Chartres BM ms 1047, ATR-IT spectra of the four differently degraded areas.

Some clear modifications occur at different steps of the burning process.

In detail, Fig. 2.28 shows an increasing slope between 2000-3000 cm^{-1}, which is probably due to the superimposition of the carbon signal originating from the cellulose carbonisation process and a decreasing of the peak at 1000 cm^{-1}, related to the degradation of the C-O bond stretching, here especially significant for strongly burnt paper.

As known, the region between 1500 and 1800 cm^{-1} is the most sensitive to the effect of degradation. The spectrum of an unburnt area of the leaf shows at 1540 and 1640 cm^{-1} the two typical peaks related to the amide I and II stretching vibrations. After a weak burning, the area between 1600 and 1750 cm^{-1} changes significantly. Two bands are observed: the first band occurs at 1635 cm^{-1} in weakly burnt areas, shifting down to 1600 cm^{-1} in strongly burnt areas.

The peak is related to conjugated carbonyl and carboxyl + carboxylate groups, the downshift being

related to the increasing conjugation with burning, as evident in Fig. 2.29.

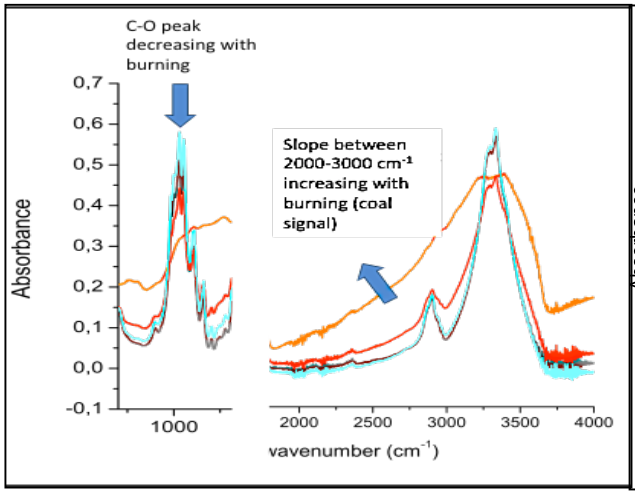

Figure 2.28. Chartres BM ms 1047, ATR-IT spectra showing cellulose degradation induced by progressive degrees of burning.

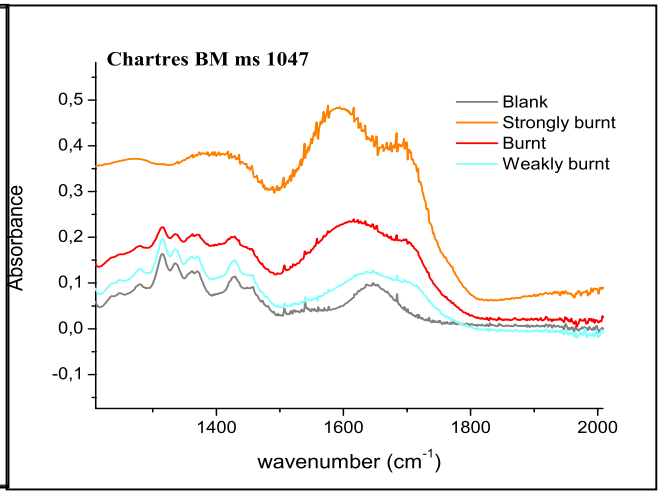

Figure 2.29. Chartres BM ms 1047, ATR-IT spectra evidencing the coniugation of carbonyl and carboxyl groups.

A second band occurs at 1700 cm^{-1} which is due to nonconjugated carbonyl and carboxylic groups. The band does not shift very much. It is to notice that the band at 1600-1635 cm^{-1} increases with respect to the band at 1700 cm^{-1} consistently with a progressive loss of CO/CO_2 (decarboxylation processes).

It is worth to stress that cellulose fibres are detected even in burnt and strongly burnt areas, both in the sample from the manuscript and, albeit in a worse state of degradation, in that from the incunabulum. The phenomenon has been observed also by Ahn and coworkers and according to the authors, the char layer shows a low thermal conductivity and can act as protection for the inner fibers from heat effects, especially in packed books [Ahn et al. 2018].

4.3.2 UV-VIS spectroscopic analysis

The Fiber Optic UV-VIS reflectance spectroscopy (FORS), with radiation wavelength ranging from the near-ultraviolet (UV, 200-350 nm) to the entire visible range (VIS, 350-700nm), was employed to evaluate the paper colour; the backscattered radiation from the sample is analyzed, recording the reflectance as a function of frequency. This spectroscopic technique is not suitable to identify chemical compounds present in the sample, but it can be particularly informative for the

composition of pigments and dyes (i.e., for works of art, frescoes, paintings and illuminated books) and allows one to evaluate the alterations occurring over natural aging time or modifications as consequence of conservation treatments (Picollo et al. 2002; Bacci 2004; Aceto et al. 2014).

In the spectra collected on the Chartres manuscript (Fig. 2.30 left) it is observed a significant reduction in the total reflectance due to a change in the paper properties induced by the combustion process. This is especially evident comparing the curve relating to the blank unburnt area of the sheet (grey) with those detected in burnt and strongly burnt areas of the same paper (the black, red and blue curves) which are almost overlapped. It is to notice the increase in spectral reflectance from UV to NIR wavelengths in the burnt areas of the manuscript, indicative of conjugated compounds. On the opposite, in the Padua incunabulum (Fig. 2.30 right), the burnt areas present an almost flat curve, indicative of a strong black, which is related to the formation of melanoidinic compounds, due to Maillard reactions between the gelatin size and the cellulosic compounds.

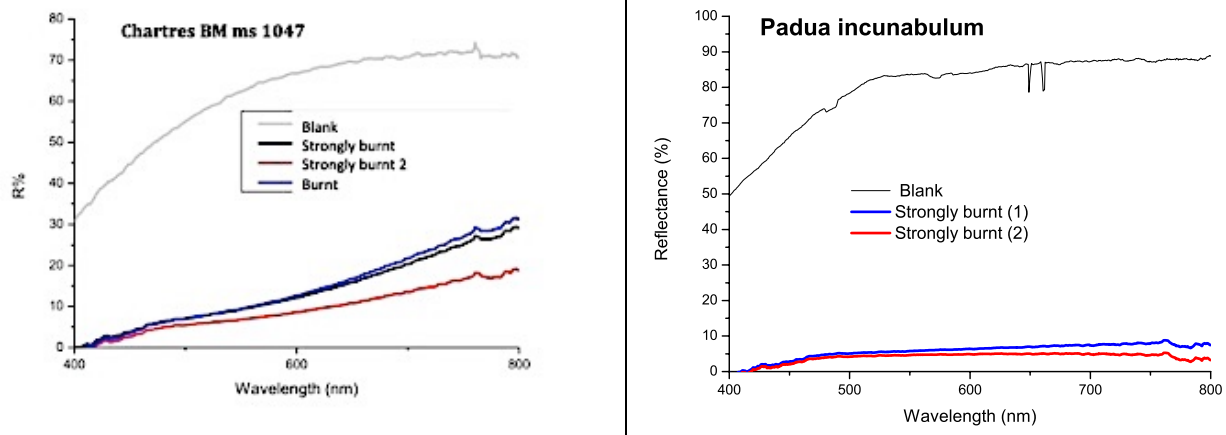

Figure 2.30. Chartres BM ms 1047, (left) and Padua incunabulum (right) UV-Vis spectra.

5. X-ray Powder Diffraction (XRPD)

X-ray Powder Diffraction (XRPD) allows the study of the crystal structure of polymeric materials. The artefact to be investigated is illuminated by a beam of specially generated monochromatic X-rays (fixed wavelengths); angles at which X-rays diffract from the sample are a function of inter-atomic spacing associated with the crystalline components. The signal coming from the sample is recorded and graphed in X-ray diffractograms; the pattern, the intensities of the diffraction maxima (peaks or lines) and their position are correlated to a specific crystal structure and can be

used to identify each specific material. As XRPD can effectively investigate the crystalline domains of the cellulose and detect the inorganic compounds present in paper (Foner and Adan 1983; Hajji et al. 2016; Hassan 2016; Gonzalez et al. 2020), some strongly burnt free fragments from the Chartres manuscript and the Padua incunabulum have been analysed.

In the first diffractogram (Fig. 2.31) referred to the Chartres ms 1047, broad peaks distinctive of crystalline cellulose are evident at 17.7, 19.5, 26.7, 40.5 and 55 [°2θ]. They are absent in the second diffractogram (Fig. 2.32), relating to the Padua incunabulum, where an amorphous band centered around 30° 2θ, indicates a remarkable decline in cellulose crystallinity, replaced by amorphous compounds. Calcite (calcium carbonate, $CaCO_3$) and talc (hydrated magnesium silicate $Mg_3Si_4O_{10}(OH)_2$) were detected in small quantities in both the samples; gypsum (dehydrated calcium sulfate, $CaSO_4{\cdot}2H_2O$) was only in the paper from the Chartres manuscript, while hydrotalcite (a hydrated magnesium aluminate often associated with talc), bassanite (calcium sulphate hemihydrate), lizarite, quartz and albite were found in the Padua incunabulum.

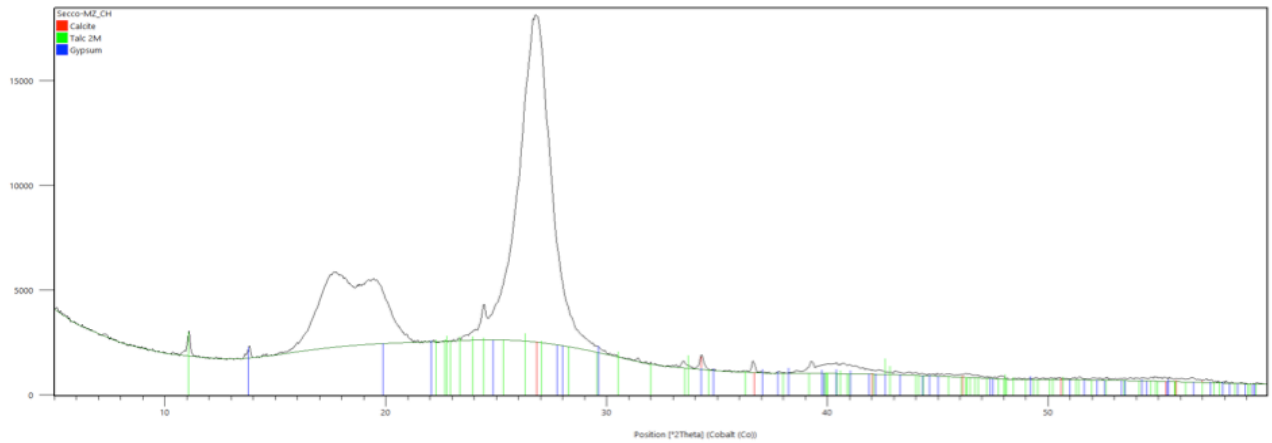

Figure 2.31. Chartres BM ms 1047, XRD difractogram. Peaks in evidence at 17.7, 19.5, 26.7, 40.5 and 55 [°2θ] are distinctive of cellulose, still present despite burning.

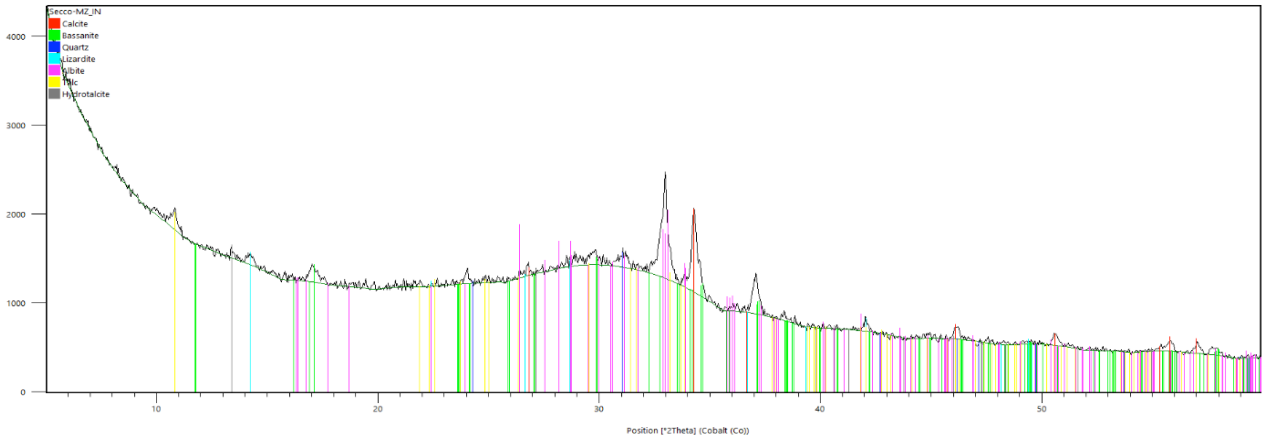

Figure 2.32. Padua Incunabulum, XRD difractogram. Cellulose peaks are not present and an amorphous band is evident at around 30 [°2θ], probably corresponding to amorphous compounds replacing the crystalline structure of cellulose.

Such trace amounts of mineral components in these historical papers are probably due to a residue of the manufacturing process (from water or from lime, for example) or accidental pollution during the long time spent in libraries, subject to access and to the deposit of particles of inorganic origin. Most of them are found on the surface of the sheets, as highlighted by SEM analysis of the cross section (§ 4.2.2). Mineral fillers were indeed deliberately introduced later, in the 19th century, into the industrial process of machine-made paper production. This considered, since the "relational life" of the incunabulum is about four centuries longer than those of Chartres manuscript, it is not surprising that the quantity and quality of the "dust" collected by paper is greater.

6. Conclusions

In this chapter, the physico-chemical characterization of burnt paper areas was carried out on two historic papers belonging respectively to a manuscript from the Municipal Library of Chartres – nowadays held in the Médiathèque L'Apostrophe in Chartres – and to an incunabulum from the Library of the Episcopal Seminary in Padua, both damaged by fire in 1944.

The measure of paper acidity was performed in the unburnt areas and in areas at different burning degree. As a piece of evidence, the fire-induced effects did not seem to dramatically affect the paper pH and only a mild acidification of the charred paper was found.

The morphological analysis of the burnt paper was carried out with optical microscopy: the surface of the samples was examined in reflected-light, bright field and dark field mode, such a way to

obtain a complete view of the paper. It was evident a conserved network of intertwined fibers. Although damaged, the outer part of the cellulose fibres remained clearly distinguishable and even identifiable as linen and hemp, both in the sample from the manuscript and from the incunabulum. The same samples were examined by SEM/EDS, both in surface and in cross section, confirming that the cellulosic structure was retained despite the burning process. EDS analysis detected the presence of other elements, beside C and O (cellulose main elements): mainly Ca, (attributed to calcite), Mg, Si, Al (attributed to talc), and Ca and S (attributed to gypsum), this latter compound only in the sample from the manuscript.

The X-ray Powder Diffraction (XRPD) analyses showed the persistence of peaks distinctive of the crystalline domain of cellulose only in the paper from the Chartres manuscript, while they were remarkably declined in the Padua incunabulum, which was actually more deeply damaged by fire.

Infrared spectroscopic analyses (ATR-FTIR) were used to investigate the nature of the compounds evolving with burning, examining areas with different degree of burning (weakly burnt, burnt, and strongly burnt). In particular, the progressive reduction of the peaks of cellulose was observed with increasing burning. Two broad bands at about 1600 and 1700 cm^{-1} developed and increased with burning, shifting to lower wavenumbers as the degradation process went on, due to the formation of conjugated carboxyl and carbonyl compounds. Formation of carboxylic compounds was probably also responsible of the light drop in pH of the burnt areas of the samples respect to the unburnt areas. Moreover, an increasing slope of the spectral profile between 2000 and 3000 cm^{-1} was also clearly seen, indicating the formation of carbonaceous compounds. The marker signal of cellulose (1030 cm^{-1}) was anyway detected in all the burnt areas of the manuscript, indicating that cellulose was still present inside the burnt fibers.

UV-Vis reflectance (FORS) spectra were also collected on the unburnt areas of the paper, as well as on areas burnt at different degrees. A significant drop in reflectance was observed, related to the progress of carbonization. In the Chartres manuscript, the spectral reflectance increased from UV to NIR wavelengths, indicating that paper was not really black (flat FORS curve in all the visible range), which is also coherent with a progressive formation of conjugated compounds, as enhanced by ATR-FTIR. Interestingly, in the Padua manuscript FORS curves of burnt areas are almost flat and are likely indicative of melanoidinic compounds resulting from Maillard reactions between the gelatin and the cellulose.

On the basis of these results, the following conclusions can be obtained: 1) crossing data from FORS, SEM-EDS, IR, XPRD and optical microscopy is a very efficient way to trace the progress of burning in terms of morphological and chemical changes in differently burnt areas; 2) the fiber network is often preserved in the examined burnt papers, even in the most fragile areas; 3) the examined burnt papers were very fragile well before a complete carbonization, and amorphous and crystalline cellulose was still present inside the fibers in most of the burnt areas.

The spectrochemical and morphological data obtained from the naturally burnt samples of the Padua incunabulum and of the Chartres manuscript provide a base for the evaluation of suitable artificial burning protocols using the efficient crossing of FORS, SEM, IR, XRPD and optical microscopy.

Chapter 2 | References

Aceto, M., Agostino, A., Fenoglio, G., Idone, A., Gulmini, M., Picollo, M., Ricciardi, P., Delaney, J. K. (2014). «Characterisation of colourants on illuminated manuscripts by portable fibre optic UV-visible-NIR reflectance spectrophotometry». *Analytical Methods,* 6, 1488-1500; https://doi.org/10.1039/C3AY41904E

Ahn K., Schedl, A., Zweckmair, T., Rosenau, T., Potthast, A. (2018). «Fire-induced structural changes and long-term stability of burned historical rag papers». Scientific Reports, 8, 12036; https://doi.org/10.1038/s41598-018-30424-7

Armstong, L., Scapecchi, P., Toniolo, F. (2008). *Gli incunaboli della Biblioteca del Seminario Vescovile di Padova: catalogo e studi.* Padova: Istituto per la storia ecclesiastica padoana, 33.

Bacci, M. (2004). «Optical Spectroscopy and Colorimetry» In: Martini, M. et al. (eds), *Physics Methods in Archaeometry*. Bologna; SIF-Amsterdam: IOS Press, 1-16.

Barrett, T. D., Mosier, C. (1995). «The role of gelatine in paper permanence». *Journal of American Institute for Conservation,* 34, 173-186.

Barrett, T., Ormsby M., Lang, J. B. (2016). «Non-Destructive Analysis of 14th–19th Century European Handmade Papers». *Restaurator*, 37(2), 93-135. https://www.degruyter.com/document/doi/10.1515/res-2015-0017/html

Barrett, T. et al. (2021). *Paper through Time: Nondestructive Analysis of 14th- through 19th-Century Papers.* The University of Iowa. Last modified October 01, 2021; https://paper.lib.uiowa.edu

Barrett, T. (2021). «European Papermaking Techniques 1300–1800». *Paper through Time: Nondestructive Analysis of 14th- through 19th-Century Papers*. The University of Iowa. Last modified November 11, 2021; http://paper.lib.uiowa.edu/european.php

Bibliotheque virtuelle des manuscrits médiévaux, https://www.manuscrits-de-chartres.fr

Bicchieri, M., Sodo, A., Piantanida G., Coluzza C. (2006). «Analysis of degraded papers by non-destructive spectroscopic techniques», *Journal of Raman Spectroscopy*, 37, 1186-1192; https://doi.org/10.1002/jrs.1603

Bicchieri, M., Biocca, P., Colaizzi, P., Pinzari. F. (2019) . «Microscopic observations of paper and parchment: the archaeology of small objects». *Heritage Sci*ence 7 (47). https://doi.org/10.1186/s40494-019-0291-9

Bitossi G., Giorgi R., Mauro M., Salvadori B., Dei L. (2005). «Spectroscopic techniques in cultural heritage conservation: a survey». *Applied Spectroscopic Reviews*, 40, 187-228. https://doi.org/10.1081/ASR-200054370

Bloom J. M. (2001). *Paper before print. The history and impact of paper in the Islamic world*. New Haven and London: Yale University Press.

Brillard, A., Habermacher, D., Brilhac, J. F. (2017). «Thermal degradations of used cotton fabrics and of cellulose: kinetic and heat transfer modeling». *Cellulose* 24, 1579-1595; https://doi.org/10.1007/s10570-017-1200-6

Brückle, I. (1993). «The role of alum in historical papermaking». *The Abbey Newsletter*, 17, 53-57.

Calvini, P., Gorassini, A. (2002). «FTIR-Deconvolution spectra of paper documents». *Restaurator,* 23, 48-66; https://doi.org/10.1515/REST.2002.48

Calvini, P., Gorassini, A., Chiggiato, R. (2006a). «Fourier Transform Infrared Analysis of Some Japanese Papers». *Restaurator,* 27, 81-89; http://dx.doi.org/10.1515/REST.2006.81

Calvini, P., Gorassini, A., Luciano, G., Franceschi, E. (2006b). «FTIR and WAWS analysis of periodate oxycellulose: Evidence for a cluster mechanism of oxidation». *Vibrational Spectroscopy*, 40, 177-183; https://doi.org/10.1016/j.vibspec.2005.08.004

Collings, T., Milner, D. (1984). «The Nature and Identification of Cotton Paper-Making Fibres in Paper». *The Paper Conservator.* 8, 59-71; https://doi.org/10.1080/03094227.1984.9638458

de Lalande, J. J. L. (1761). «Art de faire le papier». In: *Description des arts et métiers*, vol. 4. Paris: Académie royale des sciences.

Dupont A.-L. (2003) *Gelatine sizing of paper and its impact in the degradation of cellulose during aging – a study using size-exclusion chromatography*. Ph.D Thesis, Amsterdam: University of Amsterdam; https://dare.uva.nl/search?identifier=050fd247-6e8f-4dc9-a512-9e82e82f61d3

Foner, H. A., Adan, N. (1983). «The characterization of papers by X-Ray Diffraction (XRD): Measurement of Cellulose Crystallinity and Determination of Mineral Composition». *Journal of the Forensic Science Society,* 23 (4), 313-321; https://doi.org/10.1016/S0015-7368(83)72269-3

Gonzalez, V., Cotte, M., Vanmeert, F., de Nolf, W., Janssens, K. (2020). «X-ray Diffraction Mapping for Cultural Heritage Science: a Review of Experimental Configurations and Applications». Chemistry, 26 (8), 1703-1719; https://doi.org/10.1002/chem.201903284

Hassan, R. (2016). «Thermal degradation of paper: the structural changes of fibres». *Egyptian Journal of Archaeological and Restoration Study,* 6, 71-84; http://dx.doi.org/10.21608/ejars.2016.23543

Hajji, L., Boukir, A:, Assouik, J., Pessanha, S., Figueirinhasc, J. L., Carvalho, M. L. (2016). «Artificial aging paper to assess long-term effects of conservative treatment. Monitoring by infrared spectroscopy (ATR-FTIR), X-ray diffraction (XRD), and energy dispersive X-ray fluorescence (EDXRF)». *Microchemical Journal,* 124, 646-656; https://doi.org/10.1016/j.microc.2015.10.015

Hu, J., Jahid, Md., A., Venkatesan, H., Kumar, N. H. (2020). «Fundamentals of the fibrous materials». In: Hu, J. et al. (eds) *Handbook of fibrous materials.* Wiley-VCH Verlag GmbH&Co. KGaA, 1-36.

Hunter, D. (1947, reprint 1978). *Papermaking, the history and technique of an ancient craft.* New York: Dover Publication.

Kolbe, G. (2004). «Gelatine in historical paper production and as inhibiting agent for iron-gall ink corrosion on paper». *Restaurator*, 25 (1), 26-39; https://doi.org/10.1515/REST.2004.26

Kolbe, G. (2002). «Gelatine in historical paper production and present-day restoration of paper manuscripts». In: Fellows-Jensen, G. and Springborg, P. (eds) *Care and conservation of manuscripts 6. Proceedings of the sixth international seminar held at the Royal Library, Copenhagen 19th-20th October 2000*. University of Copenhagen: Museum Tusculanum Press, 33-46.

Lavoine, N., Desloges, I., Dufresne, A. Bras, J. (2012). «Microfibrillated cellulose, its barrier propertiesand applications in cellulosic materials: a review». *Carbohydrate polymers*, 90(2), 735-764; https://doi.org/10.1016/j.carbpol.2012.05.026

Lee, C.M., Mohamed, N.M.A., Watts, H.D., Kubicki, J.D., Kim, S.H. (2013). «Sum-frequency generation vibration spectroscopy and density functional theory calculations with dispersion corrections (DFT-D2) for cellulose Ia and Ib». *Journal of Physical Chemistry B*, 117, 6681-6692; https://doi.org/10.1021/jp402998s

Lojewska, J. (2005). «Cellulose oxidative and hydrolytic degradation: In situ FTIR approach». *Polymer Degradation and Stability, 89*, 883-887; https://doi.org/10.1016/j.polymdegradstab.2004.12.012

Lojewska, J. (2007). «Carbonyl groups development on degraded cellulose. Correlation between spectroscopic and chemical results». *Applied Physics A*, 89, 883-887; http://dx.doi.org/10.1007/s00339-007-4220-5

Lojewski, T. (2010a). «FTIR and UV/Vis as methods for evaluation of oxidative degradation of model paper: DFT approach for carbonyl vibrations». *Carbohydr. Polym.* 82, 370-375; https://doi.org/10.1016/j.carbpol.2010.04.087

Lojewski, T. (2010b). «Evaluating paper degradation progress. Cross-linking between chromatographic, spectroscopic and chemical results». *Applied Physics A*, 100, 809-821; https://doi.org/10.1007/s00339-010-5657-5

Makarem, M., Lee, C.M., Kabindra, K., Huang, S., Chae, I., Yang, H., Kubicki, J.D., Kim, S.H. (2019). «Probing cellulose structures with vibrational spectroscopy», *Cellulose*, *26*, 35-79; https://doi.org/10.1007/s10570-018-2199-z

Manso, M., Carvalho, M.L. (2009). «Application of spectroscopc techniques for the study of paper documents: a survey». *Spectrochimica Acta Part B,* 64, 482-490; https://doi.org/10.1016/j.sab.2009.01.009

Marini Bettolo, R., Migneco, L. M., Plossi Zappalà, M. (2007). «I materiali cellulosici e le loro materie prime». In: *Chimica per l'arte.* Bologna: Zanichelli, 411-483.

Mossini, V., Calvini, P., Mattogno, G., Righini, G. (1990). «Derivative infrared spectroscopy and electron spectroscopy for chemical analysis of ancient paper documents». *Cellulose Chemistry and Technology*, 24, 263-272; https://www.academia.edu/31828124/Derivative_infrared_spectroscopy_and_electron_spectroscopy_for_chemical_analysis_of_ancient_paper_documents

Omont, H., Molinier, A., Couderc, C., Coyecque, E. (1890). *Catalogue général des manuscrits des bibliothèques publiques de France*, t. XI, Paris.

https://www.manuscrits-de-chartres.fr//fr/bibliographie#biblio

Picollo M., Bacci, M., Casini, A., Lotti, F., Porcinai, S., Radicati, B., Stefani, L. (2002). «Fiber Optics Reflectance Spectroscopy: A Non-destructive Technique for the Analysis of Works of Art». In: Martellucci S. et al. (eds), *Optical Sensors and Microsystems*. Springer, Boston, MA.

Preston, J. (2018). «The surface analysis of paper». In: l'Anson, S. J. (ed.) *Advances in Pulp and Paper Research, Oxford 2009*, *Trans. of the XIVth Fund. Res. Symp. Oxford, 2009*. Manchester: FRC, 749–838; DOI: 10.15376/frc.2009.2.749.

Scheirs, J., Camino, G., Tumiatti, W. (2001). «Overview of water evolution during the thermal degradation of cellulose». *European Polymer Journal*, 37, 933-942; https://doi.org/10.1016/S0014-3057(00)00211-1

Strlic, M, Kolar, J., Kocar, D., Drnovsek, T., Selih, V.S., Susic, R., Pihlar, B. (2004). «What is the pH of alkaline paper?» *e-Preservation Science,* 1, 35-47; https://www.researchgate.net/publication/26412854_What_is_the_pH_of_alkaline_paper

Völkel, L., Beaumont, M., Czibula, C., Rusakov, D., Mautner, A., Teichert, C., Kontturi, E., Rosenau, T., Potthast, A. (2022). «Assessing Fire-Damage in Historical Papers and Alleviating Damage with Soft Cellulose Nanofibers». Small, 18, 2105420, 1-14; https://doi.org/10.1002/smll.202105420

Wertz, J-L., Mercier,J. P., Bédué, O. (2014). *Cellulose Science and Technology.* EPFL Press.

Chapter 3

Samples preparation and investigation of burnt paper

1. Handmade paper samples preparation

Investigation of the burnt papers from the Chartres manuscript and from the Padua incunabulum was a fundamental step for the reproduction of burnt samples as similar as possible to the historical ones. To this purpose, a handmade paper produced by the Ruscombe Paper Mill, a traditional mill established in Margaux (http://ruscombepaper.com) was employed. This paper reproduces the basic features of the historical (13^{th} -19^{th} century) paper manufacture as it is made from rags, composed of hemp (70%) and linen fibres (30%), buffered with calcium carbonate, grammage 100 g/m^2. The sheets supplied by Ruscombe Paper Mill were 50 x 70 cm^2.

In view of the fundamental role played by protein sizing in providing partial waterproofing and also of its influence on the physical qualities of the paper [Chapter 2, § 1], the experimental part of this research was carried out on both unsized Ruscombe Paper Mill (from now on called RPM) samples and on gelatin-sized RPM samples sized in the laboratory. Gelatin type B (bovine origin), 250 Bloom degree supplied by Italgelatine S.p.A. was selected as sizing agent [Tamburin 2009; GMIA 2012]. It was prepared at a concentration of 3% wt/vol in distilled water, allowing it to swell and then dissolving it by moderate heating (40°C) for about one hour in a closed beaker to minimize evaporation. Then it was used liquid and still hot to size the sheets both recto and verso by brushing.

Samples 5 x 7 cm^2 from unsized and sized RPM paper were prepared. As the sheets were handmade produced and differences in thickness were expected, a micrometer Mitutoyo was employed to measure the average thickness of 15 samples cut from different areas in 3 sheets. Measures were performed in 4 points of each sample as showed in Fig. 3.1. The values indicate that the RPM sheets were relatively uniform for a handmade product, the variation in thickness being lower than 7% (Table 3.1).

Figure 3.1. Ruscombe Paper Mills paper: the four points where thickness was measured on each sample are marked with a pencil mark.

Table 3.1. Thickness average values, the error is provided as maximum half-dispersion.

Samples	Sample average thickness (µm)
15 unsized RPM 100 g/m^2 paper samples	193 ± 6
15 sized RPM 100 g/m^2 paper samples	218 ± 6

2. Burning tests

To reproduce charring (i.e., a non-complete combustion process with blackening) observed in historical papers, several burning methods were tested, chemically and heat induced.

2.1 Chemically induced burning

Inducing chemical burning using sulfuric acid was tested, as it is a time-saving procedure to obtain uniformly burnt and fragile samples. It is known that sulfuric acid is a strong dehydration agent and, when reacting with paper, it extracts molecules of water from cellulose, inducing a heavy dehydration of the material. As a result, the paper progressively degrades until it turns into black products [Kim et al. 2001].

Unsized and gelatine-sized RPM paper samples were spread with a solution of H_2SO_4 (0.5 M) using a pipette Pasteur and allowed to dry in air. The chemical degradation process was enhanced by heating with a hot air gun set at 400°C and kept at a distance of 3 cm from the samples. 7-8

seconds were needed to have the treated areas deeply blackened and prone to fragmentation (Fig. 3.2).

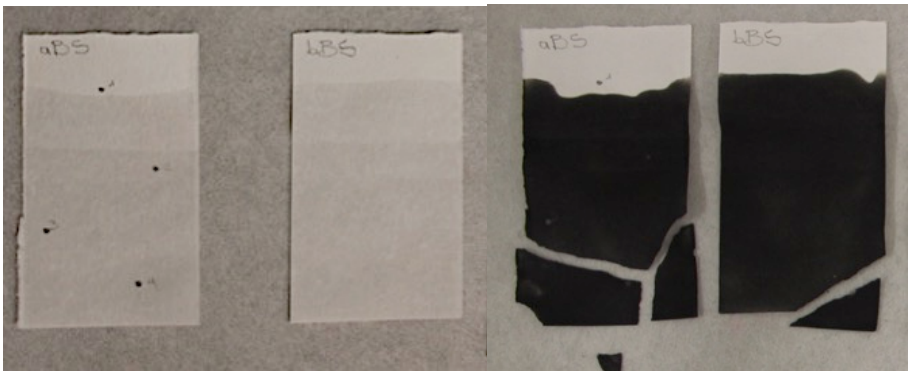

Figure 3.2. RPM paper spread with the sulfuric acid solution (left) and after heating with the hot air gun.

With the above-mentioned advantages of execution speed, aspect and brittleness, the suitability of the chemical burning method was investigated by measuring the pH of the papers after burning. Standard cold extraction procedure was carried out according to TAPPI T 509 om-11 (Table 3.2).

Table 3.2. Surface and aqueous extract pH of RPM samples before treatment and after sulfuric acid treatment and hot gun burning (data from S. Paris – CRCC).

Samples	average pH aq. Extract untreated samples	STD	average pH aq. Extract after chemical burning	STD
unsized RPM paper	7.6	0.3	2.0	N/A
sized RPM paper	7.3	0.3	2.1	N/A

Part of the burnt samples was washed by immersion in a bath of deionized water to discharge any residual excess of sulfuric acid. Surface pH measures were carried out before and after washing, according to TAPPI T 529 om-99 (Table 3.3).

Table 3.3. Surface pH of RPM samples before treatment, after burning and after washing to discharge acid residues (data from S. Paris – CRC).

Samples	surface pH average reference sample	STD	surface pH average after chem. Burning and before washing	STD	surface pH average after chem. Burning and after washing	STD
unsized RPM paper	6.3	0.6	1.6	0.5	3.4	0.4
sized RPM paper	5.7	0.1	1.4	0,4	3.5	0.4

Two to three measurements were done per sample at the Centre sur la conservation des collections – CRC. Data shows that the pH of the chemical burnt paper is very acidic, sulfuric acid remains deeply embedded in the paper and resulting pH is significantly lower than the average pH of the RPM untreated sample (reference) and of the pH of historical burnt papers, resulting in pH 6.2 in the charred areas of the Padua incunabulum and in pH 4.6 in those of the Chartres manuscript (Chapter 2, § 4.1). The burning method with sulfuric acid was thus not suitable for the purpose of this research. Chemical burning was then ruled out and new procedures, closer to natural burning by fire, were developed.

2.2 Heat-only induced burning

2.2.1 Burning by means of hot air gun and live flame

Burning of the RPM samples was achieved completely with the hot air gun set at 400°C and kept at distance of 3 cm from the samples with no addition of sulfuric acid. The resulting burned areas were small, and it took much longer to obtain a degree of burning comparable to the samples treated with the acid solution: 25 minutes for the unsized paper and 10 minutes for the sized paper to darken in a similar way (Fig. 3.3).

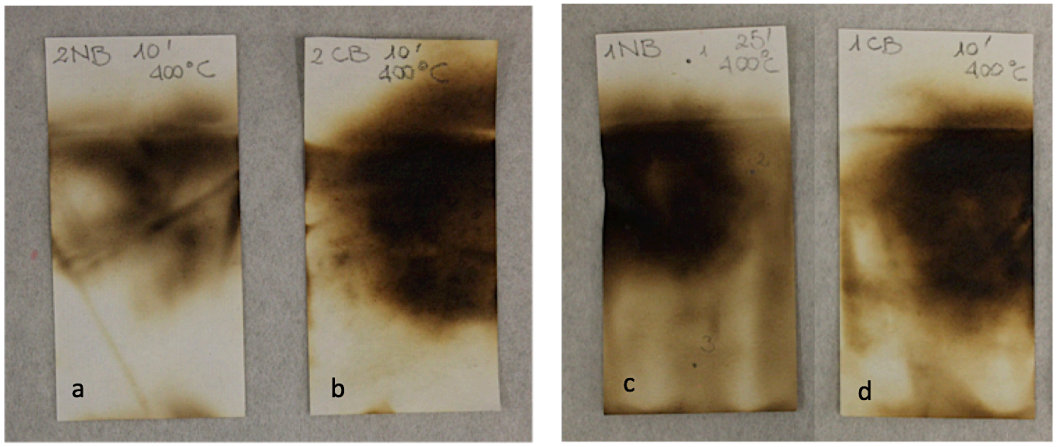

Figure 3.3. Left: unsized (a) and gelatine-sized RPM samples after 10 minutes heating with hot gun at 400°C (b); right: unsized sample (c) burnt for 25' is visually comparable with the gelatin-sized sample after 10' burning (d).

As it was not possible to obtain acceptably homogeneous samples with the hot air gun, faster burning closer to natural combustion was achieved over a larger area for both unisized and gelatin-sized RPM samples using a live flame, resulting in progressive darkening of the paper until burnt fragments were produced. Uniform charring was difficult to achieve and loss of burnt fragments occurred, as the samples tended to wear out permanently (Fig. 3.4).

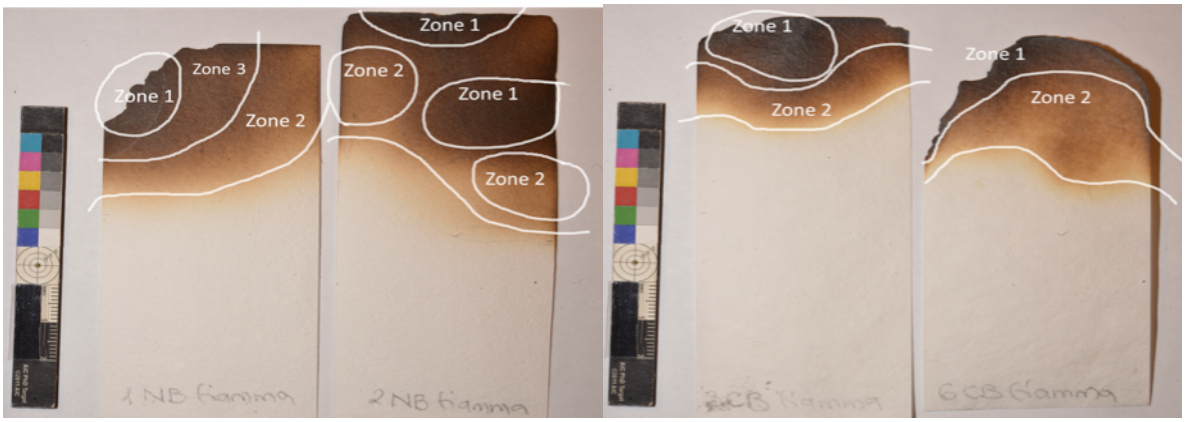

Figure 3.4. Unsized (left) and gelatine-sized RPM samples (right) burnt on live flame. Surface pH was detected in the areas 1, 2 and 3 (corresponding to different grades of combustion) and then averaged (data from S. Paris – CRC).

Two to three measurements were done per sample at the CRC. Surface pH was detected in the areas Zone 1, Zone 2 and Zone 3, corresponding to different grades of combustion, then averaged and compared to the pH values of the reference, unburnt samples. The direct flame did not seem to affect the pH so severely as the chemical burning and only a slight lowering of the values in the acid range was measured (Table 3.4).

Table 3.4. Surface pH values of RPM samples before treatment and after burning at the live flame, in zones 1, 2 and 3 of unsized and sized samples (data from S. Paris - CRC). The pH values decline, but not as much as in the chemically burnt samples.

Samples	Surface pH average reference	STD	Surface pH average Zone 1	STD	Surface pH average Zone 2	STD	Surface pH average Zone 3	STD
unsized RPM samples	6.3	0.6	4.6	0.4	5.0	-	5.6	-
sized RPM samples	5.7	0.1	4.7	1.0	6.0	0.6	-	

The areas named “Zone 1”, which were the most heavily affected by fire, deeply black and close to fragmentation, showed the lowest pH values. This would confirm a decrease in pH in relation to the paper degradation during combustion and, in particular, to the production of conjugated carbonyl and carboxyl groups.

In general, the effects on the paper material of these heat-only burning methods were best comparable with those in historical papers harmed by fire. Disadvantages were the long time required for hot air gun method and the inhomogeneity of the samples obtained, in addition to the risk of losing part of the sample during the burning over a flame.

2.2.2 Burning on hot plate

Given the disadvantages of the previous combustion methods, burning paper samples on a hot plate was tested. Some experimental steps were useful in establishing an efficient burning procedure, limiting the risk of paper fragmentation and obtaining a large and uniform burnt area. This was crucial to allow for subsequent reinforcement testing.

The experimental work was conducted in controlled stable climatic conditions of temperature

(T 23°C) and relative humidity (RH 50%). The experimental setup consisted of a standard hot plate, whose temperature was measured with a thermocouple immersed in a silicone oil bath put on the plate.

In the first test, unsized and gelatin-sized RPM samples were put on the plate and heated to observe the progress of the burning and how paper reacted with the temperature rising (Fig. 3.5).

The sample began to deform at 60°C due to water evaporation, to darken at 86°C and turn progressively brown. At 180°C the sample started to blacken with an uneven pattern: the more burnt areas shrank and the less burnt areas swelled creating blisters (Fig. 3.6) caused by water and carbon dioxide leaving the paper. This occurred primarily because the samples were free, with no weight holding them to the plate.

Figure 3.5. Progression in the burning process of unsized RPM sample from 95° to 194°C.

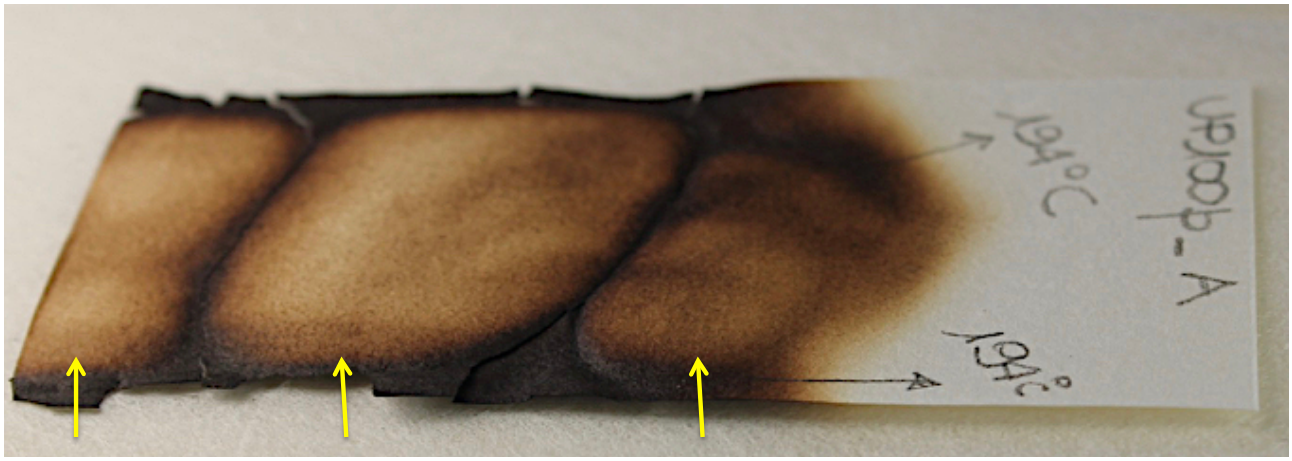

Figure 3.6. Unsized RPM sample burnt at 194°C, blisters are put in evidence by yellow arrows.

In order to limit the effect of water desorption, with blister formation and paper bending, and in order to evaluate the trend of weight loss during thermal degradation, unsized and sized RPM samples (5 x 5 cm^2) were prepared, weighed to the 10^{-4} g before and after being placed in an oven for 10 minutes at 130°C, as this was the maximum temperature reached by the oven. Then it was placed in the oven for 10 more minutes.

Leaving the samples 10 or 20 minutes in the oven at 130° yielded the same result in terms of weight loss (Table 3.5). This is a good indication that the treatment at 130°C involves only water desorption, and after 10 minutes most of water was removed: if chemical processes involving cellulose (e.g., VOC or CO_2 release) were already active at 130°C, then after 10 minutes of heating at 130°C paper was still loosing weight. Only data 20' is reported in table 3.5. It is worth pointing out that this followed procedure in desorption regime does not correspond to the Standard TAPPI method for determining moisture content in paper (T 412 om-11 Moisture in pulp, paper and paperboard), which is conducted in sorption regime, at lower temperature (105°C ± 2°C) for a longer time (30 + 3 minutes). Raising the oven temperature shortened the procedure time, although moisture data obtained in this way are less precise; however, more precise data on moisture amount have been obtained through Dynamic Vapor Sorption measurements (§ 3.2).

The samples dried for 20 minutes in the oven were then burnt on the plate, gradually heated up to 185°C. To avoid deformations, they were kept under a transparent glass to limit blister formation (Fig. 3.7). It should be noted that the temperature measured on the hotplate does not correspond to the temperature of the samples during the induced combustion process, since the latter causes exothermic reactions in paper. Temperature is further enhanced by the "thermic hood" created by

the glass, inducing the inside temperature to rise above the hotplate setting. After 30' burning, the samples were weighed once more.

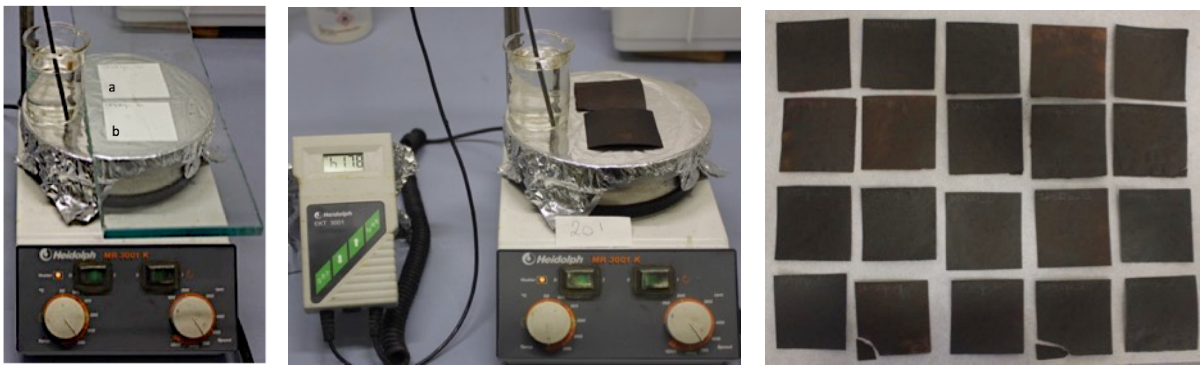

Figure 3.7. Left: Unsized (a) and gelatin-sized RPM sample (b) on the plate; centre: burning resulting after 20', plate temperature 178 °C; right: unsized and sized samples after 30' burning on the hot plate, max T 185°C reached by the plate.

Table 3.5 highlights the progressive percentage of weight loss of the samples:

Table 3.5. Samples weight modifications during the burning process on the hot plate (185°C, 30').

Samples (5x5cm^2)	Av. sample weight (mg)	Av. sample weight (mg) after oven drying (130°C, 20')	% weight loss after oven drying (130°C, 20')	Av. sample weight (mg) after oven drying + hot plate burning (185°C, 30')	% weight loss after oven drying + hot plate burning (185°C, 30')	% total weight loss
10 unsized RPM paper	220.5 ± 10.6	210.6 ± 10.1	4.4 ± 0.2	144.3 ± 20.4	31.5 ± 10.1	34.5 ± 8.6
10 sized RPM paper	225.4 ± 12.9	213.4 ± 12.3	5.3 ± 0.2	161.0 ± 15.2	24.6 ± 10.0	28.6 ± 6.4

Unsized samples lost about 4.4% w/w in water in the oven, while burning on the hot plate results in a further 31.5% weight loss; the total weight loss at the end of the process results in 34.5%. This loss represents carbon dioxide and water, and other VOC compounds.

Under the same dehydration conditions and burning process, the weight loss of sized samples in the oven was higher (5.3%) but the reduction caused by the hot plate combustion was minor (24.6%), and the total weight loss was around 28.6%.

As 200-240°C is considered the temperature range at which paper thermal decomposition of cellulosic materials begins [Molton 1977; Hirata, 1985; Scheirs et al. 2001; Shen et al. 2011; Ahn et al. 2018], further tests were performed at higher temperatures. Unsized and gelatine-sized samples were dehydrated in the oven (130°C, 20 minutes) in the same conditions as before, put under the transparent glass on the metal plate and progressively heated to 210°C, for 30 minutes, then weighed again to measure the weight loss.

Results are summarized in Table 3.6a and Table 3.6:

Table 3.6a. Modifications in the weight of paper samples during dehydration and burning process on the hot plate (210°c, 30').

Samples (5x5cm^2)	Av. sample weight (mg)	Av. sample weight (mg) after oven drying (130°C, 20')	% weight loss after oven drying (130°C, 20')	Av. sample weight (mg) after oven drying + hot plate burning (210°C, 30')	% weight loss on anhydrous after burning (210°C, 30')	% total weight loss
10 unsized RPM paper	232.7 ± 14.1	221.4 ± 14.3	4.9 ± 0,2	61.3 ± 8.6	72.3 ± 4.8	73.7 ± 5.0
10 sized RPM paper	257.9 ± 11.1	242.3 ± 10.8	6.0 ± 0.3	85.4 ± 7.9	64.8 ± 4.0	66.9 ± 4.0

Table 3.6b. Samples weight variations as effect of 30' additional burning on the hot metal plate (210°C, 30'+ 30').

Samples (5x5cm)	Av. sample weight (mg) after oven drying (130°C, 20')	Av. sample weight (mg) after oven drying + hot plate burning (210°C, 30')	% total weight loss	Av. sample weight after additional 30' burning (210°C)	% additional weight loss (210°C, 30'+30')	% additional weight loss on sample weight after oven drying
10 unsized RPM paper	221.4 ± 14.3	61.3 ± 8.6	73.7 ± 5.0	53.4 ± 10.4	12.9 ± 3.0	3.6 ± 3.2
10 sized RPM paper	242.3 ± 10.8	85.4 ± 7.9	66.9 ± 4.0	75.9 ± 8.0	11.1 ± 2.8	3.9 ± 3.5

Respect to previous tests, higher temperature (210°C) actually induced a more significant weight loss, approximately 74% in case of the unsized samples and 67% for sized samples.

On the other hand, an extension of 30 minutes on the hot plate at 210°C led to a minimal additional reduction in weight: +3.6% in the unsized samples and of +3.9% in case of sized samples.

In the experiments carried out by Ahn and coworkers and by Völkel and coworkers involving historical paper from the 19th century, degradation processes (cellulose oxidation, chain cleavage, crosslinking, progressive carbonization) result in progressive steps as dehydration, thermal scissions, and gas evolution. According to the authors, at temperature < 240 °C the weight variation is probably due to the dehydration process and most of the cellulose depolymerization and formation of carbonyl groups along the cellulose molecules occur at temperature > 240 °C.

Charring is expected at temperatures between 250° and 350 °C, which, however, does not induce a complete destruction of the fibers [Ahn at al. 2018; Völkel et al. 2022].

In order to better evaluate the efficiency of reinforcing treatments, it was decided that preferable conditions for samples to be used in the experimental part of the present research would have been brittle paper in which cellulose fibres were still present: such a type of samples was very challenging, being the most difficult to treat, since minimal movements could determine

destruction. On the other hand, samples burnt at temperatures higher than 310°C are so fragile, that it is very unlikely to find paper leaves in historic manuscripts in these conditions. Thus, the plate temperature was raised in two further burning test. In the first one, unsized and sized samples were burnt on the hot plate set at 250°C for 15 minutes, under a marble weight (20 x 20 cm^2, 400 g), turning the sample at half time to obtain a homogeneous effect, comparable recto verso.

It should be considered that, as already stressed by Suzuki and coworkers [Suzuki et al. 1992], the combustion of fibrous materials – even in historical paper – goes in a heterogeneous way, so that perfect uniformity in burning seems not to be a reasonable goal to achieve.

In the second test, the plate temperature raised at 310°C, keeping the same time and burning procedure. Samples charred at different temperatures were thus obtained and analysed with ATR to compare the effects induced by combustion on the main components of the RPM paper, essentially cellulose and gelatin (when present).

Surface pH of the samples burnt at 250°C was measured (TAPPI T 529 om-99) and found to be quite similar to those of historical burnt paper (Table 3.7). Average pH of burnt areas of the Padua incunabulum was in fact 6.2 and those of the Chartres manuscript was pH 4.6, as shown in Chapter 2, § 4.1).

Table 3.7. pH average values from RPM samples burnt on hot plate, T 250°C, 15 minutes.

Samples	**surface pH average untreated samples**	**STD**	**surface pH average after burning on hot plate (T 250°C, 15')**	**STD**
unsized RPM samples	6.9	0.1	6.1	0
sized RPM samples	6.7	0.1	5.5	0.2

It is worthy to note that paper burnt by means of sulfuric acid followed by heat emits VOCs for a long time. The smell is liquorice-like, very similar to those of manuscripts damaged by iron gall inks; on the contrary, samples burned on the hot plate with heat only, once cooled did not give off any such odour.

3. Investigation of the physico-chemical changes incurred in paper samples upon burning

So far, the different burning methods have been ranked for their ability to mimic real burnt paper according to the pH of the samples. Other physico-chemical characterizations were carried out after burning with different methods (chemically induced, hot air gun, live flame, and hot plate) to assess some of the other changes induced by the burning process, and to confirm which method was best to obtain samples comparable with the burnt historical ones.

3.1 Degree of polymerization

The degree of polymerization (DP) is a reliable index of the paper quality and condition as the main chemical degradation processes – hydrolysis and oxidation – result in the shortening of the cellulosic chain, in the formation of low molecular weight products and in a consequent DP decrease. DPv measures were performed according to the standard procedure TAPPI T 230 om-99 to determine the solution viscosity of the paper pulp dissolved in cupriethylenediamine (CuEn) solvent. This method was possible only for the unburnt RPM paper, both unsized and sized. For the unsized unburnt paper, DPv average was 1872 ± 13 and for sized unburnt paper it resulted 1890 ± 23. It was not possible to dissolve any burnt fragments: it may be inferred that the level of carbonization was too high and almost no intact cellulose and hydrogen bonds remained. Since this test could not be informative about the condition of the cellulose degraded by heat and fire and in consideration of the fact that it requires to destruct a certain mass of sample (from 10 to 100 mg), the measurement of the degree of polymerization could not be determined for the historical papers from Chartres and from Padua.

3.2 Moisture in the samples

The paper response to water was verified for RPM samples produced on plate at 250°C. In sized RPM samples, a drop of double-distilled water in the white, unburnt area and a drop in the burnt area both maintain a high contact angle for some seconds. This effect was expected, as this is exactly the function of the gelatin to make it more difficult for water to enter the sheet. On the contrary, the drop of water in the white area of the unsized RPM samples, more absorbent, expanded immediately, while remained well defined and with a high contact angle on the burnt

area, which is really hydrophobic (Fig. 3.8). Water progressively went deeper in the paper but did not expand and after more than 30' it was still well defined on the sample surface.

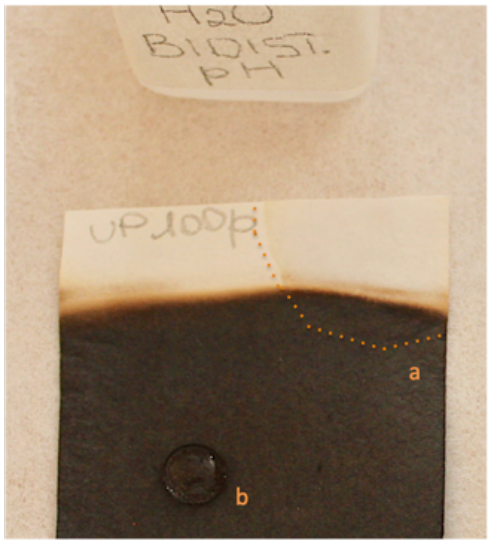

Figure 3.8. Unsized RPM samples. The water drop is immediately absorbed in the unburnt area of the paper (a), while remains longer with a high contact angle in the burnt area (b).

In the investigation of historical books made of rag paper exposed to fire, conducted by Ahn et al. (2018) and Völkel et al. (2022), the higher hydrophobicity of the burnt paper is described in association with the increase in carbon content and decrease in C-O bonds. The authors observe heat-induced crosslinking and a sort of "densification" of the cellulose chains, concurrent with cellulose depolymerization [Ahn et al. 2018; Völkel et al. 2022].

The average equilibrium moisture content of the unsized RPM unburnt paper was measured according to TAPPI T 412 om-02 as 6.0 % ± 0.1. A more in-depth investigation of the moisture sorption capacity of the samples was carried out on unburnt unsized and sized RPM paper (Fig. 3.9). The isotherms at 23°C of both samples, in the unburnt area, the interface area between totally burnt and unburnt area and in the totally burnt area were measured by a Dynamic Vapor Sorption (DVS) experiment. This instrument generating humidity is fully automated, maintains the relative humidity and temperature conditions of the material for the duration of the experiment, and is sensitive also in case of small size samples to study the dynamic uptake of moisture in paper.

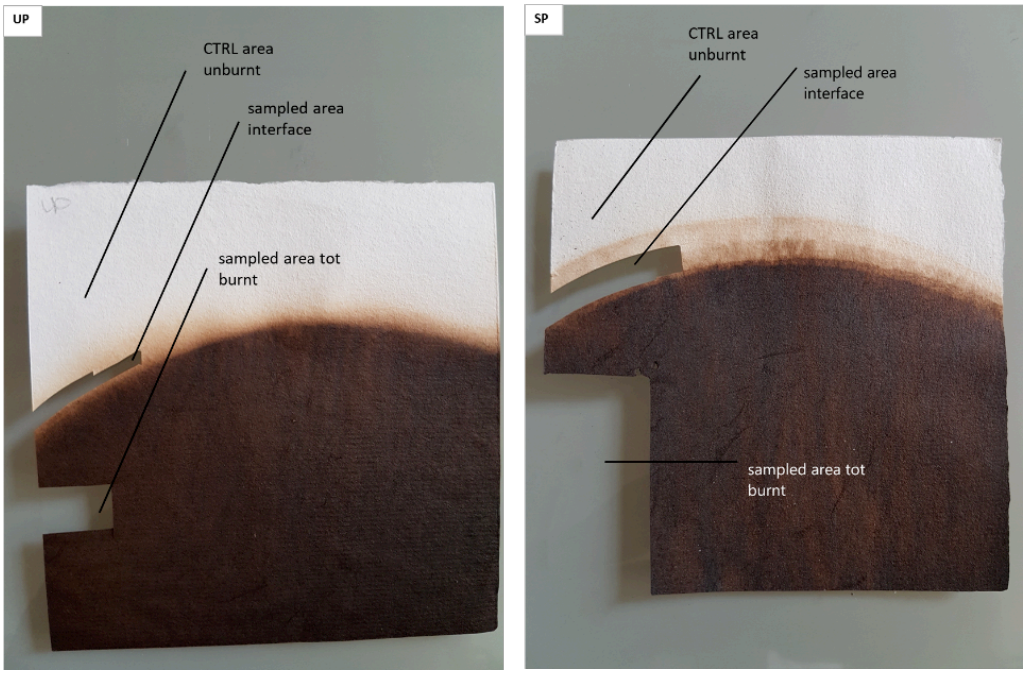

Figure 3.9. Unsized (left) and sized (right) RPM burnt on hot plate (250°C, 15') used for the investigation of moisture capacity with DVS instrument. From both samples, paper portions for the test were taken both from the totally burnt area and from the interface area between totally burnt and unburnt paper.

Fig. 3.10 represents the isotherms of the % change in mass (related to moisture content) of unsized, unburnt RPM paper (UP-CTRL) and of sized, unburnt RPM paper (SP-CTRL) for one cycle sorption/desorption.

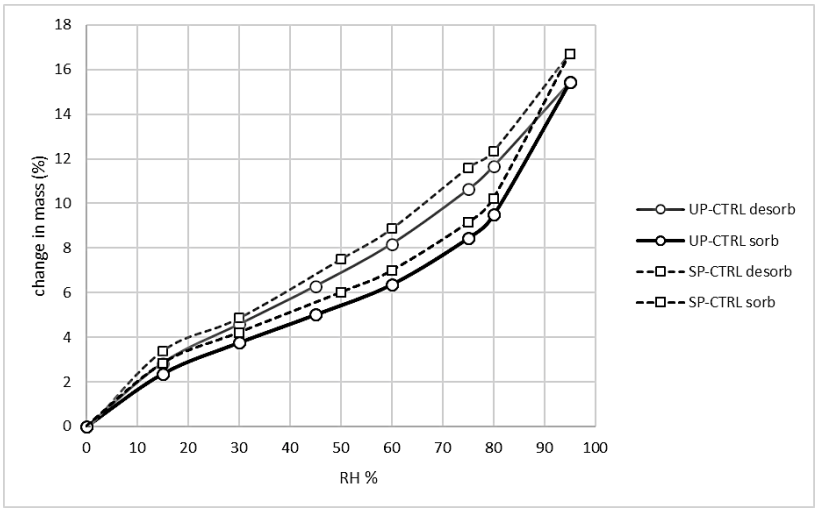

Figure 3.10. Change in mass (%) related to moisture content of unsized, unburnt RPM paper (UP-CTRL) and sized, unburnt RPM paper (SP-CTRL) at various RHs. Sorption (full lines) and desorption (dashed lines) are shown (data from A-L. Dupont and O. Belhadj – CRC).

The equilibrium moisture content (EMC) at 23°C and 50% RH is slightly higher for sized paper that unsized paper in both sorption and desorption regimes; this was also previously observed by the

modifications in weight of paper samples during dehydration (Table 3.6a and 3.6b) and was also shown in [Dupont, 2003]. The span in the sorption vs desorption for both unsized and sized RPM samples indicates that UP and SP show the normal expected hysteresis behaviour.

In Fig. 3.11 the behavior of totally burnt unsized (UP tot) and sized (SP tot) RPM paper is compared to control papers, that is unburnt unsized (UP-CTRL) and sized (SP-CTRL) RPM paper.

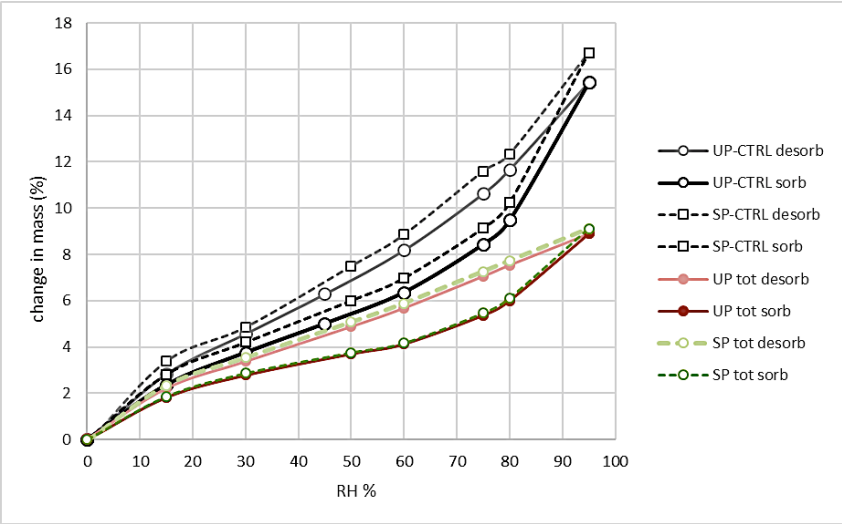

Figure 3.11. Change in mass (%) related to moisture content of the totally burnt unsized and sized RPM paper at various RHs in adsorption and desorption regime, compared to CTRL papers (data from A-L. Dupont and O. Belhadj – CRC)

Totally burnt areas of both unsized and sized RPM paper have become similar in their sorption/desorption behavior. Their EMC is systematically lower than in the CTRL papers, but they still show a distinct hysteresis in that the span in their sorption vs desorption water retention is as large as in the UP-CTRL and SP-CTRL samples. Even though the entire span of mass change does not reach the same levels as the control samples (9% vs 16.5 % at 95% RH), it is remarkable that they still show a ‘’cellulose-like’’ behavior.

Finally, Fig. 3.12 compares the behavior of paper taken from the interface area between totally burnt and unburnt in unsized and sized paper (UP int and SP int) with the behavior of UP-CTRL and SP-CTRL samples.

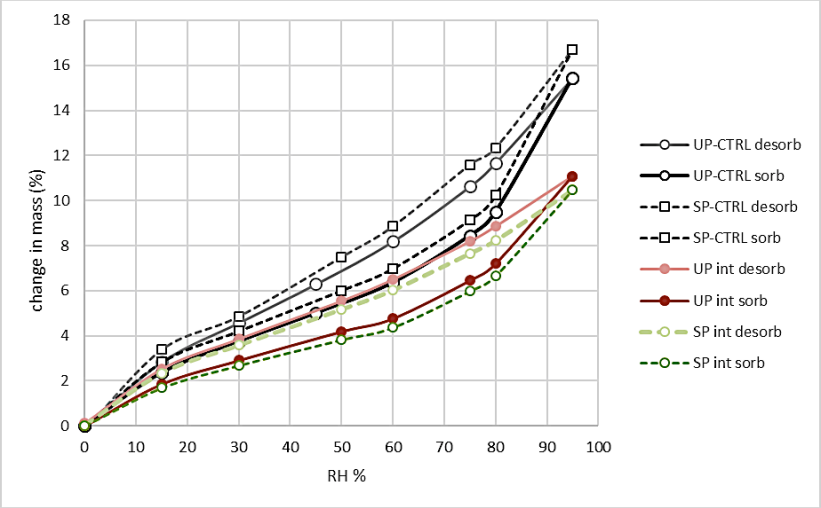

Figure 3.12. Change in mass (%) related to moisture content of the burnt, sized and unsized interface area at various RHs in adsorption and desorption regime compared to the behavior of CTRL papers (data from A-L. Dupont and O. Belhadj – CRC)

Interface areas have also lower EMC than CTRL samples but higher than totally burnt samples, both sized and unsized. UP int and SP int show in fact a trend which is intermediate between the behaviour of the UP-CTRL and SP-CTRL samples and that of the totally burnt papers. DVS data for EMC at 23°C and 50% RH in sorption regime are summarized in Table 3.8, where % hysteresis is also considered:

Table 3.8. DVS data for EMC at 23°C and 50% RH in sorption regime.

Samples	EMC (23°C, 50%RH	Hysteresis
UP int	4.2%	1.4%
UP tot	3.7%	1.2%
SP int	3.8%	1.4%
SP tot	3.8%	1.3%

3.3 ATR-FTIR spectroscopy

ATR-FTIR analyses were carried out with the same equipment and in the same experimental conditions already used for the characterization of the historical papers from the Chartres manuscript and the Padua incunabulum, the study of which is presented in Chapter 2 (§ 4.3.1) of this thesis. The main purposes were to investigate the effects of artificial burning and to compare them with the degradation caused by fire in the historical papers, so to set up and standardize, as

much as possible, a protocol to prepare suitable burnt paper samples for the tests of mechanical reinforcement.

Unburnt unsized and sized RPM were also checked as control samples, but spectra were acquired mainly on the areas burnt with the different procedures.

A first comparison among unsized paper samples burnt with chemical burning (0,5 M H_2SO_4 + heating), hot air gun burning, and flame burning is shown in Fig. 3.13. The most affected regions are between 1500 and 1800 cm^{-1} and therefore a magnification of this region is shown in Fig. 3.14.

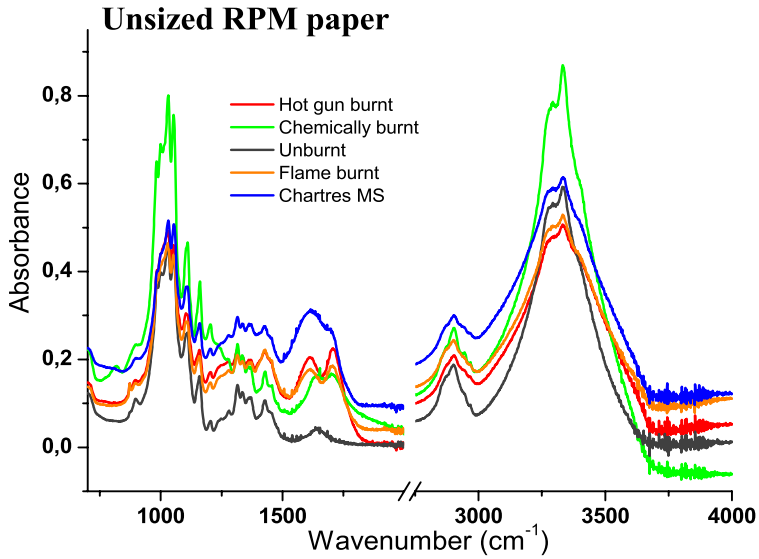

Figure 3.13. ATR-IR spectra of unsized RPM samples artificially burnt with different procedures. In blue, the burnt area in the Chartres BM ms 1047.

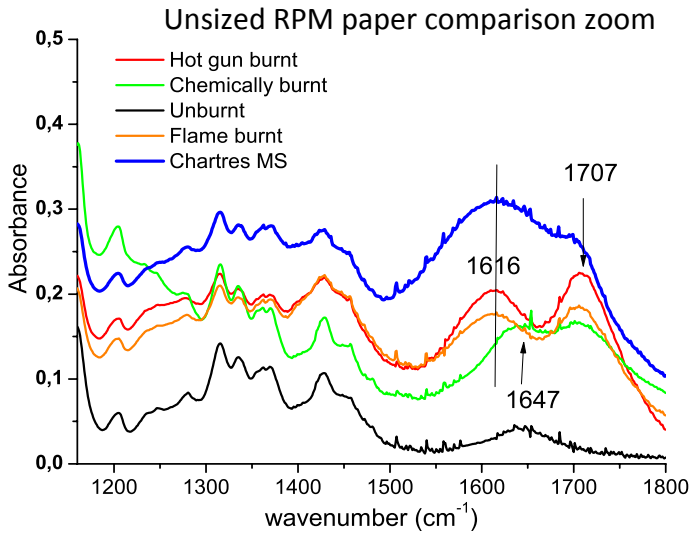

Figure 3.14. Magnification of the region 1200-1800 in Figure 3.13.

The hot air gun and the flame burning gave spectra closer to natural burnt areas of Chartres manuscript: two peaks around 1620 and 1710 cm^{-1} in the same position are observed on burnt areas of these samples, matching well to the bands observed in the burnt areas of the manuscript. Instead, in the spectrum of the chemically burnt areas, the peak at 1616 cm^{-1} is shifted to 1647 cm^{-1}, a higher wavenumber which is indicative of a likely loss of conjugated compounds and the transformation of carboxylates into carboxylic compounds. Both the effects are related to protonation in acidic environment. Moreover, the region between 1200-1300 cm^{-1} is also affected, with bands due to the stretching modes of sulphates.

In the analyses of sized RPM samples artificially burnt in different ways (Fig. 3.15) it is to notice that amide I (1540 cm^{-1}) and II (1640 cm^{-1}) typical peaks of gelatin are overlapped in this region.

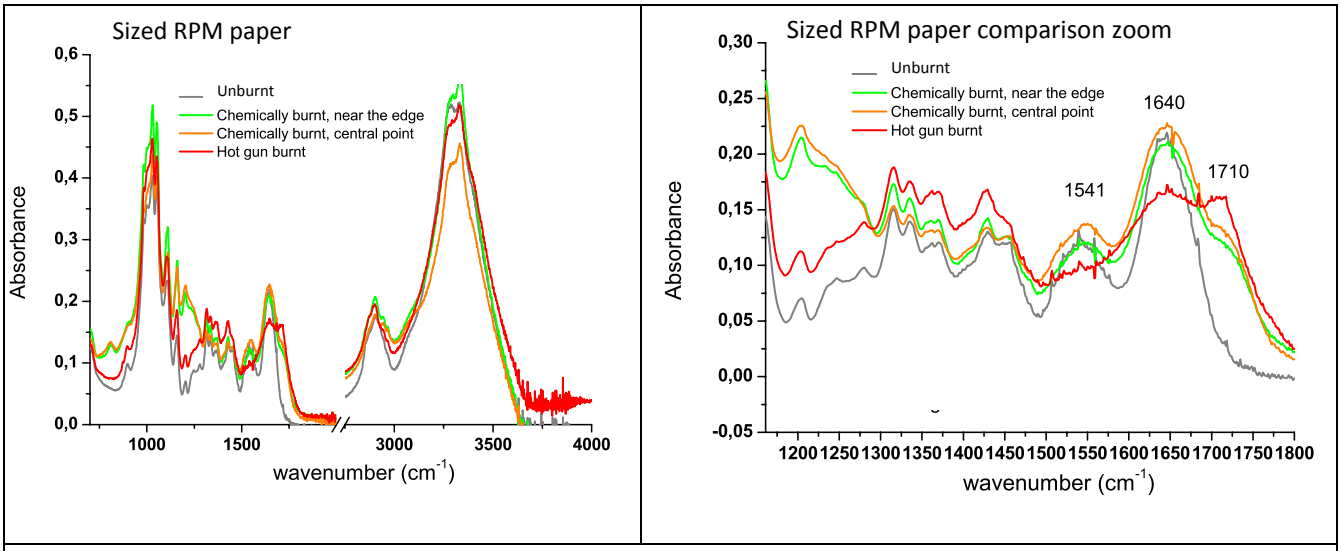

Figure 3.15. ATR-IR spectra of sized RPM samples artificially burnt with different procedures (left) and magnification 1200-1800 cm^{-1} (right).

The chemically burnt sized paper shows a spectrum very similar to the unburnt sample: only a shoulder due to carbonylic compounds is observed at 1710 cm^{-1}, but gelatin seems to have protected the paper. On the other hand, the hot gun burnt sized paper presents a spectrum similar to that observed in unsized paper, with reduction of the peaks amide I and II, and formation of peaks related to cellulose degradation. This indicates that the gelatin is mainly destroyed, and the cellulose fibers are damaged in hot gun burning, as expected, and as opposed to the chemical burning.

The unsized and sized RPM samples burnt on hot plate at different temperatures (185°C and 210°C for 30') were also investigated by ATR-IR. It should always be recalled that the given temperature refers to the plate, not to the actual temperature of burning paper, which is presumably higher due to the exothermic reactions induced by the burning process.

Burning at 185°C, albeit blackening and damaging the external part of the fibres, seems not to affect the inner cellulosic part: the conservation of the main cellulose skeleton is evident from the main, structured peak at 1031 cm^{-1}, related to the C-O stretching in cellulose. The effects are radically different when using higher temperature (i.e., 210°C), as evident in Fig. 3.16 and 3.17:

- carbonization increases rising temperature (increased slope 2000-3000)
- conjugation compounds (blackening) increase rising temperature (the feature at 1615 cm^{-1} increases and shifts lower wavenumber)

- C-O features, around 1030 cm^{-1}, indicative of cellulose, are not present at 210°C-30' burning
- OH band (water and cellulose OH) is strongly suppressed at 210°C.

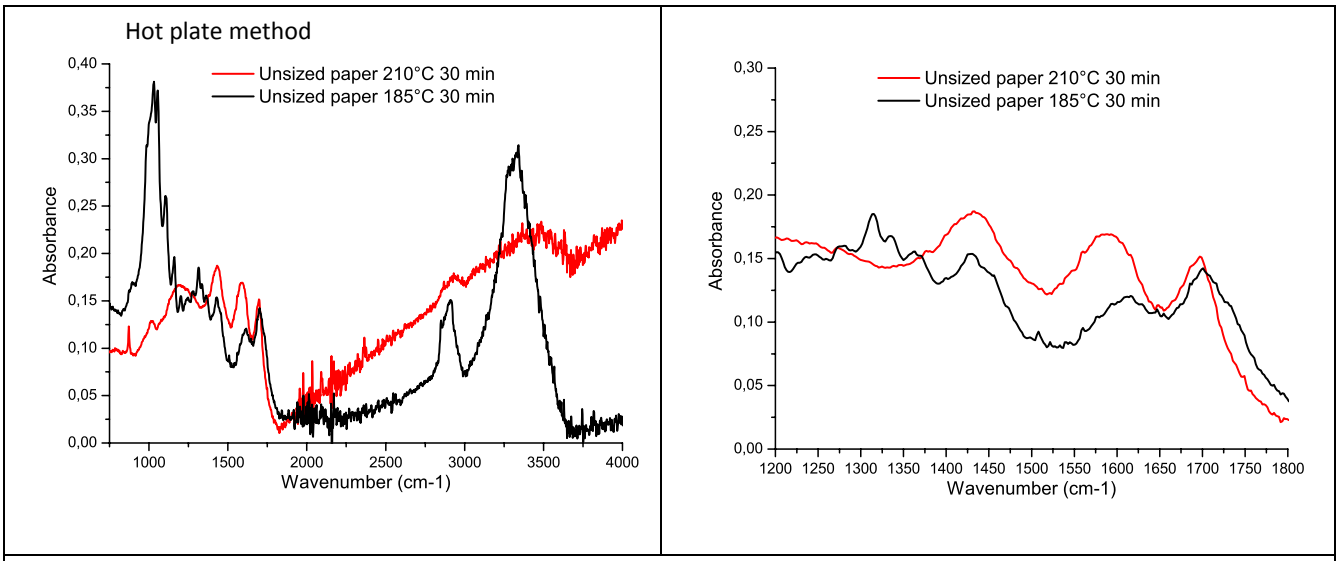

Figure 3.16. ATR-IR spectra of unsized RPM samples artificially burnt on hot plate at two different temperatures (left) and magnification 1200-1800 cm^{-1} (right).

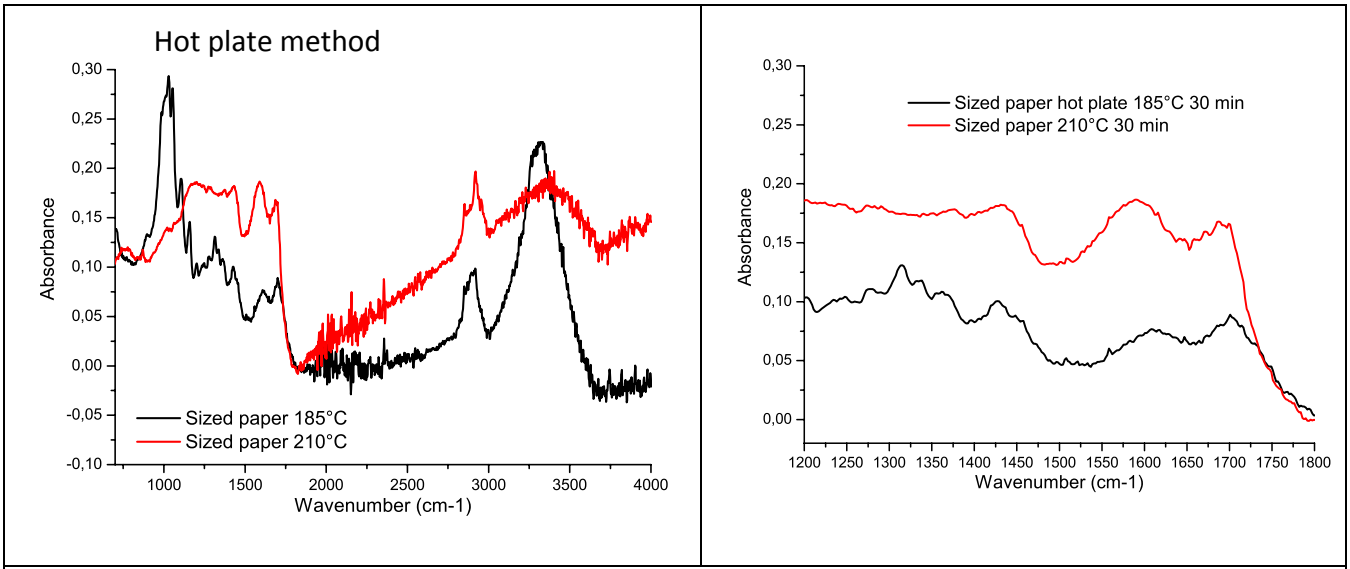

Figure 3.17. ATR-IR spectra of sized RPM samples artificially burnt on hot plate at two different temperatures (left) and magnification 1200-1800 cm^{-1} (right).

Nevertheless, the hot plate method, at lower temperature, induces an IR pattern in the region 1200-1800 cm^{-1} which is very similar to hot gun and flame burning in sized and unsized RPM paper.

Finally, hot plate and natural burning effects were compared based on the spectra obtained.

In Fig. 3.18 spectra from the unsized RPM samples, from the Chartres manuscript and from the Padua incunabulum are compared. The metal plate method is efficient: 30' at 185°C on unsized paper already reduces significantly the amount of water and the degradation IR region, between 1200 and 1800 cm^{-1}, shows that the hot plate is comparable to hot gun burning in terms of type of degradation by-products, similar to the natural flame burning of the historical paper from the Chartres manuscript and the Padua incunabulum.

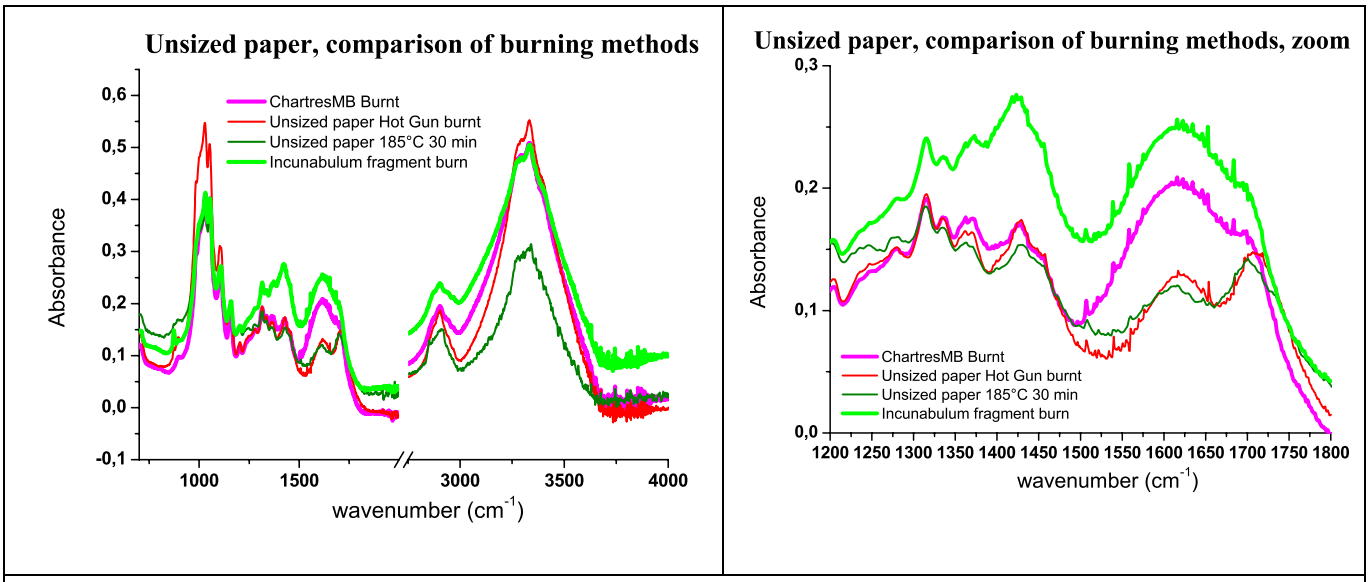

Figure 3.18. Comparison among hot gun burnt, hot plate burnt and naturally burnt samples (left) and magnification 1200-1800 cm^{-1} (right).

We must also consider that historical paper from the Chartres manuscript and from the Padua incunabulum – as well as almost all the papers used in the production of manuscripts and printed books up to the 19th century – are sized with gelatin. So, the comparison with burning of sized paper is more relevant, as shown in Fig. 3.19. Here, the general spectrum of 185°C hot plate burnt paper is very similar to the spectrum of the paper form the Chartres manuscript and the Padua incunabulum.

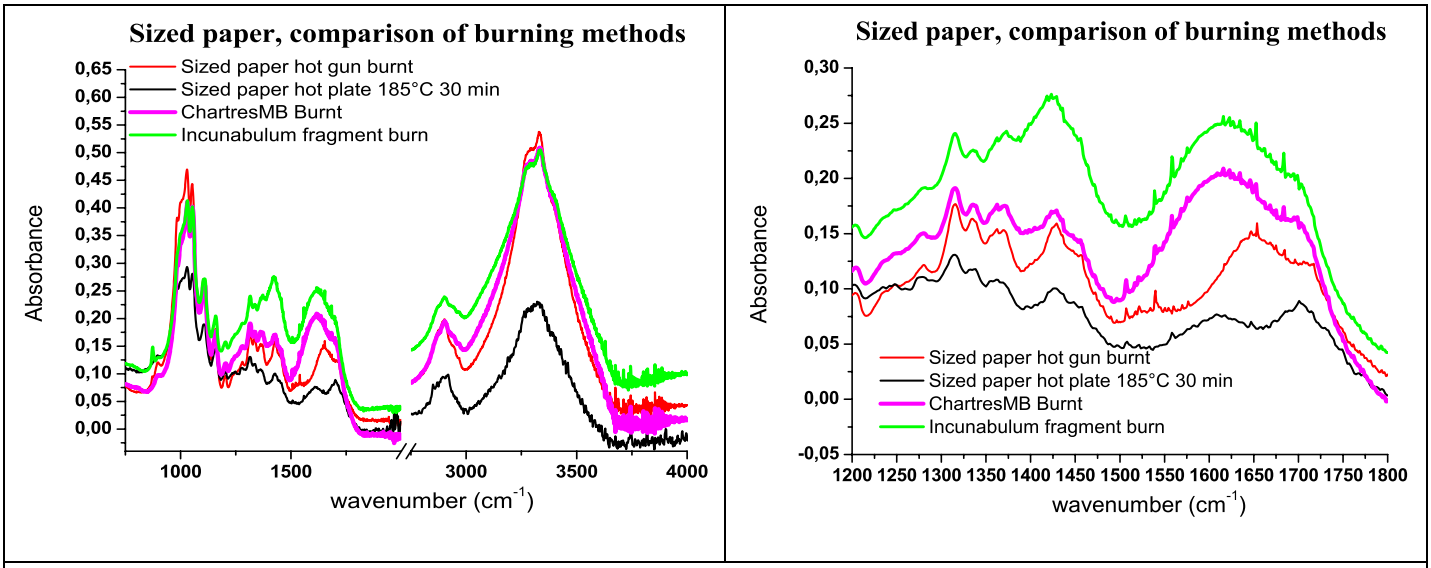

Figure 3.19. Comparison among hot gun burnt, hot plate burnt and naturally burnt samples (left) and magnification 1200-1800 cm^{-1}(right).

More important, the region between 1500 and 1800 cm^{-1} is very similar between the hot plate burnt paper and the Chartres manuscript and incunabulum: differences in band intensity in this region are essentially related to difference in sizing and/or temperature of burning, parameters clearly highly variable among the naturally burnt papers. However, considering the large variability of burning, the spectral profile between 1200 and 1800 cm^{-1} are close enough. It should also be pointed out that in both unsized and gelatin-sized samples, chemical burning produced the most dissimilar effects when compared to the paper from the Chartres manuscript and from the Padua incunabulum. In addition to the pH values of the samples treated with sulfuric acid (§ 2.1), evidence from the IR investigation supported the decision to rule out this method of combustion.

Finally, we considered the effect of increasing the burning temperature, but with reduced burning times (15 minutes instead of 30 minutes). We observe that in the sized paper spectrum at 250°C-15 minutes the cellulose peak at 1030 cm^{-1} is still present, while in the spectrum at 210°C-30 minutes is disappeared (fig. 3.20).

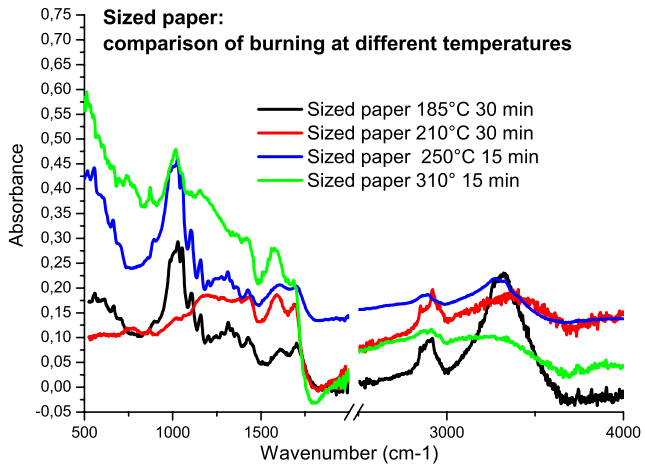

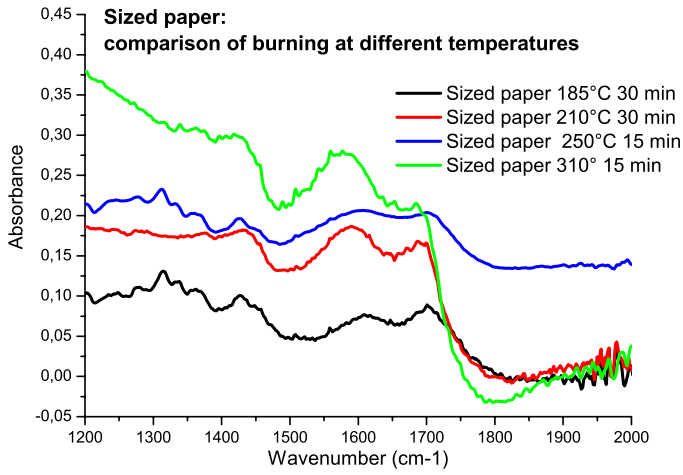

Figure 3.20. Comparison among sized papers hot plate burnt at different temperatures.

This is an indication that 250°C-15 minutes induces less damage than 210°C-30 minutes. The region between 1500 and 1800 cm^{-1} presents comparable degradation peaks between 250°C-15 minutes and 210°C-30 minutes spectra. However, at 310°C-15 minutes, the induced degradation is higher: the degradation peak at 1600 cm^{-1} is shifted at lower wavenumber than the corresponding peak at 210°C or 250°C. The peak around 1000 cm^{-1}, which we observe in the spectrum at 310°C-15 minutes, is likely not related to the cellulose peak, since it is not structured: it could be due to C-O-C cross-links created in the high temperature pyrolysis of cellulose. Spectra of unsized paper hot plate burnt at different temperatures (Fig. 3.21) show a very similar trend, indicating that burning at 310°C-15 min induces a strong degradation. Compared to sized paper, pyrolysis of unsized burnt paper seems to induce a larger amount of carbonylic-carboxylic compounds, as highlighted by the strongest peak around 1700 cm^{-1}. This is likely related to a protective role of gelatin against oxydation and acidification, even in paper pyrolysis.

As a general remark, we notice that both the Chartres and the incunabulum burnt papers present still a well-structured cellulose peak, while this peak is absent in the papers burnt at 210°C-30 minutes or 310°C-15 minutes. Therefore, we can speculate that 310°C-15 minutes is a treatment inducing a very strong degradation, with very fragile papers, prone to fragment, and represents an upper limit situation.

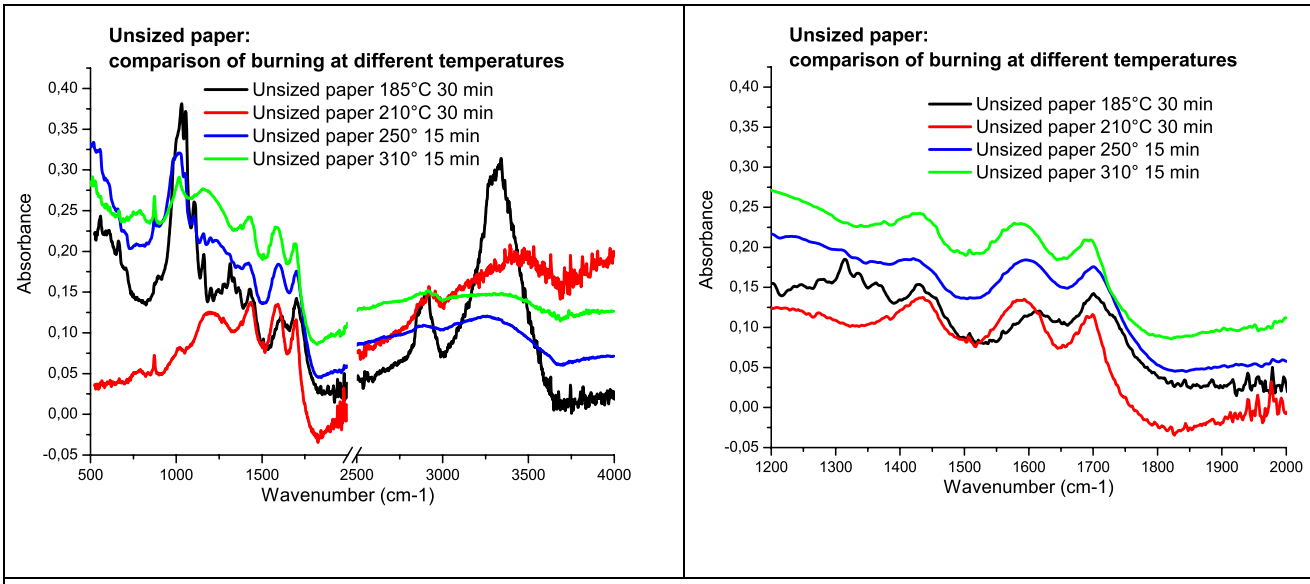

Figure 3.21. Comparison among unsized papers hot plate burnt at different temperatures.

According to ATR-FTIR analysis, samples obtained by burning on hot plate at 250°C-15 minutes best achieved a severe combustion while still retaining detectable cellulose fibers.

3.4 UV-VIS spectroscopic analysis

Fiber optics UV-VIS reflectance spectra were acquired with the same equipment and in the same experimental conditions already used for the characterization of the historical papers (Chapter 2, § 4.3.2).

As already suggested by the visual inspection, chemical burning on sized paper resulted in a strong reduction of global reflectance compared to unsized paper (Fig.3.22). This can be attributed to Maillard reactions between the gelatin and the paper, resulting in the production of melanoidinic compounds (deep black).

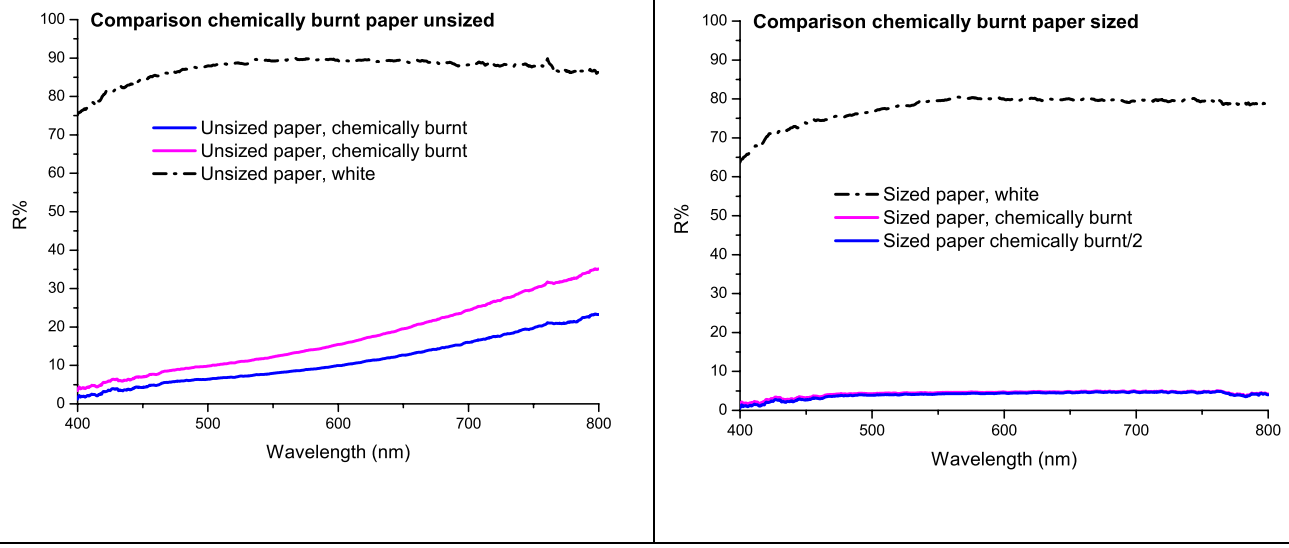

Figure 3.22. FORS spectra of chemically burnt paper, unsized (left) and sized (right).

Also, with the use of hot air gun on burning sized paper became blacker than unsized (Fig. 3.23).

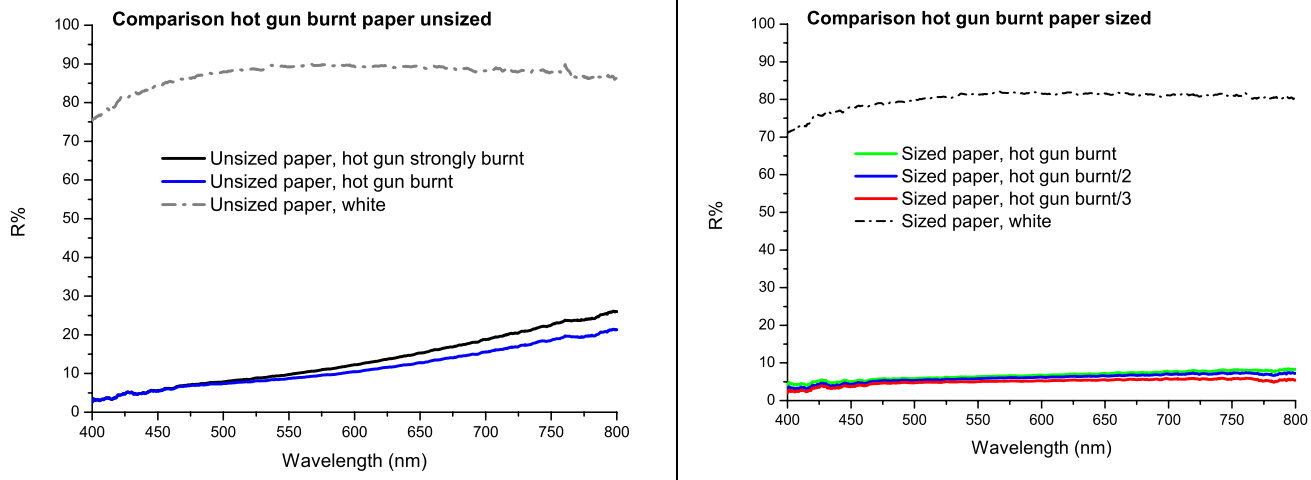

Figure 3.23. FORS spectra of hot gun burnt paper, unsized (left) and sized (right).

A comparison between Fig. 3.17 and Fig. 3.18 shows that chemical burning on sized paper results in a flatter curve than hot gun burning on sized paper, indicating a deeper black induced by chemical burning. The flame burning process resulted in a very inhomogeneous reflectance, with regions more blackened than others (Fig. 3.24, on unsized paper). This result, which is coherent with the visual examination of the samples as shown in Fig. 3.3, made flame burning unsuitable for obtaining samples for the purpose of use in the experiments.

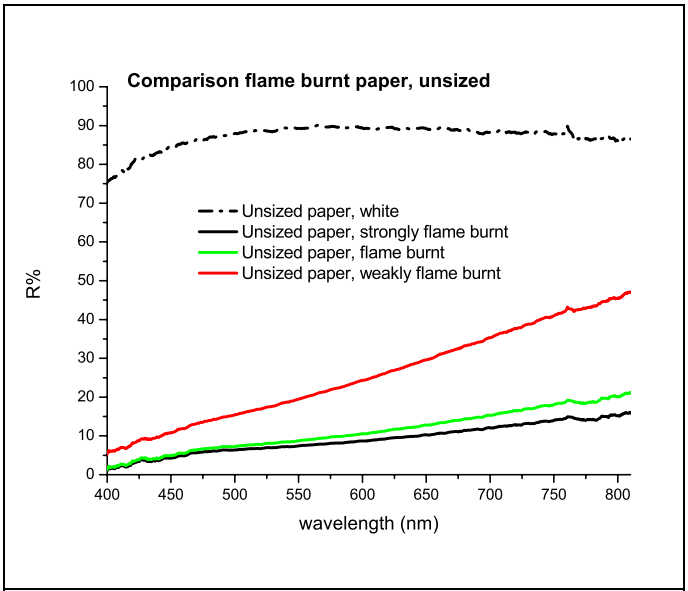

Figure 3.24 . FORS spectra of flame burnt unsized paper.

On the opposite, hot plate burning results in a very homogeneous blackening of the paper (Fig. 3.25):

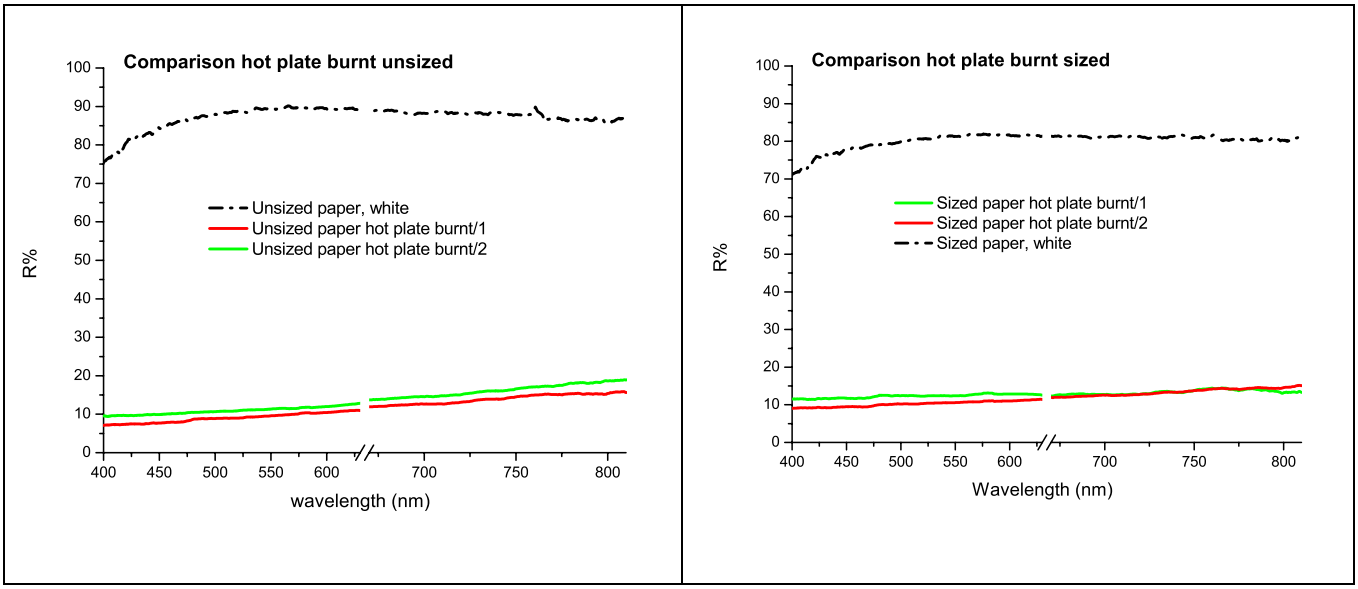

Figure 3.25. FORS spectra of hot plate burnt paper, unsized (left) and sized (right). Hot plate burning at 250°C for 15 minutes.

A general comparison of burning methods both in unsized and sized burnt papers is shown in Fig. 3.26: on unsized paper, all the methods induced a similar spectral profile, but in sized paper the general reflectance of chemical burning is lower. However, from the optical point of view hot gun, flame and hot plate seem to induce the formation of similar chromophore compounds.

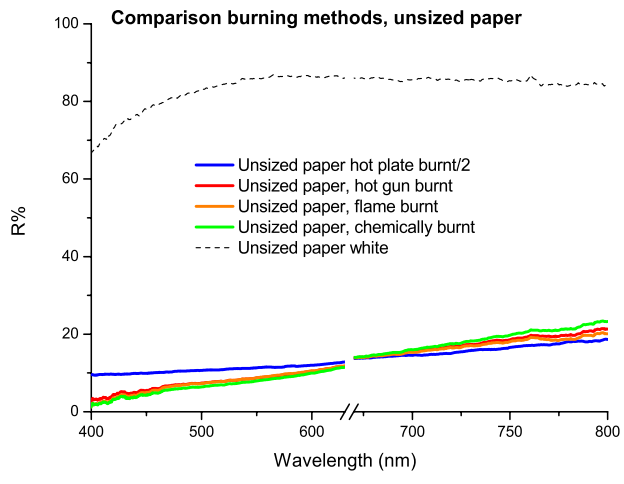

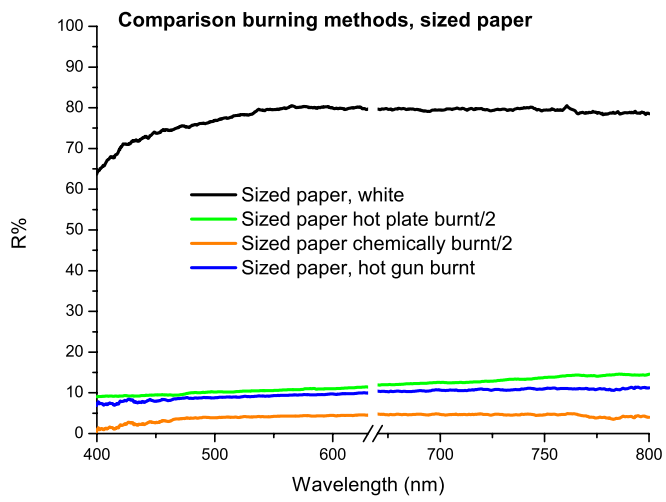

Figure 3.26. Comparison of burning methods on unsized (left) and sized (right) paper. Hot plate burning at 250°C for 15 minutes.

3.5 X-ray Powder Diffraction (XRPD)

XRPD measurements were carried out on sized and unsized RPM paper after burning on hot plate with the same equipment and in the same experimental conditions used for the historical samples (Chapter 2, § 5)

The structure of the unsized RPM paper after hot plate burning [250°C] is shown in the diffractogram in Fig. 3.27. Cellulose is identified by the well-known peaks of crystalline fraction at 17.7, 19.5, 26.7, 40.5 and 55 [°2θ]. These diffraction features are comparable to the XRD pattern of the Chartres manuscript (Chapter 2, § 5), reproposed in Fig. 3.28. A limited mineral amount was detected, consisting in calcium carbonate ($CaCO_3$), talc (MgO_3Si) and hydrotalcite (a hydrated magnesium aluminate, often associated with talc).

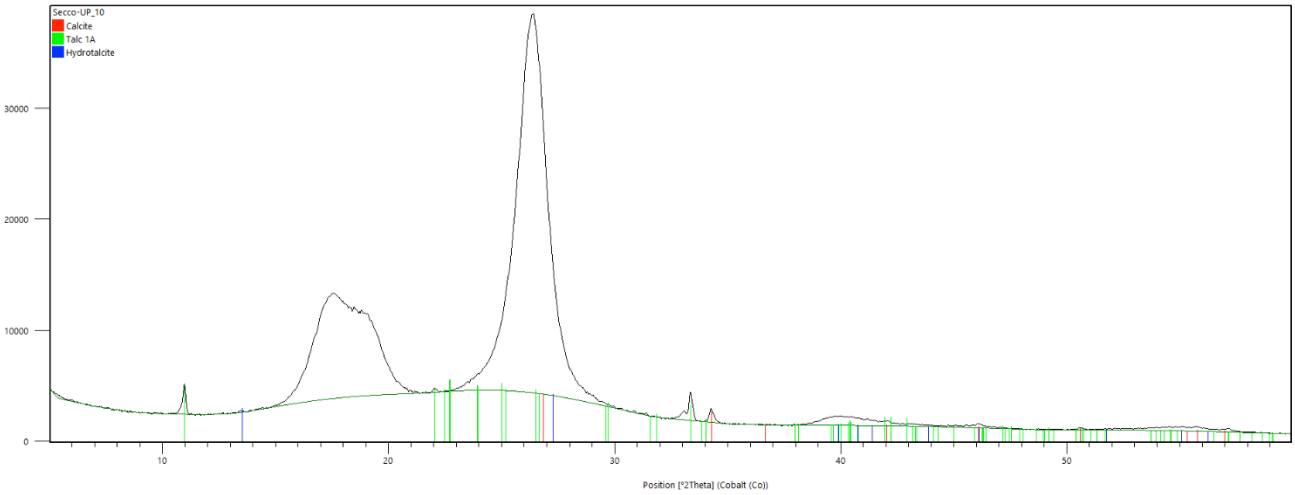

Figure 3.27. Unsized RPM paper, XRD difractogram. Peaks of crystalline fraction in evidence at 17.7, 19.5, 26.7, 40.5 and 55 [°2θ]. Limited amounts of calcite, talc and hydrotalcite are present. Crystalline cellulose peaks are comparable to the peaks of the Chartres manuscript, reproposed in Figure 3.28.

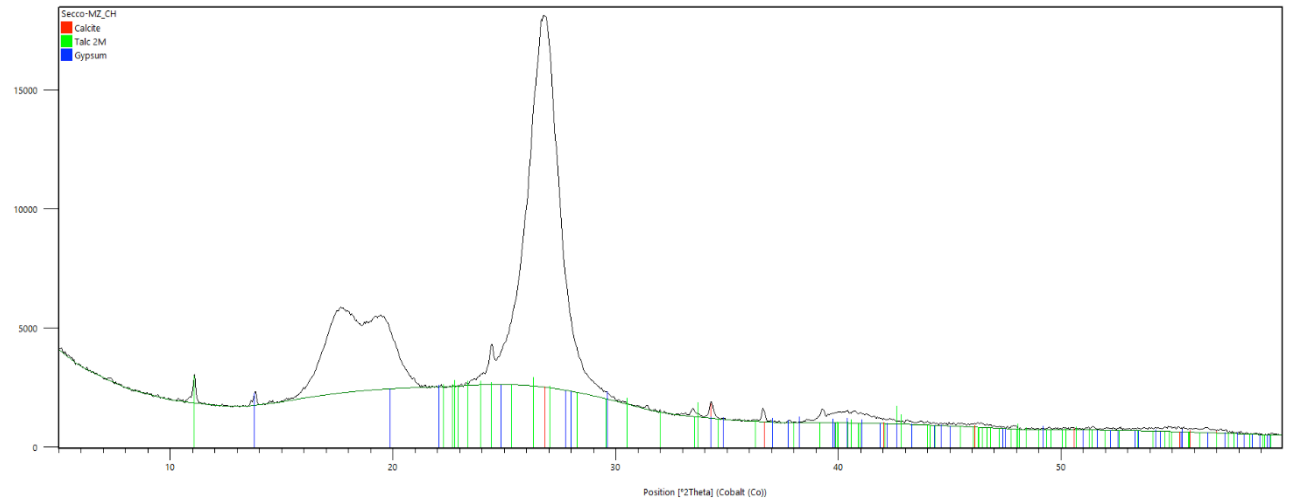

Figure 3.28. Chartres BM ms 1047, XRD difractogram. Crystalline cellulose peaks are comparable to the peaks of the unsized RPM paper in Figure 3.27. Amounts of calcite, gypsum and talc are present.

This is congruent with the ash content that was measured according to TAPPI T 211 om-02 and measured upon charring at 525°C for the unburnt unsized RPM only (average ash content= 2.211 ± 0.077).

Gelatin-sized RPM sample looks very similar to the unsized one – which is expected, being non-crystalline gelatin the only added compounds – and crystalline cellulose peaks are clearly identified. Crystalline peaks related to calcium carbonate and talc, compounds which were part of the sheet composition, are also detected (Fig. 3.29).

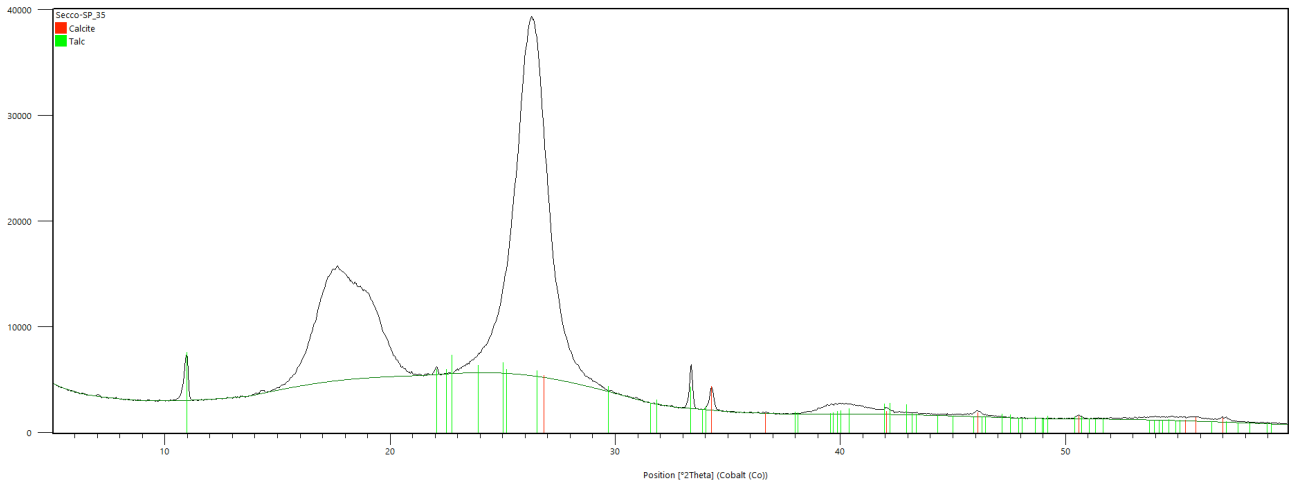

Figure 3.29. Sized RPM paper, XRD difractogram, very similar to the one in Fig. 3.27 (unsized RPM sample) and to the XRD pattern of the Chartres manuscript in Fig. 3.28.

4. SEM/EDS investigation of the burnt paper samples

SEM observations of 5 unsized and 5 sized RPM paper samples burnt by hot plate at 250° for 15' were carried out directly on the paper with the same equipment and in the same experimental conditions already used for the characterization of the historical papers (Chapter 2, § 4.2.2).

The surface morphology of unsized RPM samples was observed mapping several fibrous areas as well as some inclusions, as shown in Fig. 3.30. Long fibers are still clearly visible. They have different diameters and are morphologically still well individualized. A preferential orientation and very small white inclusions are also visible. The most significative analyses of the several points investigated are here proposed.

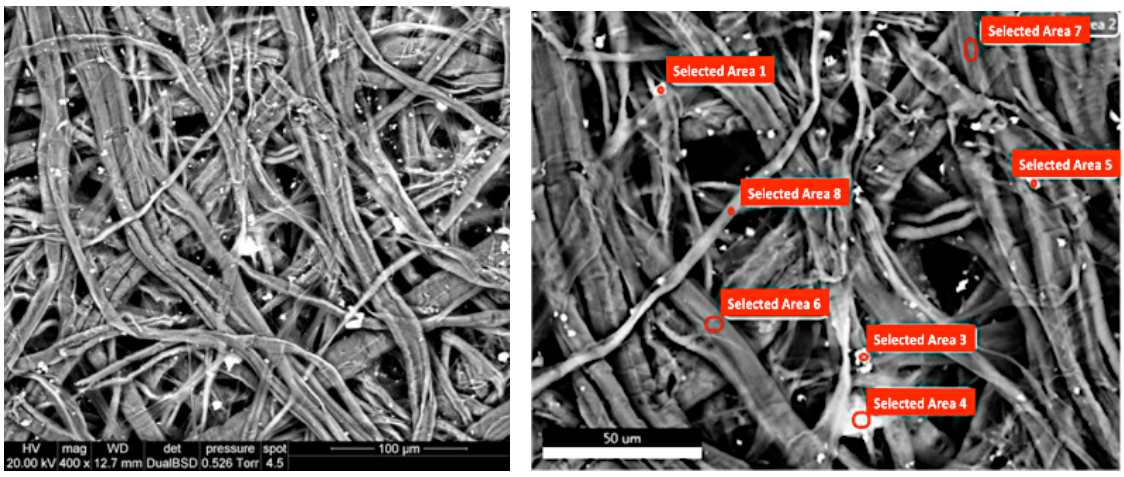

Figure 3.30. Unsized RPM sample, surface. SEM image (left) and areas investigated with EDS (right).

The representative spectrum of a point on a fibre is shown in Fig. 3.31 and semi-quantitative estimation of elements weight percentages are in Table 3.9.

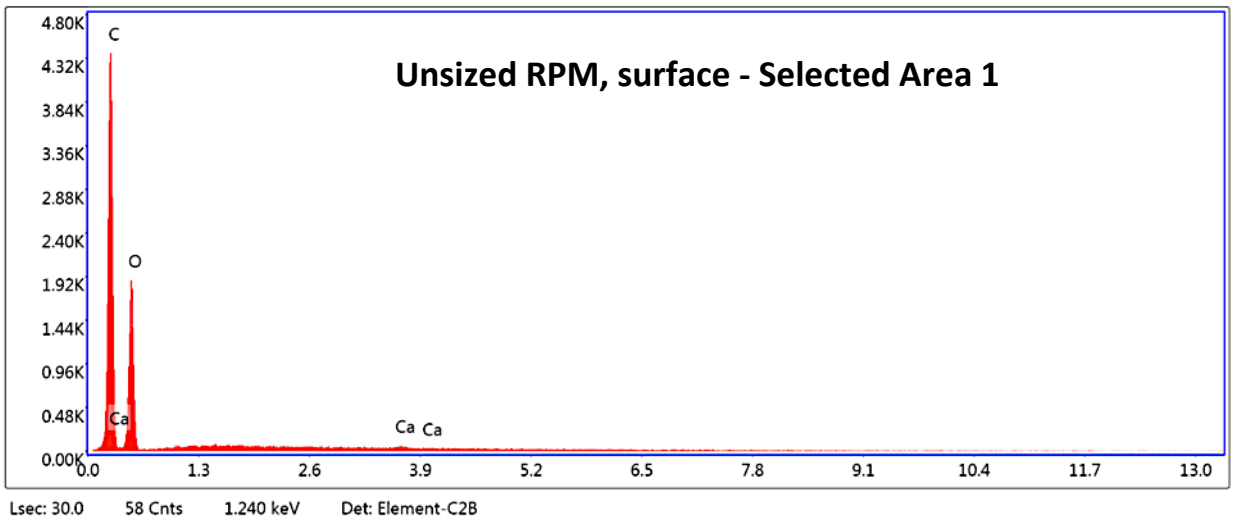

Figure 3.31. Unsized RPM sample, surface. Representative spectrum of a point on a fibre.

Table 3.9. Unsized RPM sample, surface. Estimation of elements weight percentages on a point on a fibre.

Selected Area 1 **eZAF Smart Quant Results**

Element	Weight %	Atomic %	Net Int.	Error %	Kratio	Z	A	F
C K	59.3	66.5	617.7	5.1	0.4016	1.0195	0.6642	1.0000
O K	39.3	33.1	190.6	11.0	0.0710	0.9741	0.1855	1.0000
CaK	1.4	0.5	19.8	17.7	0.0127	0.8325	1.0291	1.0403

The points consist of cellulose (98.6%, that is 59.3% C and 39.3% O) and calcium, which relates to the presence of calcium carbonate as evidenced by XRPD analysis (§ 3.5 in this chapter).

In the Selected Areas 2 calcium was also found. Since in calcium carbonate the theoretical percentage of Ca, C and O should be 40%, 12% and 46%, respectively, the lower amount of C in the Area 2 with respect to the cellulosic areas is indicative of a region enriched in calcium carbonate (Fig. 3.32, Table 3.10).

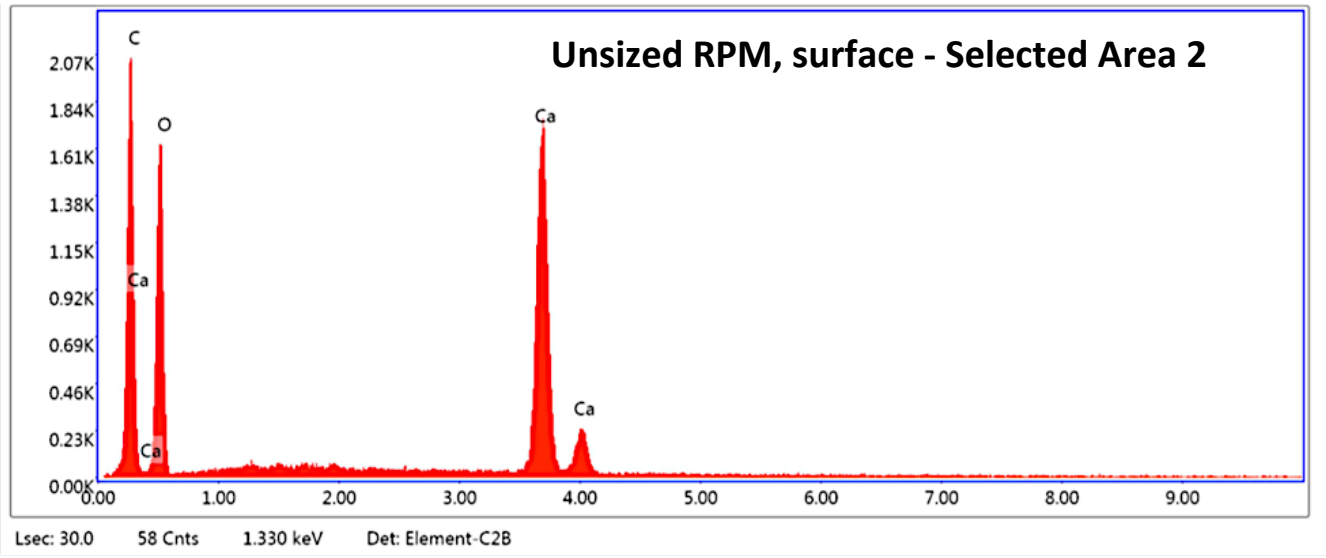

Figure 3.32. Unsized RPM sample, surface, Selected Area 2, EDX spectrum.

Table 3.10. Unsized RPM sample, surface, Selected Area 2. Semi-quantitative estimation of elements weight percentages.

Selected Area 2 eZAF Smart Quant Results

Element	Weight %	Atomic %	Net Int.	Error %	Kratio	Z	A	F
C K	27.1	38.7	433.1	6.7	0.1528	1.0652	0.5284	1.0000
O K	46.8	50.1	376.6	10.6	0.0761	1.0201	0.1594	1.0000
CaK	26.1	11.2	672.0	2.3	0.2339	0.8767	1.0159	1.0059

In case of the Selected Area 4, the presence of Mg and Si in the SEM-EDS analysis (Fig. 3.33, Table 3.11) suggests that the inclusion observed in the Area 4 is probably talc (magnesium silicate, MgO_3Si), which confirms the identification made by XRPD analyses (§ 3.5 in this chapter).

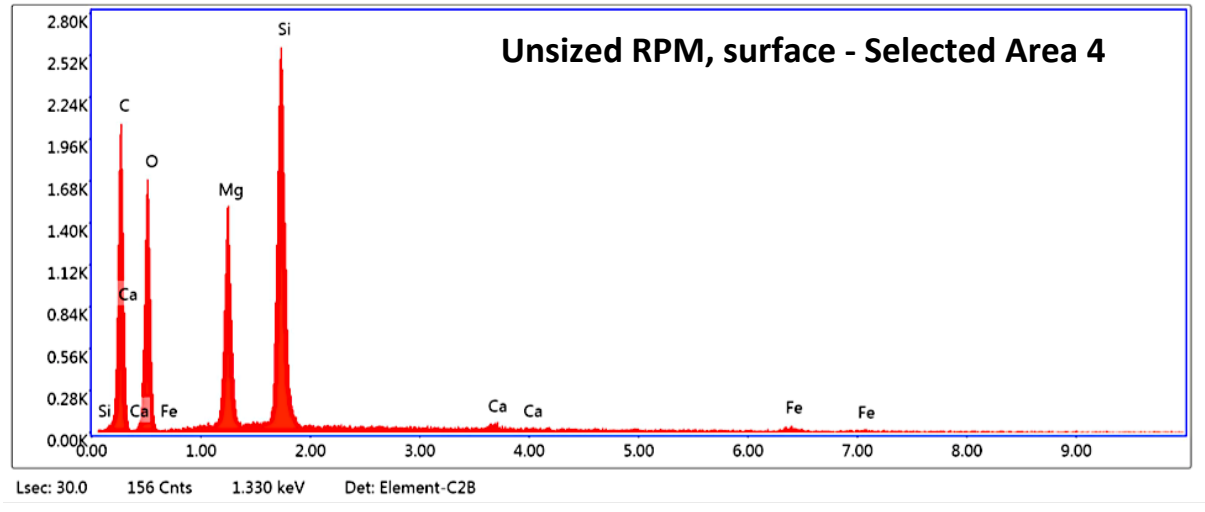

Figure 3.33. Unsized RPM sample. Representative spectrum of an area rich in inclusions.

Table 3.11. Unsized RPM sample, surface. Estimation of elements weight percentages. The large amount of Mg and Si are indicative of an inclusion, probably a talc particle.

Selected Area 4 eZAF Smart Quant Results

Element	Weight %	Atomic %	Net Int.	Error %	Kratio	Z	A	F
C K	46.6	58.6	439.4	9.4	0.1248	1.0426	0.2570	1.0000
O K	30.1	28.4	369.3	10.2	0.0601	0.9971	0.2007	1.0000
MgK	8.6	5.3	392.4	5.5	0.0521	0.9203	0.6582	1.0036
SiK	13.6	7.3	757.6	3.7	0.1008	0.9054	0.8142	1.0021
CaK	0.6	0.2	17.5	20.4	0.0049	0.8541	0.9913	1.0242
FeK	0.6	0.2	10.3	29.6	0.0050	0.7609	1.0142	1.1215

Additionally to the surface examination, cross sections examinations of the burnt samples were also made. In the cross section of the unsized sample, the fibrous material is rarefied, and large empty spaces appear between fibres (Fig. 3.34).

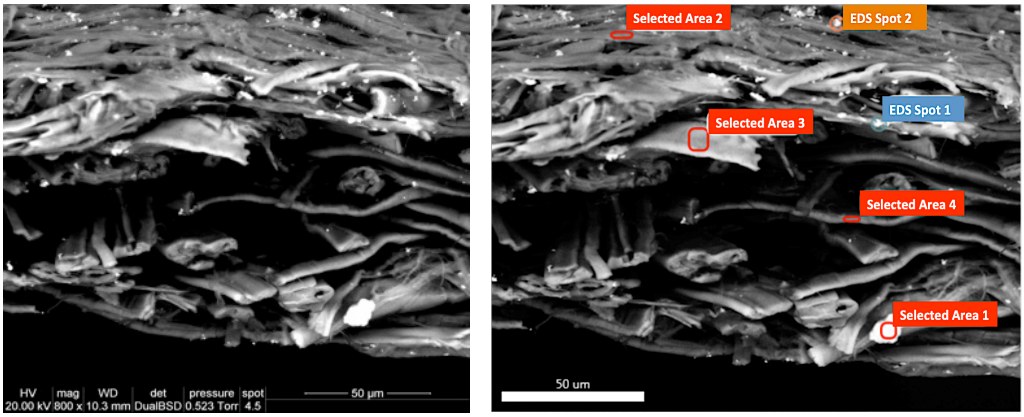

Figure 3.34. Unsized RPM sample, cross section. SEM image (left) and areas investigated (right).

C average amount and O average amount constitute about the 90% of the total weight and the EDS spectra are close to those already examined for the sample surface.

As already observed on the surface images, the white particles in Selected Area 1, Spot 1 and Spot 2 are calcium carbonate, whose representative spectrum is given for the only Selected Area 1 in Fig. 3.35 and the element analyses in Table 3.12.

Talc was not detected in the cross sections of the unsized samples.

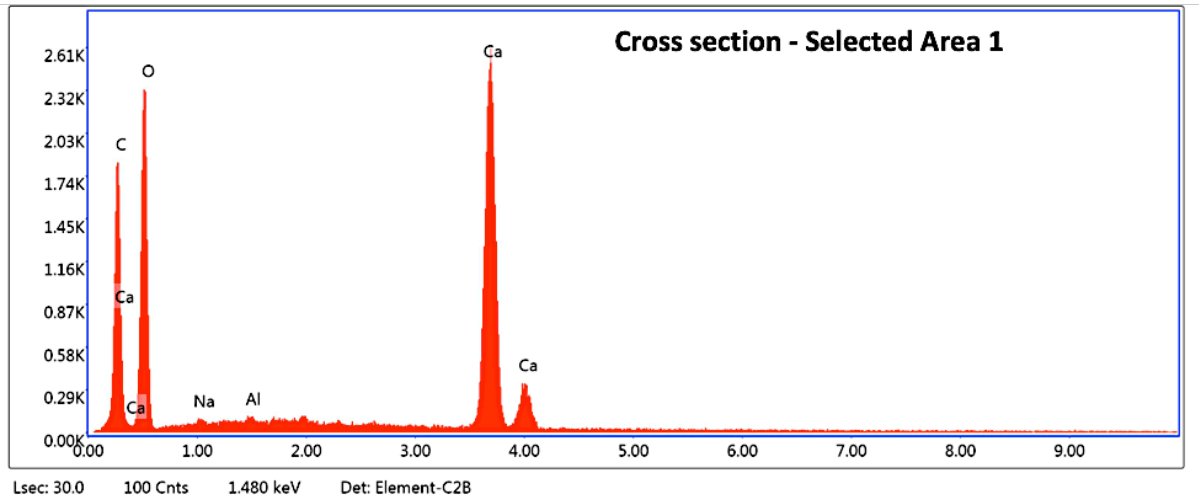

Figure 3.35. Unsized RPM sample, cross section. Analysis of the selected Area 1, an inclusion composed of calcium.

Table 3.12. Unsized RPM sample, cross section. Selected Area 1, estimation of elements weight percentages: calcium is present in large amount.

			Selected Area 1	**eZAF Smart Quant Results**				
Element	Weight %	Atomic %	Net Int.	Error %	Kratio	Z	A	F
C K	20.7	30.4	372.6	7.3	0.1071	1.0702	0.4838	1.0000
O K	51.9	57.3	528.5	10.3	0.0824	1.0250	0.1550	1.0000
NaK	0.3	0.3	6.6	45.7	0.0010	0.9317	0.3079	1.0012
AlK	0.1	0.1	5.5	64.6	0.0007	0.9128	0.6209	1.0043
CaK	27.0	11.9	979.2	2.0	0.2427	0.8812	1.0158	1.0057

The SEM images of sized samples show that the fibres network is better structured than in the unsized paper: the different morphology of linen (yellow arrow) and hemp (red arrow) could be observed (Fig. 3.36). Compared to unsized samples (Fig. 3.30), sizing allowed the fiber network to retain a more compact aspect despite the burning C average amount is 46.3% while O average amount is 40.7%; about 87% of the sample is composed by these elements, indicative of cellulose as main component.

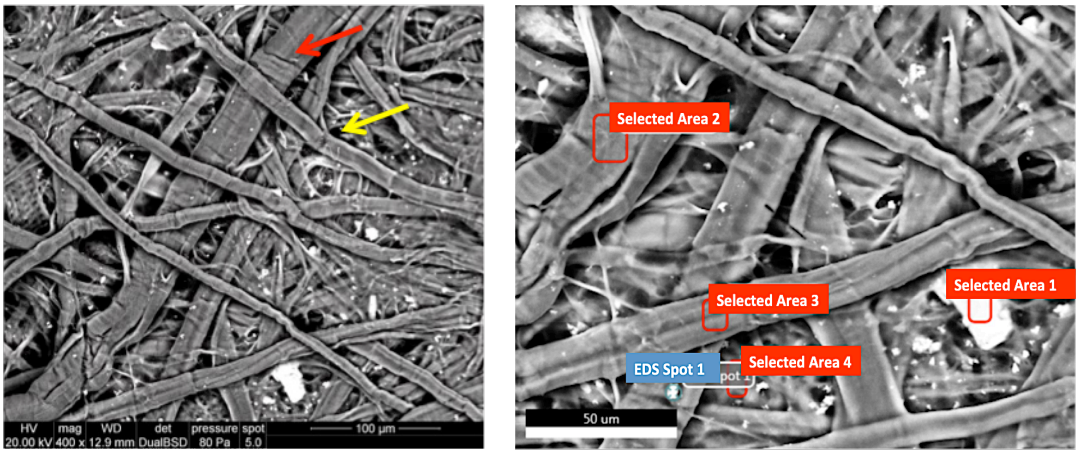

Figure 3.36. Sized RPM sample, surface. SEM image (left) and areas investigated (right).

Talc is also present together with calcium carbonate (Fig. 3.37, Table 3.13), as already observed in the unsized RPM paper and verified by XRPD (§ 3.5 in this chapter).

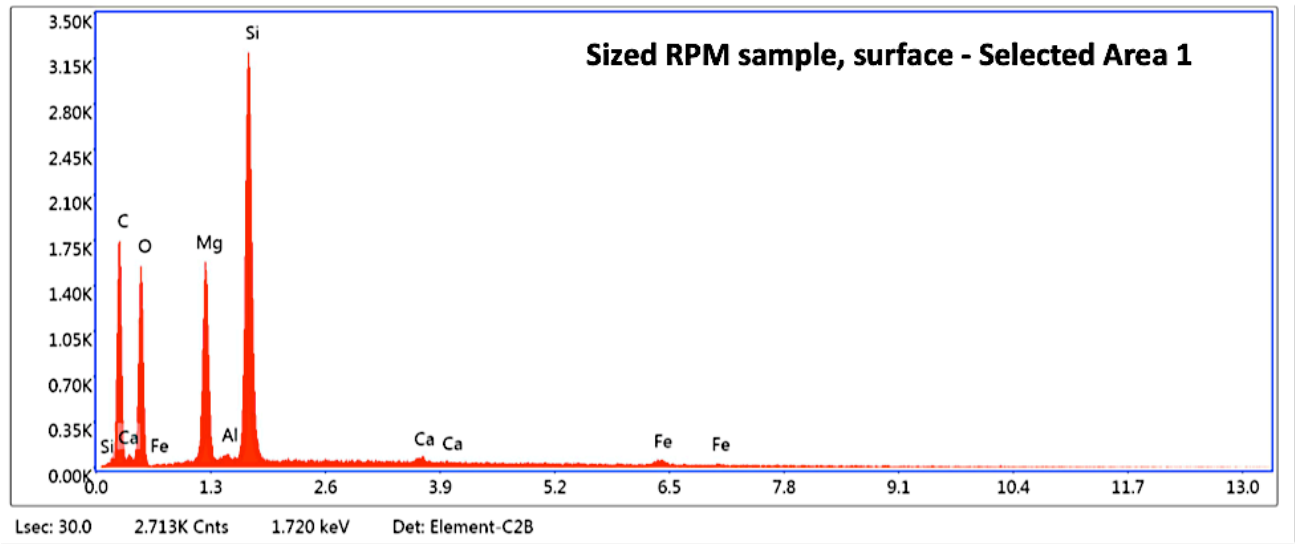

Figure 3.37. Sized RPM sample, surface. Analysis of the selected Area 1, a talc inclusion.

Table 3.13. Sized RPM sample, surface. Selected Area 1, corresponding to a talc inclusion.

Selected Area 1 eZAF Smart Quant Results

Element	Weight %	Atomic %	Net Int.	Error %	Kratio	Z	A	F
C K	43.5	56.8	341.6	10.0	0.1004	1.0505	0.2199	1.0000
O K	26.8	26.3	320.8	10.2	0.0542	1.0050	0.2010	1.0000
MgK	9.3	6.0	419.2	5.5	0.0579	0.9280	0.6689	1.0037
AlK	0.4	0.3	20.2	22.0	0.0028	0.8935	0.7009	1.0068
SiK	17.7	9.9	944.7	3.6	0.1309	0.9130	0.8088	1.0019
CaK	1.1	0.4	31.7	12.7	0.0093	0.8615	0.9814	1.0216
FeK	1.2	0.3	20.3	20.1	0.0103	0.7677	1.0116	1.0966

Similarly, the cross section of the sample shows a large disruption of the fiber bed, but it is usually denser and more compact compared to the morphology of the unsized burnt paper (Fig. 3.38).

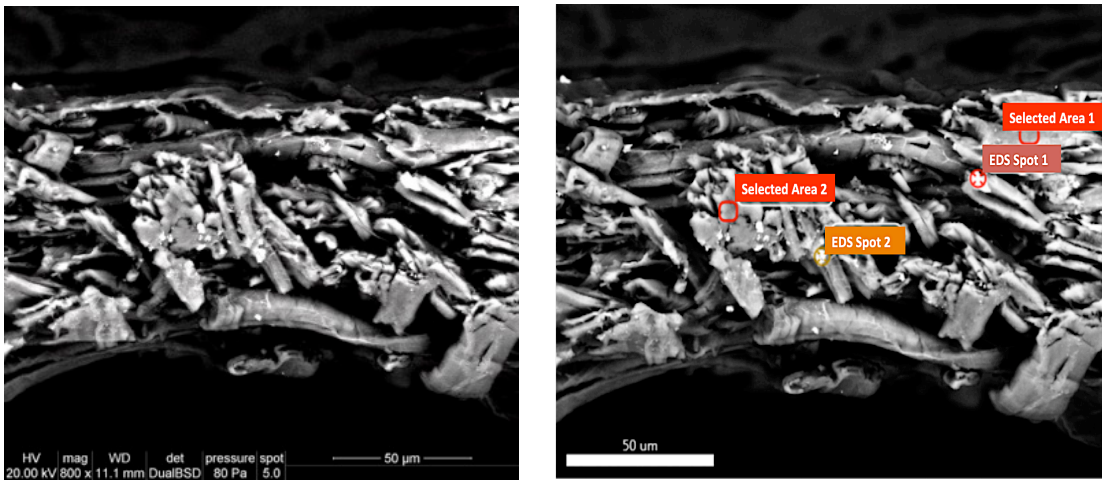

Figure 3.38. Sized RPM sample, cross section. SEM image (left) and areas investigated (right).

On the Selected Area 2, representative of the fibrous matter (Fig. 3.39), an amount of 54.9% for C and of 44.6% for O was detected, indicating that 99.4% is composed of cellulose; the remaining is calcium (Table 3.14).

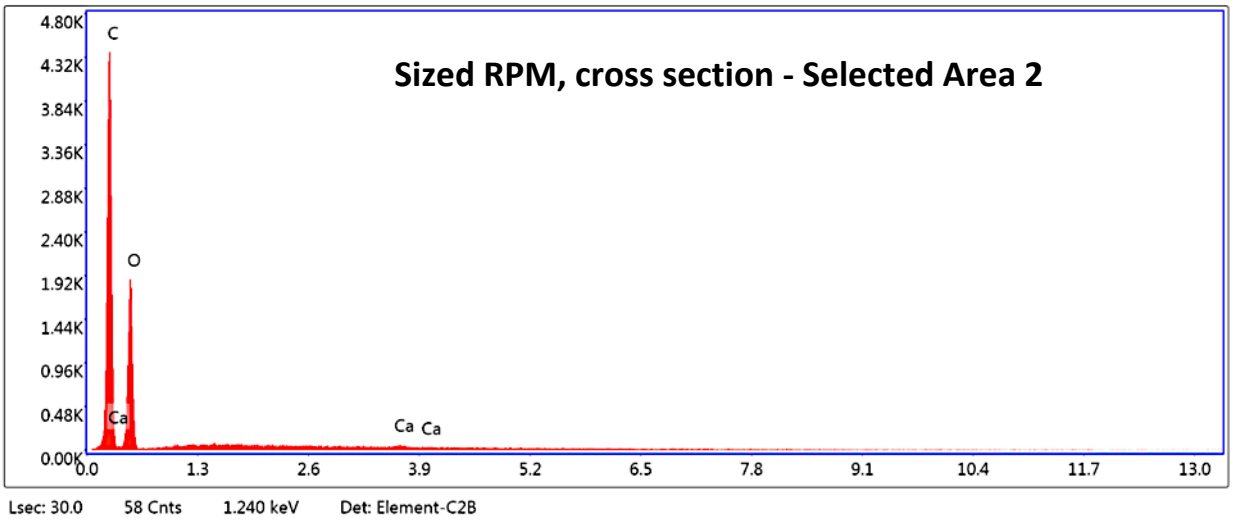

Figure 3.39. Sized RPM sample, cross section. Analysis of the selected Area 2, on a fibre.

Table 3.14. Sized RPM sample, cross section. Selected Area 2 corresponding to a fibre.

Selected Area 2 eZAF Smart Quant Results

Element	Weight %	Atomic %	Net Int.	Error %	Kratio	Z	A	F
C K	54.9	62.0	940.2	5.3	0.3518	1.0206	0.6281	1.0000
O K	44.6	37.8	404.5	10.3	0.0839	0.9751	0.1930	1.0000
CaK	0.6	0.2	15.1	25.0	0.0051	0.8333	1.0308	1.0464

5. Conclusions

Samples for the experimental part of this research were produced with a handmade paper (RPM paper) composed of hemp and linen fibres and buffered with calcium carbonate, in thus reproducing some of the main features of the historical paper dated to 13^{th}-19^{th} century. Part of the samples were sized with gelatine, in consideration of the role played by this protein sizing as waterproofing and of its influence on the physical and chemical qualities of the paper. Further tests involved therefore both unsized and sized samples.

Several burning procedures were carried out to develop the method that best fulfilled the conditions of reproducibility of samples, burning uniformity and formation of charred areas in which degradation induced by carbonization were comparable to those of the historic paper from the Chartres manuscript and from the Padua incunabulum investigated in Chapter 2. On the burnt samples the same analyses were performed (pH measure, infrared analyses ATR-FTIR, UV-VIS spectroscopic analysis, X-ray Powder Diffraction and SEM/EDS) to assess physico-chemical changes incurred in paper upon burning.

Chemically induced burning was obtained by treating the RPM samples with sulfuric acid and heat. This was a time-saving procedure achieving uniformly degraded paper. However, on the basis of pH and ATR-IR results, the degradation effects produced on cellulose were found to be quite dissimilar from the real ones. This procedure was therefore ruled out.

Combustion with heat alone was achieved, either by using a hot air gun or by exposing the paper to live flames. This method took longer but allowed more similar cellulose decay results to those observed in fire-damaged historical papers. However, the burnt areas were very heterogeneous, and the procedures did not guarantee reproducibility. Moreover, in the burning with live flame the risk of paper fragmentation with the loss of part of the sample was verified and such defects led to discard also these methods.

Finally, burning on a hot plate was tested at different plate temperature (185°C, 210°C, 250°C, 310°C) and for different burning time (30 and 15 minutes) and the evolution of the paper combustion process was especially investigated by ATR-FT.

Hot plate burning at 310°C for 15 minutes resulted in a very severe paper degradation advancing the destruction of the cellulose fibres, but the lower temperature of 250°C and a time of 15 minutes could grant a uniform charring of the paper, which was brittle but with cellulose fibres

still persisting and detectable. A “cellulose-like” behaviour of these samples was also confirmed by the hysteresis of the burnt areas of both unsized and sized samples, despite the paper hydrophobicity were enhanced by carbonization.

Burning unsized and sized RPM paper on a hot plate (250°C for 15 minutes) was therefore adopted as the procedure to obtain paper samples to be used in the experimental part, dedicated to the development of a reinforcement treatment for the charred paper, as will be presented in the following chapters.

Chapter 3 | References

Ahn K., Schedl, A., Zweckmair, T., Rosenau, T., Potthast, A. (2018). «Fire-induced structural changes and long-term stability of burned historical rag papers». *Scientific Reports*, 8, 12036; https://doi.org/10.1038/s41598-018-30424-7

Kim, DY., Nishiyama, Y., Wada, M., Kuga, S. (2001). «High-yield Carbonization of Cellulose by Sulfuric Acid Impregnation». *Cellulose,* 8, 29-33; https://doi.org/10.1023/A:1016621103245.

GMIA, Gelatin Manufacturers Institute of America (2012). *Gelatin Handbook*; http://www.gelatin-gmia.com/uploads/1/1/8/4/118450438/gmia_gelatin_manual_2019.pdf

Hirata, T. (1985), *Pyrolisis in cellulose, an introduction to the literature.* U.S. Department of Commerce, National Bureau of Standards.

Molton P. M., Demmit T.F. (1977). *Reaction Mechanisms in Cellulose Pyrolysis. A Literature Review*. Battelle, Pacific Northwest Laboratories. Richland, Washington.

Shen, D., Xiao, R., Gu, S. & Luo, K. **«**The pyrolytic behavior of cellulose in lignocellulosic biomass: a review**»**. *RSC Advances* **1**, 1641–1660.

Suzuki, M., Dobashi, R., Hirano, T. (1992). «Burning process of cellulosic fibers composing filter paper during flame spread**»**. *Fire Safety Science 1,* 499-504.

Tamburin, M. (2009). *Le gelatine animali. Tecnologia di produzione e caratteristiche igienico-sanitarie*. Thesis, University of Padua, a.a.2008-2009; http://tesi.cab.unipd.it/21620/1/TESI_Tamburin_Marta.pdf

TAPPI T 509 om-11 (2011). Hydrogen ion concentration (pH) of paper extracts (cold extraction method). *TAPPI test method.* Technical Association of the Pulp and Paper Industry. TAPPI press, Atlanta, US.

TAPPI T 230 om-99 (1999). Viscosity of pulp (capillary viscometer method). *TAPPI test method.*Technical Association of the Pulp and Paper Industry. TAPPI press, Atlanta, US.

TAPPI 412 om-11 (2011). Moisture in pulp, paper and paperboard. *TAPPI test method.* Technical Association of the Pulp and Paper Industry. TAPPI press, Atlanta, US.

Völkel, L., Beaumont, M., Czibula, C., Rusakov, D., Mautner, A., Teichert, C., Kontturi, E., Rosenau, T., Potthast, A. (2022). «Assessing Fire-Damage in Historical Papers and Alleviating Damage with Soft Cellulose Nanofibers». Small, 18, 2105420, 1-14; https://doi.org/10.1002/smll.202105420

Chapter 4

Nanostructured materials in cultural heritage conservation

1. Introduction to nanomaterials and nanotechnology

Nanostructured materials are substances composed by particles of size less than 0.1 μm, that can occur in nature, can be created in chemical reactions (e.g., combustion process), or produced through engineering and aimed at performing a specialized function. They have been used in human artefacts since prehistoric times, even if men were not fully aware of the peculiar chemical, mechanical and optical properties conferred by their very small size and shape-related characteristics.

The prefix ‘nano' comes from the ancient Greek word νάνος, which means 'very small', and nanomaterials have at least one dimension < 100 nanometres (1 nanometre = 10^{-9} metres, 1 billionth of a metre according to the International System of Units). Only the application of microscopic techniques – first through the electron microscope, which has been used since the late 1930s and progressively implemented to investigate individual atoms and the bonds that make up matter – has made it possible to identify the presence of nanoparticles in historical pigments, dyes, clay minerals, metal artefacts and ceramics, testifying to their widespread use in the distant past. [Bayda et al 2019; Barhoum et al 2022].

If the terms “nanometre” and “nanomaterial” were introduced at the beginning of the 20th century to define very small particle sizes [Nunes et al. 2019], it was 1959 when the American physicist and Nobel Prize Richard Feynman expressed his conceptual vision of the accrued benefits that might arise in manipulating and controlling the matter on a very reduced scale, even at the atomic scale, in arranging the molecular structure of materials to change their intrinsic properties and obtain others with revolutionary applications [Feynman 1959].

Nanoparticles possess in fact unique physical and chemical properties due to their minimal size and large surface-to-volume ratio that significantly affect their optical, physical and chemical properties, profoundly different from the original features of their larger material counterparts (Fig. 4.1).

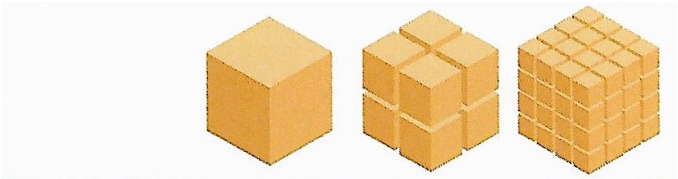

Edge length	4	2	1
Total surface area	96	192	384
Total volume	64	64	64
Surface-to-volume ratio	1.5	3	6

Figure 4.1. Large materials divided into nanoparticles result in surface-to-volume ratio increasing while total volume remains constant, as clear from this model cubic mass divided in sub-units. Reproduced from Baglioni et al. 2015, p. 3.

Today we currently refer to nanoscience as a multidisciplinary domain that studies phenomena on a miniaturised scale, and to nanotechnology as the ability to manipulate, assemble, control and manufacture matter on a nanoscale with emerging utility in various fields. Widespread international interest in nanotechnology has grown since the 2000s, not only in terms of scientific research but also as a booming economic sector in many large-scale commercial and domestic applications. In the last two decades, nanostructured materials have been synthesized for application in a variety of fields, from chemistry to biomedical engineering, electronic development, food packaging and preservation, innovative textiles, renewable energy production and environmental protection, to name but a few of the best-known fields. [Whatmore 2006; Bayda et al 2019; Barhoum et al 2022].

The rapid expansion of nanotechnology and of nanomaterial production has also led to a focus on the impact that these new materials may have on humans, animals, plants, and the environment (soil and aquatic systems), in terms of risk for inhalation, ingestion and/or contact with nanoparticles and/or any of their residues. Increasing research efforts and economic resources are being investigated in green synthesis methods and in environmentally friendly production processes for obtaining smaller, stable and safe nanoparticles [Jeevanandam et al 2018; Barhoum et al 2022].

In this perspective, the European Commission promoted the communication “Towards a European Strategy for Nanotechnology” in 2004 and in 2008 released the “Code of conduct for responsible nanosciences and nanotechnologies research”. Moreover, in absence of a standard international method for nanomaterials toxicological assessment, nanomaterials are subjected in Europe to the same regulation concerning the registration, evaluation, authorisation and restriction of

chemicals: REACH, issued in 2006 by the European Parliament (regulation No 1907/2006) [Nunes et al. 2019].

2. Nanotechnology contribution in paper conservation treatments

In the last two decades, nanotechnology has provided an important contribution also in cultural heritage conservation by developing new products and innovative methodologies that allow one to overcome some of the limits of traditional interventions. They are already successfully applied to contrast degradation of different kind of artefacts, from stone and wall painting to cellulose-based materials such as canvas, wood and paper [Chelazzi et al. 2013; Baglioni and Chelazzi 2013; Baglioni et al. 2015; David et al. 2020].

Of particularly great impact in the field of paper conservation has been the introduction of cleaning systems based on nanostructured fluids (micelles and microemulsions) that can be confined in chemical gels and used in localized treatments for removing dust, softening aged detrimental adhesives or materials of previous intervention also from water-sensitive paper artifacts [Domingues et al 2013; Domingues et al. 2014; Baglioni et al. 2013 and 2015; Mirabile et al. 2020]. Based on a three-dimensional network of covalent bonds, chemical gels are carriers with a high retention capacity, resulting in a very slow release of the fluids they are loaded with. They guarantee wettability while the cleaning agent does not diffuse in the paper matrix, the solubilised material to be removed does not tend to redeposit on the surface of the artefact and the side effects that frequently occur when using free solvents (i.e., non-selective penetration of the solvent into the porous matrix of the paper, swelling of the paper fibres, formation of halos and tidelines) are avoided or, at least, very limited. Structured in rigid or more flexible forms, these gels can adequately adapt to the morphology of the artefact, working in direct contact with the paper surface without leaving residues after treatment. For their part, the size of the nanoparticles allows good progressive and controlled penetration of the detergent, while their large interaction surface makes it possible to limit the amount of product required to carry out an effective treatment.

The use of nanoparticles of calcium hydroxide $Ca(OH)_2$ dispersed in alcohols such as ethanol or isopropanol represents a second important innovative tool in paper conservation. Similarly as the regular particle size $Ca(OH)_2$ it is aimed to counteract acid degradation in cellulose-based artifacts, at the same time preventing future acidification processes, especially due to the intrinsic artifact composition and/or to the presence of unstable elements in the writing media, as in the case of

iron gall inks used in manuscripts until the 19th century [Giorgi et al 2002; Giorgi et al. 2005; Poggi et al. 2010; Poggi et al. 2011; Poggi et al. 2014].

Calcium carbonate was usually involved in the manufacture of historical paper: lime was added to enhance the rags maceration and precipitates and accumulates between the fibres in the form of calcium carbonate, due to reaction with air CO_2. Employing calcium hydroxide to neutralize the impending acidity and to grant a long-term buffer capacity is therefore a choice fully congruent and compatible with the nature of historical pre-industrial papers. Neverthless, the traditional formulation of calcium hydroxide in semi-saturated aqueous solution cannot be recommended because the strong alkalinity of the compound can lead to an excessive rise in pH and induce alkaline degradation processes in the cellulose as well as variations in ink tonality [Stephens et al. 2009]. Calcium hydroxide nanoparticle dispersions in alcohols present some advantages over the application of saturated aqueous solutions, avoiding the use of the water, which is more polar and is more prone to induce solubilization of writing/drawing media as well as migration of metallic ions such as iron in the inks, thereby catalysing paper degradation processes. Compared to the traditional calcium hydroxide particles, present in the saturated solutions, nanoparticles allow a more homogeneous distribution and penetration within the paper matrix and, given their higher specific surface, they are better exposed to the reaction with carbon dioxide from the air to form calcium carbonate on the paper fibers. Deacidification treatment can be carried out in progressive steps by brushing or (better) spraying up to reach a pH value (usually pH 7.5-8, verified also after complete carbonatation of the nanoparticles) that ensures the neutralization of acidity and the formation of an alkaline reservoir limiting the risk of alkaline degradation reactions.

In the last years, a large and growing interest has been given to nanocellulose – nanoparticles obtained from very pure cellulose fibers – involving the use of nanocelluloses of different origin, crystallinity, and aspect ratio, as a very promising material in paper conservation. Nanocellulose films made from a water-based gel of cellulose microfibrils have been tested and employed in the mending of translucent supports of a wide range of graphic, photographic, and cinematographic objects [Dreyfuss-Deseigne 2017a; Dreyfuss-Deseigne 2017b] or for lining degraded paper areas with the aim to recover part of the lost paper physical-mechanical properties [Santos et al. 2015a, Santos et al. 2015b]. It is a very promising coating technique due to the ability of nanocellulose to form a film with very high tensile strength while maintaining good transparency (Klemm et al. 2011).

In both cases, ‘nanocellulose paper’ (paper films entirely composed of pure nanofibers) offers an advanced-quality alternative – more transparent and highly resistant – to the well-known long-fibers and very thin Japanese, Chinese or Korean papers employed in conservation treatments. It is however worth to note that the application of nanocellulose films for mending or lining has been so far carried out in a very traditional method, employing alcohol-based or water-based adhesives.

Only the most recent studies have focused on applying nanocellulose in aqueous dispersions, directly brushed onto degraded paper areas as an adhesive-free reinforcement coating [Völkel et al. 2017; Operamolla et al. 2021] or even as a mending material for tears and filling in losses [Völkel et al. 2017]. Ethanol-based “hybrids”, composed of stable dispersions of alkaline $Ca(OH)_2$ nanoparticles and nanocrystalline cellulose (CNC), have been tested to improve paper strengthening in addition to a deacidification effect [Xu et al. 2020]. To this aim, nanocellulose structure has been chemically modified and grafted with oleic acid increasing nanoparticles dispersibility in organic solvents and the paper samples have been treated by brush with the liquid formulation.

The most recent and most closely related study on the subject is the application of aqueous nanocellulose suspensions on burnt papers from historical printed collections. According to these experiments, bacterial nanocellulose, applied with an airbrush to the charred areas of the leaves, acts as a coating and reinforcing film, with a surface veiling and much reduced optical interference compared to that caused using more conventional materials as Japanese papers [Völkel et al. 2022].

From the point of view of the book and paper conservator, the unquestionable advantage in relying on advanced nanostructured materials is that they can significantly reduce the invasiveness of the intervention: localised cleaning, deacidification and consolidation make it possible to limit the intervention to the paper areas that are in need for it. In case of bound leaves, it means to avoid unsewing and unbinding a book for treating individual paper sheets or *bifolios*, working *in situ* in the respect of the historical, polymateric structure of the artefacts. Moreover, the physico-chemical compatibility of nanoparticles together with their high reactivity and effectiveness reduces the quantity of products/materials required for counteracting degradation phenomena compared to traditionally formulated materials. As a result, the original, intrinsic composition of the artefact is minimally altered, thus safeguarding as far as possible its authenticity, which is the deontological core of cultural heritage. The formulations can be gradually applied – keeping a constant control of their actual effects on the originals – and eventually repeated. A lower

quantity of products involved in the treatment leads also to a minor health risk and environmental impact: ecological advantages are also considered in conservation treatments, especially in the perspective to treat historical artifacts *in loco*, in the library/archive where they are held, therefore avoiding them the stress and risks caused by handling, moving and changes in environmental conditions.

3. Nanocomposites in the present research

The innovative perspectives offered by nanostructured materials have been the basis of the present research with a particular interest to the role of nanocellulose in the formation of polymer nanocomposites, i.e. polymers embedding low content of well-dispersed nanofillers aimed to improve many properties of the hybrid material [Siqueira et al., 2010; Moon et al. 2011; Dufresne 2017, Dufresne 2018; Trache et al. 2020].

In this research work, the application of nanocomposites based on nanocellulose dispersed in polysilicates has been studied and developed to treat the areas of historical papers damaged in blaze. As assessed in Chapter 3 and corroborated by Ahn et al 2018 and by Völkel et al. 2022, the fragility of burnt areas is a result of complex chemical degradation processes triggered by fire, including paper oxidation, chain cleavage, crosslinking, and carbonization. This latter leads to the progressive disintegration of cellulose fibers and to the formation of char.

Charred areas are lighter than the adjacent, unburnt paper areas, lack in cohesion due to the effect of heat and fire and also a minimal vibration can cause their fragmentation, as they cannot absorb the energy introduced by mechanical stress. The more severe the effect of the burning process, the more the paper is liable to break at the slightest bending or even “up and down” flexing of the leaf.

Complete carbonization means total destruction of cellulose, transformed to carbon and in this extreme situation charred fragments are usually no longer cohesive to the sheet, as they do not retain any flexibility nor the elastic property of cellulose, that is the ability to bend without cracking and to resist a distorting stress force returning to the original size and shape when that force is removed.

On the other hand, in the charred areas still *in situ* on burnt sheets, chemical and physical investigation can detect the presence of persisting cellulose fibers, however degraded, as verified in the study of the papers from the Chartres manuscript and the Padua incunabulum (§ Chapter 2),

where IR spectroscopy indicated the presence of residual cellulose structures, albeit degraded, and microscopic observations by SEM highlighted poor fiber density and cohesion, with large gaps between the fibers.

For these and similar cases, the present research has focused on the ability of nanocellulose to enter the paper matrix and to establish chemical interactions with the weakened fibres, acting as a structural agent that can stabilize and partly restore paper mechanical performances.

The simultaneous or subsequent application of polysilicates will be intended to coat the charred area with a thin, elastic film, increasing the immediate and long-term mechanical strength of severely damaged areas of paper while providing transparency, so not to interfere with the readability of the text – both manuscript and printed text – still present on the charred areas of historic papers.

It is worth remembering that the aim of the present research was to develop a conservation treatment for reinforcing burnt areas of historical handwritten/printed paper so to secure their preservation thus allowing scholars to access and researchers to digitally reproduce information born on the paper (text, drawing, etc.). Great importance was given to the possibility of setting up materials and methods that would allow the conservation treatment to be carried out *in situ*, directly in libraries and archives where the historical written heritage is kept.

3.1 Nanocellulose

Among nanomaterials, nanocellulose is considered one of the most promising ecological, renewable and sustainable biobased resources, modifiable in its chemical functionalities to fulfill a wide range of innovative biomedical, pharmaceutical, industrial and technological applications. [Klemm et al. 2006, Dufresne 2013, Trache 2018, Foster et al. 2018, Bakarova et al 2019, Thomas 2018].

Commitment in nanocellulose production and use has grown steadily over the last three decades and in particular in the last years, according to the increasing number of research and scientific articles published on the topic (compared to 2015-16 in 2021-22 the increase is tenfold) and to the activity developed by well-known international organizations, i. e. the International Organization for Standardization (ISO) and the Technical Association of the Pulp and Paper Industry (TAPPI) in the definition and dissemination of standards in nanocellulose development and in nanocellulose nomenclature [Dufresne, 2017; Klemm et al., 2018, Trache et al. 2020].

In the paper industry, nanocellulose is in use as nanofiller for paper coating improving the printing properties, as reinforcing agent for packages, or even added to paper pulp before sheet formation. As previously highlighted, an outstanding interest in the potential of cellulose nanoparticles has arisen also in the field of cultural heritage conservation.

Cellulose nanoparticles have an average length of few hundred nanometres and the width in the order of few nanometres, depending on the cellulose sources and production process. They can derive either from bacteria (bacterial or microbial nanocellulose) or from plant sources (cellulose nanofibrils and cellulose nanocrystals).

The production of bacterial nanocellulose (BNC) is a bottom-up process, where cellulose is biosynthesized from glucose by specific types of bacteria. BNC nanofibers are usually 20-100 nm in diameter and micrometers in length; they are extremely pure and ultrafine, have high cristallinity and high elastic modulus [Lavoine et al 2012, Trache 2018]. They are suitable to produce three-dimensional networks and are expecially appreciated in medical implants, skin tissue and bone engineering, just to mention a few major applications. On the other hand, the synthesis of BNC remains so far the most expensive process in the field of nanocellulose production [Trache 2018, Reshmi et al. 2021].

Like BNC, microfibrillated cellulose (MFC) and crystalline nanocellulose (CNC) consist of pure cellulose, but they are extracted from natural fibers, where the hierarchical and multi-level organization of native cellulose fibers includes these two different kinds of nanoscaled cellulosic structures (Fig. 4.2); alkaline and bleaching pre-treatments are used to eliminate hemicelluloses and lignin, as well as other extracts eventually present in the raw source [Siqueira 2010; Trache et al. 2020].

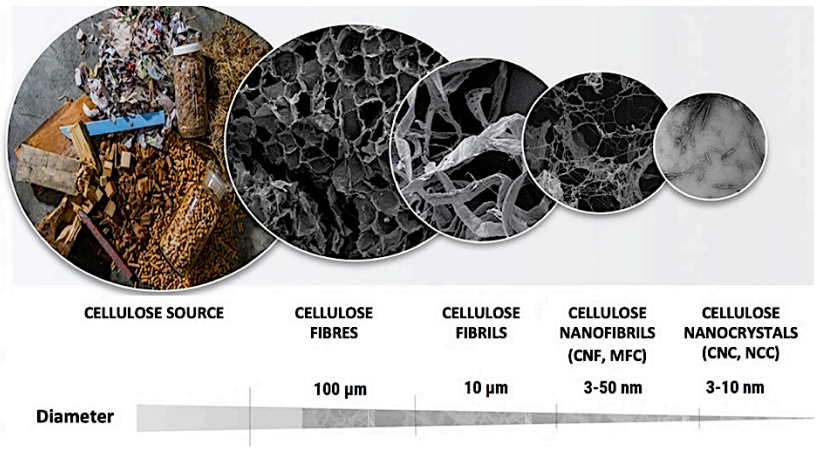

Figure 4.2. Hierarchical structure of cellulose, from cellulose source to nanoparticles. Adapted from Amoroso et al. 2021.

The top-down process to obtain cellulose nanofibrils (CNF, also called microfibrillated cellulose, henceforth MFC), consists of a mechanical delamination of the plant source material through high-pressure homogenization and/or grinding. During the process, the rupture of the cellulose fibres from wood, annual plants or even agricultural residues is induced to obtain nanofibrils, that are the smallest elements constituting the original cellulose fibre [Klemm et al 2006, Padberg et al. 2016] (Fig. 4.3).

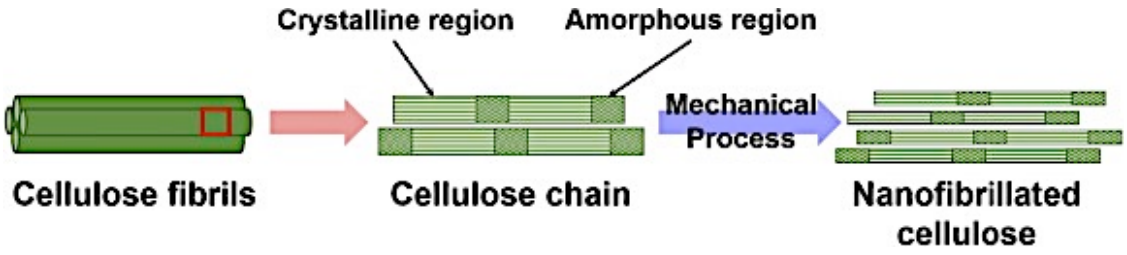

Figure 4.3. Nanofibrillated cellulose (also called microfibrillated nanocellulose) is extracted from cellulose chains through mechanical process, resulting in microfibrils of few nanometers in diameter. From Phanthong et al. 2018.

Depending on the preparation process, nanoparticles can result very small in width (3-10 nm), but they are typically in the range of 20-50 nm, since MFC usually consists of entanglements of cellulose microfibrils, from few to more than 10 micrometers in length [Samir et al. 2005; Sirò and Plackett 2010; Siqueira 2010; Moon et al. 2011; Isogai et al 2011; Trache 2019]. Their strong tendency for association depends on the abundance of interacting surface hydroxyl groups and on their large surface area, which is higher than in the bulk cellulose material [Dufresne 2013; Klemm et al. 2018; Trache 2018; Trache et al 2020, Barhoum et al 2022].

The high aspect ratio (length/width) and the presence of both crystalline and amorphous domains ensures MFC an appreciable tensile strength (i.e., the maximum load that a material can support without fracture when being stretched) and flexibility (capability of bending without breaking) at the same time [Moon et al. 2011; Trache 2019; Padberg et al 2016].

Usually obtained as aqueous dispersion, MFC has a gel-like appearance and when indagated with a scanning electron microscope (SEM), it appears as an intertwined network (Fig. 4.4).

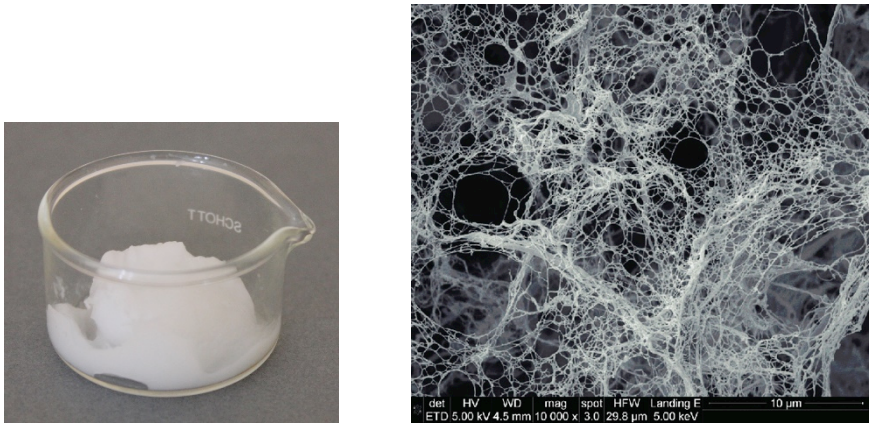

Figure 4.4. Gel-like consistency of a 2.0% (wt/v) aqueous suspension of MFC (left) and SEM image (10 000x) of MFC mechanically isolated from oat straw cellulose powder (right): the tight network of cellulose microfibrils is clearly shown. Micrograph from Tingaut et al 2011.

Cellulose nanocrystals (CNC, also called nanocrystalline cellulose) are obtained from the cellulose microfibrils through a top-down chemical process. Acid hydrolysis, usually induced by sulfuric acid, produces the cleavage of the glycosidic bonds, decreasing the cellulose degree of polymerization to the size of a crystallite, called LODP (Levelling-Off Degree of Polymerisation), with dissolution of amorphous domains and release of the crystalline elements (Fig. 4.5). After hydrolysis, CNC is neutralized by sodium hydroxide (NaOH) to remove free acid residues and is mechanically dispersed to form aqueous colloidal gels [Samir et al. 2005, Dufresne 2013, Dufresne 2017, Dufresne 2020, Naz et al. 2019].

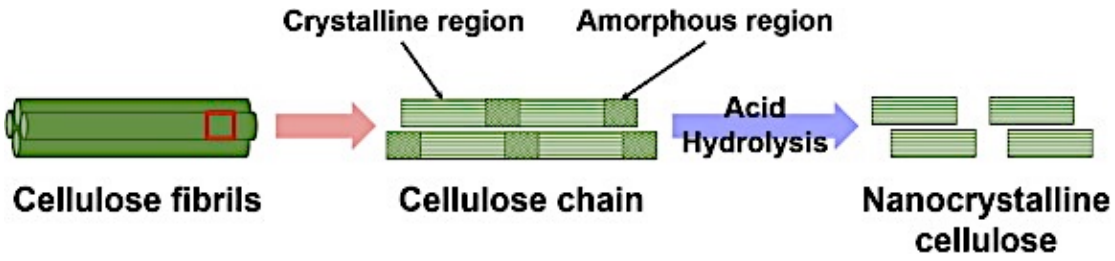

Figure 4.5. Cellulose nanocrystals (also called nanocrystalline cellulose) are obtained through acid hydrolisis resulting in the cleavage of the cellulose chain down to LODP (Levelling-Off Degree of Polymerisation) and in the isolation of the crystalline elements. From Phanthong et al. 2018.

Under SEM examination, nanocrystals appear cylindrical, elongated, rod-like in form, also identified as “whiskers”. Shape and size can vary influenced by the original cellulose source and quality and hydrolysis conditions (time and temperature): according to different works, cellulose nanocrystals are 3-5 nm in width and 50-500 nm in length [Moon et al. 2011], 5-10 nm wide and

50-200 long [Isogai et al. 2011], 4-70 nm in width and 100-6,000 nm in length [Trache et al. 2020]. In all cases, they are characterized by a high aspect ratio (Fig. 4.6).

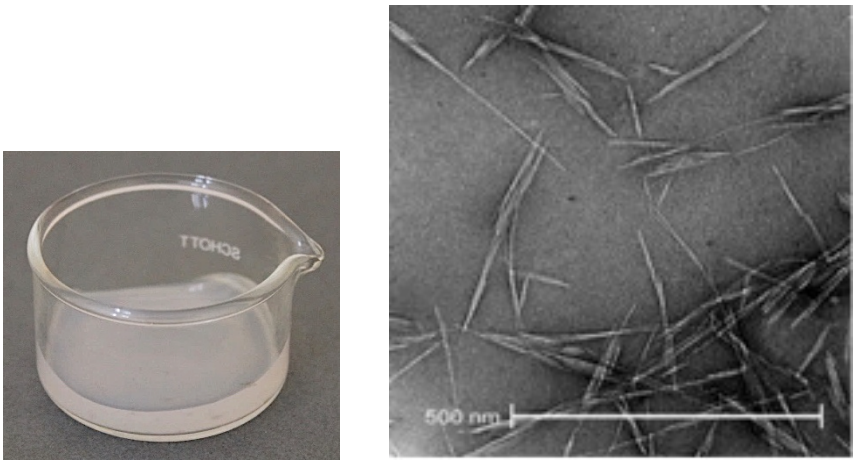

Figure 4.6. A 3.0% (wt/v) NCC aqueous dispersion (left) and a TEM micrograph of a dilute suspension of sisal nanocrytals (right). Micrograph from Siqueira et al. 2009.

Nanocrystals are negatively charged due to sulfate ester groups created on the fibril surface during the hydrolysis step, which ensures the repulsion between nanoparticles and a better stabilization of the aqueous suspensions, avoiding agglomeration/flocculation reactions [Samir et al 2005, Dufresne 2013, Dufresne 2017, Dufresne 2020, Naz et al. 2019]. Compared to microfibrils, nanocrystals are reduced in size and are straight, resulting in higher stiffness [Dufresne 2020]. However, the reinforcement effect of CNC nanoparticles in nanocomposites is impressive when related to the low volume fractions involved. It can probably be explained not only with the stiffness of the CNC whiskers but rather with a mechanical percolation effect, i.e., the movement of the nanoparticle dispersion through the porous matrix of the paper and the formation of a continuous network of cellulosic filler in which the individual CNC crystals are fastened by hydrogen bonds. This phenomenon, already observed by Favier and colleagues [Favier et al. 1995] and confirmed by Siqueira and collaborators [Siqueira et al. 2009 and 2010] leads to a significant increase in the elastic modulus of the nanocomposite (the greater the modulus, the stiffer the material). In the work of Siqueira and coworkers the reinforcing effect of CNC and MFC in a nanocomposite is compared [Siqueira et al. 2009]. The authors note that both when adding 3% (w/v) of CNC crystals and when adding 3 wt% of MFC microfibres to reinforce a polymer of polycaprolactone (PCL), an increase of stiffness is obtained, although the different nanoparticles morphology affected the mechanical properties of the nanocomposite in a different way: PLC nanocomposite added with CNC keeps a higher level of elongation at break (the increase in length

that material will achieve before breaking), while the MFC nanocomposite retains the higher value of strength, [Siquieira et al. 2009], thanks to the high level of entanglements of MFC.

Nanofilms were prepared from a 0.2% w/v aqueous dilution of the commercial MFC gel and from a 0.3% w/v CNC aqueous dispersion. It is obvious that a higher transparency is obtained with the CNC, despite its slightly higher concentration (Fig. 4.7). On the other hand, the MFC film allows a better handling and is less prone to break or tear than the CNC film.

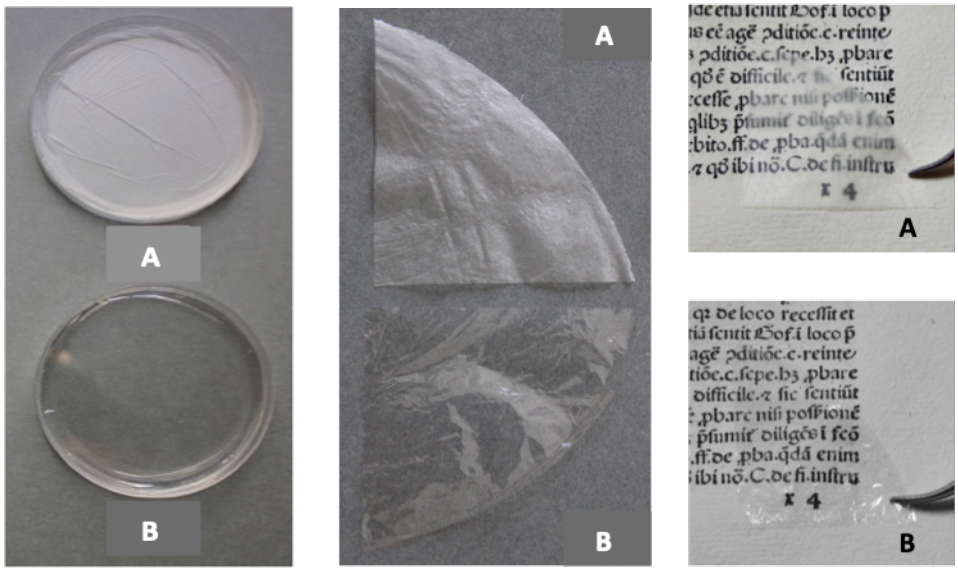

Figure 4.7. Visual comparison of nanocellulose films A, composed of a 0.2% aqueous dilution of MFC gel and B, composed of a 0.3% dilution of NCC gel. They both were prepared through casting evaporation.

Regardless of the differences determined by the quality of the source material, the production process, and the structural features, both MFC and CNC show very interesting properties, which make them particularly attractive in the formation of cellulose films and structures for paper conservation.

Being 100% composed of cellulose, they are perfectly compatible with the paper matrix; because of their small size, the surface-to-volume ratio of nanoparticles is considerable; they are rich in hydroxyl functional groups, allowing for strong hydrogen bond capacity, thus able to link tightly to the native paper. Moreover, cellulose nanoparticles can undergo a wide range of functionalizations via surface chemical reactions, so to graft specific groups and to enhance their effectiveness for tailored applications [Trache et al 2020], as already proposed by Xu and co-workers [Xu et al. 2020] in paper conservation treatments (see § 2 in this chapter).

Chemical inertness, appreciable optical qualities (good transparency), low coefficient of thermal expansion and good thermal stability of the cellulose nanoparticles up to more than 200°C have

already been outlined in several works [Siqueira et al 2009; Lavoine et al. 2012; Dufresne 2013; Salmi et al 2019; Naz et al. 2019; Trache et al. 2020; Völkel et al. 2022].

In addition to its outstanding physico-chemical compatibility with paper and to its mechanical qualities in nanocomposites, nanocellulose also provides long-term stability to light, temperature and humidity ageing [Dreyfuss-Deseigne 2017a, Völkel et al. 2017], which is an important factor to consider when selecting materials for treating an object belonging to cultural heritage.

While commercial bacterial nanocellulose has recently been proposed as reinforcing agent in the conservation treatment of historical burnt papers [Völkel et al. 2022], for the same purpose the present research has focused on the use of commercial nanocellulose nanofibrils and cellulose nanocrystals.

3.2 Polysiloxanes polymers for the protection of historical artifacts

Polysiloxanes (also called silicones) are organosilicon polymers composed by siloxanes, chemical compounds whose functional, repeated group $(R_2SiO)_n$ consists of silicon atoms linked to oxygen and to organic alkyl groups (R) (Fig. 4.8).

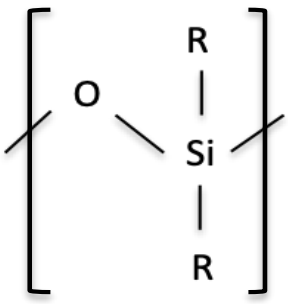

Figure 4.8. Siloxane backbone structure composed by Si, O, and organic groups.

Introducing variations in the silicon-oxygen chain length or in the side groups, polysiloxanes with completely different consistency and features can be synthesized. [Colas and Curtis 2005; Hacker et al. 2019].

As general rule, polysiloxanes show very interesting structure-property relationships, such as controllable water repellence, low surface tension, chemical, photochemical and thermal stability. Usually applied with organic solvents, they have been widely employed at least since the 1940s in several fields, for medical applications (artificial organs, facial reconstruction, artificial skin, contact lenses, drug delivery systems and many others), industrial production of membranes, electrical

insulators, water repellants, anti-foaming agents, mold release agents, anti-corrosion agents, adhesives, and protective coatings [Mark et al. 2015; Hacker et al. 2019].

Siloxanes with four alkoxy reactive groups RO are called alkoxysilanes (AS), with general formula $Si(OR)_4$, where the four RO groups can be different (Fig. 4.9).

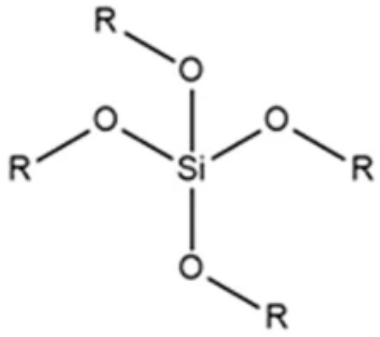

Figure 4.9. Alkoxysilane.

Alkoxysilanes polymerizes in protic solvents (water or alcohols) to give a glass film (polysilicate film).

High flexibility and hydrophobicity, combined with permeability to gas molecules while being impermeable to particles, make polysilicate films formed by alkoxysilanes interesting materials also in the field of cultural heritage and particularly suitable as consolidation and protective coatings of monuments and artifacts exposed outdoor. In the last 20 years, they have been extensively used to preserve historical stone materials [Wheeler 2005; Remzova et al. 2019; Sena de Fonseca et al. 2019; Cecchin et al. 2020], glasses [Carmona et al. 2004; Bertoncello et al. 2006; Dal Bianco et al. 2008; Dal Bianco and Bertoncello 2008; de Ferri et al. 2011; De Bardi et al. 2014] ceramics (Constâncio et al. 2008; Bortolussi et al. 2012; Bertoncello et al. 2014; Baratti Rava et al. 2018] metallic [Baratti Rava et al. 2018] and wood artifacts [Hübert and Mahr 2017; Broda et al. 2019] subjected to degradation processes induced by climatic factors, in particular water and relative humidity, light, temperature and atmospheric pollutants.

Alkoxysilanes usually present low viscosity and after their application can easily permeate the matrix of the object through a sol-gel type reaction, a synthesis technique used to produce various 1D, 2D and 3D silicate nanostructures, as in this case.

In the reaction, alkoxysilanes are hydrolyzed by water – both from the atmosphere and from the material itself – to produce alkoxysilanols, which polymerize in a condensation reaction to form a silicate network.

Several reagents are involved in the sol-gel process: precursors, water, solvents, and catalysts. In the first step, a colloidal suspension (**sol,** solid nanoparticles in a liquid) is obtained from the hydrolysis of the **precursor** (starting molecules) dissolved in a liquid medium, mostly water or a protic solvent such as ethanol or isopropanol. An acid or alkali is added as a hydrolysis catalyst and the hydrolysates are aggregated into nanoscale particles to produce the sol.

In the second step, the sol evolves into a **gel** (i.e., a substance formed by a continuous solid phase enclosing and supporting a continuous liquid phase) through condensation. Finally, the gel dries to form inorganic nanostructures. Alcohol or water molecules are produced in the condensation phase, as shown in the following sol-gel reactions [Schmidt et al. 1984; Brinker and Scherer 1990; Wheeler 2005; Mark et al. 2015; Bokov et al. 2021]:

1) **HYDROLYSIS**, where an alkoxy group (OR) is removed by water and replaced by hydroxyl group (OH) generating silanol (Si-OH) and alcohol (ROH)

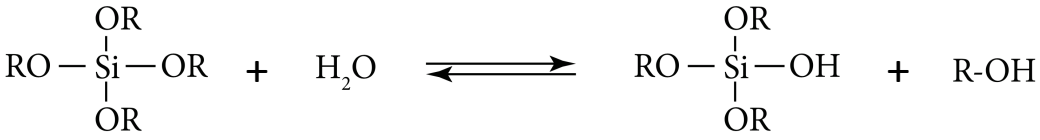

2) **CONDENSATION**, where partially hydrolyzed silanol molecules can link together to produce siloxane bonds (Si-O-Si) such as

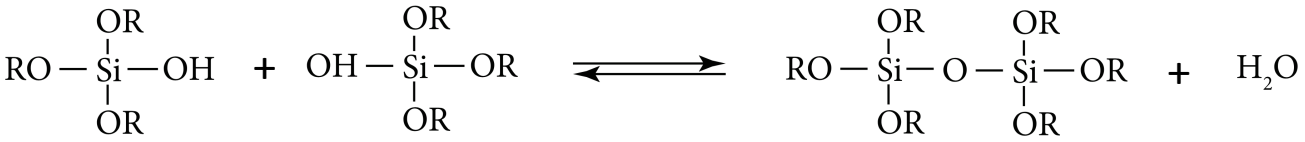

(water condensation)

or

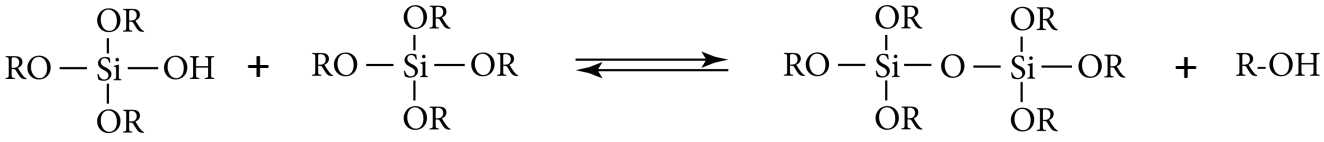

(alcohol condensation)

R is an alkyl chain (e.g., R= $-CH_2CH_3$ for tetraethyl orthosilicate, TEOS, the basis of the formulations tested in Chapter 6) and the condensation reactions lead to the formation of Si-O-Si siloxane bonds. As a consequence of a continuing sol-gel process, a three-dimensional silicate network is formed via polymerization. These polysiloxanes can link through hydrogen or condensation bonds with hydroxyl groups present on the matrix of the historical material, so to consolidate it, to improve its dimensional stability, while retaining its aesthetic features, thanks to the transparency of the polysiloxane film. Also, the mesoporous structure of the film allows for a good release of volatile organic compounds, evolving from the artifact, into the environment.

Moreover, functional groups like amine groups (in the aminoalkylalkoxysilanes used in this research) have enhanced affinity with cellulose through the possibility of forming hydrogen bonds between

$-NH_2$ and –OH groups.

It was observed that hydrolysis and polycondensation reactions of alkoxysilanes can be affected by temperature [Brochier Salon et al. 2008; Hatte et al. 2019] and can proceed with either an acid or base as catalyst. In general, lower pH seems to be particularly favorable while neutral environment should be the most unfavourable, making alkoxysilanes hydrolysis very slow [Schmidt et al 1989; Brinker and Scherer 1990; Choinowski and Cypryk 2000; Monredon-Senani 2004]. For obvious reasons, in paper conservation acid hydrolysis would not be recommended in case of residual acids in the compounds. Alkali hydrolysis is better suited.

3.2.1 TEOS-based alkoxysilane application to cellulose materials

Tetraethoxysilane, or tetraethyl orthosilicate (TEOS, $SiO_4C_8H_{20}$), is one of the most common alkoxysilanes, widely employed as precursor for the deposition of a thin nanosilica protective film on the matrix of historical objects, due to its many advantages, such as low density, chemical stability, elasticity, resistance to ageing, harmlessness of the compounds formed during gelation, relatively simple application and cost effectiveness [Brinker and Scherer 1990; Wheeler 2005]. TEOS is composed of four ethoxide groups bonded to a silicon atom (Fig. 4.10) and exhibits very good sol-phase properties (Fig. 4.11) [Miliani et al. 2007, Dal Bianco and Bertoncello 2008; Mark et al. 2015; Hacker et al. 2019].

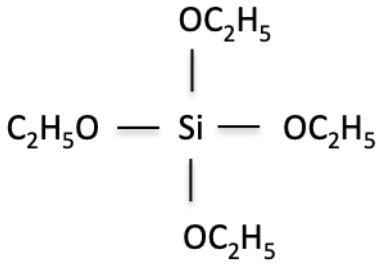

Figure 4.10. Tetraethoxysilane (TEOS) structure.

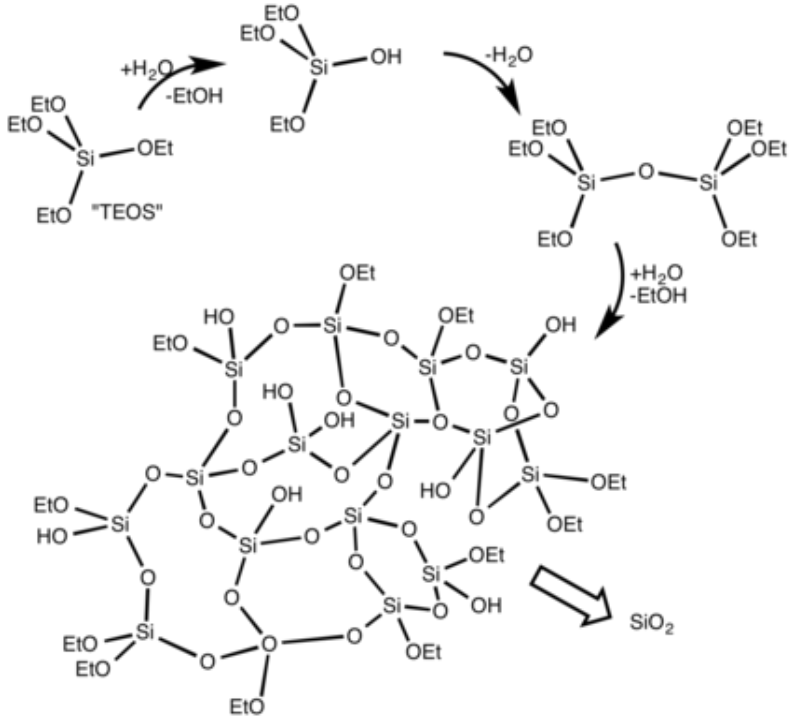

Figure 4.11. TEOS sol-gel process [adapted from: https://en.wikipedia.org/wiki/St%C3%B6ber_process]

In the frame of the present study, TEOS-based formulations with addition of different co-precursors were tested for treatment of burnt paper areas. The original formulation was developed by the University of Padua, patent no. 0001370457 released in 2007, "Synthesis of silica protective films by tin-catalyzed sol-gel process", as reliable solution for the protective, consolidating and coating treatment of mineral surfaces, mainly stone, glass and ceramic, resulting in a film that usually reaches stability in few days (more or less 72 hours), has a composition of pure, amorphous SiO_2, is transparent, colorless and isotropic [Bertoncello et al. 2006; Dal Bianco et al. 2008; Dal Bianco and Bertoncello 2008; Bertoncello et al. 2014]. It is to note that the reaction to produce such protective films is not so deeply affected by the treatment conditions – as usual for alkoxysilanes sol-gel process – and takes place at ambient temperature and relative humidity

conditions. Last but not least, the solvent used is isopropanol, a widely employed solvent in conservation interventions because of its low toxicity.

Over the last ten years, several formulations have been implemented by SILTEA Srl – born in 2012 as start-up of the Padua University – developing different products to be directly used on historical artifacts and making them potentially suitable also for the application on organic materials. Being tetrafunctional, TEOS tends to form rigid interpenetrated films, whose properties in term of viscosity, rigidity, flexibility can however be tailored by the addition of co-precursors modifying the qualities of the gel phase so that it fits better also into a porous organic matrix such as paper.

Although not yet commercially proposed for paper treatment, SILTEA had carried out preliminary laboratory tests to demonstrate the potential of certain TEOS and co-precursor formulations as coatings for cellulose-based materials exposed to the outdoor environment such as wood. In this latter case, the coating was intended to create a protective surface layer on the cellulose-based material. It should be noted that the purpose of the present study was different and aimed at reinforcing the burnt paper matrix, and that the improvement in mechanical and physical properties given by the deposition of the product on paper materials had not yet been investigated by SILTEA.

The effect of alkoxysilane and crystalline cellulose nanocomposite polymers had also been investigated [Favier et al. 1995; Dufresne 2017a and b] but no reference concerning their application on paper, and in particular on burnt paper, could be found. Testing commercial TEOS-based formulations in the treatment of charred paper was therefore one of the specific goals of the present research.

3.2.2 Aminoalkylalkoxysilanes: AMDES and APTES in paper treatment

Polysiloxanes containing alkyl groups and amine functions are called aminoalkylalkoxysilanes (AAAS). Some of them have long been investigated, tested, and optimized in their application in the field of paper conservation, to contrast acidification phenomena while simultaneously strengthening paper, a dual purpose never achieved before with a single chemical product in conservation. The pioneering work [Cheradame et al. 2003; Rousset et al. 2004; Ipert et al. 2005 and 2006] was followed by a number of publications where the physicochemical mechanisms of the paper/AAAS interactions were thoroughly studied and the formulations were optimized.

These experimental works on paper deacidification combined with strengthening treatment were carried out at the Centre de Recherche sur la Conservation des collections (CRC, CNRS) in collaboration with University of Evry Val d'Essonne and University of Cergy-Pontoise. The optimized formulations included two of the AAAS that were tested in the present work: 3-aminopropylmethyldiethoxysilane (from now on: AMDES) (Fig. 4.12) and 3-aminopropyltriethoxysilane (from now on: APTES) (Fig. 4.13). They have been used separately, as they form linear (AMDES) or network (APTES) polymers [Ipert 2005 and 2006; Dupont et al. 2010; Dupont et al. 2011; Souguir et al. 2011 and 2012; Piovesan 2017] as well as in mixtures to form co-polymers (AMDES:APTES, in various proportions, usually 1:1) [Piovesan 2014, 2017 and 2018; Ferrandin-Schoffel 2020, 2021a&b].

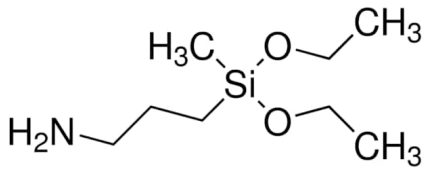

Figure 4.12. 3-aminopropylmethyldiethoxysilane (AMDES) structure.

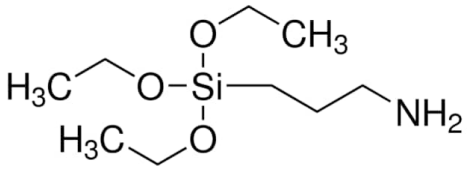

Figure 4.13. (3-aminopropyltriethoxysilane (APTES) structure.

The amine function achieves the effect of neutralising paper acidity and introducing an alkaline reserve in the fibres. On the other hand, the polymerization of the alkoxy component of AAAS through the sol-gel process (hydrolysis and polycondensation) in ambient conditions leads to a simultaneous improvement in paper mechanical properties due to hydrogen bonds established between the amine functions and the OH groups in cellulose [Dupont et al. 2010; Souguir et al. 2011; Ferrandin-Schoffel 2021a]. Papers of different qualities have been involved in deacidification and strengthening treatments with application of AMDES and APTES diluted in hexamethyldisiloxane (HMDS) by immersion or spraying the AAAS directly - without dilution in a solvent- on the paper surface. Specifically, unsized and sized papers made of pure cellulose (cotton linters) or cellulose with a very low impurity amount were tested [Dupont et al. 2010; Piovesan 2014 and 2017], as well as cellulose with considerable lignin amounts from unpurified wood pulp (mechanical pulp such as in case of newspapers newsprint), chemically affected by different degrees of acidity and oxidation and with various mechanical strength, from reasonable to low (brittle papers) [Piovesan 2016, 2017 and 2018; Ferrandin Schoffel 2021]. The solvent, HMDS, was selected as it belongs to the same chemical family (siloxane) and hence has perfect chemical

inertness towards the AAAS compounds, and consequently it grants good dimensional stability of the paper during treatment, limiting cellulose fibres swelling and does not induce solubilization/modification of inks and adhesives eventually present [Dupont 2010]. SEM-EDS mapping of the silicon atoms in treated paper samples confirmed the ability of the aminoalkylalkoxysilanes to coat the sample surface, as well as to permeate through the fiber cross section, ensuring a homogeneous distribution in the whole paper matrix [Dupont et al. 2010 and 2011; Souguir 2011, Piovesan 2017]. Investigations agree that the AMDES and APTES influence the mechanical properties of cellulose-based materials to varying degrees depending on their functionalities. Being bifunctional (two alkoxy functions), AMDES forms linear polymers of limited length and is effective in restoring some plasticity to the paper matrix, while the trifunctional APTES (three alkoxy functions) builds larger, cross-linked networks improving paper tensile strength (tensile modulus and breaking length) but thereby also increases paper stiffness to some degree. Moreover, paper treated with APTES has higher hydrophobicity compared to AMDES which does not modify paper natural hydrophilicity [Dupont 2010, Piovesan 2014 and 2016]. Last but not least, the AAAS have been shown to exhibit fungistatic properties [Rakotonirainy et al. 2008], which is a significant asset for libraries and archives collections where water damage unfortunately happens in storage areas more frequently in the recent years due to climate change and floodings, sometimes also as a consequence of extinguishing a start of fire.

Building on this body of work, mixtures combining a bifunctional and a trifunctional AAAS, AMDES/APTES were investigated, with the aim of inserting flexible linear chains into the rigid polymer network to improve the flexibility of the resulting structure [Piovesan et al. 2014 and 2017; Ferrandin Schoffel 2021]. These properties of strength and flexibility are highly compatible with the very nature of cellulose, which itself combines these two properties in the fiber, i.e., highly ductile regions (amorphous) alternating with highly stiff regions (crystallites).

In all types of tested papers, cotton linters, linen rags, and lignin-containing papers, naturally or artificially aged, copolymers APTES/AMDES were found the most efficient in improving the fiber resistance, flexibility and plasticity, as evidenced by the results of folding endurance and tensile strength tests performed on samples treated with APTES, AMDES and APTES/AMDES copolymer (1:1 and 0.5: 0.95) in comparable conditions [Dupont et al. 2010; Piovesan et al. 2014, 2017 and 2018].

Some limits have been observed in the treatment of highly oxidised, very brittle paper (defined by the authors as having less than 10 to 20 double folds resistance). These papers are the kind that

are lignin-rich (mechanical pulp) where mostly lignin, but also cellulose, is very oxidized. In these cases, the efficiency of both AMDES and APTES in improving mechanical performance is greatly reduced [Dupont et al. 2010, Souguir et al. 2011 and 2012; Piovesan et al. 2014 and 2016; Ferrandin Schoffel 2021a]. These observations led to an in-depth study of the chemical interactions between AAAS and cellulose, in order to identify the reasons of this lack of efficiency for this specific type of papers: degraded lignocellulosic papers.

The interest thus focused in overcoming the reactivity of carbonyl and carboxyl groups in oxidized paper containing a considerable amount of lignin – which is considered one of the main reasons for the ineffectiveness of the strengthening treatment – to optimize the effect of the copolymers APTES/AMDES also on very oxidized and fragile papers [Ferrandin Schoffel 2021]. It is pointed out by the authors that the mechanical properties improvement also depends on the matrix porosity and on its hydrophilic/hydrophobic properties, and this remains an open field for further research. Optimization routes such as the neutralization of the paper using $Ca(OH)_2$ and/or its reduction using sodium borohydride, before the APTES/AMDES treatment were investigated and were shown to enhance the treatment efficiency considerably, leading to an unprecedented reinforcement of highly brittle mechanical pulp papers (Ferrandin Schoffel 2021a).

Optical properties must also be taken into account when developing conservation treatments of historical archival and library material, which is written or printed, as text readability can be affected by changes in the paper color or even in opacity/transparency. In general, no major alterations have been observed after treatment with APTES, while AMDES can induce a certain loss of opacity (Piovesan et al. 2014). Small changes in opacity can occur in papers treated with APTES/AMDES [Piovesan 2014 and 2016]. A good stability of AMDES, APTES and AMDES/APTES polymers towards ageing processes has been systematically confirmed by all the authors.

Based on the results of these previous studies and applications, APTES and AMDES polymers were included in the experimental part of this research in conservation treatments of papers damaged by fire (Chapter 6).

4. Conclusions

In the last two decades, cultural heritage conservation has benefited from an important contribution with the development of innovative solutions based on nanomaterials and nanotechnologies. In the light of these innovations, some of the limits of traditional conservation

workshop practice intervention methodologies can be overcome, so to face conservation issues that cannot be solved with conventional materials and techniques. The development of new methodologies for reinforcing treatments of historical papers severely damaged by fire, which is the goal of the present research project, is among them.

In the field of paper conservation, nanocellulose – both microfibrillated cellulose (MFC) characterized with thin and flexible high aspect-ratio micro-fibrils, and crystalline nanocellulose (CNC), with shorter, rigid fully cristalline whiskers – is considered a very promising material, which is starting to make its way to the conservation workshop. Nanocellulose is extracted from cellulose fibers, is perfectly compatible with the paper matrix and offers the appreciable properties of the nanostructured materials together with very interesting optical and mechanical features (transparency, flexibility and tensile resistance). Therefore, it has been recently proposed as a suitable alternative to the more conventional Japanese, Chinese, Korean papers in tear repairs, mending and lining of paper brittle areas. As for burnt paper strengthening, a very recent application of nanocellulose (published during the course of the present research) showed interesting results as a coating for areas severely damaged by fire. The size and the reactivity of the nanocellulose nanoparticles, allowing their penetration and distribution in the paper matrix, are some factors that explain why they raised interest for this specific application. It was observed that the creation of hydrogen bonds with the original paper fibres helped partly restore the mechanical features mostly lost during thermal degradation. Based on this, nanocelluloses were tested as strengthening agents for burnt papers in Chapter 5.

Polysiloxane polymers are another chemical family of compounds commonly used for the consolidation, reinforcing and protective treatments of cultural artifacts due to their outstanding properties such as low viscosity and low surface tension, flexibility, hydrophobicity combined with permeability to gas molecules, chemical, photochemical and thermal stability. Through a sol-gel reaction, such compounds can permeate the original matrix and form linear or interpenetrated silicate networks, enhancing the matrix physico-mechanical performances. In the field of paper conservation, aminoalkylalkoxysilanes have long been investigated and tested with positive results for deacidification and simultaneous strengthening treatment of paper artifacts through a green chemistry process. Although not yet fully characterised, nor commercially proposed for paper treatments, alkoxysilane formulations - originally developed for coating treatments of historical inorganic artifacts, mainly stone, glass and ceramic - show the potential of being implemented for the application on organic, cellulose-based matrices.

Starting from the previous studies and experimental works, in this research work aminoalkyalkoxysilanes AMDES and APTES, and TEOS-based alkoxysilanes were tested on burnt paper samples. The efficiency of the resulting nanostructured materials to combine reinforcement and protective coating of paper areas embrittled by fire were investigated (Chapter 6).

Chapter 4 | References

Amoroso, L., Agkün, B., Limbo, S. (2021). «GSICA / Nanocellulosa da biomasse di scarto», *Com.pac news,* Online magazine, April 9th 2022;
https://www.compacknews.news/it/news/2021/nanocellulosa-da-biomasse-di-scarto/

Baglioni P., Chelazzi D., (eds.) 2013. *Nanoscience for the conservation of works of art*. Royal Society of Chemistry.

Baglioni P., Chelazzi D., Giorgi R., Poggi G. (2013). «Colloid and meterial science for the conservation of cultural heritage: cleaning, consolidation, and deacidification». *Langmuir*, 5110-5122.

Baglioni, P., Chelazzi, D., Rodorico G. (2015). *Nanotechnologies in the conservation of cultural heritage. A compendium of materials and techniques.* Springer Netherlands.

Bacalova L., Pajorova, J., Backiva, M., Skogberg, A., Kallio, P., Kolarova, K., Svorcik, V. (2019). «Versatile application of nanocellulose: from industry to skin tissue engineering and wound healing». *Nanomaterials*, 9, 164. https://doi.org/10.3390/nano9020164

Baratti Rava R., Cappellina, M., Cecchin, M., Lattanzi, D., Mapelli, M. (2018). «La chiesa di Santa Maria Annunciata all'Ospedale San Carlo Borromeo a Milano. Interventi conservativi sulle superfici di un'opera di Gio' Ponti e sull'Annunciazione della facciata settentrionale». In: Biscontin, G., Driussi, G. (eds), Proceedings of the 34th International Meeting *"Scienza e Beni Culturali. Intervenire sulle superfici dell'architettura tra bilanci e prospettive. Acting on architectural surface between budgets and perspectives",* Bressanone 2018. Edizioni Arcadia Ricerche, 581-590.

Barhoum, A., García-Betancourt, M.L., Jeevanandam, J., Hussien, E.A., Mekkawy, S.A., Mostafa, M., Omran, M.M., Abdalla, M.S., Bechelany, M. (2022). «Review on natural, incidental, bioinspired, and engineered nanomaterials: history, definitions, classifications, synthesis, properties, market, toxicities, risks, and regulations». *Nanomaterials,* 12(2), 177;
https://doi.org/10.3390/nano12020177

Bayda S., Adeel M., Tuccinardi T., Cordani M., Rizzolio F. (2019). «The history of nanoscience and nanotechnology: from chemical-physical applications to nanomedicine». *Molecules*, 25(1), 112; https://doi.org/10.3390/molecules25010112

Bertoncello, R., Milanese, L., Dran, J.C., Bouquillon, A., Sada, C. (2006). «Sol-gel deposition of silica films on silicate glasses: influence of the presence of lead in the glass or in precursor solutions». *Journal of Non-Crystalline Solids,* 352, 315-321; https://doi.org/10.1016/j.jnoncrysol.2005.12.005

Bertoncello, R., Bortolussi, C., Cecchin, M., Lattanzi, D. (2014) «Silica thin film synthetized by sol-gel process for the protection of outdoor artistic ceramic in architecture». Proceedings of the 6th International Congress on "*Science and Technology for the Safeguard of Cultural Heritage in the Mediterranean Basin",* Athens, 22-25 October 2013. Editore Valmar, 340-346.

Bokov, D., Turki Jalil, A., Chupradit, S., Suksatan, W., Javed Ansari, M., Shewael, I.H., Valiev, G. H., Kianfar, E. «Nanomaterial by Sol-Gel Method: Synthesis and Application». *Advances in Materials Science and Engineering*, Volume 2021, Article ID 5102014, 1-21; https://doi.org/10.1155/2021/5102014

Bortolussi, C., Cecchin, M., Lattanzi, D., Mapelli, M., Mischiatti, F., Munerato, E., Righetti, M., Bertoncello, R. (2012). «Film di silice sol-gel per la protezione della ceramica nell'architettura di Gio Ponti a Milano». In: Biscontin, G., Driussi, G. (eds), Proceedings of the 28th International Meeting "*Scienza e Beni Culturali. La conservazione del patrimonio architettonico all'aperto. Superfici, strutture, finiture e contesti*", Bressanone 2012. Edizioni Arcadia Ricerche, 405-415.

Brinker, C. J., Scherer, G.W. (1990). *Sol-Gel Science: The Physics and Chemistry of Sol-Gel Processing*. Academic Press, Inc.: New York; https://doi.org/10.1016/C2009-0-22386-5

Broda, M., Mazela, B., Dutkiewicz, A. (2019). «Organosilicon compounds with various active groups as consolidants for the preservation of waterlogged archaeological wood». *Journal of Cultural Heritage,* 35, 123-128; https://doi.org/10.1016/j.culher.2018.06.006

Carmona, N., Villegas, M.A., Fernández Navarro, J.M. (2004). «Protective silica thin coatings for historical glasses». *Thin Solid Films,* 458 (1-2), 121-128; https://doi.org/10.1016/j.tsf.2003.12.064

Cecchin, M., Bortolussi, C., Pellizzari, G., Basso, E. (2020). «L'utilizzo di protettivi sol-gel su lapidei e stuccature. Il caso del pavimento in opus sectile e tessellatum della Galleria Franchetti alla Ca' d'Oro di Venezia». In: Biscontin, G., Driussi, G. (eds), Proceedings of the 36th International Meeting "*Scienza e Beni Culturali. Gli effetti dell'acqua sui beni culturali. Valutazioni, critiche e modalità di verifica. The effects of water on Cultural Heritage. Critical assessements and verification methods*", Venezia 2020. Edizioni Arcadia Ricerche, 81-90.

Chelazzi, D., Poggi, G., Jaidar, Y., Toccafondi, N., Giorgi, R., Baglioni, P. (2013). «Hydroxide nanoparticles for cultural heritage: consolidation and protection of wall paintings and carbonate materials». *Journal of colloid and interface science,* 392, 42-49; https://doi.org/10.1016/j.jcis.2012.09.069

Choinowski, J., Cypryk, M. (2000). «Synthesis of linear polysiloxanes». In: Jones, R. G., Ando, W., Choinowski, J. (eds), *Silicon containing polymers: the science and technology of their synthesis and applications.* Springer Netherlands, Dordrecht, 3-41.

Colas, A., Curtis, J. (2005). «Silicone biomaterials: history anc chemistry». In: Ratner, B. D., Hoffman, A. S., Schoen, F. J., Lemons, J. R. (eds), *An introduction to materials in medicine.* Elsevier, 80-86; https://www.pentasil.eu/images/Silicone%20Biomaterials.pdf

Constâncio, C., Franco, L., Russo, A., Anjinho, C., Pires, J., Fátima Vaz, M., Carvalho, A.P. (2010). «Studies on Polymeric Conservation Treatments of CeramicTiles with Paraloid B-72 and Two Alkoxysilanes». *Journal of Applied Polymer Science,* 116(5), 2833-2839; https://doi.org/10.1002/app.31743

Dal Bianco, B., Bertoncello, R., Bouquillon, A., Dran, J-C., Milanese, L., Rohers, S., Sada, C., Salomon, J., Voltolina, S. (2008a). «Investigation on sol–gel silica coatings for the protection of ancient glass: Interaction with glass surface and protection efficiency». *Journal of Non-Crystalline Solids,* 354(26), 2983-2992; https://doi.org/10.1016/j.jnoncrysol.2007.12.004

Dal Bianco, B., Bertoncello, R. (2008). «Sol-gel silica coatings for the protection of cultural heritage glass». *Nuclear Instruments and Methods in Physics Research Section B: Beam Interactions with Materials and Atoms,* 266, 2358-2362.

De Bardi, M., Hutter, H., Schreiner, M., Bertoncello, R. (2014). «Sol-Gel silica coating for potash-lime-silica glass: applicability and protective effect». *Journal of Non-Crystalline Solids*, 390, 45-50; https://doi.org/10.1016/j.jnoncrysol.2014.02.016

de Ferri, L., Lottici, P.P., Lorenzi, A., Montenero, A., Salvioli-Mariani, E. (2011). «Study of silica nanoparticles – polysiloxane hydrophobic treatments for stone-based monument protection». *Journal of Cultural Heritage,* 12(4), 356-363; https://doi.org/10.1016/j.culher.2011.02.006

David, M. E., Ion, R-M., Grigorescu, R. M., Iancu, L., Anrei, E. R. (2020). Nanomaterials Used in Conservation and Restoration of Cultural Heritage: An Up-to-Date Overview. *Materials*, *13(9),* 2064; https://doi.org/10.3390/ma13092064

Domingues, Joana; Bonelli, Nicole; Giorgi, Rodorico; Fratini, Emiliano; Gorel, Florence; Baglioni, Piero. (2013). «Innovative hydrogels based on semi-interpenetrating p(HEMA)/PVP networks for the cleaning of water-sensitive cultural heritage artifacts». *Langmuir*, 29(8), 2746–55; doi: 10.1021/la3048664

Domingues, Joana; Bonelli, Nicole; Giorgi, Rodorico; Baglioni, Piero (2014). «Chemical semi-IPN hydrogels for the removal of adhesives from canvas paintings». *Applied Physics A*, 114(3), 705-10; doi 10.1007/s00339-013-8150-0

Dreyfuss-Deseigne, R. (2017a). «Nanocellulose Films: Properties, Development, and New Applications for Translucent and Transparent Artworks and Documents». *The Book and Paper Group Annual* 36, 108;
https://cool.culturalheritage.org/coolaic/sg/bpg/annual/v36/bpga36-20.pdf

Dreyfuss-Deseigne, R. (2017b). «Nanocellulose films in art conservation. A new and promising mending material for translucent paper objects». *Journal of Paper Conservation* Volume 18, 18-29; https://doi.org/10.1080/18680860.2017.1334422

Dufresne, A. (2013). «Nanocellulose: a new ageless bionanomaterial». *Materials Today,* 16 (6), 220-227; https://doi.org/10.1016/j.mattod.2013.06.004

Dufresne, A. (2017a). «Cellulose nanomaterial reinforced polymer nanocomposites». *Current opinion in colloid & interface science*, 29, 1-8. https://doi.org/10.1016/j.cocis.2017.01.004

Dufresne, A. (2017b).«Cellulose nanomaterials as green nanoreinforcements for polymer nanocomposites». *Philosophical Transactions Royal Society A,* 376:20170040*;*
http://dx.doi.org/10.1098/rsta.2017.0040

Dupont A-L., Lavédrine, B., Cheradame, H. (2010). «Mass deacidification and reinforcement of papers and books VI – Study of aminopropylmethyldiethoxysilane treated papers». *Polymer Degradation and Stabiity*, 95(12), 2300-2308;
https://doi.org/10.1016/j.polymdegradstab.2010.09.002

Dupont A-L., Lavédrine, B., Cheradame, H., Souguir, Z. (2011). «Deacidification and Strengthening of Degraded Papers With Aminosilanes: The Example of AMDES». Proceedings *Adhesives and Consolidants for Conservation: Research and Applications*, CCI Symposium 2011, Ottawa, Canada.

Favier, V., Chanzy, H., Cavaille, J.Y. (1995). **«**Polymer nanocomposites reinforced by cellulose whiskers**»**. *Macromolecules*, 28, 6365-6367; https://pubs.acs.org/doi/pdf/10.1021/ma00122a053

Feynman R. P. (1959). *Plenty of room at the bottom.* Transcription of the talk presented to the annual meeting of the American Physical Society at the California Institute of Technology (Caltech) in Pasadena.
https://web.pa.msu.edu/people/yang/RFeynman_plentySpace.pdf

Feynman, R. (1960). **«**There's plenty of room at the bottom**»**, *Engineering Science*, vol. 23(5), 22-36.

Ferrandin-Schoffel, N., Haouas, M., Martineau-Corcos, C., Fichet, O., Dupont, A.-L. (2020). **«**Modeling the reactivity of aged paper with aminoalkylalkoxysilanes as strengthening and deacidification agents**»**. *ACS Applied Polymer Materials* 2, 1943-1953.
DOI: 10.1021/acsapm.0c00132

Ferrandin-Schoffel, N. (2021a). *Renforcement et désacidification de papers patrimoniaux par des réseaux de copolymères de polyaminoalkylalcoxysilanes. Mécanism, stabilitè et optimisation.* PhD Thesis, CY Cergy Paris Université.
https://hal.archives-ouvertes.fr/tel-03221504v1/document

Ferrandin-Schoffel, N., Martineau-Corcos, C., Piovesan, C., Paris-Lacombe, S., Fichet, O., Dupont, A.-L. (2021b). **«**Long-term stability of lignocellulosic papers strengthened and deacidified with aminoalkylalkoxysilanes**»**. *Polymer Degradation and Stability*, 183, 10941 ;
DOI: 10.1016/j.polymdegradstab.2020.109413

Foster E. J., Moon, R. J., Agarwal, U. P., Bortner, M. J., Bras, J., Camarero-Espinosa, S., Chan, K. J., Clift, M.J.D., Cranston, E.D., Eichhorn, S. J., Fox, D. , Hamad, W. Y., Heux, L., Jean, B., Korey,M., Nieh, W., Ong, K. J., Reid, M. S., Scott Renneckar, S., Roberts, R., Shatkin, J. A., Simonsen, J., Stinson-Bagby, K., Wanasekara, N., Youngblood, J. (2018). **«**Current characterization methods for cellulose nanomaterials». *Chemical Society Reviews,* 47(8), 2511-3006;
https://doi.org/10.1039/C6CS00895J

Giorgi, R., Dei, L., Ceccato, M., Schettino, C., Baglioni, P. (2002). «Nanotechnologies for Conservation of Cultural Heritage: Paper and Canvas Deacidification». *Langmuir*, 18, 8198-8203; https://doi.org/10.1021/la025964d

Giorgi, R., Chelazzi, D., Baglioni, P. (2005). «Nanoparticles of calcium hydroxide for wood conservation. The deacidification of the Vasa warship». *Langmuir,* 21, 10743-10748.

Hacker, M. C., Krieghoff, J., Mikos, A. G. (2011). «Sinthetic Polymers». In: Atala, A., Lanza, R., Milos, A. G., Nerem, R. (eds), *Principles of Regenerative Medicine,* Academic Press, 559-590; https://doi.org/10.1016/C2009-0-61040-0

Hatte, Q., Dubos, P-A., Guitter, N., Richard-Plouet, M., Casari, P. (2019). «Influence of relative humidity and temperature on the sol-gel transition of a siloxane surface treatment». *Journal of Sol-Gel Science and Technology,* 90 (2), 230-240;
https://doi.org/10.1007/s10971-019-04929-0

Hübert T., Mahr M.S. (2017) «Sol-gel Wood Preservation». In: Klein, L., Aparicio, M., Jitianu, A. (eds) *Handbook of Sol-Gel Science and Technology*. Springer, Cham, 1-48; https://doi.org/10.1007/978-3-319-19454-7_106-2

Ipert, S, Rousset, E., Cheradame, H. (2005). «Mass deacidification of papers and books III: Study of a paper strenghtening and deacidification process with Amino Alkyl Alkoxy Silanes». *Restaurator*, 26, 250-264; https://doi.org/10.1515/REST.2005.250

Ipert, S, Dupont, A.-L., Lavédrine, B., Bégin, P., Rousset, E., Cheradame, H. (2006). «Mass deacidification of papers and books. IV. A study of papers treated with aminoalkylalkoxysilanes and their resistance to ageing». *Polymer Degradation and Stability*, 91(12), 3448-3455; https://www.academia.edu/17759550/Mass_deacidification_of_papers_and_books_IV_A_study_of_papers_treated_with_aminoalkylalkoxysilanes_and_their_resistance_to_ageing

Isogai A., Saito, T., Fukuzumi, H. (2011). «TEMPO-oxidized cellulose nanofibers».*Nanoscale*, 3, 71-85; https://pubs.rsc.org/en/content/articlelanding/2011/nr/c0nr00583e

Jeevanandam, J., Barhoum, A., Chan, Y. S., Dufresne, A., Danquah, M. K. (2018). «Review on nanoparticles and nanostructured materials: history, sources, toxicity and regulations». *Beilstein Journal of Nanotechnology,* 9, 1050-1074; https://doi.org/10.3762/bjnano.9.98

Khan. I., Saeed, K., Khan, I. (2019). «Nanoparticles: Properties, applications and toxicities». *Arabian Journal of Chemistry,* 12 (7), 908-931.

Klemm, D., Schumann, D., Kramer, F., Heßler, N., Hornung, M., Schmauder, H.P., Marsch, S. (2006) «Nanocelluloses as innovative polymers in research and application». In: Klemm D. (ed.), *Polysaccharides II*. Springer, 49–96.

Klemm, D., Kramer, F., Moritz, S., Lindström, T., Ankerfors, M., Gray, D., Dorris, A. (2011). «Nanocelluloses: A new family of nature-based materials». *Angewandte Chemie International Edition,* 50 (24), 5438-5466; https://doi.org/10.1002/anie.201001273

Klemm, D., Cranston, E. D., Fischer, D., Gama, M., Kedzior, S. A., Kralisch, D., Kramer, F., Kondo, T., Lindström, T., Nietzsche, S., Petzold-Welcke, K., Rauchfuß, F. (2018). «Nanocellulose as a natural source for groundbreaking applications in materials science: today's state». *Materials Today,* 21 (7), 720-748; https://doi.org/10.1016/j.mattod.2018.02.001

Lavoine, N., Desloges, I., Dufresne, A. Bras, J. (2012). «Microfibrillated cellulose, its barrier propertiesand applications in cellulosic materials: a review». *Carbohydrate polymers*, 90(2), 735-764; https://doi.org/10.1016/j.carbpol.2012.05.026

Mark, J., M., Schaefer, D.W., Lin, G. (2015). *The Polysiloxanes.* Oxford University Press.

Miliani, C., Velo-Simpson, M.L., Scherer, G. W. (2007). «Particle-modified consolidants: A study on the effect of particles on sol–gel properties and consolidation effectiveness». *Journal of Cultural Heritage,* 8 (1), 1-6; https://doi.org/10.1016/j.culher.2006.10.002

Mirabile, A., Chelazzi, D., Ferrari, P., Montis, C., Berti, D., Bonelli, N., Giorgi, R., Baglioni, P. (2020). «Innovative methods for the removal, and occasionally care, of pressure sensitive adhesive tapes from contemporary drawings». *Heritage Science,* 8; https://doi.org/10.1186/s40494-020-00387-y

Monti, M., Dal Bianco, B., Bertoncello, R., Voltolina, S. (2008).«New protective coatings for ancient glass: Silica thin-films from perhydropolysilazane». *Journal of Cultural Heritage* 9, e143-e145; https://doi.org/10.1016/j.culher.2008.08.002

de Monredon-Senani, S. (2004). *Interaction Organosilanes/Silice de précipitation du milieu hydro-alcoolique au milieu aqueux*. Thèse de doctorat. Université Pierre et Marie Curie - Paris VI https://tel.archives-ouvertes.fr/tel-00012113/document

Moon, R. J., Martine, A., Nairn, J. A., Simonsen. J. (2011). «ChemInform Abstract: Cellulose Nanomaterials Review: Structure, Properties and Nanocomposites». *Chemical Society Reviews*, 40(7), 3941-3994; http://dx.doi.org/10.1039/c0cs00108b

Nunes, D., Pimentel, A., Santos, L., Barquinha, P., Pereira, L., Fortunato, E., Martins, R., Korotcenkov, G. (2019). *Metal Oxide Nanostructures. Synthesis, Properties and Applications.* Elsevier Science.

Operamolla, A., Mazzuca, C., Capodieci, L., Di Benedetto, F., Severini, L., Titubante, M., Martinelli, A., Castelvetro, V., Micheli, L. (2021). «Toward a reversible consolidation of paper materials using cellulose nanocrystals». *ACS Applied Materials & Interfaces,* 13, 44972-44982; https://doi.org/10.1021/acsami.1c15330

Padberg, J., Gliese, T., Bauer, W. (2016). «The influence of fibrillation on the oxygen barrier properties of films from microfibrillated cellulose». Biorefinery *Nordic Pulp & Paper Research Journal*, 31(4), 548-560; https://doi.org/10.3183/npprj-2016-31-04-p548-560

Phanthong, P., Reubroycharoen, P., Hao, X., Xu, G., Abudula, A., Guan, G. (2018). «Nanocellulose: Extraction and application». *Carbon Resources Conversion,* 1, 32-43; https://doi.org/10.1016/j.crcon.2018.05.004

Piovesan, C., Dupont, A-L., Fabre-Francke, I. *,* Fichet, O., Lavédrine, B., Chéradame, H. (2014). **«**Paper strengthening by polyaminoalkylalkoxysilane copolymer networks applied by spray or immersion: a model study**»**. *Cellulose,* 21, 705–715;
https://doi.org/10.1007/s10570-013-0151-9

Piovesan, C. (2016). *Elaboration de traitements de conservation à base de réseaux de polysiloxanes pour le renforcement et la désacidification simultanés adaptables à differents papiers: exemple des papiers de presse*. PhD Thesis. Université de Cergy-Pontoise.

Piovesan, C., Fabre-Francke, I., Dupont, A-L., Fichet, O., Paris-Lacombe, S., Lavédrine, B., Chéradame, H. (2017). **«**The impact of paper constituents on the efficiency of mechanical strengthening by polyaminoalkylalkoxysilanes**»**. *Cellulose,* 24, 5671-5684;
https://doi.org/10.1007/s10570-017-1513-5

Piovesan, C., Fabre-Francke, I., Paris-Lacombe, S., Dupont, A-L., Fichet, O. (2018). **«**Strenghtening naturally and artificially aged paper using polyaminoalkylalkoxysilane copolymer networks**»**. *Cellulose,* 25, 6071-6082; https://doi.org/10.1007/s10570-018-1955-4

Poggi, G., Giorgi, R., Toccafondi, N., Katzur, V., Baglioni, P. (2010). «Hydroxide Nanoparticles for Deacidification and Concomitant Inhibition of Iron-Gall Ink Corrosion of Paper». *Langmuir*, 26(24), 19084-19090; https://doi.org/10.1021/la1030944

Poggi, G., Baglioni, P., Giorgi, R. (2011). «Alkaline Earth Hydroxide Nanoparticles for the Inhibition of Metal Gall Ink Corrosion». *Restaurator*, 32(3), 247-73; https://doi.org/10.1515/rest.2011.012

Poggi, G., Toccafondi, N., Melita, L.N., Knowles, J.C., Bozec, L., Giorgi, R., Baglioni P. (2014). **«**Calcium hydroxide nanoparticles for the conservation of cultural heritage: new formulations for the deacidification of cellulose-based artifacts**».** *Applied Physics A*, 114, 685- 693;
https://doi.org/10.1007/s00339-013-8172-7

Rakotonirainy, M. S., Dupont, A.-L., Lavédrine, B., Ipert, S., Cheradame H. (2008). **«**Mass deacidification of papers and books. V – Fungistatic properties of papers treated with aminoalkylakoxysilanes**»**. *Journal of Cultural Heritage* 9, 54-59.
DOI: 10.1016/j.culher.2007.12.002

Remzova, M., Zouzelka, R., Lukes, J., Rathousky, J. (2019). **«**Potential of advanced consolidants for the application on sandstone**»**. *Applied Sciences*, 9(23), 5252;
https://doi.org/10.3390/app9235252

Reshmy, R., Eapen, P., Deepa, T., Aravind, M., Raveendran, S., Parameswaran, B., Sunita, V., Awasthi, M. K., Ashok, P. (2021). «Bacterial nanocellulose: engineering, production, and applications». Bioengineered , 12 (2), 11463-11483;
https://doi.org/10.1080/21655979.2021.2009753

Rousset, E., Ipert, S., Cheradame, H. (2004). **«**Mass deacidification of papers and books II - deacidification in the liquid phase using aminosilanes**»**. *Restaurator*, 25 (2), 104-118.

Salimi, S., Sotudeh-Gharebagh, R., Zarghami, R., Chan, S. Y., and Yuen, K. H. (2019). **«**Production of nanocellulose and its applications in drug delivery: a critical review**»**. *ACS Sustainable Chemistry Engineering* (7), 15800–15827; https://doi.org/10.1021/acssuschemeng.9b02744

Samir, A., Alloin, F., Dufresne, A. (2005). «Review of Recent Research into Cellulosic Whiskers, Their Properties and Their Application in Nanocomposite Field». *Biomacromolecules*, 6(2), 612–626; https://doi.org/10.1021/bm0493685

Santos, S., Carbajo J.M., Gómez, N., Quintana, E., Ladero, G., Sánchez, A., Chinga-Carrasco, G., Villar, J. C. (2015a). «Use of bacterial cellulose in degraded paper restoration. Part. I: application on model papers». *Journal of Material Science,* online publication
http://dx.doi.org/10.1007/s10853-015-9476-0

Santos, S., Carbajo J.M., Gómez, N., Quintana, E., Ladero, G., Sánchez, A., Chinga-Carrasco, G., Villar, J. C. (2015b). «Use of bacterial cellulose in degraded paper restoration. Part. II: application on real samples». *Journal of Material Science,* online publication
http://dx.doi.org/10.1007/s10853-015-9477-z

Schmidt, H., Scholze, H., Kaiser, A. (1984). «Principles of hydrolysis and condensation reaction of alcoxysilanes». *Journal of Non-Crystalline Solids* 63, 1-11;
https://doi.org/10.1016/0022-3093(84)90381-8

Sena De Fonseca, B., Joao Ferreira, M., Taryba, M. G., Picarra, S., Ferreire Pinto A. P., Montemor, M. F. (2019). «Alkoxysilane-based sols for consolidation of carbonate stones: Impact of the carbonate medium in the sol-gel processes». *Journal of Cultural Heritage,* 37, 63-72;
https://doi.org/10.1016/j.culher.2018.11.007

Siqueira, G., Bras, J., Dufresne, A. (2009). «Cellulose whiskers versus microfibrils: influence of the nature of the nanoparticle and its surface functionalization on the thermal and mechanical properties of nanocomposites». *Biomacromolecules,* 10(2), 425-32;
https://doi.org/10.1021/bm801193d

Siqueira, G., Bras, J., Dufresne, A. (2010). «Cellulosic bionanocomposites: a review of preparation, properties and applications». *Polymers,* 2, 728-765;
https://doi.org/10.3390/polym2040728

Siró, I., Plackett, D. (2010). «Microfibrillated cellulose and new nanocomposite materials: a review». *Cellulose* 17, 459–494; https://doi.org/10.1007/s10570-010-9405-y

Souguir, Z., Dupont, A-L., d'Espinose de Lacaillerie, J-B., Lavédrine, B., Cheradame, H. (2011). «Chemical and physicochemical investigation of an aminoalkylalkoxysilane as strengthening agent for cellulosic materials». *Biomacromolecules*, 12(6), 2082–2091**;**
https://doi.org/10.1021/bm200371u

Souguir, Z., Dupont, A-L., Fatyeyva, K., Mortha, G., Cheradame, H., Ipert, S., Lavédrine, B. (2012). «Strenghtening of degraded cellulosic material using a diamine alkyalcoxysilane ». *RSC Advance,* 19; https://pubs.rsc.org/En/content/articlelanding/2012/ra/c2ra20957h

Stephens, C. H., Whitmore, P. M., Morris, A. H., Smith, T. (2009). «Assessing the risks of alkaline damage during deacidification treatments of oxidized paper». *JAIC* (48), 235-249;

https://doi.org/10.1179/019713612804514251

Thomas, B., Raj, M. C., Rubiyah, A. K. B. Jithin Joy, M. H., Moores, A., Drisko, G. L., and Sanchez, C. (2018). «Nanocellulose, a Versatile Green Platform: From Biosources to Materials and Their Applications». *Chemical Reviews,* 2018**,** *118* (24), 11575-11625.

Tingaut, P., Eyholzer, C., Zimmermann, T. (2011). «Functional polymer nanocomposite materials from microfibrillated cellulose». In: Hashim, A. A. (ed.), *Advances in Nanocomposite Technology*. Intechopen, 319-334; http://dx.doi.org/10.5772/20817.

Trache, D. (2018) «Nanocellulose as a promising sustainable material for biomedical applications». *AIMS Material Science* 5, 201–205; doi: 10.3934/matersci.2018.2.201.

Trache, D., Tarchoun, A. F., Derradji, M., Hamidon, T. S., Masruchin, N., Brosse, N., Hazwan Hussin, M. (2020). «Nanocellulose: from fundamentals to advanced applications». *Frontiers in Chemistry,* 8:392; https://doi.org/10.3389/fchem.2020.00392

Völkel, L., Ahn, K., Hähner, U., Gindl-Haltmutter, W., Potthast, A. (2017). «Nano meets the sheet: adhesive-free application of nanocellulosic suspensions in paper conservation». *Heritage Science,* 5, 23, https://doi.org/10.1186/s40494-017-0134-5

Völkel, L., Beaumont, M., Czibula, C., Rusakov, D., Mautner, A., Teichert, C., Kontturi, E., Rosenau, T., Potthast, A. (2022). «Assessing Fire-Damage in Historical Papers and Alleviating Damage with Soft Cellulose Nanofibers». Small, 18, 2105420, 1-14; https://doi.org/10.1002/smll.202105420

Whatmore, R. W. (2006). **«**Nanotechnology-what is it? Should we be worried?**».** *Occupational Medicine*, 56(5), 295-299; https://doi.org/10.1093/occmed/kql050

Xu, Q., Poggi, G., Resta, C., Baglioni, M., Baglioni, P. (2020). «Grafted nanocellulose and alkaline nanoparticles for the strengthening and deacidification of cellulosic artworks». *Journal of Colloid Interface Scence,* 576, 147–157; https://doi.org/10.1016/j.jcis.2020.05.018

Xu, E., Zhang, Y., Lin, L. (2020). «Improvement of mechanical, hidrophobicity and thermal properties of Chinese Fir Wood by impregnation of nanosilica sol». *Polymers,* 12(8):1632. https://doi.org/10.3390/polym12081632

Wheeler, G. (2005). *Alkoxysilane and the consolidation of stone.* The Getty Conservation Institute: Los Angeles, CA, USA;
https://books.google.it/books?hl=it&lr=&id=GNgxCwAAQBAJ&oi=fnd&pg=PP1&ots=PEPFMRDvdO&sig=VlTTNOFaui_JEK1lXWIgeP66jcw&redir_esc=y#v=onepage&q&f=false

Chapter 5

Burnt paper strengthening with nanocellulose: treatment development and optimization

1. Preliminary tests

Nanocrystalline cellulose (CNC) (supplier Melodea Ltd) and microfibrillated cellulose (MFC) (supplier Borregaard SpA) were supplied respectively in a 3% and in a 2% aqueous dispersion in a thick gel-like consistence (§ Chapter 4, Fig. 4.4 and 4.6; see section Materials and methods) and had to be further dispersed at lower concentrations to be employed for the purpose of this study. The aim of the first, preliminary tests was thus to select the most suitable dilution solvent that could be mixable with the aqueous commercial nanocellulose formulations, effective in distributing the nanocellulose on the samples and in delivering it within the paper fibres. It was stated that carriers inducing side effects such as surface deposits, tidelines formation and stains had to be avoided in the context of this study, aimed at developing materials and methods to be applied on historical documents and books.

CNC and MFC were diluted, individually and combined, and applied on the artificially burnt unsized (called UP) and sized (called SP) Ruscombe Paper Mill (RPM) paper samples. Treated samples were then visually examined for eventual undesirable effects and to optimize the method.

1.1 Samples preparation (Cfr Chapter 3, § 2.2.2)

Charred samples were produced by burning UP and SP RPM paper (5x10 cm^2) on a hot plate set at 250°C for 15', covered by a marble slab (20 x 20 cm^2, thickness 1.5 cm, weight 400 g) and turned once to induce a recto/verso burn as even as possible. Samples were then usually cut in 4/5 strips (1x10 cm^2) to be treated with the different nanocellulose dispersions; one or two strips per sample were left untreated as control samples.

1.2 Nanocellulose dispersion preparation and distribution on the charred samples

Water, ethyl alcohol (Merck, 96%) and isopropyl alcohol (Merck 99,5%) were selected as solvents. Both alcohols are widely in use in the conservation field in combination to, or as an alternative to,

water in key conservation treatments of water-sensitive materials. They exhibit lower polarity and lower surface tension compared to water, and hence penetrate better into the paper matrix and evaporate faster. They also induce less fiber swelling. The reduced time of direct contact with the paper, inks and graphic media prevents, as far as possible, the swelling of the fibres and the bleeding of inks and colored media. In addition, the fast evaporation of alcohols limits the migration of the solvents beyond the defined area of operation, allowing more precise localization of the treatment and a better control. In recent decades, ethanol and isopropanol have also been employed as carriers for nanoparticles, e.g., in the deacidification of paper and cellulose-based materials.

Cellulose nanocrystals (CNC) dispersions were prepared at a concentration of 0.3% w/v in water, in ethanol and in isopropanol and microfibrillated cellulose (MFC) dispersions at a concentration of 0.2 % w/v in the same solvents. According to Dreyfuss-Deseigne [2017], these concentrations were the more suitable for a good nanocellulose film preparation through casting-evaporation method. A rod was used to mix the dispersions before applying them to the samples by brushing recto and verso on the whole charred area, including a few millimeters of the white, unburnt adjacent area. Samples were then allowed to dry at room conditions (21°C ± 2°, 45% ±2% RH).

1.3 Visual assessment of the treatment impact on paper

Whatever the kind of nanocellulose (CNC or MFC), water, ethyl alcohol and isopropyl alcohol penetrated the samples at different speed and unwanted effects were observed particularly on the unsized (UP) samples, since they are not hydrophobized by the sizing, regardless of the type of nanocellulose used, as summarized in Table 5.1.

Table 5.1. Side effects observed on unsized RPM paper treated with 0.3 % w/v CNC and 0.2 % w/v MFC aqueous dispersion in ethyl alcohol and in isopropyl alcohol.

	NANOCELLULOSE DISPERSION WATER	**NANOCELLULOSE DISPERSION ETHYL ALCOHOL**	**NANOCELLULOSE DISPERSION ISOPROPYL ALCOHOL**
UNSIZED SAMPLES	slow solvent penetration long drying time tideline formation consistent surface deposits no sample deformation	fast solvent penetration short drying time tideline formation minimal surface deposits possible sample deformation	very fast solvent penetration very short drying time very rare tideline formation evident surface deposits not frequent sample deformation

The CNC and MFC aqueous dispersions took the longest time to enter the sample, remaining on the charred surface for 25-30 minutes before drying. The hydrophobicity of the burnt areas was an expected effect already observed in the investigation of the burnt samples presented in Chapter 3 (§ 3.2). After drying, treated areas showed white surface deposits. On the other hand, water was rapidly absorbed by the unburnt areas of the unsized samples, dragging the brown compounds and inducing tide stains formation (Fig. 5.1). In the sized samples, the penetration of water within the paper was more uniformly slow both in the burnt and in the unburnt areas and tidelines occurred less frequently.

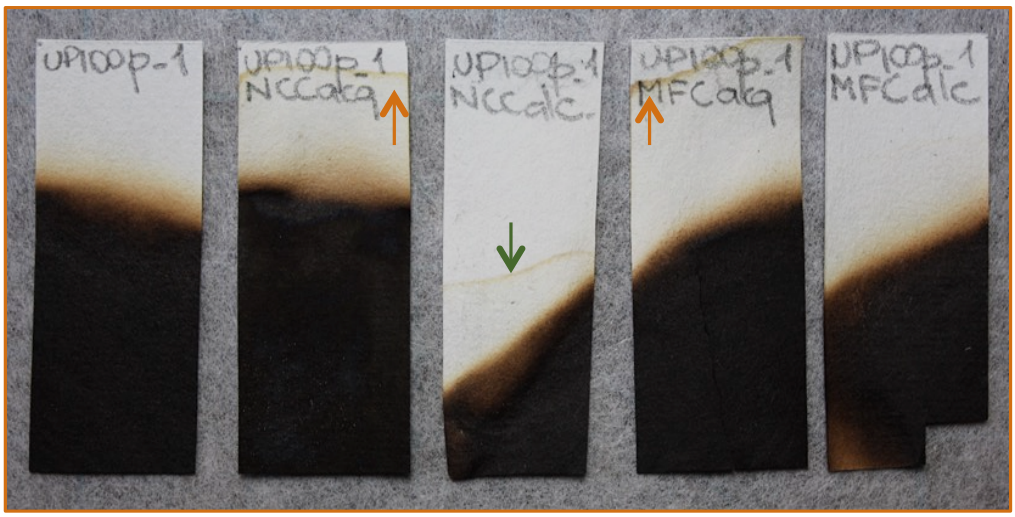

Figure 5.1. Unsized RPM burnt paper: control (left) and samples treated with nanocellulose aqueous dilutions (CNCacq, MFCacq) and with ethyl alcohol dilutions (CNCalc, MFCalc). Tide stains appeared in CNCacq and MFCacq (orange arrows), a less marked tideline is also on CNCalc (green arrow).

Compared to water, both ethanol and isopropanol entered the paper faster, tideline formation was not frequent and occurred exclusively on the unsized paper samples, as shown for ethanol in Fig. 5.1.

White surface deposits were observed in all cases on the charred areas of the unsized and sized samples: the most conspicuous deposits were observed in the samples treated with nanocellulose in water, the less evident ones in samples treated with nanocellulose in ethanol. Such deposits had the appearance of shiny particles on the paper surface treated with CNC and a milky appearance

on those treated with MFC (Fig. 5.2). This is consistent with the crystalline and amorphous structure of these two products, respectively.

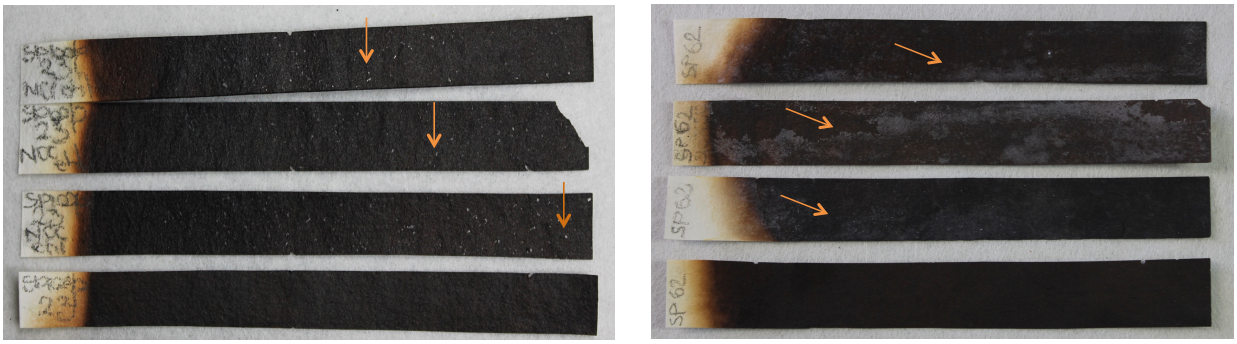

Figure 5.2. Sized RPM samples treated recto/verso with 0.3% w/v CNC (left) and 0.2% w/v MFC (right) in ethanol. One strip (at the bottom in the figure) was left as control.

Deformations were absent in the samples treated with aqueous dispersion, but sometimes appeared on samples brushed with nanocellulose in propanol and in ethanol, more frequent and accentuated in the latter case (Fig. 5.3). Deformations were probably due to a short-term paper dehydration, as the samples left at room temperature returned to flatness within a few hours.

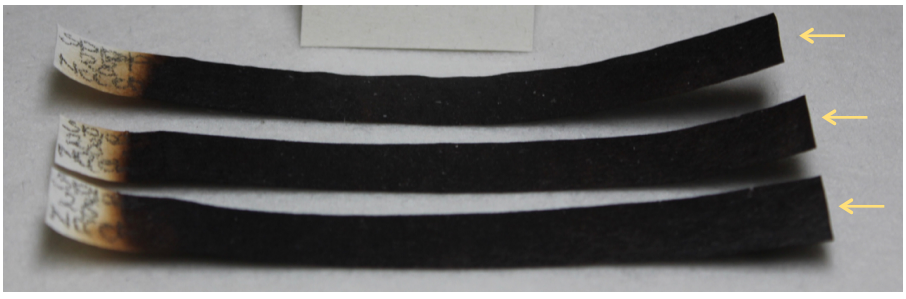

Figure 5.3. Deformation of sized RPM sample treated recto/verso with the 0,3% w/v CNC dispersion in ethyl alcohol.

In general, unwanted effects, like tidelines and surface deposits, were relevant for CNC or MFC in water, and also longest drying times were needed. Therefore, water was excluded and only ethanol and isopropanol were employed in the dilution of CNC and MFC for further tests.

1.4 Treatment optimization

On the basis of the preliminary tests, some variations were introduced in the method of nanocellulose dilution and distribution on the samples.

1.4.1 Stirring nanocellulose in solvent

Nanocellulose dispersed in a solvent tended to separate from the solvent and to sediment within a few hours after preparation. This probably led to a varying amount of nanocellulose deposited on the paper during treatment and favored some accumulations on its surface, resulting in shining particles or in the matt white spots shown in Fig. 5.2. More uniform and stable dispersions for further testing were obtained by stirring vigorously the nanocellulose in solvent (5' at 10,000 rpm) using a High Speed Power Blender (Philips).

1.4.2 Nanocellulose deposition

Nanocellulose application by brushing had also contributed to the non-uniform deposition on the paper surface, depending on the friction of the brush bristles. In addition, the minimal pressure produced by brushing could induce mechanical stress on the burnt, fragile areas and sometimes led to their fragmentation. Spraying was therefore tested in later applications.

2. Development of a fold test procedure for burnt paper

Folding endurance is a property representing the mechanical resistance of the paper and allows estimating its ability to withstand repeated bending, folding, and creasing before breaking. It was considered the key test to evaluate the evolution of strength improvement in treated versus untreated samples (also called control samples).

The extreme fragility of the burnt paper did not allow the use of standardized mechanical strength procedures or tools (e.g., TAPPI T-404 Tensile Strength Tests of Paper and Paperboard or T-494 Tensile properties test, TAPPI T 423 and TAPPI T 511 om-02 Folding endurance of paper). A simpler folding endurance test was therefore developed, using a customized instrument for measuring the critical folding angle (CFA) of the samples, i.e., the folding angle at which paper started to break.

2.1 The custom instrument to test burnt paper fold resistance

The tailor-made tool for the fold test was realized mounting a transparent plastic protractor on a transparent base. A sample holder (a) and a lever (b) were fixed to the base by hinges made of transparent tape so that they can move to be raised and lowered (Fig. 5.4).

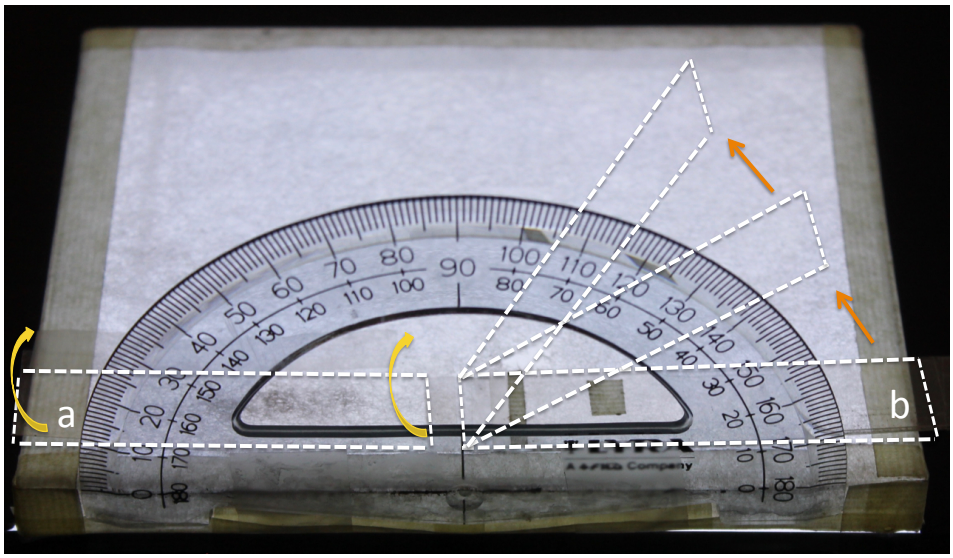

Figure 5.4. The custom tool to test the burnt paper folding resistance. The sample holder (a) was movable as indicated by the yellow arrows, and the lever (B), could move up and down in the direction shown by the orange arrows.

When perfectly vertical, the lever resulted at a right angle to the base and its position corresponded to 90° on the protractor (Fig. 5.5).

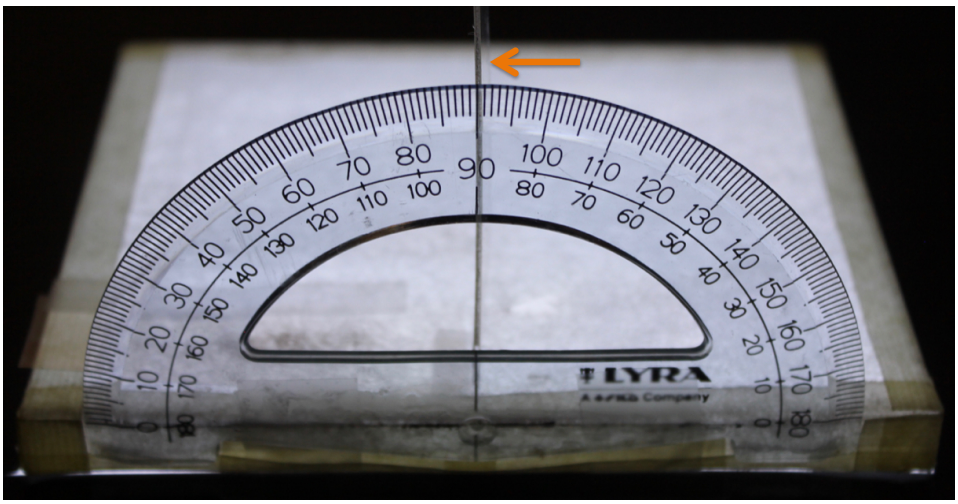

Figure 5.5. Once fully up, the lever is in vertical position (orange arrow), corresponding to 90° on the protractor.

The sample was placed horizontally on the base and secured by the slight pressure exerted by the holder (a), 5 mm^2 overlapping the lever (b) (Fig. 5.6). Each sample involved in the fold resistance test, when positioned on the apparatus, presented the same orientation of the chain (horizontal) and of the laid line (vertical) so that they all were tested in the same fiber direction.

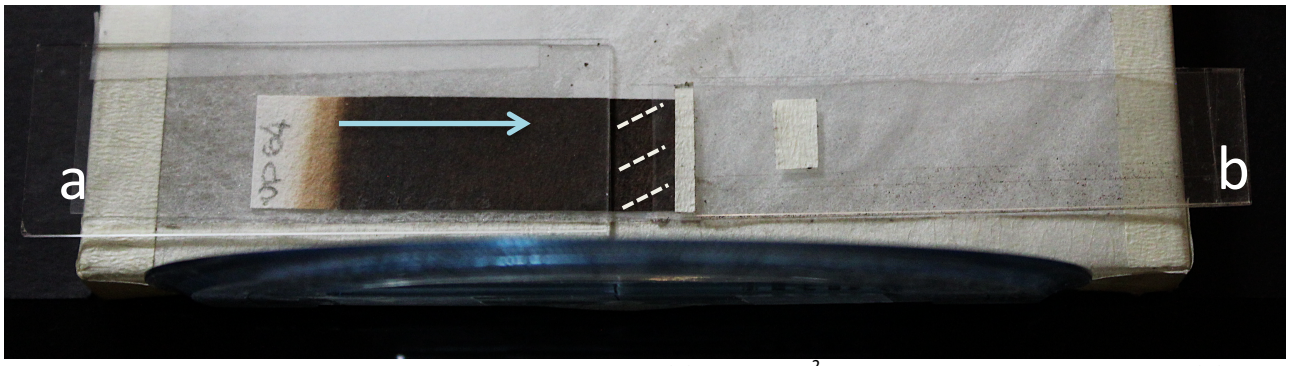

Figure 5.6. The sample kept in position by the sample holder (a), the 5 mm^2 dotted area overlapping the lever (b). The blue arrow indicates the chains direction of the paper

The part of the paper overlapping the lever was therefore free and, when pushed by the upward movement of the lever, moved with it, bending until it broke. As the test was carried out with the instrument positioned on a light pad, the transmitted light allowed to better visualize the first breakage of the sample. The breaking angle corresponding to the lever position could then be read on the protractor and reported as critical fold angle (CFA), see Fig. 5.7. The test was repeated at fixed 5 mm intervals on the same sample, the sample resulting progressively shorter. This allowed to maximize the numbers of tests on a single sample.

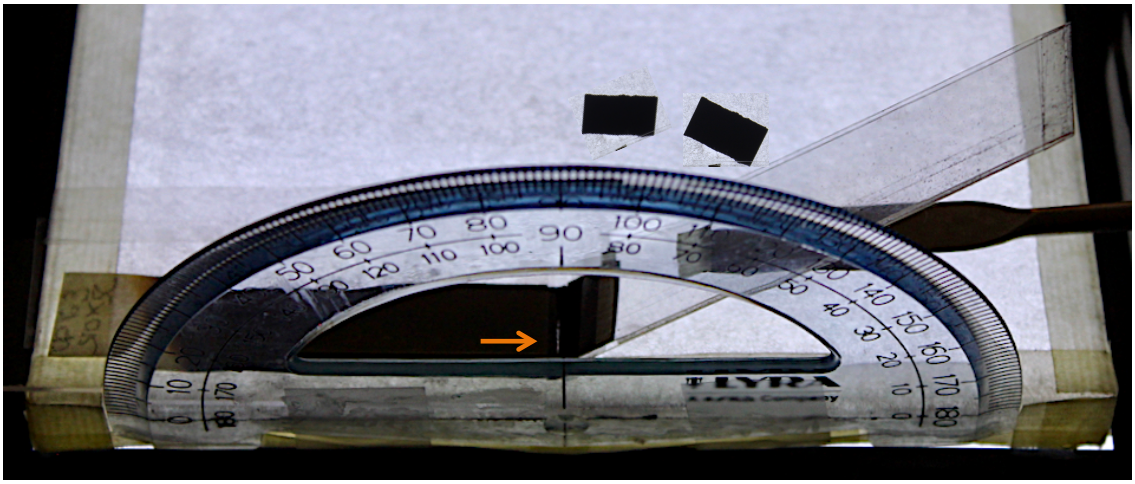

Figure 5.7. Fold test in progress: the lever progressively raised forcing the sample to bend and the transmitted light filtered through the first paper breaking point (enahnced by the orange arrow). The amplitude of the angle (50°) is readable on the protractor and defined as critical fold angle (CFA).

3. Burnt paper treatment with cellulose nanocrystals (CNC)

Upon the preliminary tests and the adoption of a measuring tool (CFA), further treatments were carried out with crystalline nanocellulose dispersed in alcohol with the aim of selecting a suitable concentration of the CNC dispersion and the most effective combination of nanocellulose and solvent.

3.1 CNC dilution and distribution in the charred samples

Nanocellulose dispersions were obtained by stirring 0.3% w/v CNC in isopropyl alcohol, in ethyl alcohol and in a mix isopropyl/ethyl alcohol (1:1). Each dispersion was tested on 5 unsized (UP10-14) and 5 sized (SP10-14) burnt RPM paper samples, which were strips of 5 cm x10 cm. Each strip was longitudinally cut in 5 substrips (1x10 cm^2): 2 of them were left untreated as control and the other 3 sprayed with the nanocellulose dispersion at a distance of 10 cm using a KAKUYI Airless Aerosol Mister sprayer. Single applications recto and verso were done, double application recto and verso was performed only with CNC in alcohol.

In order to evaluate the amount of product entered within the paper (uptake), samples were weighed before and after each application with a balance Mettler AE166 Delta Range.

Once dried, charred area of the samples treated with CNC did not show shining deposits, confirming a better product distribution achieved by spray compared to the brush used in the previous applications. Fold test was therefore carried out.

3.2 Fold resistance evolution of samples treated with cellulose nanocrystals

The fold test was performed under constant conditions of temperature (21°C ± 2°) and relative humidity (45% ± 2%). As already mentioned, the critical fold angle (CFA) corresponded to the measurement of the amplitude (degree) of the break angles of successive portions of the sample, and breaks occurred at 5 mm interval distances, with a minimum of 10 breaks per substrip (1 x 10 cm^2). Consequently, a minimum of 100 breaks, and corresponding CFA values, were obtained for the control substrips in the five UP10-UP14 samples (2 control substrips x 10 breaks x 5 UP samples). From these values, the average CFA for the UP10-14 control substrips was worked out (CFA_{CTRL}). For the treated substrips, a minimum of 150 breaks, and corresponding CFA values, were obtained (3 treated substrips x 10 breaks x 5 UP10-14 samples). From these values, the

average CFA for the UP10-14 treated substrips was worked out (CFA_{TRT}). The same was done for the SP10-14 samples.

Fold resistance variation (FRV) between treated and control was calculated as a percentage according to the formula (CFA_{TRT}-CFA_{CTRL})/CFA_{CTRL} * 100.

In order to evaluate the errors, standard deviations were worked out for CFA_{CTRL} and CFA_{TRT}. Standard deviation gives the statistical error expected for a single CFA measurement. However, we must point out that the average CFA values, CFA_{CTRL} and CFA_{TRT}, have a much lower standard error, which is given by: $\varepsilon = \frac{\sigma}{\sqrt{n}}$, σ being the standard deviation and *n* the number of measurements. In the tables, the indicated errors for CFA_{CTRL} and CFA_{TRT} are the so calculated standard mean errors.

Based on this consideration, all the observed variations between CFT_{TRT} and CFA_{CTRL} are always above the actual error, and therefore indicative of actual variations.

FRV% errors were calculated with the error propagation formula:

$$\varepsilon_{FRV} = FRV\% \cdot \frac{\sqrt{\varepsilon_{ctrl}^2 + \varepsilon_{trt}^2}}{|CFA_{trt} - CFA_{ctrl}|}$$

Table 5.2 gathers the variations in weight (indicative of the uptake of nanocellulose) and in fold resistance of RPM burnt samples (UP10-14 and SP10-14) treated recto and verso with the 0,3% dispersion of CNC in isopropyl alcohol by spraying with the KAKUYI Airless Aerosol Mister sprayer.

Table 5.2. UP and SP burnt RPM samples treated by spraying once recto and verso the 0.3% dispersion of CNC in isopropyl alcohol. Uptake is intended as average sample weight variation before and after treatment, CFA is given as average break angle amplitude. Errors in CFA are given as standard mean errors, while standard deviations are reported in brackets under the CFA values. Errors in the fold resistance variation percentage were calculated as indicated in the main text.

Unsized samples	Average weight before	Average weight after 0.3%CNC_isop. 1r/1v	Weight variation (uptake)	CFA_{CTRL} (106 breaks)	CFA_{TRT} (150 breaks)	%Fold Resistance Variation
UP10-14	mg 118.2	mg 118.5	+0.4%	102° ± 1° (St.Dev = 12°)	105° ± 1° (St.Dev = 13°)	**+3.0 ± 1.5%**

Sized samples	Average weight before	Average weight after 0.3%CNC_isop. 1r/1v	Weight variation (uptake)	CFA_{CTRL} (106 breaks)	CFA_{TRT} (150 breaks)	%Fold Resistance Variation
SP10-14	mg 110.8	mg 112.1	+1.1%	59° ± 1° (St.Dev = 10°)	62° ± 1° (St.Dev = 11°)	**+5.0 ± 2.0%**

The treatment seemed to affect the sized samples in a more consistent way, in terms of both uptake (+1.1% versus +0.4% of the unsized samples) and paper resistance improvement (FRV% +5% vs. +3% of the unsized samples).

It is to be noted that standard deviation of CFA_{CTRL} was quite high (12° in unsized samples and 10° in sized samples), probably due to the imperfect uniformity in the samples (burning procedure), resulting in slight differences in the resistance of the charred fibers when forced to fold. As expected, the CNC treatment performed by spraying did not attenuate this variability and the standard deviation of average CFA in the treated samples was even higher, resulting in 13° in the unsized samples and 11° in the sized ones. This can be explained by the spraying methodology which inherently bears a variability in the deposit and adds up to the overall paper resistance variability.

A positive influence of the CNC dispersion was however achieved, as it was able to enter the charred paper and somewhat increased its mechanical performance.

The results of the fold test performed on the set of samples UP20-24 (UP20, UP21, UP22, UP23, UP24 and SP20-24 (SP20, SP21, SP22, SP23, SP24) treated recto and verso with the 0.3% CNC dispersion in ethyl alcohol are presented in Table 5.3.

Table 5.3. UP and SP burnt RPM samples treated by spraying once recto and verso the 0,3% dispersion of CNC in ethanol. Uptake is intended as average sample weight variation before and after treatment, CFA is given as average break angle amplitude. Errors in CFA are given as standard mean errors, while standard deviations are reported in brackets under the CFA values. Errors in the fold resistance variation percentage were calculated as indicated in the main text.

Unsized samples	Average weight before	Average weight after 0.3%CNC_ethyl. 1r/1v	Weight variation (uptake)	CFA_{CTRL} (102 breaks)	CFA_{TRT} (151 breaks)	%Fold Resistance Variation
UP20-24	mg 107.0	mg 108.6	+1.5%	105° ± 1° (St.Dev = 13°)	113° ± 1° (St.Dev = 13°)	**+8.0 ± 1.6%**
Sized samples	Average weight before	Average weight after 0.3%CNC_ethyl. 1r/1v	Weight variation (uptake)	CFA_{CTRL} (113 breaks)	CFA_{TRT} (158 breaks)	%Fold Resistance Variation
SP20-24	mg 112.8	mg 114.4	+1.4%	55° ± 1° (St.Dev = 9°)	58° ± 1° (St.Dev = 10°)	**+5.0 ± 2.0%**

The resulting uptake was greater compared to the weight increase obtained using CNC in isopropanol and was higher for the unsized samples, which were evidently more permeable to alcohol than the sized ones: +1.5% for the unsized samples (it was +0.4% when using the dispersion in isopropanol) and +1.4% for the sized ones (it was +1.1% in the previous test). The average CFA confirmed the trend already observed in the previous test: CNC induced positive variations in the mechanical resistance of the charred samples and the improvement was directly proportional to the uptake. The FRV was +8% for the unsized samples and +5% for the sized ones, with a rather high standard deviation of average CFA (respectively 13° and 9°) which was not reduced after the treatment (13° in the unsized samples and 10° in the sized ones).

Table 5.4 shows the uptake and CFA variations in the set of samples UP30-34 and SP30-34 treated recto and verso with the 0.3 % w/v dispersion of CNC in a mixture composed of ethyl alcohol and isopropyl alcohol (1:1).

Table 5.4. UP and SP burnt RPM samples treated by spraying once recto and verso with the 0,3% dispersion of CNC in a mixture composed of ethyl alcohol and isopropyl alcohol (1:1). Uptake is intended as average sample weight variation before and after treatment, CFA is given as average break angle amplitude. Errors in CFA are given as standard mean errors, while standard deviations are reported in brackets under the CFA values. Errors in the fold resistance variation percentage were calculated as indicated in the main text.

Unsized samples	Average weight before	Average weight after 0.3%CNC_et/iso 1r/1v	Weight variation (uptake)	CFA_{CTRL} (110 breaks)	CFA_{TRT} (156 breaks)	%Fold Resistance Variation
UP30-34	mg 107.59	mg 109.24	+1.5%	105° ± 1° (St.Dev = 14°)	112° ± 1° (St.Dev = 14°)	**+6.7 ± 1.7%**
Sized samples	Average weight before	Average weight after 0.3%CNC_et/iso 1r/1v	Weight variation (uptake)	CFA_{CTRL} (113 breaks)	CFA_{TRT} (158 breaks)	%Fold Resistance Variation
UP30-34	mg 119.3	mg 120.8	+1.2%	57.0° ± 0.8° (St.Dev = 8°)	59.0° ± 0.6° (St.Dev = 8°)	**+3.5 ± 1.8%**

The treatment performed with the 0.3% CNC dispersion in the alcohol mixture led to a paper uptake of +1.5% in the unsized samples and +1.2% in the sized ones. The fold resistance also increased: a +6.7% in the unsized samples and a +3.5% in the sized samples were obtained. Both uptake and CFA variations were lower than those obtained treating samples with the dispersion of CNC in ethyl alcohol only, which had already demonstrated to work better than isopropanol as nanocellulose carrier (cfr. Table 5.3). Data resulted from this fold test also showed a high standard deviation of average CFA both in control (14° for the unsized and 8° for the sized samples) and in treated samples (respectively 14° and 8°).

On the basis of the interesting results obtained from the treatment with 0.3% w/v CNC in ethyl alcohol recto and verso, a double application recto and verso with the same dispersion was also performed on the samples; once sprayed, samples were allowed to dry perfectly before the second application. Results are summarized in Table 5.5.

Table 5.5. UP and SP burnt RPM samples treated by spraying with the 0,3% dispersion of CNC in ethyl alcohol twice recto and verso. Uptake is given as average sample weight variation before and after treatment, CFA is given as average break angle amplitude. Errors in CFA are given as standard mean errors, while standard deviations are reported in brackets under the CFA values. Errors in the fold resistance variation percentage were calculated as indicated in the main text.

Unsized samples	Average weight before	Average weight after 0.3%CNC_ethyl. 2r/2v	Weight variation (uptake)	CFA_{CTRL} (108 breaks)	CFA_{TRT} (150 breaks)	%Fold Resistance Variation
UP25-29	mg 121.0	mg 123.5	+2.7%	107° ± 1° (St.Dev = 14°)	115° ± 1° (St.Dev = 14°)	**+7.5 ± 1.7%**
Sized samples	Average weight before	Average weight after 0.3%CNC_isop. 2r/2v	Weight variation (uptake)	CFA_{CTRL} (113 breaks)	CFA_{TRT} (158 breaks)	%Fold Resistance Variation
UP25-29	mg 127.8	mg 131.0	+2.5%	56.0° ± 0.7° (St.Dev = 7°)	59.0° ± 0.7° (St.Dev = 9°)	**+5.4 ± 1.8%**

Comparison between Table 5.3 and Table 5.5 confirmed a higher uptake for samples treated twice. In the unsized paper, it went from +1.5% achieved with the single application to +2.7% induced by the second application and from +1.4% to +2.5% in the sized samples. However, the double application did not produce an improvement in the mechanical resistance. For the unsized samples, FRV was +8.0% in the single application and +7.5% in the double treatment. For the sized samples, FRV was +5% in the single treatment and +5.4% in the double treatment.

In conclusion, a double application of nanocellulose seemed not to be advantageous. This piece of evidence, together with the appearance of shiny surface residues in the samples treated twice, led to the decision to use the single treatment in further tests. Single application was also less stressful and preferable in a perspective of future application on historical material, especially considering that the reinforcement with nanocellulose should possibly be followed by, or combined to, the coating with polysiloxanes, as will be discussed in the next chapter, and such a three-step treatment would have cause an overstress to the fragile burnt paper of the originals.

4. Burnt paper treatment with microfibrillated cellulose (MFC)

The method followed in treating the samples with CNC dispersions, was used also for testing MFC dispersions to evaluate the efficiency of the different alcohol-based solvents as nanocellulose carriers.

4.1 MFC concentration and distribution in the charred samples

Preliminary tests performed by brushing with 0.2% MFC suspensions in ethyl and in propyl alcohol had manifested the formation of white surface deposits, larger and considerably more interfering compared to those observed on samples treated with the 0.3% CNC suspensions (cfr § 1.3 in this chapter). Lower MFC concentrations (0.1% w/v, 0.08% w/v, 0.06% w/v) were tried by stirring (5' at 10,000 rpm) in isopropyl and in ethyl alcohol and were sprayed on the UP and SP samples to check for any undesirable effects. Once dried, only the samples treated with the 0.06% MFC dispersion did not show any noticeable residue on the surface of the treated charred areas.

As it is a pre-requisite for any real paper treatment not to modify the optical properties of the paper surface, unsized and sized burnt RPM paper (5x10 cm^2) were thus treated with the 0.06% MFC dispersions, both in ethyl and in isopropyl alcohol. 5 strips (1x10 cm^2) per sample were cut: 2 of them were left untreated as control and the other 3 sprayed recto and verso with the 0.06 % MFC at a distance of 10 cm with the KAKUYI Airless Aerosol Mister sprayer.

As done in previous tests, the samples were weighed before and after each application and the folding test was performed to assess the resulting improvement in paper strength using the CFA criterion. The same procedure used for CNC was used for determining CFA_{CTRL}, CFA_{TRT} and FRV in the samples treated with MFC, as well as their errors.

4.2 Fold resistance evolution in samples treated with microfibrillated nanocellulose

Uptake and variations in the fold resistance of the sample sets UP20-24 and SP20-24 treated recto and verso with a 0.06% dispersion of MFC in isopropyl alcohol are displayed in Table 5.6.

Table 5.6. UP and SP burnt RPM samples treated by spraying once recto and verso with the 0,06% dispersion of MFC in isopropanol. Uptake is given as average sample weight variation before and after treatment, CFA is stated as average break angle amplitude. Errors in CFA are given as standard mean errors, while standard deviations are reported in brackets under the CFA values. Errors in the fold resistance variation percentage were calculated as indicated in the main text.

Unsized samples	Average weight before	Average weight after 0.06%MFC_isop. 1r/1v	Weight variation (uptake)	CFA_{CTRL} (109 breaks)	CFA_{TRT} (156 breaks)	%Fold Resistance Variation
UP20-24	mg 115.85	mg 116.43	+0.5%	101° ± 1° (St.Dev = 13°)	101° ± 1° (St.Dev = 11°)	**0%**
Sized samples	Average weight before	Average weight after 0.06%MFC_isop. 1r/1v	Weight variation (uptake)	CFA_{CTRL} (109 breaks)	CFA_{TRT} (152 breaks)	%Fold Resistance Variation
SP20-24	mg 118.06	mg 119.47	+1.2%	77° ± 1° (St.Dev = 10°)	80.0° ± 0.7° (St.Dev = 9°)	**+3.9% ± 1.6%**

According to the weight variations in the treated samples compared to the controls, the uptake of the unsized samples was very low (+0.5%) and no improvement in the paper mechanical resistance was observed, with a high standard deviation in average CFA both for the untreated (13°) and the treated samples (11°). These outcomes were less satisfying than those obtained treating the samples with CNC in isopropyl alcohol, shown in Table 5.2. The uptake for the sized samples seemed to be more in line with that resulting from tests carried out with CNC. The 0.2% w/v MFC increased the sample weight of +1.2% and improved FRV of +3.9%, with standard deviations of average CFA lower than 10°.

In Table 5.7, the results of the applications performed on the set samples UP25-29 and SP25-29 with a 0.06% w/v of MFC dispersion in ethyl alcohol are summarized.

Table 5.7. UP and SP burnt RPM samples treated by spraying once recto and verso with the 0,06% dispersion of MFC in ethyl alcohol. Uptake is given as average sample weight variation before and after treatment, CFA is stated as average break angle amplitude Errors in CFA are given as standard mean errors, while standard deviations are reported in brackets under the CFA values. Errors in the fold resistance variation percentage were calculated as indicated in the main text.

Unsized samples	Average weight before	Average weight after 0.06%MFC_eth. 1r/1v	Weight variation (uptake)	CFA_{CTRL} (111 breaks)	CFA_{TRT} (152 breaks)	%Fold Resistance Variation
UP25-29	mg 112.7	mg 115.48	+2.5%	98.0° ± 0.9° (St.Dev = 9°)	103.0° ± 0.9° (St.Dev = 11°)	**+5.1 ± 1.3%**
Sized samples	Average weight before	Average weight after 0.06%MFC_eth. 1r/1v	Weight variation (uptake)	CFA_{CTRL} (112 breaks)	CFA_{TRT} (155 breaks)	%Fold Resistance Variation
SP25-29	mg 119.5	mg 122.36	+2.4%	71.0° ± 0.9° (St.Dev = 9°)	77.0° ± 0.9° (St.Dev = 11°)	**+8.4 ± 1.8%**

The application of a 0.06%MFC in ethyl alcohol led to a considerable uptake, +2.5% for unsized samples and a +2.4% for the sized ones; the lower weight increase of the sized paper confirmed, once again, the same trend observed in all the previous tests. As for the fold resistance variation, a +8.4% increase was obtained for the sized sample, and lower for the unsized one (+5.1%).

Interestingly, if we compare the results for CNC in ethanol (Table 5.3) and MFC in ethanol (Table 5.7) there is a sort of "inversion", with MFC/ethanol enhancing the fold resistance in sized samples and performing worse on unsized samples.

Comparing FRV for MFC dispersion in isopropanol and ethanol, it is evident that MFC/ethanol involves a strong improvement in mechanical resistance with respect to MFC/isopropanol. Therefore, MFC in ethanol:isopropanol mixture was not further considered, and ethanol was chosen as the best solvent for CNC and MFC dispersions to be applied on the burnt samples.

5. Optimised reinforcement treatment with a CNC/MFC dispersion

5.1 Dispersion of the combined nanocelluloses and distribution in the charred samples

Tests were also performed by combining CNC and MFC in ethanol. The main objective of these applications was to compare the improvements in absorption and CFA with those resulting from the application of CNC and MFC separately.

0.3% CNC and 0.06% MFC were mixed in ethyl alcohol by stirring at 10 000 rpm for 5 minutes to achieve a stable nanocellulose dispersion. The resulting dispersion was thicker than the separated CNC and MFC dispersions, and the sprayer was unfit to carry the dispersion on the paper in a uniform way. Therefore, the dispersion was applied on the samples sets UP94-96 (composed of the samples UP94, UP95, UP96) and SP94-96 (composed of SP94, SP95, SP96) by airbrush (Belkits BEL-AIR 005 with a compressor piston type Typhoon supplied by the Kaiser Trading Srl) carrying a 0.8 mm needle, working at a pression pressure of 1.5 bar and kept at a distance of more or less 10 cm from the sample.

5.2 Fold resistance evolution of samples treated with the combination of nanocrystals (CNC) and microfibrillated (MFC) cellulose

Table 5.8 shows the results of the tests performed combining CNC and MFC in ethyl alcohol and treating samples by airbrush.

For each samples set UP94-96 (composed of UP94, UP95 and UP96) and SP94-96 (SP94, SP95 and SP96) a minimum of 60 breaks were obtained from the control strips and a minimum of 90 breaks from the treated strips.

Table 5.8. UP and SP burnt RPM samples treated by airbrushing once recto and verso with the dispersion of combined nanocelluloses (0.3% CNC + 0.06% MFC) in ethyl alcohol. Uptake is given as average sample weight variation before and after treatment, CFA is stated as average break angle amplitude. Errors in CFA are given as standard mean errors, while standard deviations are reported in brackets under the CFA values. Errors in the fold resistance variation percentage were calculated as indicated in the main text.

Unsized samples	Average weight before	Average weight after 0.3%CNC+0.06%MFC_ eth_1r/1v_airbrush	Weight variation (uptake)	CFA_{CTRL} (60 breaks)	CFA_{TRT} (90 breaks)	%Fold Resistance Variation
UP94-96	mg 106.07	mg 106.87	+1.4%	95° ± 1° (St.Dev = 8°)	104.0° ± 0.8° (St.Dev = 8°)	**+9.5 ± 1.5%**
Sized samples	Average weight before	Average weight after 0.3%CNC+0.06%MFC_ eth_1r/1v_airbrush	Weight variation (uptake)	CFA_{CTRL} (60 breaks)	CFA_{TRT} (90 breaks)	%Fold Resistance Variation
UP94-96	mg 115.92	mg 117.45	+1.5%	76° ± 1° (St.Dev = 8°)	83.0° ± 0.6° (St.Dev = 6°)	**+9.2 ± 1.7%**

Compared to the treatment with the 0.06% w/v MFC dispersion in ethanol (Table 5.7), the uptake in the application of a mix of CNC and MFC resulted lower and more similar to the weight increase in samples treated with the 0.3 % w/v CNC in ethanol (Table 5.3). Despite this limited increase in weight, a greater improvement in mechanical resistance was achieved and was the best improvement of all the fold tests reported above, amounting to +9.5% for UP and to +9.2% for SP, therefore also reducing the gap in the treatment effect between the unsized and the gelatin-sized paper, and indicating a synergistic effect of CNC and MFC.

Standard deviations were also the lowest so far achieved, thus indicating a better uniformity of the product distribution in the samples.

On the basis of these encouraging results, a larger number of UP and SP burnt samples were treated with the combined nanocellulose dispersion composed of 0.03%CNC and 0.06% MFC in ethyl alcohol, in the same conditions and application method, to obtain a more significant number of fold tests and uptake values.

Table 5.9 summarizes the results of the uptake and the fold resistance improvement of the treated samples. Each set (e.g., UP88-90) was composed of 3 samples (UP88, UP89, UP90), 5 substrips per sample, 2 kept untreated (control) and 3 treated. Minimum 10 breaks per substrip were done, so that for each set of samples, an average number of 60 breaks were obtained as control (2 substrips x 10 breaks x 3 samples) and 90 breaks for the treated substrips (3 substrips x 10 breaks x 3 samples).

Table 5.9. UP burnt RPM samples treated by airbrush once recto and verso with the dispersion of combined nanocelluloses (0.3% CNC + 0.06% MFC) in ethyl alcohol. Uptake and fold resistance variation in the treated samples are displayed.

Unsized Samples	**Average weight variation after nano treat. recto/verso (mg)**	**Average %weight variation after nano treat. recto/verso**	**Average fold resistance variation after nano treat. recto/verso**
UP88-90	+ 0.83	+ 1.3%	+ 8.7% ± 1.5%
UP 94-96	+ 0.99	+ 1.4%	+ 9.9% ± 1.3%
UP97-99	+ 1.13	+ 1.5%	+ 8.4% ± 1.3%
UP118-120	+ 1.52	+ 2.1%	+ 10.7% ± 1.5%
UP121-123	+ 1.40	+ 2.1%	+ 13.7% ± 1.3%
UP 103-105	+ 1.33	+ 2.3%	+ 15.7% ± 1.2%

The uptake – given both as average weight variation and average % weight variation of the samples after treatment – and the fold resistance improvement confirmed that the deposition of the nanocellulose dispersion in the paper induced systematically an improvement in its mechanical strength, in this fulfilling the expectations that nanocellulose could play a positive role in reinforcing even severely deteriorated paper fibres. A relationship between the uptake and the resulting increase in the fold strength of the samples was generally observed, especially true for uptakes higher than 2%, which could lead to a fold resistance increase higher than 10%. This trend is best visualised in the graph (Fig. 5.10).

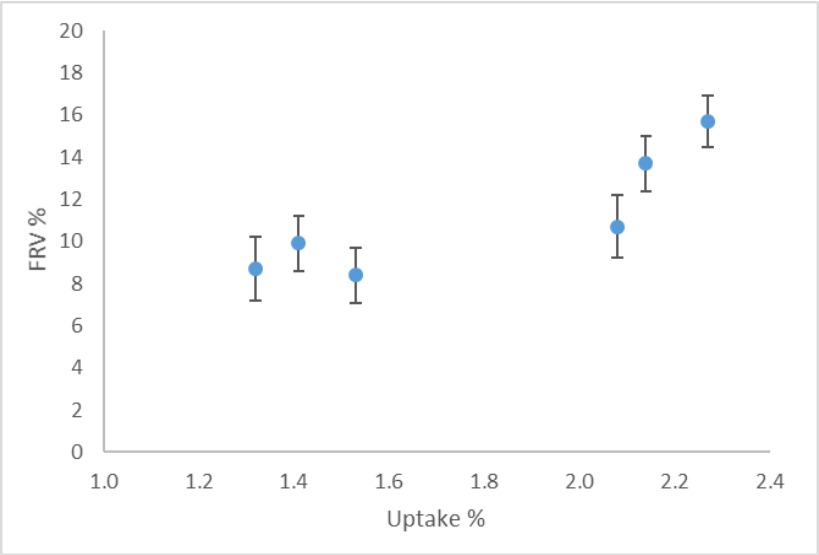

Figure 5.10. Trend of average fold resistance variation percentage (FRV%) vs. average weight variation percentage (Uptake%), from the data in Table 5.9 relative to unsized samples treated with the combined nanocellulose dispersion composed of 0.03%CNC and 0.06% MFC in ethyl alcohol.

The results in Table 5.10 are referred to the sized samples treated with the combined 0.3%w/v CNC and 0.06%w/v MFC dispersion in ethyl alcohol.

Also in this case, for each set of samples (i.e. SP85-87, SP88-90 and so on) an average number of 60 breaks were induced during the fold test in the control strip samples and about 90 in the treated sample strips.

Table 5.10. SP burnt RPM samples treated by airbrush once recto and verso with the dispersion of combined nanocelluloses (0.3% CNC + 0.06% MFC) in ethyl alcohol. Uptake and fold resistance variation in the treated samples are displayed.

Sized Samples	Average weight variation after nano treat. recto/verso (mg)	Average %weight variation after nano treat. recto/verso	Average fold resistance variation after nano treat. recto/verso
SP94-96	+ 1.05	+ 1.2%	+ 7.5% ± 1.6%
SP88-90	+ 1.07	+ 1.4%	+ 5.7% ± 1.6%
SP97-99	+ 1.07	+ 1.5%	+ 9.4% ± 1.5%
SP103-105	+ 1.53	+ 2.0%	+ 9.9% ± 1.7%
SP121-123	+ 1.47	+ 2.1%	+ 15.6% ± 1.5%
SP118-120	+ 1.57	+ 2.2%	+ 13.5% ± 1.5%

The results obtained from the sized treated samples showed a similar trend in absorption and fold strength variation to that observed in the unsized samples. The nanocellulose acts effectively within the charred areas by reinforcing the fibres: as a general trend, a higher weight variation of the samples treated with the nanocellulose dispersion - reported in Table 5.10 as average weight variation and average % weight variation - led to a better performance in the fold test, with higher positive variations in mechanical strength, as shown in the graph (Fig. 5.11).

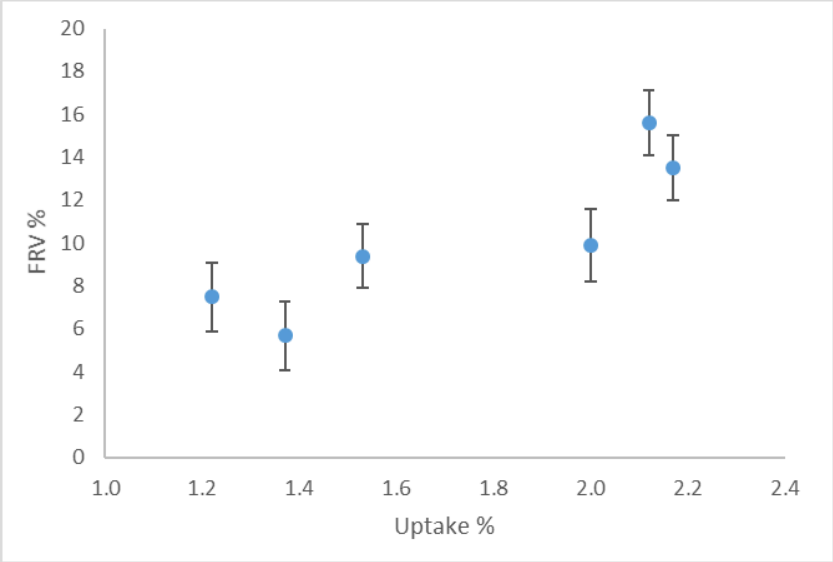

Figure 5.11. Trend of average fold resistance variation percentage (FRV%) vs. average weight variation percentage (Uptake%), from the data in Table 5.10 relative to sized samples.

It is important to note that paper breakage during folding tests occurred differently in untreated than in treated samples. In the former, the first fracture led to the immediate fragmentation of the paper. In the latter, on the other hand, despite the occurrence of crack points, the sample did not fragment completely and could be further forced to bend, confirming the firm interaction of the nanocelluloses with the paper matrix.

5.3 Inside the paper: nanocellulose distribution highlighted by SEM investigation

The effects and the morphological changes induced on the charred paper matrix by the introduction of nanocelluloses through the combined treatment with 0.3 % w/v CNC and 0.06 %

w/v MFC in ethyl alcohol were investigated by SEM/EDS both in the unsized and in the sized RPM samples.

The composition of the burnt RPM samples was analysed in Chapter 3 (§ 4) and will therefore not be discussed again in this chapter. Cellulose fibres of the control RPM paper were clearly visible in the SEM images, as were the countless, white particles, consisting in calcium carbonate or, more rarely, in magnesium silicate inclusions. However, the understanding of the modifications induced by the treatment was important. The element analysis (EDS) could not distinguish the original paper matrix from nanocellulose material, as the examination of the elements present in the sample indicated C and O as the predominant elements, fully congruent with cellulose.

The morphological study from the SEM images was more informative. The variation in the fibre density was particularly evident comparing the images of the charred paper before and after the nanocellulose application, especially when observing the unsized sample, as it was the case of UP94 shown in Fig. 5.12. The burnt samples had been treated with the combined nanocellulose dispersion recto and verso by airbrush, increasing its fold resistance by 8.4%.

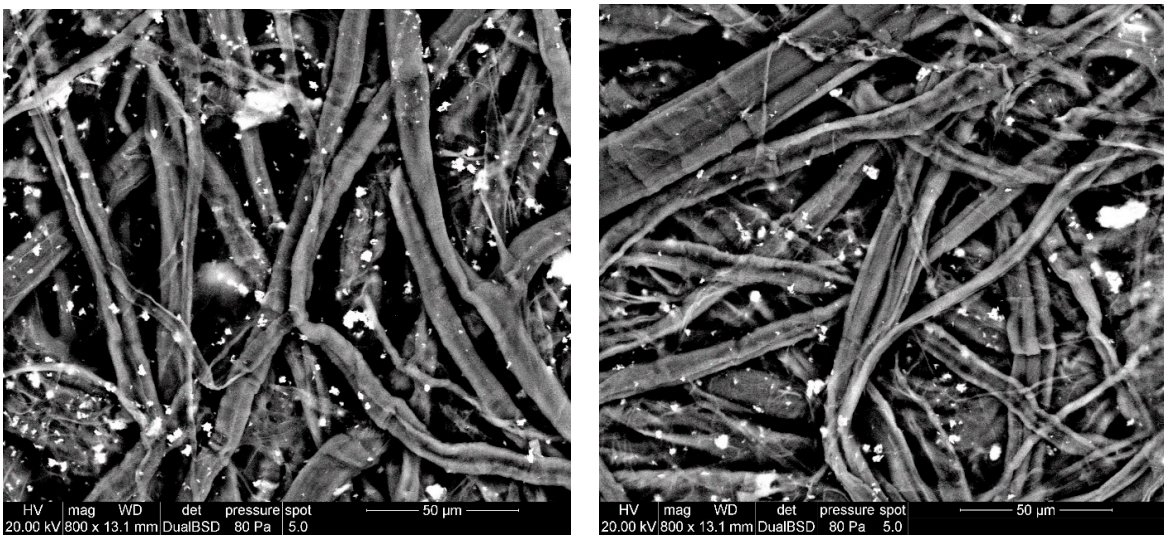

Figure 5.12. Unsized burnt sample UP94. SEM images (surface area, 800 x) before (left) and after (right) the application of the dispersion composed of 0.3%w/v and 0.06%w/v MFC in ethyl alcohol.

Before treatment, the fibers appeared rarefied, with large air gaps in between (Fig. 5.12, left), which appeared considerably reduced after the nanocellulose application. The paper matrix was consolidated by the insertion of the nanocelluloses (Fig. 5.12, right).

The SEM image of the dispersion of nanocrystals and cellulose microfibrils in ethyl alcohol used for the treatment (Fig. 5.13) indicates the presence of long, thin MFC microfibrils as main component, whose shape is comparable to that of the filaments intertwining with the larger fibres in the treated sample showed in Fig. 5.12.

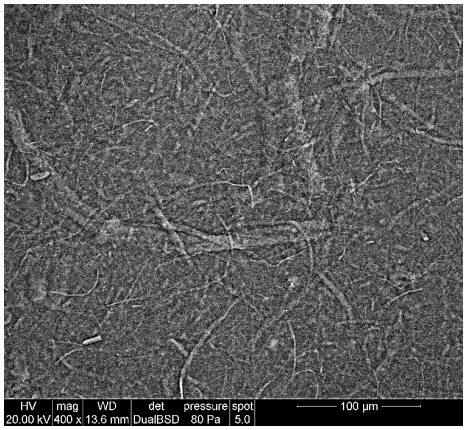

Figure 5.13. SEM image (400 x) of the dispersion composed of 0.3%w/v nanocrystal cellulose and of 0.06%w/v microfibrillated cellulose in ethyl alcohol.

In Fig. 5.13 the filaments of microfibrillated cellulose are the most visible, but nanocrystal whiskers, which are more difficult to distinguish in the UP94 sample, are also present as a sort of filler between the microfibrils.

This effect of density increase of the fibrous material was even more obvious when examining the cross sections of the same sample UP94 (Fig. 5.14), largely deprived of fibres.

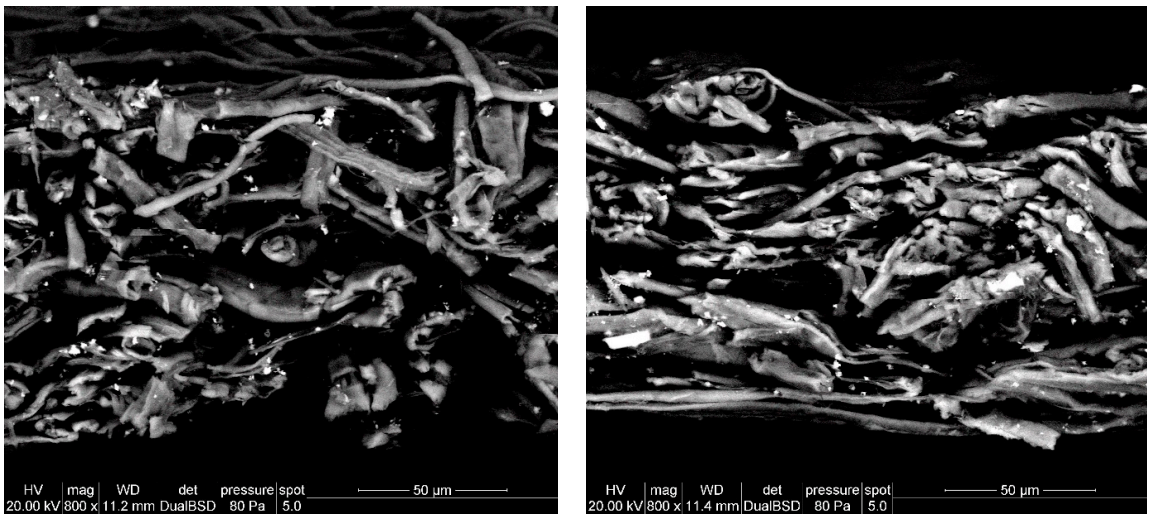

Figure 5.14. Unsized burnt sample UP94. SEM images (cross section, 800 x) before (left) and after (right) the application of the dispersion composed of 0.3%w/v CNC and 0.06%w/v MFC in ethyl alcohol.

Before treatment, the persisting fibres were sparse in the cross section (Fig. 5.14 left). After the treatment, nanocellulose penetrated into the paper thickness filling the voids and acting as a structural stabilising agent of the paper matrix.

Comparison of the SEM images of the sized burnt samples SP97 before and after the nanocellulose application is shown in Fig. 5.15.

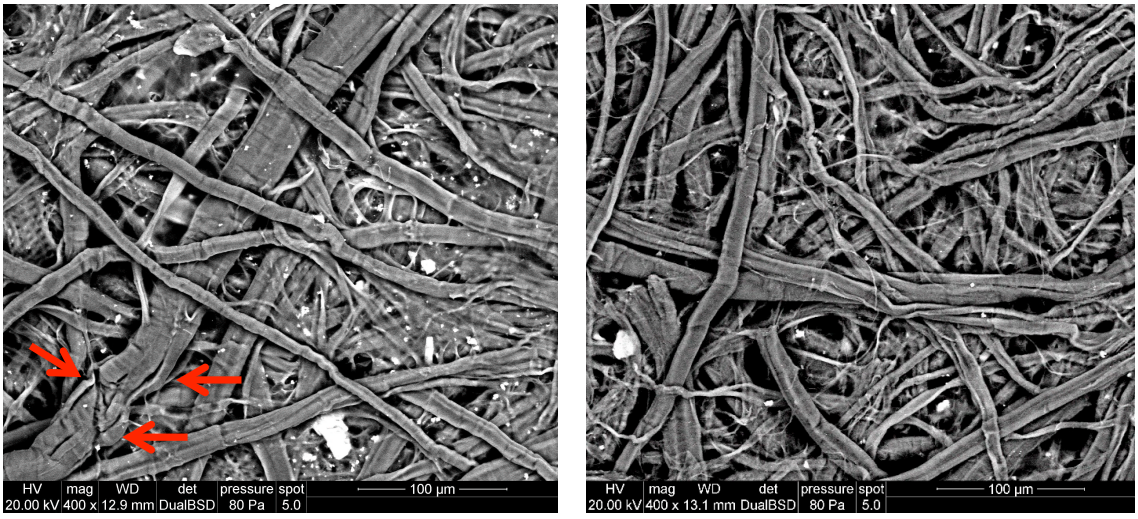

Figure 5.15. Sized burnt sample SP97. SEM images (surface area, 800 x) before (left) and after (right) the application of the dispersion composed of 0.3%w/v CNC and 0.06%w/v MFC in ethyl alcohol.

Despite being severely damaged by burning – as evident from the cuts on the larger cellulose fiber on the left in the Fig. 5.15 (red arrows) – the fiber network retained a compact appearance, probably due also to the role played by gelatin in somewhat protecting the fibre structure, as already explained in Chapter 3. However, in the treated sample (Fig. 5.15, right) the fibers density is higher and a larger number of thin, embedding filaments was observed.

The good penetration of the nanocellulose dispersion and its densification of the fiber network is clearly shown in Fig. 5.16, presenting the cross section of the sized sample SP97.

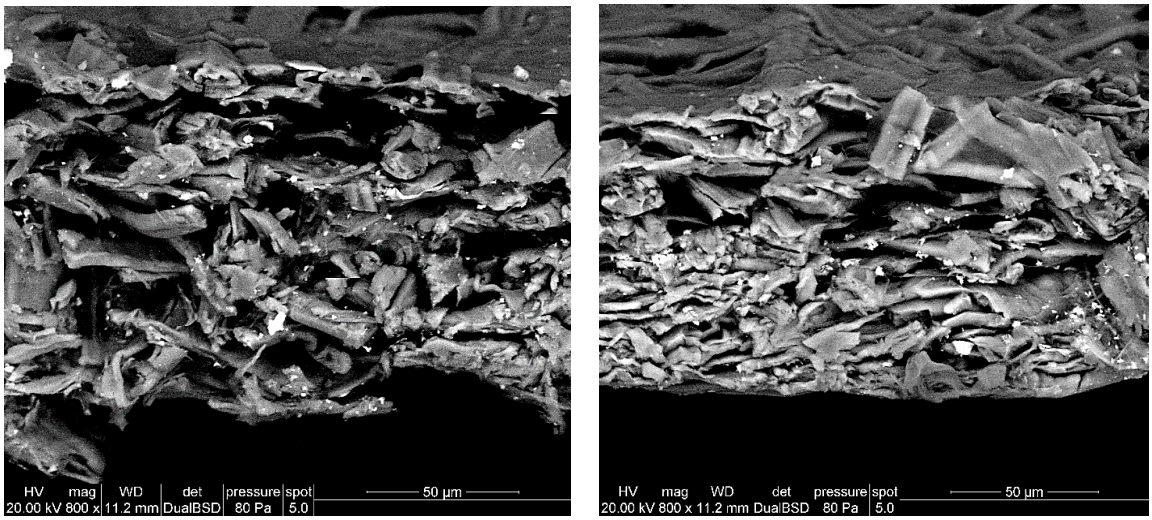

Figure 5.16. Sized burnt sample SP97. SEM images (cross section, 800 x) before (left) and after (right) the application of the dispersion composed of 0.3%w/v CNC and 0.06%w/v MFC in ethyl alcohol.

The differently "packed" aspect of the paper before (Fig. 5.16, left) and after the nanocellulose application (Fig. 5.16, right) was evident, and was certainly crucial in improving the mechanical strength of the sample, with an increasing of up to + 8.9% in its fold resistance.

6. Conclusions

Both cellulose nanocrystals and microfibrillated cellulose were tested as reinforcing agents of the charred paper areas with the application of nanocellulose dispersions on the unsized and sized RPM samples (obtained by burning for 15' on a hot plate set at 210°C).

Tests were first carried out to select the most suitable dispersing liquid for carrying the nanocellulose within the burnt fibres. Both CNC and MFC nanocellulose from the supplier jar were diluted in water, in ethyl alcohol and in isopropyl alcohol, applied on the samples by brushing and dried before assessing eventual unwanted effects. The formation of surface deposits, tidelines on the white unburnt areas as well as structure deformations were considered. On these bases, water was discarded and only the two alcohol solvents, ethanol and isopropanol, were deemed useful as dispersing liquids of the nanocellulose dispersions preparation.

Results of further treatments were achieved by visual assessment and a study of the paper mechanical properties improvement, performing the fold tests with a tailor-made instrument that

measures a critical folding angle (CFA). A 0.3 % w/v CNC dilution in ethyl or in isopropyl alcohol did not cause side effects on the paper, while giving a result in increasing the critical folding angles, especially when applied by spray. In particular, the application recto and verso by spray of a 0.3 % w/v CNC dispersion in ethanol with uptakes around 1.5% in the samples resulted to be the most effective treatment in improving the mechanical performance of the burnt paper, inducing a critical fold increase of +8.0% for the UP samples and of +5.0% for the SP samples. Double applications (twice recto/verso) were tested, but no improvement in the folding resistance was observed, while inducing more physical stress in the fragile burnt paper and additional treatment steps.

Tests performed with MFC dispersed in ethanol and in isopropanol at different concentrations (0.3 % w/v, 0.1 % w/v and 0.06 % w/v) allowed us to highlight the 0.06 % w/v MFC dispersion in ethanol as the most suitable product for obtaining an appreciable CFA improvement, both in UP

(+5.1%) and SP samples (+8.4%) for uptakes around 2.5%. Interestingly, irrespective of the slight uptakes difference, the MFC/ethanol was better on sized than on unsized, i.e., the opposite with respect to CNC/ethanol, suggesting that a combination CNC + MFC was probably the better choice.

A combination of 0.3 % CNC and 0.06 % MFC in ethyl alcohol was tested. Samples were treated by spraying with an airbrush to achieve a uniform distribution of the thick liquid dispersion, which was thicker than CNC or MFC alone. Fold resistance improvements were better than with each of the nanocelluloses separately, with a mechanical resistance average increase of +9.5% in the UP samples and +9.2% in the SP samples for uptakes around 1.5%.
The results of a large number of tests carried out with the same combined CNC/MFC dispersion under the same conditions confirmed the efficiency of the 0.3 % CNC and 0.06 % MFC dispersion in ethyl alcohol for reinforcing cellulose in the charred paper areas without any of the unwanted side effects. The tendency towards a certain relationship between the uptake and the corresponding fold resistance improvement was shown and it was observed that an uptake of over 2% generally induced an increase in strength of over 10% in both unsized and sized treated samples.

Sample investigation by SEM/EDS before and after treatments showed the higher fibers density in the treated samples, visible both on the surface and cross section, confirming the penetration of the nanocellulose into the whole thickness of the paper matrix. The reinforced cellulose network showed a higher amount of long, thin filaments intertwined in the original paper fibres. The firm

interaction between the nanocellulose introduced by the treatment and the paper matrix was evidenced also with the folding test as when the first crack occurred, untreated paper usually went into fragments, while treated paper did not and could be forced to bend further before breaking to a higher CFA. In the next chapter, the impact of polysiloxanes as reinforcement agent alone and in combination with nanocelluloses is studied.

Chapter 5 | References

Dreyfuss-Deseigne, R. (2017). «Nanocellulose Films: Properties, Development, and New Applications for Translucent and Transparent Artworks and Documents». *The Book and Paper Group Annual* 36, 108; https://cool.culturalheritage.org/coolaic/sg/bpg/annual/v36/bpga36-20.pdf

Chapter 6

Burnt paper strengthening with polysiloxanes

It was thought that the deposition of a thin, mesoporous structured nanosilica film on the burnt papers could protect the charred fragile areas, improving their cohesion and generating new chemical bonds with the paper matrix. To this end, various formulations of polysiloxanes based on tetraethoxysilane (TEOS) and aminoalkyloxysilanes were tested in this research.

1. Burnt paper strengthening with polysiloxanes based on tetraethoxysilane (TEOS)

1.1 TEOS based formulations involved in the research

As mentioned in Chapter 4 (§ 3.2.1), the alkoxysilane formulations based on tetraethoxysilane (TEOS) developed by the University of Padua and implemented by Siltea Srl had not yet been completely tested on cellulosic artifacts, and their compatibility with burnt paper was particularly to be investigated. Some polysiloxanes formulations developed especially to this purpose by Siltea Srl were then tested for the first time in the present study. They all were hydroalcoholic ready-to-use formulation (water 52% /isopropyl alcohol 43%) solutions of tetraethoxysilane (TEOS) and TEOS functionalised with one octyl group (octyltriethoxysilane, OTES) or with two methyl groups (diethoxydimethylsilane, DDMES). OTES was present in the formulations SIOX-5TO and SN1, while DDMES was present in the formulations SIOX-5S, SN1/DDMES and SIOX-5TD. The proportion TEOS/OTES and TEOS/DDMES is covered by industrial secrecy. The different formulations and the amount of active precursors in weight (percentage), with respect to the solvent, are summarized in Table 6.1.

Table 6.1. The different formulations tested, composed of tetraethoxysilane (TEOS) functionalised with octyl-triethoxyoctylsilane, OTES or diethoxydimethylsilane, DDMES, with specification of the precursor concentration.

Name	Active compounds	% Active compounds
SIOX-5TO	TEOS/ octyl-triethoxyoctylsilane	5%
SN1	TEOS/ octyl-triethoxyoctylsilane	9%
SIOX-5TD	TEOS/ diethoxydimethylsilane	5%
SN1d	TEOS/ diethoxydimethylsilane	9%
SIOX-5 S	TEOS/ diethoxydimethylsilane	30%

The addition of a co-precursor (OTES or DDMES) in the formulations influences the rigidity of the three-dimensional silicate network formed by TEOS via polymerization in the paper matrix. From experimental results by Siltea, DDMES gives a more compact and less flexible coating due to its shorter chains, while the long OTES chains provide a less rigid and more flexible coating film. These results could be counterintuitive, since OTES, thanks to three ethoxy groups, can provide cross-linking, while DDMES contains two ethoxy groups, and can give just linear polymers. However, in this case the longest octyl chains counterbalances the increased rigidity due to the induced cross-linking by OTES.

1.2 Preliminary tests with the TEOS-based polysiloxane formulations

1.2.1 Sample preparation

Unsized (UP) and sized (SP) burnt samples were produced in accordance with the standard procedure described in Chapter 3 (hot plate 250°C, 15 min). Each sample was cut in 6 strips, the first left as control and the others treated with one of the formulations, performing single and double applications. All the formulations were colourless and liquid and could be easily picked up and delivered by the brush bristles. The solvent evaporation time was quite fast, and the samples became dry to the touch in few minutes. In case of a double treatment, the second application took place before the sample was completely dry, in accordance with the procedure recommended by the producer.

The UP and SP samples intended for the visual examination (10 x 5 cm^2) were treated by brush recto and verso over an area of approximately 2 cm^2, including part of the charred paper and part of the white, unburnt paper (Fig. 6.1). In the UP and SP samples intended for the fold resistance test (6x10 cm^2), the whole charred area and few millimeters of the unburnt area were included in the application. Both single and double applications were performed and samples were allowed to dry at constant conditions (21°C ± 2° and 45% ± 2%RH).

Figure 6.1. The five formulations and the UP and SP samples prepared for the preliminary test (left). On the right, a SP sample treated with SIOX-5 S over an area of approximately 2 cm^2, including part of the charred paper and part of the unburnt paper.

1.2.2 Visual examination of the samples treated with a single application

According to the producer, the polymerisation process of the polysiloxane formulations usually takes some time (about 72 hours) to complete and stabilise. Visual examination was thus carried out a week after their application to the samples. The undesirable effects considered were the appearance of brown tide lines on the white paper area due to the spread of the product, darkening of the burnt, treated area and changes in the opacity of the paper (Fig. 6.2). In fact, an effect of transparency could be perceived on the unburnt areas of some of the treated samples, more evident when observing them with transmitted light (Fig. 6.3).

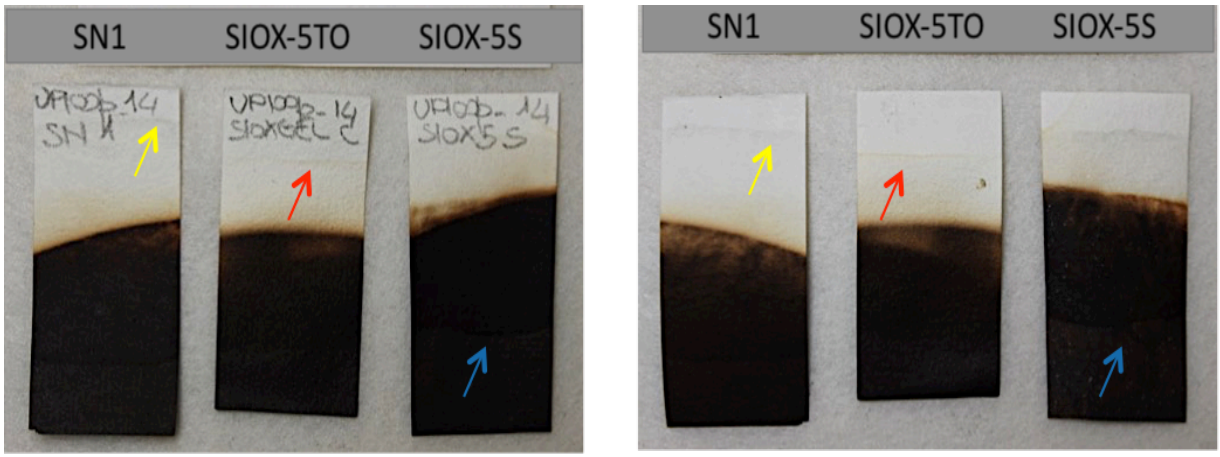

Figure 6.2. Undesirable effects on the UP burnt samples treated by brush with different poysiloxanes formulations, single application, recto and verso. On the left, the front of the samples is shown, on the right the back of the same samples. Brown tide lines (red arrow), color variation of the burnt area (blue arrow) and a transparency effect, resulting in a sort of white tidelines on the white, unburnt area (yellow arrow) were observed. SIOXGEL C, written on the sample in the middle on the left image, was the old name of SIOX-5TO. Pictures taken after drying.

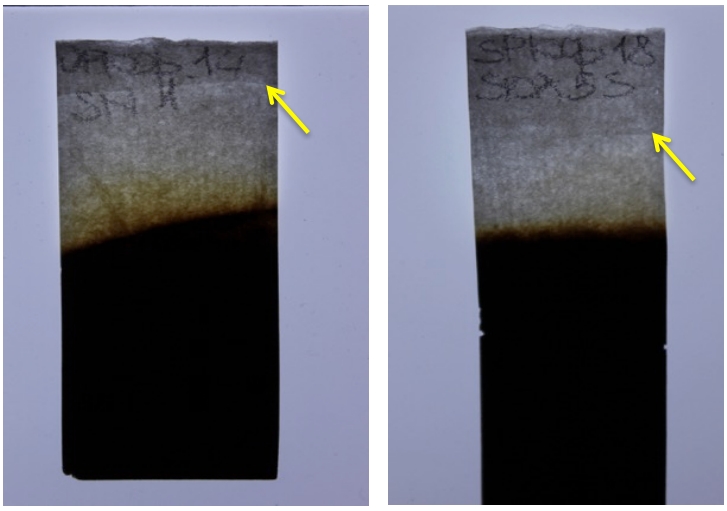

Figure 6.3. Transparency of the white area (yellow arrows) induced by SN1 on the UP sample (on the left) and by SIOX-5 S on the SP sample (on the right) distributed by brush, single application. Pictures taken after drying.

In general, unwanted effects were limited and less important in the SP samples. In Table 6.2 a rating level is expressed for each side effect observed: no = no variation; 1= slight; 2= medium; 3= heavy.

Table 6.2. Evaluation of the visual examination of the UP and SP samples, treated recto and verso by brush with the different TEOS-based formulations. Uptakes are given as % weight difference in the sample before and after treatment. Rating level: no = no variation; 1= light; 2= medium; 3= heavy.

TEOS based formulations	% weight increase after treat. (uptake)	Brown tide lines on white areas	Darkening of burnt area	White tide lines (transparency effect)
UP_SN1 (T/O 9%)	4.2%	no	2	3
UP_SN1d (T/D 9%)	5.3%	no	2	2
UP_SIOX-5TD (T/D 5%)	3.4%	3	1	no
UP_SIOX-5 S (T/D 30%)	7.4%	1	3	2
UP_SIOX-5TO (T/O 5%)	3.8%	1	no	no
SP_SN1 (T/O 9%)	2.7%	no	2	no
SP_SN1d (T/D 9%)	3.9%	1	2	no
SP_SIOX-5TD (T/D 5%)	3.0%	no	2	no
SP_SIOX-5 S (T/D 30%)	6.1%	2	3	3
SP_SIOX-5TO (T/O 5%)	2.7%	no	1	no

Different TEOS-based formulations determined different uptakes. On sized paper, the lowest uptakes, below or equal to 3%, resulted from the application of SIOX-5TO and SIOX-5TD - composed of a 5% of active matter - and of SN1 (T/O 9%). On sized paper, medium uptakes (around 4%) resulted from the application of SN1d, containing a 9% of active matter. Finally, on sized paper, the highest uptake (6%) was for SIOX-5 S, in which the amount of active compounds raised to 30%. On unsized paper, a similar trend was observed, although the uptakes, on average, are higher than for sized paper: lowest uptakes were for SIOX-5TO, SIOX-5TD and SN1 (range 3.5-4.5%). Medium uptakes for SN1d (5.3%) and highest uptakes SIOX-5S (7.4%). The difference in the uptakes between the UP and the SP paper was notable: polysiloxane was considerably more retained by the unsized samples after the solvent evaporation. This can be explained by the reduced permeability induced by the gelatin coating in the sized samples.

The lightest post-treatment side effects were observed on the samples brushed with SIOX-5TO, composed of TEOS and OTES: the appearance of brown tidelines on the UP sample and of darkening in the burnt area of the SP samples were of low impact (value: 1). Moreover, these problems are likely related to the large amount of product brushed on the paper, a defect which could be avoided by simply modifying the method of application of the polysiloxane.

SIOX-5TD, containing TEOS and DDMES, led to strong brown tide lines on the white area and slight color variation of the burnt treated area (value: 1) of the unsized samples, while no transparency effects were observed. In the sized samples, the same formulation produced a darkening of the

charred paper. The unwanted effects of the formulations SN1 (TEOS/OTES 9%) and SN1d (TEOS/DDMES 9%) were heavier, especially on the UP samples. The most important of unwanted effect was the darkening of the burnt treated area, observed in both UP and SP samples, and the transparency effect of the white area in the unsized paper.

The worst outcome was for SIOX-5 S, the product with TEOS and DDMES in the highest concentration: all the side effects were well detectable on both UP and SP samples, likely due to the very high product uptakes for this formulation.

1.2.3 Mechanical strength of the samples treated with a single application

The tailor-made instrument for the fold test, described in Chapter 5 (§ 2.1), was employed to evaluate the mechanical strength improvement induced by the polysiloxanes applications on the burnt papers. As before, the average critical fold angle (CFA) was intended as the measure of the amplitude (degree) of the break angles of progressive portions of the sample. Breaks were induced by folding the strip each 5 mm. For the control sample, and each treated sample, fold resistance was estimated as the average of CFA on 20 sample breaks, respectively CFA_{CTRL} and CFA_{TRT}. Folding resistance variation percentage (FRV%) and all the errors were calculated according to the formulas in Chapter 5 (§ 3.2).

In Table 6.3 the evolution of the mechanical fold resistance of the unsized and sized samples treated with the different polysiloxane formulations is shown and the uptake of each application is given as average % weight variation of the samples after treatment. Notice that, as described in section 1.2.1, these samples are not the same as in Table 2, but were freshly produced for the mechanical test.

Table 6.3. Fold test results of the UP and SP samples treated by brush with the different TEOS formulations SN1, SN1d, SIOX-5TD, SIOX-5 S and SIOX 5-TO, single application recto and verso. 20 breaks occurred during the fold test and the average CFA is intended as average break angle amplitude. The errors on average CFA are given as standard mean errors and standard deviations are reported in brackets.

TEOS based formulations	% weight increase (uptake) after treat. **1 recto/verso**	CFA_{CTRL} (20 breaks)	CFA_{TRT} (20 breaks)	**Fold resistance Variation**
UP_control	-	82.9±1.7° (7.7°)		
UP_SN1 (T/O 9%)	10.1%		96.5±2.8° (12.3°)	+16±4%
UP_SN1d (T/D 9%)	8.8%		100.4±3.4° (15.1°)	+12±4%
UP_SIOX-5TD (T/D 5%)	3.8%		102.2±2.0° (8.8°)	+23±3%
UP_SIOX-5 S (T/D 30%)	31.3%		75.3±2.8° (12.4°)	decrease
UP_SIOX-5TO (T/O 5%)	3.9%		106.4±2.5° (11.2°)	+28±5%
SP_control	-	65.7±2.1° (9.3°)		
SP_SN1 (T/O 9%)	10.2%		63.3±1.6 (7.0°)	decrease
SP_SN1d (T/D 9%)	8.3%		70.6±1.7° (7.6°)	+7±3%
SP_SIOX_5TD (T/D 5%)	3.6%		73.5±2.0° (8.8°)	+12±3%
SP_SIOX-5 S (T/D 30%)	25.3%		59.1±1.1° (5.0°)	decrease
SP_SIOX-5TO (T/O 5%)	3.5%		73.8±2.1° (9.5°)	+13±3%

Consistently with the results in Table 6.2, also in these latter samples the uptakes were higher for the unsized papers (UP) than for the sized ones (SP).

In the UP samples, mechanical resistance to fold was particularly enhanced by SIOX-5TO (+28%) and SIOX-5TD (+23%). The same outcome was also confirmed for the sized paper: SIOX-5TO was responsible of a +12% improvement and SIOX-5TO induced a similar fold resistance increase of +12%. This comes with uptakes that are higher than those obtained with nanocelluloses (Chapter 5). However, the best performance (SIOX-5TO) coincided with the lowest uptakes possibly achieved with the polysiloxanes in these tests. It has to be noted that the uptake for this latter sample is one of the lowest (+3.5%).

The UP papers, treated with SN1 and SN1d, were also strengthened and their fold resistance increased respectively of +21% and +16%, but only SN1d worked also for the SP samples and resulted in +7%. Also, in these samples the uptakes were higher (8-10%) than SIOX-5TO and SIOX-5TD. With uptakes around 25-30%, SIOX-5S even decreased the mechanical resistance of the samples. On the other hand, the richer formulation in TEOS and DDMES (30% of active matter), SIOX-5 S**,** affected negatively the paper strength and a decrease in fold resistance variation was observed (-12% in the UP sample, -9% in the SP one).

Fold test results showed that the SIOX-5TO formulation, containing a 5% of active compounds consisting of TEOS functionalised with OTES, was the most effective in inducing a positive variation of the mechanical resistance both in the UP and in the SP samples. Also, visual examination showed that SIOX-5TO applications did not give rise to heavy unwanted effects. Therefore, SIOX-5TO was the better choice in terms of both visual impact and mechanical resistance improvement.

1.2.4 Evaluation of the effects of a double application

The double application of the different TEOS-based formulations to the UP and SP samples yielded to the results summarized in Table 6.4. Comparison with Table 6.3 shows that, as expected, uptakes were higher (from 1.5 to 2 times).

Table 6.4. Fold test results of the UP and the SP samples double treated by brush, recto and verso with the different TEOS formulations. The number of breaks occurred during the fold test is specified and the average CFA is intended as average break angle amplitude. The errors on average CFA are given as standard mean errors and standard deviations are reported in brackets..

TEOS based formulations	% weight increase (uptake) after treat. **1 recto/verso**	CFA_{CTRL} (20 breaks)	CFA_{TRT} (20 breaks)	Fold resistance Variation
UP_control	-	108.0±3.2° (14.1°)		
UP_SN1 (T/O 9%)	16.0%		118.3±3.2° (14.5°)	+10±5%
UP_SN1d (T/D 9%)	12.4%		128.3±3.1° (14.0°)	+19±5%
UP_SIOX-5TD (T/D 5%)	14.6%		126.8±3.8° (17.2°)	+17±6%
UP_SIOX-5 S (T/D 30%)	48.4%		84.1±3.7° (16.4°)	decrease
UP_SIOX-5TO (T/O 5%)	11.5%		115.1±2.5° (11.0°)	+7±4%
SP_control	-	70.1±1.7° (7.7°)		
SP_SN1 (T/O 9%)	15.5%		69.3±1.8° (8.1°)	decrease
SP_SN1d (T/D 9%)	11.7%		63.3±2.0° (9.0°)	decrease
SP_SIOX_5TD (T/D 5%)	9.6%		77.0±1.7° (7.6°)	+10±3%
SP_SIOX-5 S (T/D 30%)	30.9%		63.5±1.1° (5.0°)	decrease
SP_SIOX-5TO (T/O 5%)	8.4%		69.0±2.2° (9.7°)	decrease

The trends in the reinforcement achieved by the various formulations was consistent with the results of the single applications. According to data, double application did not favour the improvement of flexibility in the samples. Again, an inverse proportionality relationship emerged between uptakes – given as average % weight variation of the samples after treatment – and variations in fold resistance: the greater the amount of polysiloxanes retained by the samples, the smaller the resulting reinforcing effect, or even a decrease. SIOX-5TD was the only product

working in the double application both on unsized and sized paper. In any case, in presence of a higher uptake, the result in fold resistance variation was reduced compared to those induced by the single application, as shown in Table 3 (+17% for double application vs. 23% for single application, for the UP samples, and +10% versus 12% for the SP samples). Except for SIOX-5TD, all the other formulations applied twice induced a clear decrease in paper strength.

Based on these considerations, further tests were carried out with single applications of the formulations found to be the most effective, SIOX-5TO and SIOX-5TD.

2. Development of the strengthening treatment with SIOX-5TO and SIOX-5TD

Side effects observed in the samples treated with SIOX-5TO and SIOX-5TD (Figures 6.2 and 6.3) were reduced by employing the airbrush to distribute the polysiloxane formulations on the samples with a single application recto/verso. This tool releases a very small-diameter spray and allowed a better control of the amount of product sprayed on the samples compared to the brush, preventing the appearance of the unwanted effects while allowing a more uniform coating application.

The airbrush was used with a 0.8 mm needle, pressure of 1.5 bar, at a distance of 10 cm from the sample.

2.1 Sample preparation

Samples were produced by burning unsized (UP) and sized (SP) RPM paper (3 x 10 cm^2) according to the standard procedure (hot plate, 250°, 15 min). Each sample was cut in 3 substrips (1 x 10 cm^2): one left as control and the others treated respectively with SIOX-5TO and SIOX-5TD. Applications were performed in constant thermohygrometric conditions (23°C, 50% RH) by airbrush.

2.2 Fold resistance induced by single applications of SIOX-5TO and SIOX-5TD

The samples were weighed before and after each application. The fold resistance test was performed one week after the treatment, when polymerisation was supposed to be almost complete, to study the strength evolution induced by SIOX-5TO and SIOX-5TD on the unsized and on the sized paper. Table 6.5 displays the results of the SIOX-5TO application to the UP burnt samples and is organised in increasing order of uptakes. The latter were significantly reduced compared to the applications by brush and were more in line with the uptakes achieved with the nanocelluloses (Chapter 5). They are given as average weight variation, as well as average % weight variation of the samples after treatment.

Table 6.5. Uptakes, critical fold angle (CFA) and fold test results of the UP samples treated with a single application of SIOX-5TO applied by airbrush recto and verso. 20 sample breaks were induced per sample during the fold test and the average CFA is intended as average break angle amplitude. The errors on average CFA are given as standard mean errors and standard deviations are reported in brackets..

Unsized samples	Weight before treatment (mg)	Weight after treatment (mg)	Weight variation (mg)	% weight variation (uptake)	CFA_{CTRL} (20 breaks)	CFA_{TRT} (20 breaks)	Fold resistance Variation
UP58_SIOX-5TO	102.23	103.00	0.77	+0.8%	96.5±2.2° (9.9°)	110.3±1.7° (7.6°)	+14±3%
UP68_SIOX-5TO	107.85	109.07	1.22	+1.1%	95.2±1.6° (7.0°)	102.1±1.3° (6.0°)	+7±2%
UP56_SIOX-5TO	117.66	119.01	1.35	+1.2%	98.5±1.9° (8.5°)	104.2±1.4° (6.4°)	+6±2%
UP57_SIOX-5TO	117.07	118.48	1.41	+1.2%	86.9±1.7° (7.8°)	103.0±1.7° (7.4°)	+19±3%
UP69_SIOX-5TO	113.81	115.40	1.59	+1.4%	90.8±1.8° (8.0°)	106.3±1.4° (6.2°)	+17±3%
Average				**+1.12%**			**+12.6±1.2%**

As a general trend, SIOX-5TO had an effective influence on the increase of the critical fold angle of all the unsized samples. In addition, the formulation also induced greater uniformity in the CFA resulting from the fold tests, which is reflected in the decrease of the values of the standard deviation in the treated samples compared to the controls. Also, airbrush led to minor uptakes with respect to brush (compare Table 6.5 and Table 6.3). However, there is no clear correlation between uptake percentage, which are all close to 1%, and fold resistance variation percentage which vary from +6% to +19%.

The tendency to a lower standard deviation could be observed also in the unsized burnt paper treated with the SIOX-5TD formulation. In contrast, positive results were not the rule with this

formulation and the treatment did not always induce an improvement in the mechanical resistance of the charred paper, as shown in Table 6.6.

Table 6.6. Uptakes, critical fold angle (CFA) and fold test results of the UP samples treated with a single application of SIOX-5TD applied by airbrush recto and verso. 20 sample breaks were induced per sample during the fold test and the average CFA is intended as average break angle amplitude. The errors on average CFA are given as standard mean errors and standard deviations are reported in brackets.

Unsized samples	Weight before treatment (mg)	Weight after treatment (mg)	Weight variation (mg)	% weight variation (uptake)	CFA_{CTRL} (20 breaks)	CFA_{TRT} (20 breaks)	Fold resistance Variation
UP58_SIOX-5TD	108.98	110.78	1.80	+1.7%	96.5±2.2° (9.9°)	91.3±1.8° (8.2°)	decrease
UP57_SIOX-5TD	127.60	129.97	2.37	+1.9%	86.9±1.7° (7.8°)	92.9±1.5° (6.9°)	+7±2%
UP56_SIOX-5TD	126.21	128.64	2.43	+1.9%	98.5±1.9° (8.5°)	97.2±1.8° (8.0°)	decrease
UP68_SIOX-5TD	118.93	121.40	2.47	+2.1%	95.2±1.6° (7.0°)	94.1±1.5° (6.7°)	decrease
UP69_SIOX-5TD	115.05	117.54	2.49	+2.2%	90.8±1.8° (8.0°)	106.3±1.4° (6.4°)	+17±3%
Average				**+1.96%**			**-**

For three out of five samples with SIOX-5TD, a decrease in resistance was observed while an increase was recorded for the other two. This outcome made SIOX-5TD a much less reliable formulation than SIOX-5TO as reinforcing coating for the charred paper. Table 6.7 and Table 6.8 present the results of the applications of SIOX-5TO and of SIOX-5TD to the sized burnt samples and are still organised in increasing order of uptake.

Table 6.7. Uptakes, critical fold angle (CFA) and fold test results of the SP samples treated with a single application of SIOX-5TO applied by airbrush recto and verso. 20 sample breaks were induced per sample during the fold test and the average CFA is intended as average break angle amplitude. The errors on average CFA are given as standard mean errors and standard deviations are reported in brackets.

Sized samples	Weight before treatment (mg)	Weight after treatment (mg)	Weight variation (mg)	% weight variation (uptake)	CFA_{CTRL} (20 breaks)	CFA_{TRT} (20 breaks)	Fold resistance Variation
SP69_SIOX-5TO	116.23	117.29	1.06	+0.9%	59.7±1.2° (5.5°)	62.0±1.1° (4.7°)	+4±2%
SP68_SIOX-5TO	101.12	102.05	0.93	+0.9%	75.4±2.7° (12.2°)	76.3±2.1° (9.6°)	+1±3%
SP57_SIOX-5TO	106.98	108.09	1.11	+1.0%	85.4±1.2° (5.3°)	94.4±1.0° (4.3°)	+13±2%
SP58_SIOX-5TO	105.43	106.74	1.31	+1.2%	68.9±1.9° (8.3°)	72.5±.0.9° (4.2°)	+5±2%
SP56_SIOX-5TO	117.07	118.62	1.55	+1.3%	74.9±2.3° (10.3°)	79.4±2.2° (9.8°)	+6±3%
Average				**+1.06%**			**+5.8±2.2%**

The SIOX-5TO applications on the sized samples confirm a systematic positive effect of the polysiloxane coating in improving the resistance of the charred paper to fold and all the treated papers showed an upgrade of their mechanical properties (from 4% to 13%). As observed previously for the unsized samples (Table 6.5), also for sized samples there is no clear correlation between uptake percentage around 1% and fold resistance variation percentage. As already noticed in Table 6.5, standard deviations of the values of the breakage measures decreased also in the SP samples compared to the controls, suggesting a greater uniformity induced in the charred paper by the formation of the polymeric film.

Table 6.8. Uptakes, critical fold angle (CFA) and fold test results of the SP samples treated with a single application of SIOX-5TD applied by airbrush recto and verso. 20 sample breaks were induced per sample during the fold test and the average CFA is intended as average break angle amplitude. The errors on average CFA are given as standard mean errors and standard deviations are reported in brackets.

Sized samples	Weight before treatment (mg)	Weight after treatment (mg)	Weight variation (mg)	% weight variation (uptake)	CFA_{CTRL} (20 breaks)	CFA_{TRT} (20 breaks)	Fold resistance Variation
SP69_SIOX-5TD	116.16	118.02	1.86	+1.6%	59.7±1.2° (5.5°)	65.3±1.1° (4.7°)	+9±2%
SP68_SIOX-5TD	101.28	102.98	1.67	+1.7%	75.4±2.7° (12.2°)	75.7±1.1° (4.8°)	+0±3%
SP57_SIOX-5TD	107.83	110.09	2.26	+2.1%	85.4±1.2° (5.3°)	86.0±0.9° (4.0°)	+1±1%
SP58_SIOX-5TD	129.31	132.08	2.77	+2.1%	68.9±1.9° (8.3°)	69.1±.1.0° (4.6°)	+0±2%
SP56_SIOX-5TD	109.66	112.21	2.55	+2.3%	74.9±2.3° (10.3°)	77.7±2.0° (9.0°)	+4±3%
Average				**+1.97%**			**+2.8±1.0%**

As highlighted in Table 6.8, treatment with SIOX-5TD on sized paper led to higher uptakes and less improvement of mechanical resistance to fold than with SIOX-5TO. This trend was similar to that observed in the UP samples in Table 6.6.

It was not clear the reason why, in these tests and especially for the unsized samples, SIOX-5TD induced in most cases a decrease in flexibility compared to untreated paper. Among the TEOS-based formulations tested, SIOX-5TO was the only one reliable in forming a coating which sistematically improved the flexibility of burnt paper enough to increase the CFA even when applied in small amounts, verso and recto.

Comparison of the average uptake and of the average improvement of the fold resistance of the UP and SP treated with SIOX-5TO in the test is proposed in Table 6.9.

Table 6.9. Comparison of the fold test results of the UP and the SP samples treated with SIOX-5TO.

Samples	SIOX-5TO treat. uptake	SIOX-5TO treat. fold resistance variation
UP56-58, UP68-69	+ 1.12%	+12.6%
SP56-58, SP68-69	+ 1.07%	+5.8%

2.3 Stiffness evaluation of the treated samples and its influence on the resistance to fold

Before subjecting the samples to the fold test – which is destructive – a rigidity test was performed on the sample set UP56-58 and SP56-58 to better define a possible relationship between the samples rigidity and the resistance they could oppose to fold. The paper rigidity was tested as "dynamic bending stiffness" (i.e. the resistance of the paper against bending deformation) with a rigidimetre Adamel Lhomargy, in accordance to the standard method AFNOR NF Q03-025, equivalent to T535 wd-03 *Bending stiffness of paper and paperboard - Resonance method* (see Materials and methods).

Table 6.10. Rigidity and fold variation of UP and SP samples treated with SIOX-5TO and SIOX-5TD in single application recto and verso by airbrush. The influence of the SIOX-5TO treatment on rigidity and fold resistance on the unsized and sized samples is highlighted. As for any mechanical test, a standard error of 10% should be considered .

Unsized samples	Weight before treatment (mg)	Weight after treatment (mg	% Weight increase (uptake)	Rigidity (N/n	% Rigidity (R) variation	% Fold resistance variation
UP56_ctrl	121.88			0.19		
UP57_ctrl	119.81			0.38		
UP58_ctrl	110.45			0.15		
UP56_SIOX-5TO	117.66	119.01	1.15%	0.20	- 1.2%	+ 6%
UP57_ SIOX-5TO	117.07	118.48	1.20%	0.37	- 1. 8%	+ 19%
UP58_ SIOX-5TO	102.23	103.00	0,.5%	0.11	- 24%	+ 14%
UP56_ SIOX-5TD	126.21	128.64	1.93%	0.10	- 47.1%	- 1%
UP57_ SIOX-5TD	127.60	129.97	1.86%	0.47	+ 24.8%	+ 7%
UP58_ SIOX-5TD	108.98	110.78	1.65%	0.12	-21%	- 5%
Sized samples						
SP56_ctrl	111.76			0.28		
SP57_ctrl	128.89			0.28		
SP58_ctrl	98.00			0.17		
SP56_SIOX-5TO	117.07	118.62	1.32%	0.21	- 24.5%	+ 6%
SP57_SIOX-5TO	106.98	108.09	1.04%	0.10	- 62.6%	+ 13%
SP58_SIOX-5TO	105.43	106.74	1.24%	0.21	- 22.3%	+ 5%
			Av 1,2%			
SP56_ SIOX-5TD	107.83	110.09	2.10%	0.18	- 35.3%	+ 4%
SP57_ SIOX-5TD	129.31	132.08	2.14%	0.32	+ 14.9%	+ 1%
SP58_ SIOX-5TD	109.66	112.21	2.33%	0.28	+ 60.6%	+ 0%

Here again, the only coherent data in Table 6.10 appear to be those related to the samples treated with SIOX-5TO. Indeed with SIOX-5TD, both large positive and negative values of rigidity variation were obtained, indicating sometimes a higher rigidity (+) and sometimes a higher flexibility (-) for the same type of sample. For the unsized as well as for the sized burnt paper, this formulation composed of TEOS and OTES induced a decrease in the rigidity, small for the unsized (1-2%) and much larger for the sized samples (>20%). This was concomitant with an improvement of the mechanical resistance to fold from +6% to +19% depending on the samples. The influence of SIOX-5TD, composed of TEOS and DDMES, on the rigidity of the samples was less predictable, sometimes reducing and sometimes increasing the paper stiffness. This fluctuating trend is confirmed in the fold test results, sometimes positive, indicating an increase in fold strength, sometimes negative, in an inconsistent way. It is worthy to observe that the SIOX-5TD could also induce a decrease both in rigidity and in fold resistance, as for the samples UP56 and UP58, in thus confirming a quite different behaviour from that of SIOX-5TO.

3. Development of a strengthening treatment with aminoalkylalkoxysilanes (AAAS) formulations

The aminoalkylalkoxysilanes 3-aminopropylmethyldiethoxysilane (henceforth: AMDES or AM), and 3-aminopropyltriethoxysilane (henceforth: APTES or AP) were tested, separately and in the mixture AMDES/APTES 1:1 (henceforth AM/AP). For details about AP, AM and AM/AP, see Chapter 4, § 3.2.2.

3.1 Preliminary tests with AMDES, APTES and AMDES/APTES

Preliminary tests were carried out to visually assess the impact of AMDES, APTES and of the AMDES/APTES mixture on the unsized (UP) and sized (SP) burnt samples, in order to verify the occurrence of any undesirable effects, such as those already listed previously. As previously highlighted (Chapter 4, § 3.2.2), the three products were supplied commercially by ABCR (Gelest) at high purity: AMDES (98%) and APTES (97%). In the previous experimental works, they had been applied to papers by immersion in a hexamethyldisiloxane diluted solution (HMDS) or spraying them directly, without any further dilution. In the present study, the formulations were tested as

provided (“pure”) as well as in a 5% v/v dilution in isopropanol. This was done in order to possibly compare with the TEOS-based formulations SIOX-5TO, employed at the same concentration. It has to be noted that the treatments developed by the CRC for various papers (unaged, aged, cellulosic, lignocellulosic) are based on higher concentrations (10% v/v) in HMDS (immersion treatment) or by spraying so as to target uptakes in the range 6%-12%, which were determined as the optimal range for mechanical strengthening [Souguir et al. 2011; Piovesan et al. 2014, 2017, 2018; Ferrandin-Schoffel et al. 2020, 2021].

3.1.1 Samples preparation

One UP and one SP burnt sample (4 x 10 cm^2 strips), prepared according to the standard procedure (hot plate, 250°C, 15 min), were cut in 4 substrips each (1 x 10 cm^2): one strip was left as control and the others treated recto and verso by brush with AMDES, APTES ad AM/AP. All the pure formulations are liquid and could be brushed on the samples, over an area of approximately 2 cm^2, including part of the charred paper and part of the unburnt paper. A single application, one side only, was effective in visibly permeating the paper recto/verso.

One UP and one SP sample (4 x 10 cm^2 strips), burnt as above and cut in 4 substrips, were treated with the same products diluted in isopropanol (5% v/v), applied recto and verso by airbrush. Samples dried at constant conditions of 23°C and 50% RH.

3.1.2 Visual examination of the samples treated with a single application of aminoalkylalkoxysilanes

One week after the application, the treated samples were examined according to the same criteria applied to the paper treated with the nanocellulose dispersions and with the TEOS-based formulations. The appearance of brown tide lines, of darkening of the burnt treated area and transparency or changes in the original paper opacity were considered. Table 6.11 shows what results from the visual examination of the samples treated with the pure AAAS formulations.

Table 6.11. Visual examination of the UP and SP samples treated recto only by brush with the pure aminoalkylalkoxysilanes APTES, AMDES and AM/AP (1:1). Rating level: no = no variation; 1= light; 2= medium; 3= heavy. Uptakes are given as % weight difference in the sample before and after treatment.

AAAS formulations	% Weight increase (uptake) after treat. **recto only**	Brown tide lines on white areas	Color variation of burnt area	White tide lines (transparency effect)
UP_APTES	+ 18.8%	no	no	no
UP_AMDES	+ 22.2%	1	2	3
UP_AM/AP (1:1)	+ 29.7%	no	2	3
SP_APTES	+ 7.8%	no	no	no
SP_AMDES	+ 12.3%	no	2	3
SP_AM/AP(1:1)	+ 16.7%	no	2	3

For the paper sprayed with the undiluted solutions, the gap in the uptakes between the unsized (UP) and the sized (SP) samples was very significant: UP paper, because it is more permeable, retained up to about 50% more product than the SP samples and in case of APTES, even more than 50%. The mixture AM/AP (1:1) gave the higher uptakes both in UP and in SP samples, followed by AMDES and finally by APTES. Note that these uptakes are pretty high, if compared to the AAAS uptakes observed on blank paper in previous experiments at CRC, which were never higher than 12% in weight.

The UP and SP samples treated with APTES did not show any tidelines nor paper transparency.

On the other hand, AMDES produced the worst result in terms of transparency (level 3) and darkening of the burnt area (level 2) both in the UP and in the SP samples, especially evident when oberving them at transmitted light and more accentuated in the sized samples (Fig. 6.4). On the unsized samples, light tide lines were also induced by the spread of AMDES in the very absorbent paper.

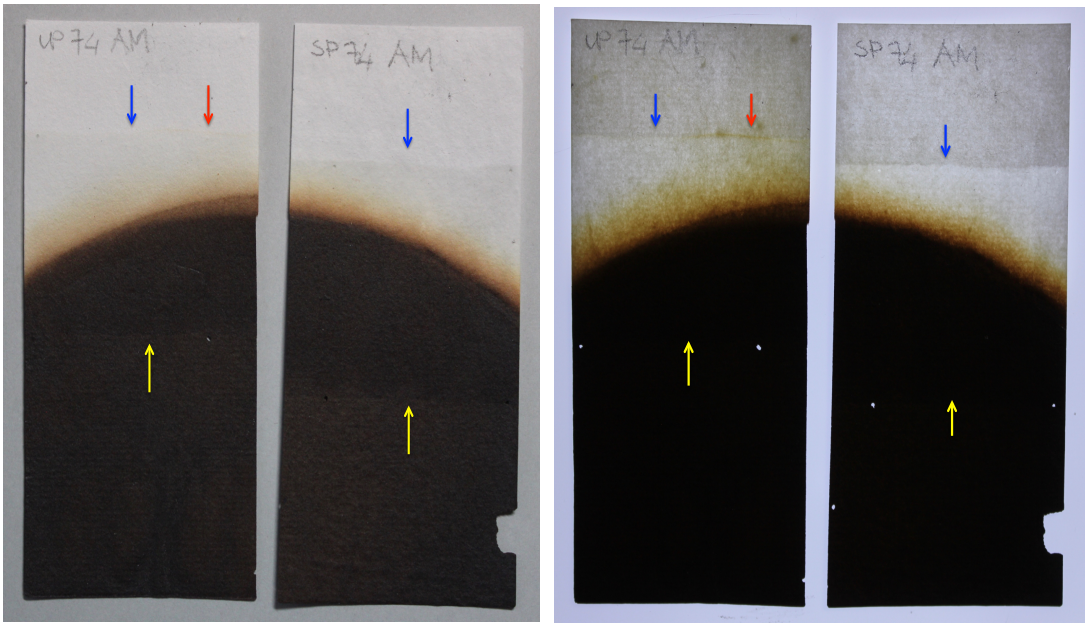

Figure 6.4. Visual examination of the UP74 and SP74 burnt samples treated with a single application of AMDES by brush, recto only. Brown tide lines (red arrow), darkening of the burnt area (yellow arrow) and transparency (blue arrow) were observed both in scattered (left) and in transmitted light (right).

Collateral effects of the AM/AP applications were equivalent to those observed in the samples treated with AMDES. Even at naked eyes, transparency and darkening in the burnt area were more accentuated in the sized samples, as evident in Fig. 6.5.

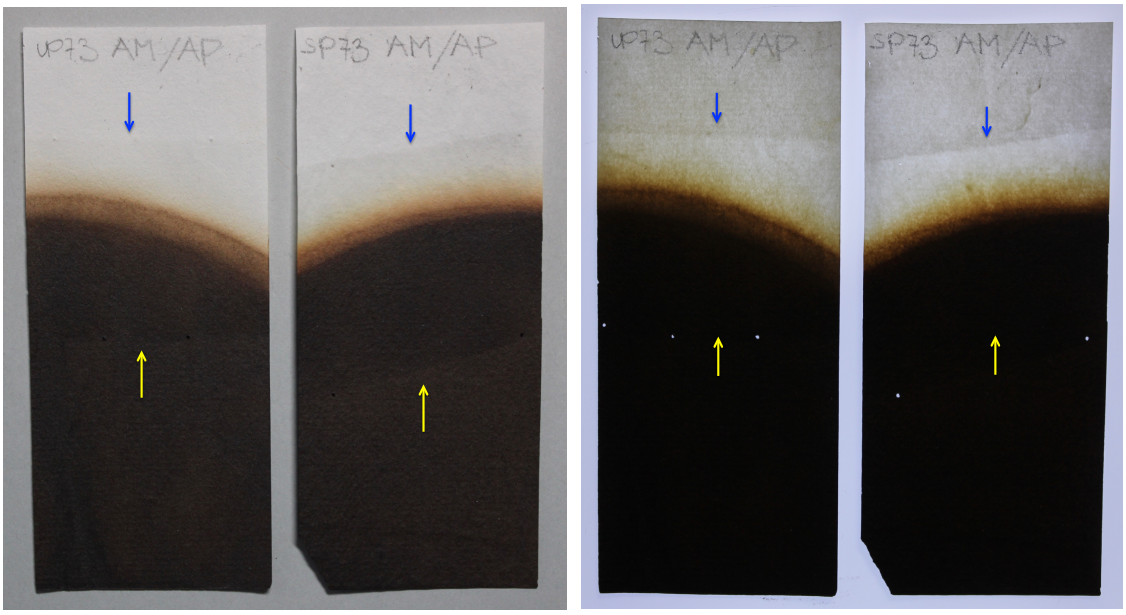

Figure 6.5. Visual examination of the UP74 and SP74 burnt samples treated with a single application of AM/AP (1:1) by brush, recto only. Transparency (blue arrow) and change in reflectance of the burnt area were noticed in the scattered (left) and in the transmitted light (right).

Table 6.12 displays the results for the samples treated with the solutions diluted 5% in isopropanol.

Table 6.12. Visual examination of the UP and SP samples treated recto and verso by brush with APTES, AMDES and AM/AP (1:1) in a 5%v/v dilution in isopropanol. Rating level: no = no variation; 1= light; 2= medium; 3= heavy. Uptakes are given as % weight difference in the sample before and after treatment.

AAAS formulations	% Weight increase after treat. (uptake)	Brown tide lines on white areas	Color variation of burnt area	White tide lines (transparency effect)
UP_APTES	+ 2.8%	1	1	no
UP_AMDES	+ 1.2%	1	1	no
UP_AM/AP (1:1)	+ 0.6%	1	1	no
SP_APTES	+ 0.3%	no	no	no
SP_AMDES	+ 0.3%	no	no	no
SP_AM/AP(1:1)	+ 0.6%	1	1	no

In the paper treated with the diluted formulations, the uptakes considerably decreased (Table 6.12). The gap in the uptakes between the UP and the SP samples was significant, at least for the APTES and AMDES. Only AM/AP seemed to be retained in the paper in similar amounts in both unsized and sized papers.

A gap was also observed with the use of alkoxysilanes, albeit not so relevant, but the uptakes induced by applications of aminoalkyloxysilanes diluted at 5% are in general lower than those resulting from TEOS-based formulations, (Cfr. Table 6.2).

In the diluted formulations, all the side effects were attenuated, no opacity loss was detectable and only light tidelines appeared both on the unburnt, white sample areas, probably due to the large amount of the polar isopropanol applied by brush. This defect was considered of low impact, avoidable by distributing the products evenly on the samples with an airbrush.

3.1.3 Rigidity and fold resistance in the samples treated with the AAAS

Unsized (UP) and sized (SP) samples (4 x 10 cm^2 strips) were prepared according to the standard procedure (hot plate, 250°C, 15 min). The set of samples UP56-58 and SP56-58, cut in 4 substrips

1 x 10 cm^2 each (one kept as control) were treated recto only by airbrush (0.8 mm nozzle, pressure 1.5 bar, sample distance 10 cm) with AMDES, APTES or AM/AP.

The evolution of the uptakes and the fold resistance in the treated UP and SP samples are presented in Table 6.13. Each sample substrip (UP56, UP57, UP58, SP56, SP57 and SP58, size 1x10 cm^2) underwent an average of 15 breaks during the fold test, so that the breaks amounted to 45 for each set of samples (UP56-58, SP56-58).

Table 6.13. Uptakes, critical fold angle (CFA) and fold test results of the UP and of the SP samples treated with a single application of the pure AM, AM/AP (1:1) and AP applied by airbrush. Each set of samples undertaken 45 breaks during the fold test, the average CFA is intended as average break angle amplitude. Errors are provided as standard mean errors, while standard deviations are reported in the brackets.

Samples	Weight before treatment (mg)	Weight after treatment (recto only) (mg)	% Weight variation (uptake)	CFA_{CTRL} (15 breaks)	CFA_{TRT} (15 breaks)	Fold resistance variation
UP56_ctrl				98.5°±2.2° (8.5°)		
UP57_ctrl				86.9°±2.0° (7.8°)		
UP58_ctrl				96.5°±2.6° (9.9°)		
UP56_AM	118.83	153.24	29.0%		84.4°±2.9° (11.2°)	-14±3%
UP57_AM	137.48	172.56	25.5%		72.6°±2.3 (9.1°)	-16±3%
UP58_AM	104.43	117.64	12.7%		94.8°±2.3° (8.8°)	-2±3%
Average			**22.4%**			**-10.6±2.0%**
UP56_AP	126.30	143.05	13.3%		56.2°±1.0° (3.7°)	-43±1%
UP57_AP	137.80	157.70	14.4%		52.5°±1.7° (6.6°)	-40±2%
UP58_AP	111.43	121.55	9.1%		66.6°±2.1° (8.3°)	-31±3%
Average			**12.3%**			**-38.0±2.0%**
UP56_AM/AP	120.94	147.22	21.7%		41.8°±2.1° (8.1°)	-58±2%
UP57_ AM/AP	138.48	159.29	15.0%		49.6°±1.9° (7.3°)	-43±2%
UP58_ AM/AP	106.55	124.85	17.2%		62.4°±1.9° (7.3°)	-35±2%
Average			**18.0%**			**-45.3±2.0%**
SP56_ctrl				74.9°±2.7° (10.3°		
SP57_ctrl				85.4°±1.4° (5.3°)		
SP58_ctrl				68.9°±2.1° (8.3°)		
SP56_AM	111.83	125.73	12.4%		60.4°±1.5° (5.7°)	-19±3%
SP57_AM	113.30	127.26	12.3%		85.4°±2.1° (8.0°)	0%
SP58_AM	102.44	113.95	11.2%		56.9°±2.3° (8.9°)	-17±3%
Average			**11.7%**			**-12.0±2.0%**
SP56_AP	111.36	119.43	7.3%		53.5°±1.8° (6.8°)	-29±2%
SP57_AP	118.75	138.52	16.7%		58.8°±1.6° (6.1°)	-31±2%
SP58_AP	108.39	118.02	8.9%		48.9°±1.5° (5.7°)	-29±2%
Average			**10.9%**			**-29.7±2.0%**
SP56_AM/AP	121.16	130.29	7.5%		59.1°±2.3° (9.0°)	-21±3%
SP57_ AM/AP	114.73	121.46	5.9%		65.2°±1.6° (6.1°)	-24±3%
SP58_ AM/AP	96.60	107.44	11.2%		46.4°±1.3° (5.0°)	-33±3%
Average			**8.2%**			**-26±3%**

The uptakes for the pure formulations were considerably high, even when sprayed by airbrush and the highest uptakes were observed for AM. The already noticed gap between UP and SP paper was confirmed: in the same treatment conditions, the sized samples absorbed and retained a lower amount of product compared to the unsized samples. None of the three formulations contributed to the improvement of fold resistance and all the treatments resulted in a decrease in the strength of both the SP and the UP paper.

Rigidity testing was also carried out for the sample sets UP56-58 and SP56-58 with the rigidimeter Adamel Lhomargy (see Materials and methods) to investigate the influence of the AAAS in pure form applied on the paper fold resistance. Table 6.14 summarizes the results of both rigidity and fold test.

Table 6.14. Rigidity and fold variation of UP and SP samples treated with AM, AP and AM/AP in single application recto only by airbrush. .A standard error of 10% should be considered in the rigidity test.

Samples	Weight before treatment (mg)	Weight after treatment (recto only) (mg)	% Weight variation (uptake)	Rigidity (N/m)	% Rigidity variation	Fold resistance variation
UP56_ctrl				0.192118		
UP57_ctrl				0.380009		
UP58_ctrl				0.150919		
UP56_AM	118.83	153.24	29.0%	0.277742	+ 44.6%	- 14±3%
UP57_AM	137.48	172.56	25.5%	0.657789	+ 73.1%	- 16±3%
UP58_AM	104.43	117.64	12.7%	0.167307	+ 10.9%	- 2±3%
Average			**22.4%**		**+ 42.9%**	**- 10.6±2.0%**
UP56_AP	126.30	143.05	13.3%	0.241222	+ 25.6%	- 43±1%
UP57_AP	137.80	157.70	14.4%	0.609268	+ 60.3%	- 40±2%
UP58_AP	111.43	121.55	9.1%	0.211665	+ 40.2%	- 31±3%
Average			**12.3%**		**+ 42.0%**	**- 38.0±2.0%**
UP56_AM/AP	120.94	147.22	21.7%	0.235197	+ 22.4%	- 58±2%
UP57_ AM/AP	138.48	159.29	15.0%	0.856583	+ 125.4%	- 43±2%
UP58_ AM/AP	106.55	124.85	17.2%	0.252389	+ 67.2%	- 35±2%
Average			**18.0%**		**+ 71.7%**	**- 45.3±2.0%**
SP56_ctrl				0.276776		
SP57_ctrl				0.277107		
SP58_ctrl				0.175827		
SP56_AM	111.83	125.73	12.4%	0.282101	+ 1.9%	-19±3%
SP57_AM	113.30	127.26	12.3%	0.208269	+ 24.8%	0%
SP58_AM	102.44	113.95	11.2%	0.197849	+ 12.5%	-17±3%
Average			**11.7%**		**+ 13.1%**	**-12.0±2.0%**
SP56_AP	111.36	119.43	7.3%	0.244291	+ 11.7%	-29±2%
SP57_AP	118.75	138.52	16.7%	0.313694	+ 13.2%	-31±2%
SP58_AP	108.39	118.02	8.9%	0.405639	+ 130.7%	-29±2%
Average			**10.9%**		**+ 51.9%**	**-29.7±2.0%**
SP56_AM/AP	121.16	130.29	7.5%	0.315671	+ 14.1%	-21±3%
SP57_ AM/AP	114.73	121.46	5.9%	0.298693	+ 7.8%	-24±3%
SP58_ AM/AP	96.60	107.44	11.2%	0.268991	+ 53.0%	-33±3%
Average			**8.2%**		**+ 25.0%**	**-26±3%**

All the treatments with the pure aminoalkylalkoxysilanes led systematically to an increase of the sample stiffness and to a concomitant decrease of their fold resistance. The uptake did not seem to influence this outcome, as whether 6% or >20%, a rigidity increase, and fold resistance decrease were consistently observed. This effect was exactly opposite with respect to that of SIOX-5TO, which tended to decrease the paper rigidity, enhancing its flexibility and its resistance to fold, as shown in Table 6.10.

3.1.4 Evaluation of the fold resistance in the samples treated with the diluted aminoalkylalkoxysilanes formulations

The set of samples UP94-96 and SP94-96 (4 x 10 cm^2 strips) were prepared, and each sample cut in 4 substrips (1 x 10 cm^2): one kept as control, the others airbrushed with the 5% v/v dilution of AM, AP and AM/AP in isopropanol. Samples were dried in stable conditions of 23°C and 50% RH before carrying out the fold test, whose results are presented in Table 6.15.

15 breaks were undertaken per each strip (UP94, UP95, UP96, SP94, SP95, SP96), that is 45 breaks per each sample set (UP94-96 and SP94-96).

Table 6.15. Uptakes, critical fold angle (CFA) and fold test results of the UP and SP samples treated with a single application of AM, AM/AP (1:1) and AP in a 5%v/v concentration in isopropanol and applied by airbrush recto and verso. Each set of samples undertaken 45 breaks during the fold test, the average CFA is intended as average break angle amplitude. Errors are provided as standard mean errors, while standard deviations are reported in the brackets.

Samples	Weight before treatment (mg)	Weight after treatment (recto only) (mg)	% Weight variation (uptake)	CFA_{CTRL} (15 breaks)	CFA_{TRT} (15 breaks)	Fold resistance variation
UP94_ctrl	67.0			94.6°±1.9° (7.5°)		
UP95_ctrl	59.5			94.1°±2.1° (8.3°)		
UP96_ctrl	72.6			93.6°±2.1° (8.3°)		
UP94_AM	65.3	65.5	+0.3%		94.4°±1.3° (5.1°)	0%
UP95_AM	65.3	65.4	+0.2%		93.8°±2.3 (9.1°)	0%
UP96_AM	66.2	66.7	+0.8%		90.4°±2.4° (9.3°)	-3%
Average			**+0.4%**			**-1.0%**
UP94_AP	87.6	88.2	+0.7%		78.9°±2.3° (9.0°)	-17%
UP95_AP	66.0	66.5	+0.8%		82.6°±1.8° (6.9°)	-12%
Average			**+0.7%**			**-14.5%**
UP94_AM/AP	76.4	77.0	+0.8%		84.4°±1.9° (7.5°)	-11%
UP95_AM/AP	64.4	65.0	+0.9%		86.5°±1.9° (7.5°)	-8%
UP96_AM/AP	67.6	77.7	+1.6%		79.2°±2.7° (10.4°)	-15%
Average			**+1.1%**			**-11.3%**
SP94_ctrl	64.3			74.5°±1.9° (7.4°)		
SP95_ctrl	78.8			75.9°±1.7° (6.4°)		
SP96_ctrl	87.4			67.3°±1.9° (7.5°)		
SP94_AM	68.6	69.4	+1.2%		62.2°±1.5° (5.7°)	-17%
SP95_AM	87.8	89.3	+2.0%		62.3°±2.1° (8.0°)	-18%
SP96_AM	84.8	85.3	+0.6%		64.6°±2.3° (8.9°)	-4%
Average			**+1.2%**			**-13.0%**
SP94_AP	67.9	68.2	+0.4%		71.3°±1.9° (7.5°)	-4%
SP95_AP	88.4	88.8	+0.4%		72.8°±1.7° (6.5°)	-4%
SP96_AP	85.4	85.8	+0.5%		63.9°±1.8° (7.1°)	-5%
Average			**+0.5%**			**-4.5%**
SP94_AM/AP	62.1	62.8	+1.1%		59.9°±1.4° (5.3°)	-20%
SP95_ AM/AP	82.7	84.1	+1.7%		631°±1.6° (6.3°)	-17%
SP96_ AM/AP	89.9	90.4	+0.6%		69.6°±2.8° (10.8°)	-3%
Average			**+1.1%**			**-13.3%**

Here again and despite the low uptakes, according to the results of the fold test, the effect of the diluted aminoalkylalkoxysilanes alcoholic solutions was to reduce slightly the mechanical strength of the charred paper (lower CFA in all cases). As a trend, higher uptakes tended to correspond to

poorer performance in the fold test, but this pattern was not systematic and even low uptakes led to a decrease in the mechanical fold performances.

Moreover, when forced to bend during the fold test, both UP and SP samples went into fragments, a totally different behavior from that observed in the fold test of burnt papers reinforced with the nanocellulose or with SIOX-5TO at the same 5% concentration. Rigidity was not tested on these samples. However, based on previous tests, it was assumed that a decrease in bending strength was matched by an increase in stiffness and, since the outcomes of the fold resistance tests of charred samples treated with aminoalkylalkoxysilanes had persistently given negative results, the formulations AP, AM and AM/AP were considered unsuitable for the purpose of this research and excluded from further testing.

4. Conclusions

Various formulations of polysiloxanes based on tetraethoxysilane (TEOS) and on aminoalkyloxysilanes were experimented on unsized (UP) and sized (SP) RPM samples, aimed to protect the burnt areas with a polysiloxane film, generating new chemical bonds with the damaged paper matrix and enhancing its mechanical properties.

Five hydroalcoholic (water/isopropanol) ready-to-use formulations were tested on paper for the first time in the present research: SIOX-5TO and SN1 were composed of TEOS and functionalized with the co-precursors octyltriethoxysilane, OTES, with an amount of active precursors respectively of 5% and 9% in relation to the solvent. SIOX-5TD, SN1/d and SIOX-5 S contained TEOS and diethoxydimethylsilane, DDMES, in increasing percentage, 5%, 9% and 30%.

It was known that the presence of different co-precursors in the formulation could differently affect its polymerization. Trifunctional OTES could provide cross-linking, the expected rigidity counterbalanced by the long octyl chains, while the difunctional DDMES leads to the formation of essentially linear chains.

In a first time, the five formulations were evaluated by visual assessment and compared with respect to uptakes and collateral effects (i.e., tide lines, darkening of the treated burnt paper area, changes in paper opacity) that they could induce in the paper samples treated in same conditions. Higher uptakes were observed in unsized paper compared to the sized one, whose permeability

was reduced by the gelatin coating. With respect to the other formulations, treatments by brush with SIOX-5TO and SIOX-5TD, containing the lower quantity of precursor (5%), led to the most moderate uptake both in the unsized and sized samples and to the lightest collateral effects. Fold resistance tests, according to the protocols described in Chapter 5, were also carried out, resulting in the best performances of the paper samples treated with SIOX-5TO and SIOX-5TD. The formulations SN1, SN1/d and SIOX-5 S were therefore excluded, and more mechanical tests were conducted: both fold resistance and rigidity measurements on samples treated with single application of SIOX-5TO and SIOX-5TD were performed.

As a result, the formulation SIOX-5TO was the only one reliable in inducing a stiffness decrease in the treated unsized and sized samples, positively influencing their flexibility and resistance to bend even when applied in very small amounts (around 1%).

Aminoalkylalkoxysilanes were also tested: 3-aminopropylmethyldiethoxysilane, AMDES, which is difunctional and polymerizes in linear chains, 3-aminopropyltriethoxysilane, APTES, trifunctional and leading to the formation of a stiffer network, and the mixture AMDES/APTES 1:1 showing intermediate properties. Their ability in enhancing mechanical performances, in particular strength and flexibility, in unburnt paper was well known from previous research works, but their application to charred paper had never been considered before. They were used both pure and in a 5% v/v dilution in isopropanol, in order to be compared with the TEOS-based formulations SIOX-5TO, employed at the same concentration. Visual examination and mechanical tests were carried out. As a piece of evidence, all the applications of the three AMDES, APTES and AM/AP 1.1 in the burnt paper led to high uptakes, an increase of the stiffness and a decrease of their fold resistance. Moreover, important collateral effects such as paper transparency were observed.

For the samples treated with the diluted product and according to the same criteria applied to TEOS-based formulations, the visual assessment showed minimal collateral effects. Nevertheless, even reducing the uptakes to around 1%, comparable to SIOX-5TO, the application of the AAAS to the burnt samples led to an increase of the sample stiffness, highlighted by the rigidity test, and a decrease of their fold endurance. This was exactly opposite to the influence of AMDES, APTES the mix AM/AP on the unburnt paper so far tested and, more important in the frame of the present study, an opposite behavior with respect to that of SIOX-5TO.

The nanostructured nanosilica film formed by SIOX-5TO in the charred areas, systematically enhanced the mechanical properties of the damaged paper, allowing an improvement of its fold resistance. Since the SIOX-5TO formulation solvents are water and isopropanol, and isopropanol is considered a solvent of low toxicity (H225 and H319, like ethanol) and low environmental impact, SIOX-5TO could be considered suitable, in perspective, for *in loco* application, directly in the libraries and archives holding written cultural heritage, in poor condition due to fire damages.

So far tested separately, in the last step of the experimental part of this work the polysiloxane SIOX 5-TO, composed of TEOS and OTES (5%), will be applied in combination with the nanocellulose.

Chapter 6 | References

Ferrandin-Schoffel, N., Haouas, M., Martineau-Corcos, C., Fichet, O., Dupont, A.-L. (2020) **«**Modeling the reactivity of aged paper with aminoalkylalkoxysilanes as strengthening and deacidification agents**»**. *ACS Applied Polymer Materials* 2, 1943−1953;
DOI: 10.1021/acsapm.0c00132

Ferrandin-Schoffel, N., Martineau-Corcos, C., Piovesan, C., Paris-Lacombe, S., Fichet, O., Dupont, A.-L. (2021). **«**Long-term stability of lignocellulosic papers strengthened and deacidified with aminoalkylalkoxysilanes**»**. *Polymer Degradation and Stability*, 183, 109413.
DOI: 10.1016/j.polymdegradstab.2020.109413

Piovesan, C., Dupont, A-L., Fabre-Francke, I. *,* Fichet, O., Lavédrine, B., Chéradame, H. (2014). **«**Paper strengthening by polyaminoalkylalkoxysilane copolymer networks applied by spray or immersion: a model study**»**. *Cellulose,* 21, 705–715; https://doi.org/10.1007/s10570-013-0151-9

Piovesan, C., Fabre-Francke, I., Dupont, A-L., Fichet, O., Paris-Lacombe, S., Lavédrine, B., Chéradame, H. (2017). **«**The impact of paper constituents on the efficiency of mechanical strengthening by polyaminoalkylalkoxysilanes**»**. *Cellulose,* 24, 5671-5684;
https://doi.org/10.1007/s10570-017-1513-5

Piovesan, C., Fabre-Francke, I., Paris-Lacombe, S., Dupont, A-L., Fichet, O. (2018). **«**Strenghtening naturally and artificially aged paper using polyaminoalkylalkoxysilane copolymer networks**»**. *Cellulose,* 25, 6071-6082; https://doi.org/10.1007/s10570-018-1955-4

Souguir, Z., Dupont, A-L., d'Espinose de Lacaillerie, J-B., Lavédrine, B., Cheradame, H. (2011). Chemical and physicochemical investigation of an aminoalkylalkoxysilane as strengthening agent for cellulosic materials». *Biomacromolecules***,** 12**(**6**)**, 2082–2091**;**
https://doi.org/10.1021/bm200371u

Chapter 7

Development of a nanocellulose and polysiloxane nanocomposite for the stabilization and reinforcement of burnt paper

1. Nanocellulose and TEOS-based polysiloxanes combined in a single treatment

Given the mechanical reinforcement results obtained with nanocelluloses and polysiloxanes separately, the development of a combined treatment was tested in the last step of the experimental work.

This final phase was performed on laboratory burnt samples and aimed at optimizing, as much as possible, a suitable formulation for the reinforcement treatment of historical papers belonging to the written heritage, opening up a future perspective for archives and libraries on the conservation of burnt books and documents.

Tests carried out on treated paper samples had shown the positive influence of the mixed cellulose dispersion consisting of cellulose nanocrystals (0.3%) and microfibrillated nanocellulose (0.06%) in ethyl alcohol, as well as of the polysiloxane formulation SIOX-5TO (tetraethoxysilane, TEOS, functionalized with octyl-triethoxymethylsilane, OTES, in isopropanol). Applied separately, both products succeeded in imparting greater physical and chemical consistency, cohesion, and strength to the burnt areas of the paper and did not induce visual unacceptable side effects (Chapters 5 and 6).

The two treatments were tested in a single step, as it is important to avoid over-stressing the damaged and very brittle material. Airbrushing proved to be the most suitable method to ensure even distribution and it was efficient also for thick dispersions. Based on this, the applicability and effectiveness of a formulation consisting of a combination of nanocellulose and polysiloxane was tested, and its efficiency was compared with the results obtained from the treatment with nanocellulose only.

1.1 Preparation of the nanocellulose and polysiloxane SIOX-5TO dispersion

The nanocellulose formulations that gave the best results previously (Chapter 5) were used: cellulose nanocrystals (CNC) (0.3% w/v) and microfibrillated cellulose (MFC) (0.06% w/v). They were mixed directly in the SIOX-5TO formulation and the suspension was stirred for 10 minutes. The resulting dispersion appeared to be uniform and stable over time and no sedimentation or separation of the nanocellulose from the polysiloxane was observed even after several weeks (Fig. 7.1).

Figure 7.1. Stirring of the nanocellulose in SIOX-5TO formulation (left), the freshly prepared combined formulation (centre) and the same formulation after 2 months (right).

The pH of SIOX-5TO was 4.5, as measured with a pHmeter Hanna HI 83141 with a combined electrode. This acidic pH is explained by the fact that, according to the producer, HCl is added to the polysiloxane formulation as catalyst of the sol-gel process. In the dispersion of nanocellulose and polysiloxane, the pH was 4.8, still too acidic to be used for an application on paper due to the risk of exposing cellulose to acid-catalysed degradation reactions. A neutralization of the SIOX-5TO was therefore necessary. Calcium hydroxide $Ca(OH)_2$ was regarded as a good option to this aim, because this alkaline salt is compatible with the paper composition and widely used as a paper filler, as well as for paper deacidification. However, the addition of a few drops of a semi-saturated aqueous solution of calcium hydroxide or of calcium hydroxide nanoparticles in isopropyl alcohol (as commercial formulation Nanorestore Paper ®- propanol 3) to the nanocellulose dispersions in SIOX-5TO could not be used because it induced instability of the nanocellulose, which

precipitated, with formation of a sediment (likely because CNC contains sulphate groups combining easily with Ca^{2+} ions to give insoluble aggregates). The neutralization of the dispersion of nanocellulose and SIOX-5TO was reached with the addition of a few drops of NaOH 0.1 M. The nanocomposite suspension was stable and pH was progressively raised to 7.0, to 8.0 and to 9.0.

As already mentioned, the change in environment from acidic to neutral results in a slowing of the polymerisation process of the polysiloxanes (cf Chapter 4, § 3.2). However, moving from neutral to a slightly basic environment (pH 8 or 9) promotes the basic catalysis of polysiloxane polymerization [Brinker 1988], while the cellulose is stable at these pH values.

The dispersions of nanocellulose and SIOX-5TO buffered at different pH (7, 8 and 9) were thus tested on burnt samples to verify whether and to what extent alkalinity could influence their paper-strengthening efficiency.

1.2 Application of CNC/polysiloxane to the burnt paper

Unsized sample set UP113-115 and sized sample set SP113-115 (3 x 15 cm^2), burnt following the standard procedure (hot plate, 250°C, 15 min), were cut in 3 substrips: one substrip was kept as control, one was sprayed recto and verso with the nanocellulose mixture composed of 0.3%w/v CNC and 0.06%w/v MFC in ethyl alcohol, and the last one was sprayed with the nanocellulose formulation (0.3% w/v CNC + 0.06w/v MFC) dispersed in SIOX-5TO buffered at pH 7.

The same procedure was followed for UP121-123 and SP121-123, except that the dispersion of nanocellulose in SIOX-5TO had pH 8. Finally, UP126-128 and SP126-128, prepared with the same procedure, were treated with the dispersion of nanocellulose in SIOX-5TO at pH 9.

The spraying was carried out in a single application recto/verso with the airbrush (nozzle 0.8 mm, pressure 1.5 bar, 10 cm distance from the sample) in constant thermohygrometric conditions (23°C, 50% RH). The fold resistance test was carried out a week later, using the tailor-made apparatus (Chapter 5, § 2.1). This should give time enough to the siloxane to polymerize.

1.3 Fold resistance of the charred paper treated with the neutralized dispersion of nanocellulose and SIOX-5TO

The results of the folding resistance test of samples UP113-115 treated with the nanocellulose dispersion (CNC/MFC) in ethyl alcohol and with the dispersion of nanocellulose and SIOX-5TO at pH 7 are compared in Table 7.1. Uptake is shown as weight variation (mg) and as percentage change in sample weight after treatment. The percentage change in fold resistance (FRV%) using the CFA method described previously expresses how much paper resistance to breakage improves in the treated strips compared to the control strip kept untreated. Each substrip 1 x 15 cm^2 was subjected to 14 breaks, leading to a total of 42 breaks (14 x 3 substrips) for each sample set. The estimated error in FRV% was calculated as described in Chapter 5.

Table 7.1. Uptake and fold resistance variation of the UP an SP samples treated with a single application recto/verso of the dispersion composed of 0.3% w/v CNC + 0.06w/v MFC in ethyl alcohol and with the dispersion composed of 0.3% w/v CNC + 0.06w/v MFC in SIOX-5TO at pH 7.

Unsized sample	mg weight variation after nano r/v	%weight variation after nano r/v	mg weight variation after nano&SIOX r/v	%weight variation after nano&SIOX r/v	%fold resistance variation (standard deviation of CFA angle in brackets)
UP113nano	+ 1.44	+ 1.9%			+ 4 ±1% (± 7.2)
UP114nano	+ 1.52	+ 1.9%			+ 8 ±1% (± 7.1)
UP115nano	+ 1.71	+ 2.6%			+ 12 ±2% (± 8.7)
Average	**+ 1.55**	**+ 2.1%**			**+ 8.0** ± 1.0%
UP113nano &SIOX-5TO			+ 1.75	+ 2,4%	+ 11 ±1% (± 5.6)
UP114nano &SIOX-5TO			+ 1.85	+ 2.6%	+ 13 ±1% (± 5.5)
UP115nano &SIOX-5TO			+ 2.05	+ 2,6%	+ 13 ±1% (± 7.1)
Average			**+ 1.88**	**+ 2.5%**	**+ 12.3** ± 1.0%
Sized sample					
SP113nano	+ 1.82	+ 1.9%			+ 7 ±1% (± 5.2)
SP114nano	+ 1.90	+ 2.1%			+ 11 ±1% (± 7.1)
SP115nano	+ 1.53	+ 1.7%			+ 6 ±1% (± 5.2)
Average	**+ 1.75**	**+ 1.9%**			**+ 8.0** ± 1.0%
SP113nano&SIOX-5TO			+ 1.92	+ 2.5%	+ 5 ±1% (± 4.8)
SP114nano&SIOX-5TO			+ 2.05	+ 2.4%	+ 13 ±1% (± 6.8)
SP115nano&SIOX-5TO			+ 1.73	+ 2.6%	+ 10 ±1% (± 4.8)
Average			**+ 1.90**	**+ 2.5%**	**+ 9.3** ± 1.0%

As expected, both the UP and the SP samples improved their mechanical performance after the treatment with the mix of CNC and MFC, resulting in a positive variation of the fold resistance (+8.0%).

Results of the treatment with the dispersion of nanocellulose and SIOX-5TO show that the combined formulation improved FRV in both the UP and the SP samples a bit more than nanocellulose applied alone. In the sample set UP113-115 treated with nanocellulose, the percentage fold increase was 8.0%, while it was 12.3% in UP113-115 treated with the nanocellulose and polysiloxane. In the SP samples the fold resistance increase induced by nanocellulose was 8.0% versus 9.3% resulted from the combined treatment. Standard deviation in the measurements of the critical fold angle were slightly reduced in the application of the combined formulation, both in the UP and in SP paper and this should be an indication of a more uniform distribution of the dispersion in the samples.

Table 7.2 refers to samples treated with the nanocellulose dispersion alone and with the nanocellulose and SIOX-5TO dispersion at pH 8.

Table 7.2. Uptake and fold resistance variation of the UP an SP samples treated with a single application, recto/verso, of the dispersion composed of 0.3% w/v CNC + 0.06w/v MFC in ethyl alcohol and with the dispersion composed of 0.3% w/v CNC + 0.06w/v MFC in SIOX-5TO at pH 8.

Unsized sample	mg weight variation after nano r/v	%weight variation after nano r/v	mg weight variation after nano&SIOX r/v	%weight variation after nano&SIOX r/v	%fold resistance variation (standard deviation of CFA angle in brackets)
UP121nano	+ 1.30	+ 1.93%			+ 7 ±1% (± 6)
UP122nano	+ 1.62	+ 2.39%			+ 18 ±2% (± 4.9)
UP123nano	+ 1.31	+ 2.11%			+ 16 ±2% (± 8.8)
Average	**+ 1.41**	**+ 2.1%**			**+ 13.7** ± 1.0%
UP121nano&SIO-5TO			+ 1.75	+ 2.5%	+ 14 ±1% (± 5.6)
UP122nano&SIOX-5TO			+ 1.60	+ 3.0%	+ 28 ±2% (± 5.2)
UP123nano&SIOX-5TO			+ 1.85	+ 3.1%	+ 25 ±2% (± 4.6)
Average			**+ 1.73**	**+ 2.6%**	**+ 22.3** ± 1.0%
Sized sample					
SP121nano	+ 1.52	+ 2.05%			+ 12 ±1% (± 5.9)
SP122nano	+ 1.42	+ 1.03%			+ 11 ±1% (± 5.5)
SP123nano	+ 1.53	+ 2.27%			+ 7 ±1% (± 6.5)
Average	**+ 1.49**	**+ 1.8%**			**+ 10.0** ± 1.0%
SP121nano&SIOX-5TO			+ 1.70	+ 2.5%	+ 18 ±1% (± 5.1)
SP122nano&SIOX-5TO			+ 2.65	+ 2.2%	+ 13 ±1% (± 4.6)
SP123nano&SIOX-5TO			+ 1.77	+ 2.5%	+ 14 ±1% (± 5.8)
Average			**+ 2.04**	**+ 2.4%**	**+ 15.0** ± 1.0%

The same trends as before apply to the data, i.e. an improvement of fold resistance with the nanocomposite nanocellulose + polysiloxane with respect to nanocellulose alone.

Both UP and SP samples treated with the combined formulation of nanocellulose and SIOX-5TO have much better mechanical performance than those treated with the nanocellulose dispersion alone: the UP treated with the combination has a +22.3% of fold resistance increase vs. a 13.7% induced by nanocellulose only, while the SP samples has a +15.0% improvement compared to a +10.0% for nanocellulose alone. This confirms a more efficient combined treatment in improving the flexibility of the charred paper and the resulting strengthening to bending.

As already observed in Table 7.1, standard deviation of the CFA measurements slightly decreases with the UP and SP samples reinforced with the combined formulation in favor of more homogeneous results.

The percentage fold resistance variations were the best so far achieved: +22.3% for the unsized sample set UP121-123 and +15.0% for the sized sample set SP121-123.

Also considering the variability due to non-uniformity of samples (slightly different burning conditions, different uptakes, etc.), this appeared to corroborate once again the role of the polisiloxanes, enhancing the efficiency of the nanocellulose in forming a nanocomposite that systematically induced an improvement in the mechanical performance of the treated UP and SP samples.

Moreover, it was also verified that the slight alkalinity introduced in the dispersion nanocellulose and SIOX-5TO, by raising the originally acidic pH to 8, did not compromise, its efficiency.

In Table 7.3 the results of the applications with the nanocellulose dispersion alone and with the nanocellulose and SIOX-5TO formulation adjusted to pH 9 are presented.

Table 7.3. Uptake and fold resistance variation of the UP an SP samples treated with a single application recto/verso of the dispersion composed of 0.3% w/v CNC + 0.06w/v MFC in ethyl alcohol and with the dispersion composed of 0.3% w/v CNC + 0.06w/v MFC in SIOX-5TO at pH 9.

Unsized sample	mg weight variation after nano r/v	%weight variation after nano r/v	mg weight variation after nano&SIOX r/v	%weight variation after nano&SIOX r/v	%fold resistance variation (standard deviation of CFA angle in brackets)
UP126nano	+ 1.20	+ 2.1%			+ 10 ±1% (± 5.3)
UP127nano	+ 1.50	+ 2.1%			+ 2 ±1% (± 3.9)
UP128nano	+ 1.43	+ 1.9%			+ 4 ±2% (± 7.4)
Average	**+ 1.38**	**+ 2.0%**			**+ 5.3** ± 1.3%
UP126nano&SIO-5TO			+ 2.6	+ 3.0%	+ 20 ±1% (± 5.6)
UP127nano&SIOX-5TO			+ 1.7	+ 2.4%	+ 6 ±1% (± 5.2)
UP128nano&SIOX-5TO			+ 1.7	+ 2.4%	+ 3 ±1% (± 4.6)
Average			**+ 1.66**	**+ 2.6%**	**+ 9.7** ± 1.0%
SIzed samples					
SP126nano	+ 1.50	+ 2.3%			+ 10 ±1% (± 3.7)
SP127nano	+ 1.62	+ 2.2%			+ 10 ±1% (± 5.4)
SP128nano	+ 1.63	+ 2.1%			+ 6 ±1% (± 3.1)
Average	**+ 1.58**	**+ 2.2%**			**+ 8.7** ± 1.0%
SP126nano&SIO-5TO			+ 1.32	+ 2.3%	+ 2 ±1% (± 4.6)
SP127nano&SIOX-5TO			+ 1.73	+ 2.3%	+ 2 ±1% (± 4.4)
SP128nano&SIOX-5TO			+ 1.71	+ 2.4%	+ 2 ±1% (± 3.3)
Average			**+ 1.59**	**+ 2.3%**	**+ 2.0** ± 1.0%

The samples treated with the dispersion of nanocellulose in ethyl alcohol highlight a trend in the nanocellulose strengthening efficiency and in the variability of the resulting fold resistance increase comparable with those already observed, in particular in the results in Table 7.1.

The results of treatment with the combination of nanocellulose and SIOX-5TO with pH raised to 9 show that the trend in standard deviations of the CFA measurements decrease both in the UP and SP samples, which confirms a certain reliability of the application method. The sample UP126nano&SIO-5TO presented significantly higher fold resistance increase, than the other samples in Table 3. Similarly, the sample UP126nano shows higher fold resistance at equal uptake than the two other samples in the set. It can be compared to the sample UP122nano&SIOX-5TO in Table 7.2.

In the latter UP122nano&SIOX-5TO, an uptake of 3.0%, led to a fold increase of 28%; in UP126nano &SIO-5TO, a similar uptake of 3.0%, achieved an increase in of 20% in the fold

resistance. Even being one sample over 3 that responds so much better to the treatment is a very positive outcome. It could be that this is due to the sample itself that may be slightly less charred than the two others.

The results induced by the combined treatment in the sized SP samples appeared more uniform in terms of uptake and mechanical performance but not as positive as those achieved in the tests carried out with the formulations at pH 7 (Table 7.1) and at pH 8 (Table 7.2), as summarised in Table 7.4.

Sample	mg weight variation after nano&SIOX r/v	%weight variation after nano&SIOX r/v	%fold resistance variation
UP113-115nano &SIOX-5TO pH 7.0	+ 1.88	+ 2.53%	+ 11.4%
UP121-123nano &SIOX-5TO pH 8.0	+ 1.73	+ 2.85%	+ 22.4%
UP126-128 nano &SIOX-5TO pH 9.0	+ 1.66	+ 2.62%	+ 9.7%
SP113-115nano &SIOX-5TO pH 7.0	+ 1.90	+ 2.49%	+ 9.3%
SP121-123nano &SIOX-5TO pH 8.0	+ 2.04	+ 2.38%	+ 15.2%
SP126-128 nano &SIOX-5TO pH 9.0	+ 1.59	+ 2.33%	+ 2.3%

Table 7.4. Comparison of the uptake and fold resistance improvement induced by UP and SP sample sets treated with the formulation compose of 0.3% w/v CNC + 0.06w/v MFC in SIOX-5TO at pH 7.0, 8.0 and 9.0

According to the fold tests performed on these sample sets, the combined treatment with the formulation composed of 0.3% w/v CNC + 0.06w/v MFC in SIOX-5TO adjusted to pH 8.0 induced the best increase in the resistance to folding of both unsized and sized burnt samples.

The best performance of the formulation at pH 8 is likely related to the improvement in the polymerization rate of polysiloxane with a slightly basic environment. On the other hand, the reduced performance at pH 9 could be due to an increased difficulty for nanocellulose to interact with cellulose: increasing pH, carboxylic groups on the nanocellulose surface are more deprotonated, increasing the negative charge of nanocellulose, preventing precipitation of the NCC crystals between the cellulose fibers or decreasing the affinity with the sample damaged fibres.

2. Investigation of the physico-chemical modifications induced on the burnt paper by the combined treatment of nanocellulose and polysiloxane SIOX-5TO

2.1 Infrared spectroscopic analyses (ATR-FTIR)

The physico-chemical modifications induced by the application of the nanocellulose dispersion (0.3%w/v NCC and 0.06%w/v MFC) and by the application of the nanocomposite formulation (0.3%w/v NCC and 0.06%w/v MFC in SIOX-5TO) were examined through ATR-FTIR. The IR spectra of the unsized sample UP118, the UP118 treated with the NCC/MFC dispersion (UP118nano), and the UP118 treated with the nanocomposite formulation (UP118nanosiox) are shown in fig. 7.2 left.

Practically, no detectable difference can be observed among the three spectra: maybe, very small changes are present in the CH stretching bands around 2800 cm^{-1} and in the OH stretching band around 3300 cm^{-1}, but they are hardly appreciable. The IR spectra of the sized sample SP121, the SP121 treated with the NCC/MFC dispersion (SP121nano), and the SP121 treated with the nanocomposite formulation (UP121nanosiox) are shown in fig. 7.2, right. Again, no detectable difference among the three spectra, apart from the very small changes in the band at 3300 cm^{-1} and in the CH stretching band at 2800 cm^{-1}.

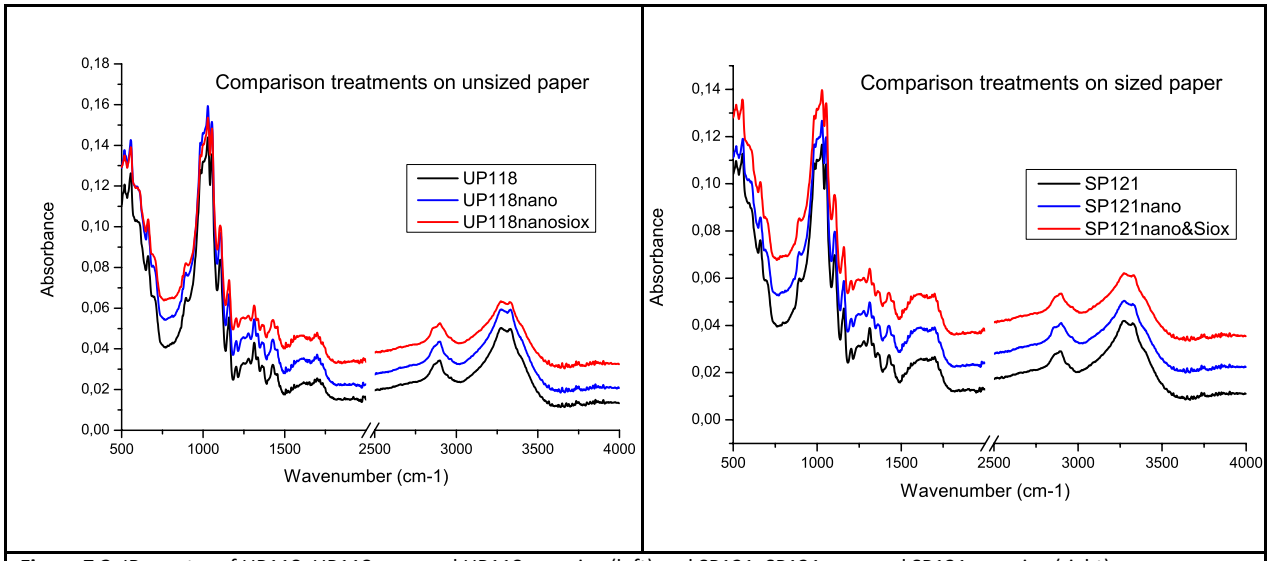

Figure 7.2. IR spectra of UP118, UP118nano and UP118nanosiox (left) and SP121, SP121nano and SP121nanosiox (right).

Therefore, ATR-IR spectra are almost unable to track differences before and after treatments on the samples, and the technique is thus useless to monitor changes. On the other side, this is a very good indication that most of the sample retains its original features: actually, product uptakes are very small compared to the entire mass of the sample (around 1-2% of sample mass), but nevertheless, as shown in the previous section, significant mechanical improvements were obtained.

2.2 Scanning electronic microscope (SEM) investigation

The physico-chemical modifications induced in the burnt paper by the application of the dispersions of the combined formulation (0.3%w/v NCC and 0.06%w/v MFC in SIOX-5TO) neutralized at pH 8 were investigated by SEM/EDS.

The cross section images of the treated samples was observed and analysed with EDS. In Fig.7.3 is the SEM image of the unsized burnt sample UP122, untreated and after the treatment performed recto/verso by airbrush.

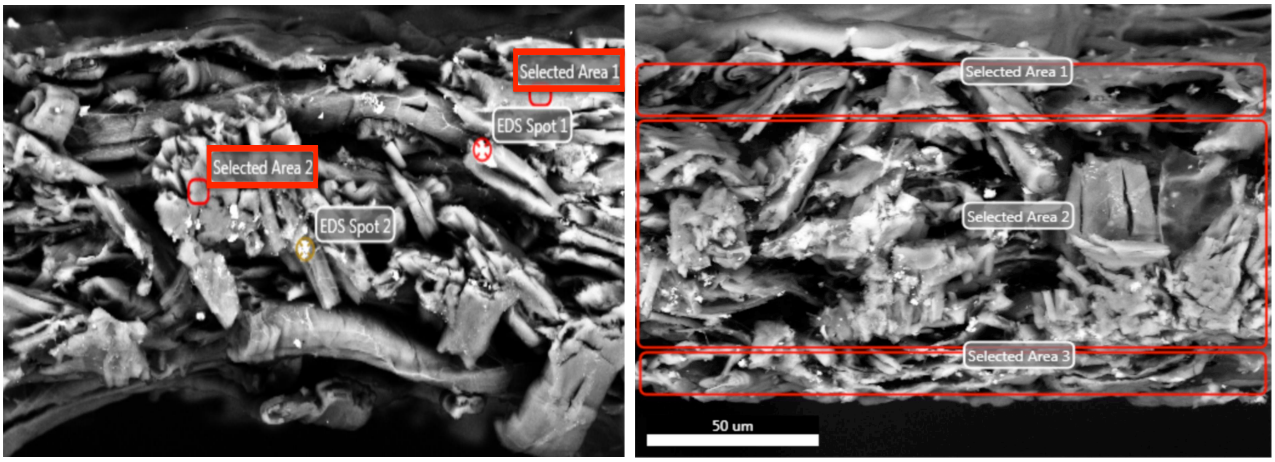

Figure 7.3. Unsized sample UP122, cross section. SEM image of the sample before (left) and after treatment (right) with the combined dispersion of nanocellulose and polysiloxane. The areas investigated with EDS are highlighted by the red frames.

As expected, and already observed by SEM in other samples treated with the mix of CNC and MFC (see Chapter 5, § 5.3), the treated paper (on the right in the figure 7.3) shows a more compact and "packed" aspect. This is due to the interaction of the nanocomposite with the damaged fibres of the original paper matrix. In the untreated sample, Spot 1 and Spot 2 are inclusions, respectively Mg (from talc, $Mg_3Si_4O_{10}(OH)_2$) (Spot 1) and Ca (from calcium carbonate) (Spot 2) compounds, that

were systematically detected in these RPM samples in the previous investigations (see Chapter 3, § 3.4). Selected Area 1 and Selected Area 2, in figure 7.3, left, are two chosen areas in the unsized sample located on the cellulose fibres, the Area 1 close to the surface and the Area 2 inside the sample.

The spectrum in Fig. 7.4 refers to the Selected Area 1 and Table 7.5 shows the elements detected by the EDS probe in this area, which is adjacent to the surface of the paper.

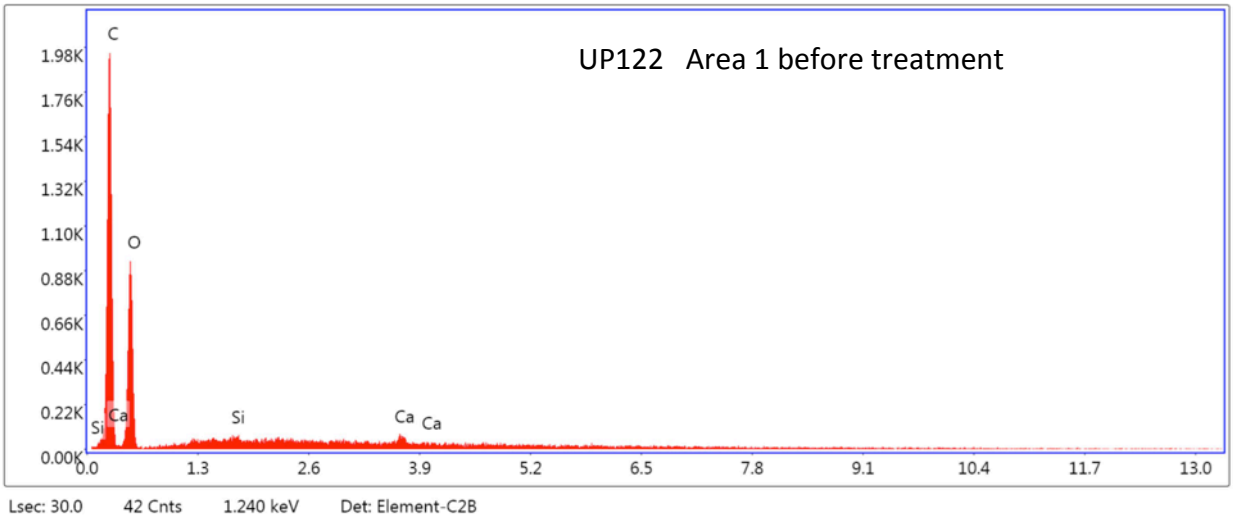

Figure 7.4. Unsized burnt sample UP122, cross section before treatment. EDX spectrum of the Selected Area 1.

Table 7.5. Unsized burnt sample UP122, cross section before treatment. Semi-quantitative estimation of the elements in Selected Area 1, located on a fibre. Apart cellulose, only calcium is present in some quantity.

			Selected Area 1 before treatment		**eZAF Smart Quant Results**			
Element	Weight %	Atomic %	Net Int.	Error %	Kratio	Z	A	F
C K	51.2	58.9	399.7	6.2	0.3112	1.0237	0.5935	1.0000
O K	46.8	40.4	210.9	10.6	0.0910	0.9782	0.1987	1.0000
SiK	0.4	0.2	8.3	39.0	0.0028	0.8871	0.8338	1.0055
CaK	1.6	0.6	20.2	22.6	0.0143	0.8363	1.0286	1.0371

Apart from C and O, characterizing cellulose, only calcium is present in some quantity, while silicon (Si) is only in trace.

In the treated sample, three macro areas were examined, corresponding to the upper (Selected Area 1) and lower (Selected Area 3) sample surface and to the centre (Selected Area 2) of the paper section, so to check the variations in the elements detected by EDS before and after treatment in the whole paper thickness.

After treatment, the area adjacent to upper surface of the sample presented in Fig. 7.5 contains silicon (Si) in a considerably higher amount, as also shown in Table7.6.

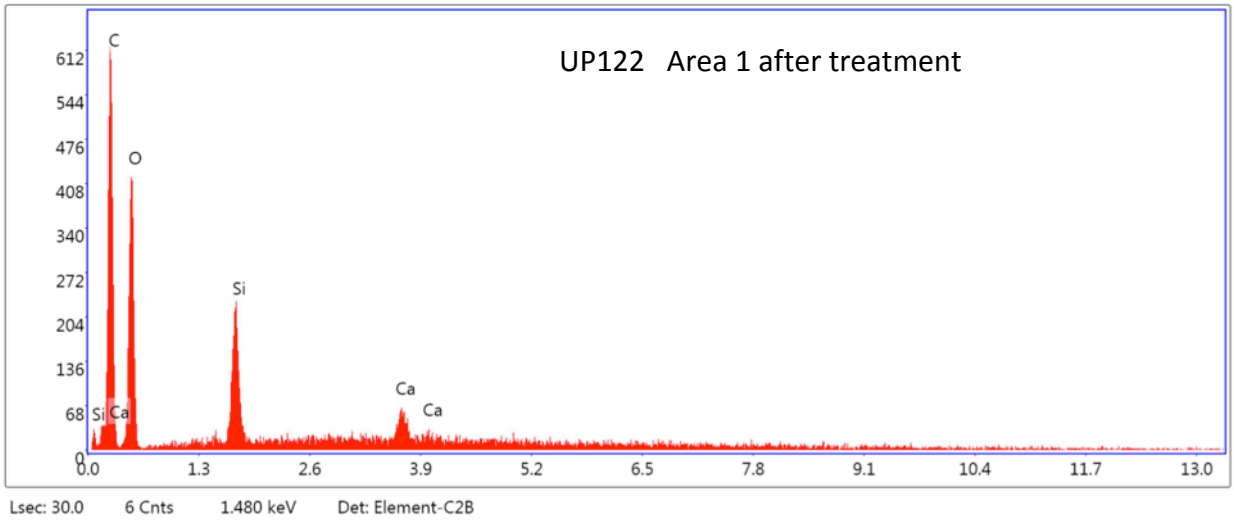

Figure 7.5. Unsized burnt sample UP122, cross section, EDX spectrum of the Selected Area 1 after treatment.

Table 7.6. Unsized burnt sample UP122, cross section after treatment. Semi-quantitative estimation of the elements in the Selected Area 1, adjacent to the sample surface, shows the presence of silicon (Si) in higher quantity compared to the untreated sample.

			Area 1 after treatment	**eZAF Smart Quant Results**				
Element	Weight %	Atomic %	Net Int.	Error %	Kratio	Z	A	F
C K	46.6	55.8	128.9	8.7	0.2022	1.0316	0.4205	1.0000
O K	44.9	40.3	98.5	11.3	0.0838	0.9861	0.1894	1.0000
SiK	5.5	2.8	62.1	6.5	0.0405	0.8948	0.8275	1.0044
CaK	3.0	1.1	19.8	14.8	0.0267	0.8438	1.0176	1.0250

Silicon is the main component of the SIOX-5TO and was therefore considered the key element to be mapped to test whether the polysiloxane has permeated the paper matrix.

The EDS spectrum of the Selected Area 2 in the untreated UP122 sample is in Fig. 7.6 and the elements detected by the EDS probe are examined in Table 7.7.

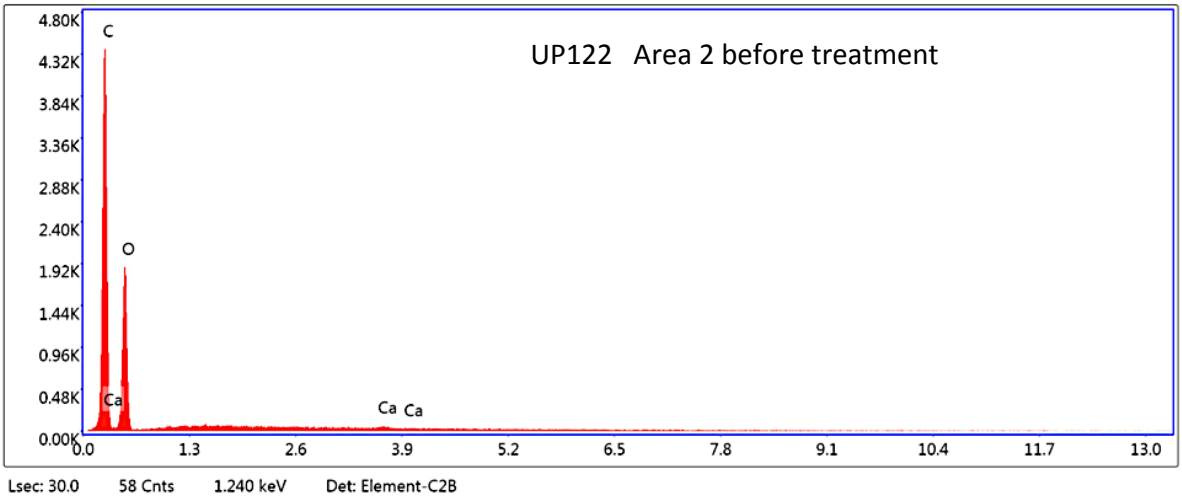

Figure 7.6. Unsized burnt sample UP122, cross section before treatment. EDX spectrum of the Selected Area 2, in a more central position in the cross section of the paper.

Table 7.7. Unsized burnt sample UP122, cross section after treatment. Semi-quantitative estimation of the elements in the central Selected Area 2,

			Selected Area 2 before treatment		**eZAF Smart Quant Results**			
Element	Weight %	Atomic %	Net Int.	Error %	Kratio	Z	A	F
C K	54.9	62.0	940.2	5.3	0.3518	1.0206	0.6281	1.0000
O K	44.6	37.8	404.5	10.3	0.0839	0.9751	0.1930	1.0000
CaK	0.6	0.2	15.1	25.0	0.0051	0.8333	1.0308	1.0464

Only the main components of the paper (C, O and traces of Ca) are present in this central area of the burnt untreated sample UP122.

The central cross area of the same UP122 sample, treated with the combined formulation composed of the mix of nanocelluloses and SIOX-5TO, is examined in Fig. 7.7 and in Table 7.8.

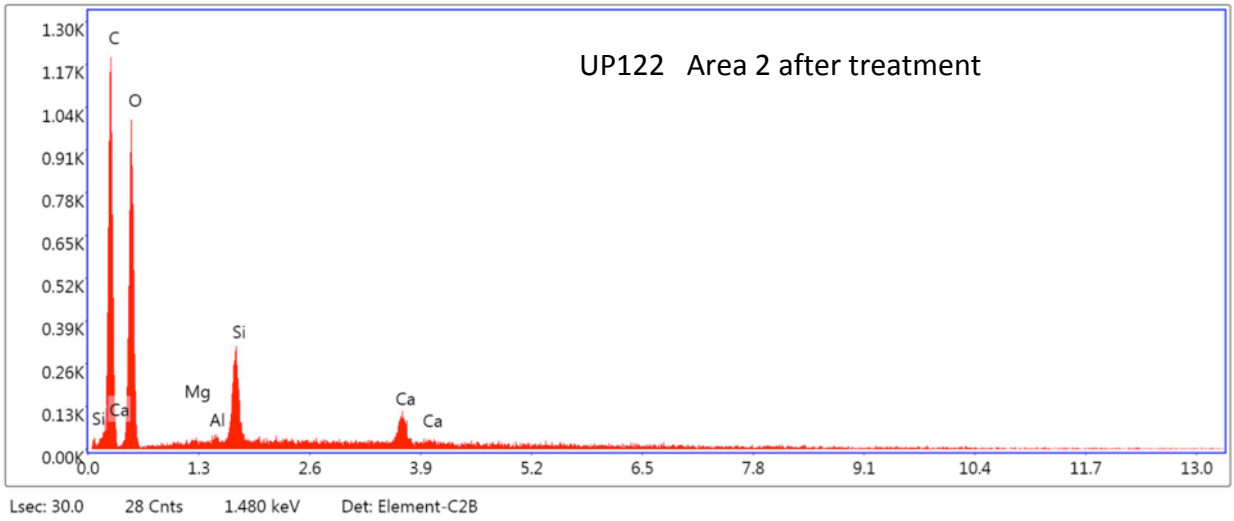

Figure 7.7. Unsized burnt sample UP122, cross section after treatment. EDX spectrum of the Selected Area 2, the core of the paper cross section.

Table 7.8. Unsized burnt sample UP122, cross section after treatment. Semi-quantitative estimation of the elements in the central Selected Area 2, highlighting the presence of silicon (Si).

Selected Area 2 after treatment eZAF Smart Quant Results

Element	Weight %	Atomic %	Net Int.	Error %	Kratio	Z	A	F
C K	43.4	52.2	238.8	8.0	0.1976	1.0319	0.4408	1.0000
O K	49.4	44.6	222.5	10.4	0.0998	0.9864	0.2046	1.0000
MgK	0.2	0.1	2.8	70.1	0.0010	0.9100	0.5362	1.0028
AlK	0.2	0.1	3.5	67.1	0.0012	0.8760	0.6928	1.0050
SiK	3.9	2.0	82.8	6.	0.0285	0.8950	0.8134	1.0046
CaK	2.8	1.0	35.2	11.6	0.0251	0.8440	1.0193	1.0264

The addition of silicon is clearly highlighted also in the central area of the sample, in such confirming the penetration of the polysiloxane within the paper matrix.

Finally, the Selected Area 3, adjacent to the lowest surface of the sample in Fig. 7.3, was also analysed after treatment and the resulting EDX spectrum is presented in Fig. 7.8.

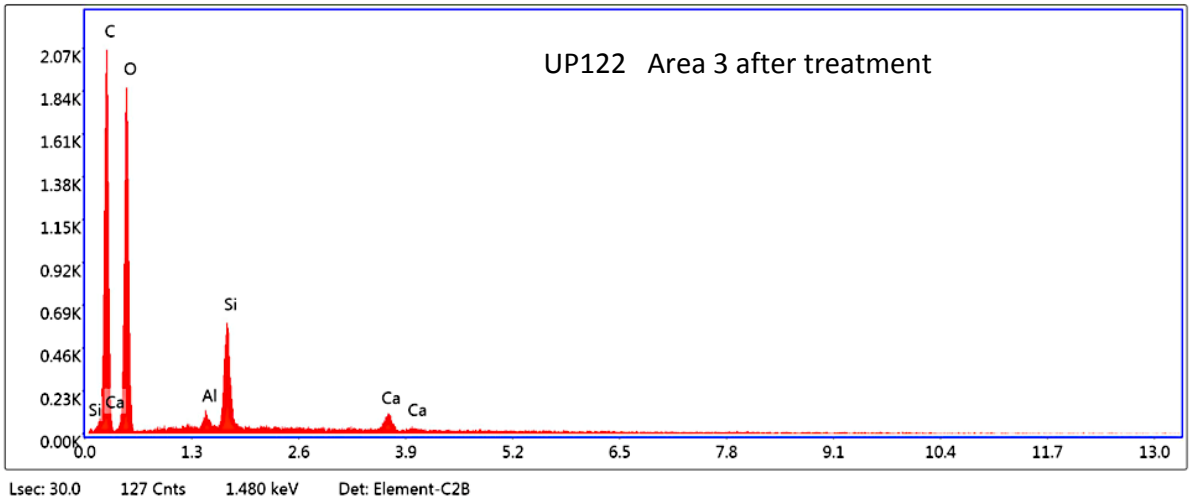

Figure 7.8. Unsized burnt sample UP122, cross section after treatment. EDX spectrum of the Selected Area 3, adjacent to the surface of the paper.

Table 7.8. Unsized burnt sample UP122, cross section after treatment. Semi-quantitative estimation of the elements in the area adjacent to the surface of the paper. The presence of silicon (Si) is clearly shown.

Selected Area 3 after treatment eZAF Smart Quant Results

Element	Weight %	Atomic %	Net Int.	Error %	Kratio	Z	A	F
C K	44.2	52.7	423.7	7.6	0.1965	1.0305	0.4313	1.0000
O K	49.5	44.3	406.7	10.0	0.1023	0.9850	0.2097	1.0000
AlK	0.6	0.3	17.9	15.7	0.0035	0.8746	0.6992	1.0052
SiK	4.2	2.1	159.0	5.3	0.0307	0.8935	0.8148	1.0041
CaK	1.5	0.6	33.8	12.5	0.0135	0.8425	1.0189	1.0309

Once again, silicon is present in the treated area. As the combined treatment was applied by airbrush, it was expected to detect the presence of the film formed by the polysiloxane on the surface areas, but SEM/EDS also confirmed its ability to permeate the whole UP sample.

The silicon amount in the central Selected Area 2 results slightly lower (3.9 weight%) than in the Selected Area 1 (5.5%) and in the Selected Area 3 (4.2 weight%), which are more adjacent to the surface and therefore directly received the airbrushed application of the product.

Sized samples were also investigated. Fig. 7.9 is the SEM image of the cross section in the sample SP122, before (left) and after (right) the combined treatment with 0.3% w/v CNC + 0.06w/v MFC in SIOX-5TO, performed recto/verso by airbrush. The macro areas investigated with EDS probe are

highlighted by red frames and correspond to the Selected Area 1, close to the upper surface of the paper, Selected Area 2, which is the central area of the cross section, and Selected Area 3, close to the lower sample surface in the image.

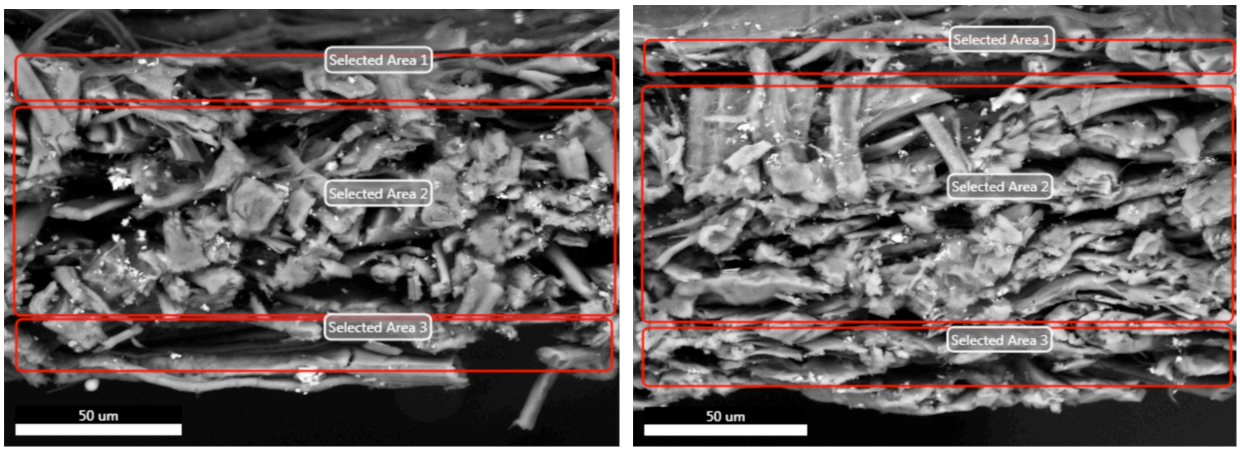

Figure 7.9. Sized burnt sample SP122, cross section, SEM images 800 x. The sample is shown before (left) and after (right) the combined treatment with 0.3% w/v CNC + 0.06w/v MFC in SIOX-5TO. The macro areas investigated are highlighted by red frames.

The EDS spectrum of the Selected Area 1 is presented in Fig. 7.10 and the elements detected with EDS are shown in Table 7.9.

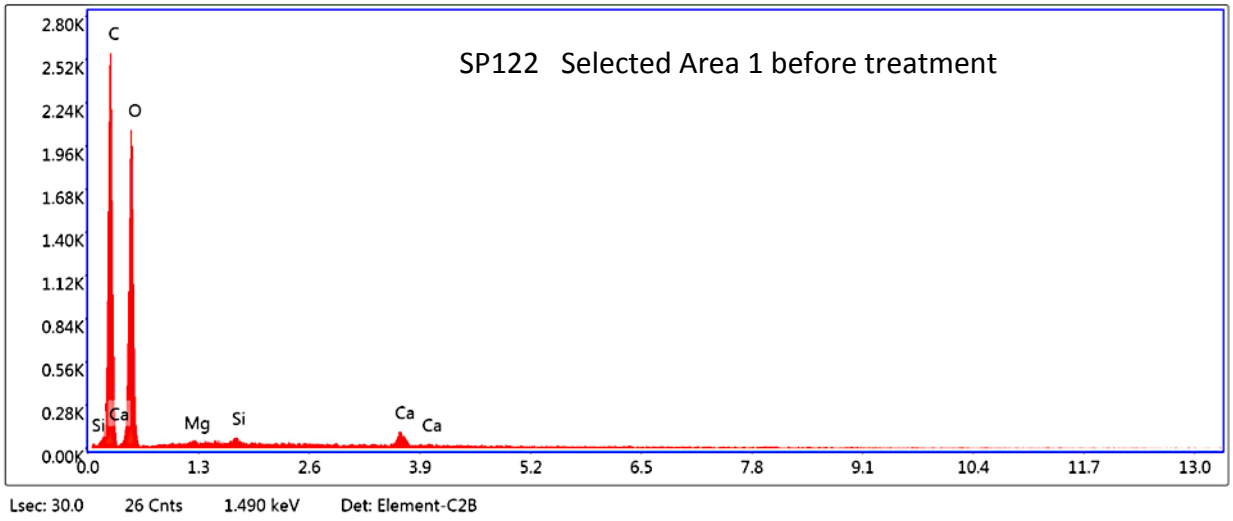

Figure 7.10. Sized burnt sample SP122, cross section before treatment. EDX spectrum of the Selected Area 1, adjacent to the surface of the paper.

Table 7.9. Sized burnt sample SP122, cross section before treatment. Semi-quantitative estimation of the elements in the area adjacent to the surface of the paper. Silicon (Si) is present in trace and probably in form of talc (magnesium silicate).

			Selected Area 1 before treatment		**eZAF Smart Quant Results**			
Element	Weight %	Atomic %	Net Int.	Error %	Kratio	Z	A	F
C K	44.0	51.6	531.6	6.2	0.2537	1.0272	0.5615	1.0000
O K	53.9	47.5	457.2	9.7	0.1215	0.9816	0.2296	1.0000
MgK	0.2	0.1	4.9	43.0.	0.0010	0.9052	0.5439	1.0018
SiK	0.3	0.1	8.7	29.1	0.0018	0.8903	0.8187	1.0053
CaK	1.7	0.6	33.6	13.9	0.0148	0.8393	1.0259	1.0358

A part from C and O, referable to cellulose, only calcium and limited amount of what is probably talc ($Mg_3Si_4O_{10}(OH)_2$) are present as part of the sheet composition (see Chapter 3, § 4).

The EDX spectrum and the analyses of the elements detected in the Selected Area 1 after treatment confirm a marked increase in the content of silicon, no longer associated in a compound with magnesium, as shown in Fig. 7.11 and in Table 7.10.

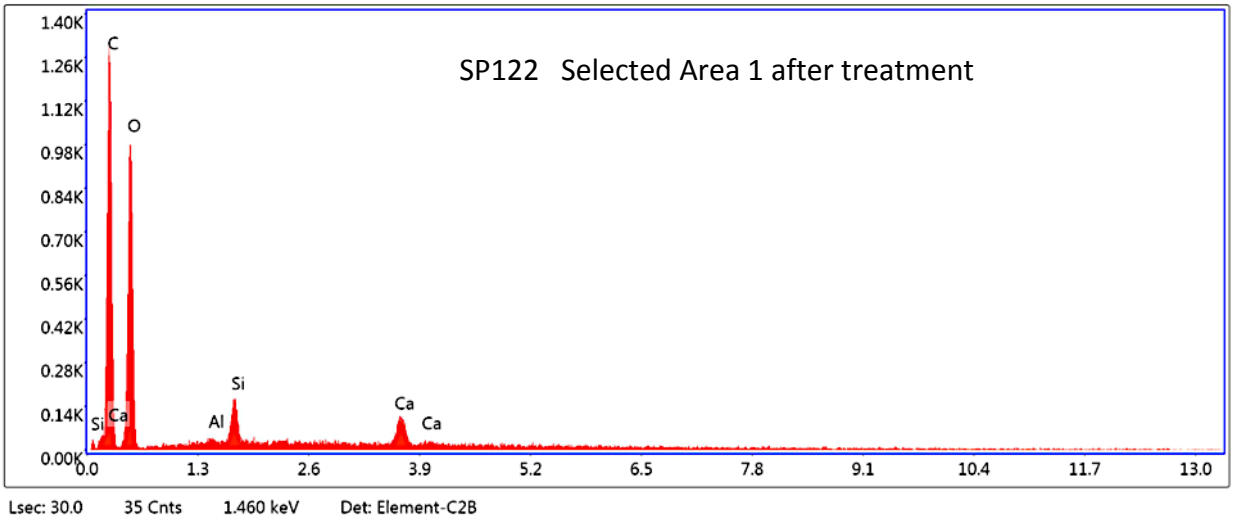

Figure 7.11. Sized burnt sample SP122, cross section after treatment. EDX spectrum of the Selected Area 1, adjacent to the surface of the paper.

Table 7.10. Sized burnt sample SP122, cross section after treatment. Semi-quantitative estimation of the elements in the Selected Area 1, adjacent to the surface of the paper. Silicon is present.

	Selected Area 1 after treatment			eZAF Smart Quant Results				
Element	Weight %	Atomic %	Net Int.	Error %	Kratio	Z	A	F
C K	43.9	52.4	267.2	7.2	0.2277	1.0304	0.5030	1.0000
O K	50.7	45.4	225.4	10.4	0.1073	0.9850	0.2149	1.0000
AlK	0.2	0.1	3.7	65.9	0.0014	0.8746	0.7071	1.0044
SiK	2.0	1.0	39.6	9.1	0.0150	0.8936	0.8228	1.0052
CaK	3.2	1.1	35.5	12.9	0.0280	0.8426	1.0218	1.0271

The composition of the Selected Area 2 in the untreated sized sample SP122 is essentially the same as observed in the Selected Area 1, shown in the EDX Spectrum in Fig. 7.12 and in the EDS results in Table 7.11, except for the complete absence of magnesium.

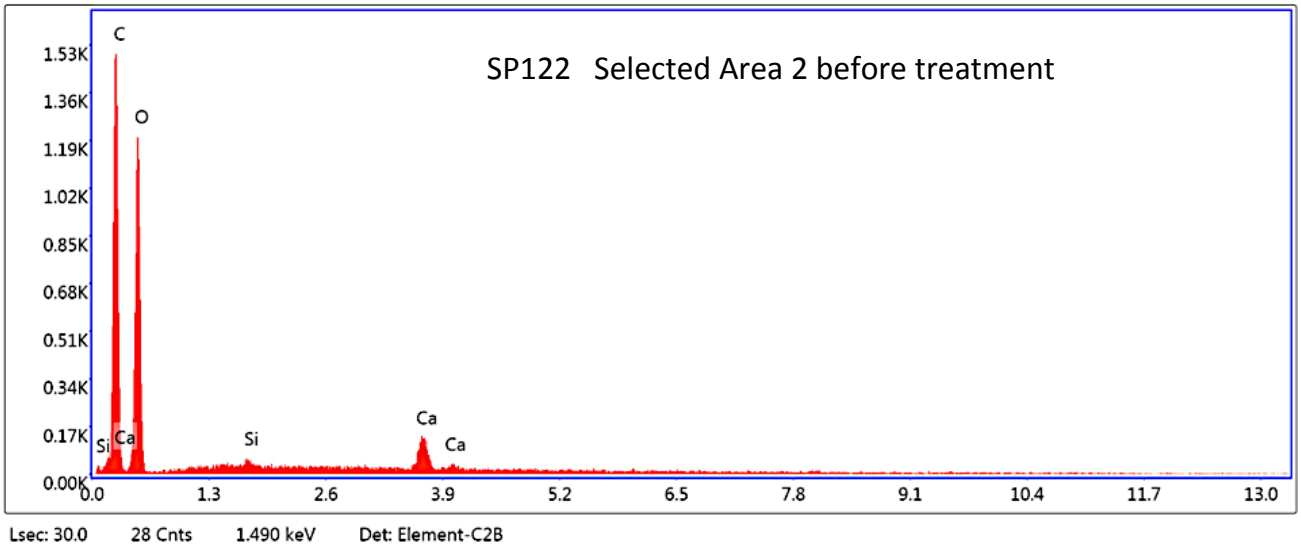

Figure 7.12. Sized burnt sample SP122, cross section before treatment. EDX spectrum of the central Selected Area 2.

Table 7.11. Sized burnt sample SP122, cross section before treatment. Estimation of the elements detected with EDS probe in the central Selected Area 2, very close to that in the Selected Area 1.

			Selected Area 2 before treatment		eZAF Smart Quant Results			
Element	Weight %	Atomic %	Net Int.	Error %	Kratio	Z	A	F
C K	42.6	50.8	305.0	6.6	0.2444	1.0303	0.5563	1.0000
O K	53.2	47.6	256.6	10.2	0.1146	0.9848	0.2186	1.0000
SiK	0.4	0.2	7.7	30.6	0.0027	0.8934	0.8166	1.0059
CaK	3.8	1.4	45.9	9.0	0.0339	0.8424	1.0251	1.0265

After the application of the combined strengthening formulation, also in this central area of the sized sample silicon is clearly detected (Fig. 7.13 and Table 7.12).

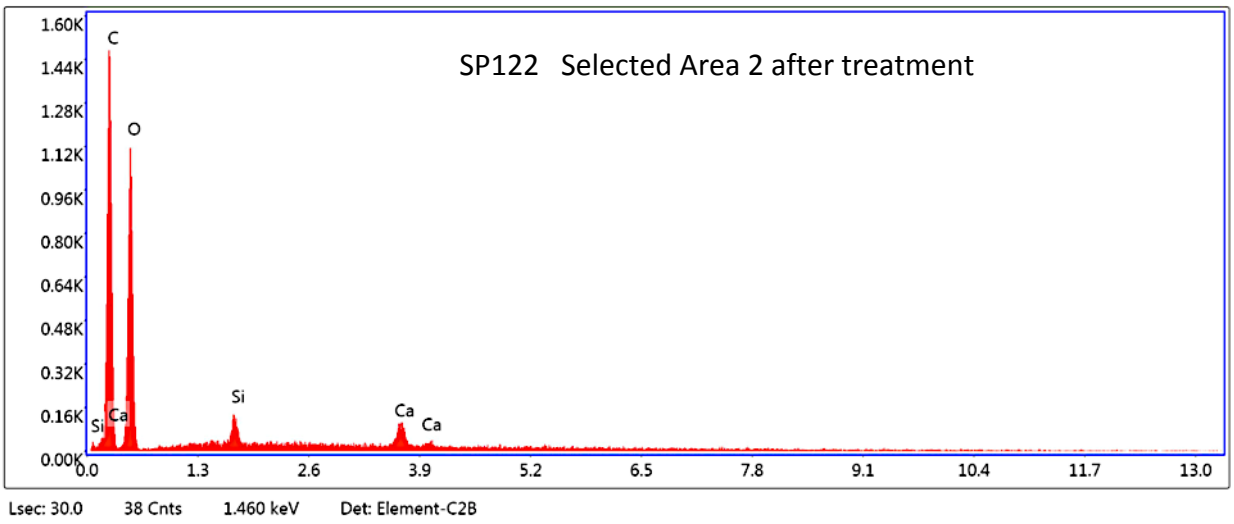

Figure 7.13. Sized burnt sample SP122, cross section after treatment. EDX spectrum of the central Selected Area 2.

Table 7.12. Sized burnt sample SP122, cross section. After treatment, the EDS probe clearly detected Silicon also in this central Selected Area 2.

			Selected Area 2 after treatment		eZAF Smart Quant Results			
Element	Weight %	Atomic %	Net Int.	Error %	Kratio	Z	A	F
C K	44.1	52.3	295.7	6.9	0.2420	1.0291	0.5326	1.0000
O K	51.8	46.1	243.8	10.2	0.1114	0.9836	0.2186	1.0000
SiK	1.3	0.6	25.7	10.9	0.0093	0.8922	0.8233	1.0054
CaK	2.8	1.0	32.8	12.2	0.0249	0.8413	1.0238	1.0293

Finally, the EDX spectra and the analysis with EDS of the Selected Area 3 located near the surface of the sample, can be compared before and after the application of the strengthening nanocomposite. In the untreated sample SP122, silicon (Si) is detected in minimum amount, as shown in Fig. 7.14 and in Table 7.13.

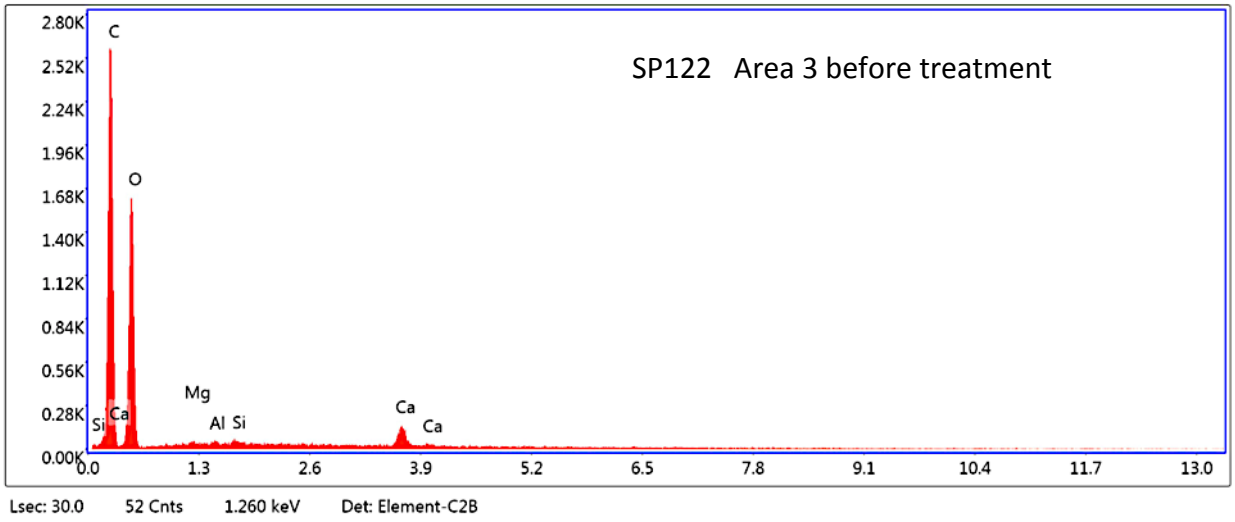

Figure 7.14. Sized burnt sample SP122, cross section before treatment. EDX spectrum of the central Area 3, near the paper surface.

Table 7.13. Sized burnt sample SP122, cross section. Before treatment, the EDS probe detected limited traces of silicon (Si).

		Selected Area 3 before treatment		**eZAF Smart Quant Results**				
Element	Weight %	Atomic %	Net Int.	Error %	Kratio	Z	A	F
C K	46.8	54.7	542.1	6.1	0.2782	1.0268	0.5787	1.0000
O K	50.3	44.2	364.9	10.1	0.1043	0.9813	0.2111	1.0000
MgK	0.2	0.1	3.4	70.2	0.0008	0.9049	0.5511	1.0020
AlK	0.1	0.0	2.1	76.3	0.0005	0.8712	0.7058	1.0035
SiK	0.1	0.1	3.9	65.9	0.0009	0.8900	0.8237	1.0057
CaK	2.5	0.9	47.4	9.8	0.0224	0.8391	1.0269	1.0319

Once treated, In the Selected Area 3 of sample SP122, the presence of silicon is more consistent (Fig. 7.15, Table 7.14).

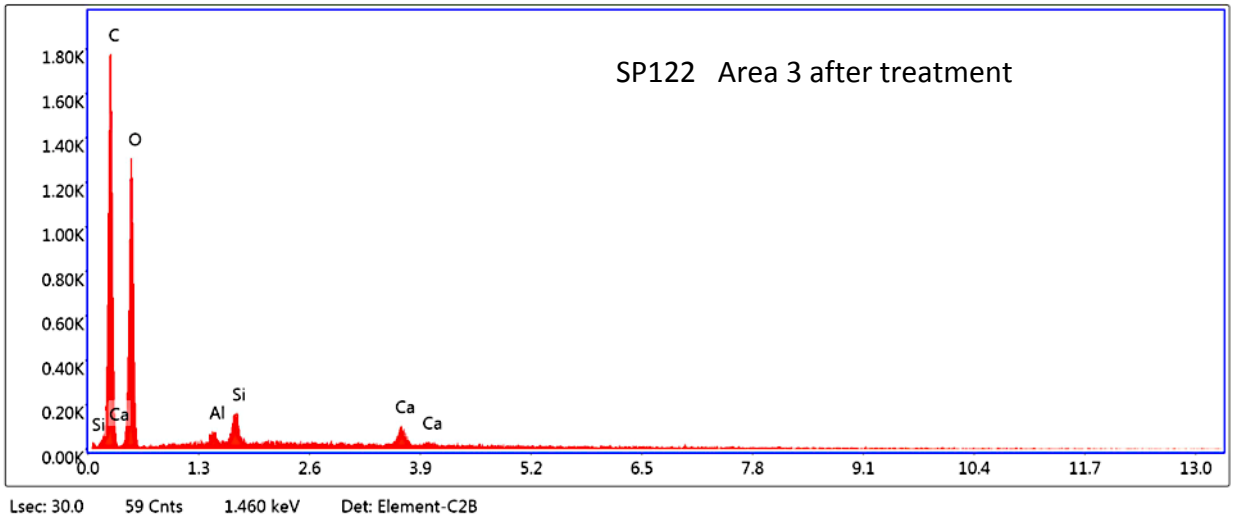

Figure 7.15. Sized burnt sample SP122, cross section before treatment. EDX spectrum of the Selected Area 3, near the paper surface.

Table 7.14. Sized burnt sample SP122, cross section. After treatment, the EDS probe detected traces a more consistent amount of Silicon (Si).

Selected Area 3 after treatment eZAF Smart Quant Results

Element	Weight %	Atomic %	Net Int.	Error %	Kratio	Z	A	F
C K	45.3	53.5	366.0	6.9	0.2396	1.0285	0.5142	1.0000
O K	50.5	44.7	295.7	10.1	0.1081	0.9830	0.2179	1.0000
AlK	0.6	0.3	11.9	21.7	0.0035	0.8727	0.7106	1.0041
SiK	1.5	0.8	39.2	10.0	0.0114	0.8916	0.8224	1.0050
CaK	2.1	0.7	30.1	14.8	0.0183	0.8407	1.0229	1.0318

On the basis of the SEM/EDS results, the formulation of 0.3% w/v CNC + 0.06w/v MFC in SIOX-5TO permeated the whole cross section of the sized paper. As already realized for the unsized sample UP122, in the treated sample SP122 silicon was detected in slightly lower quantity in the central Selected Area 2 (1.3 weight%) than in the Selected Area 1 (2.0 weight%) and in the Selected Area 3 (1.5 weight%), both adjacent to the paper surfaces.

Compared to the UP122, in SP122 the silicon amount is lower in all the three areas. This evidence is in line with the uptakes resulting from the sample treatment, which were always higher for the unsized paper (UP), prone to absorb the products applied on its surface, than for the gelatin size paper (SP), less easily permeable in general.

3. Conclusions

In the last step of the experimental phase of the present research, a new nanocomposite, based on the mix of nanocelluloses and polysiloxane, was developed to achieve the structural strengthening and the consolidating coating of the utterly fragile burnt paper areas in a single treatment application.

The new product is composed of a mix of cellulose nanocrystals (CNC, 0.3% w/v) and microfibrillated nanocellulose (MFC, 0.06% w/v) dispersed in a formulation of SIOX-5TO, a polysiloxane based on tetraethoxysilane, TEOS, functionalized with octyl-triethoxymethylsilane, OTES, in isopropanol. The formulation had a low pH (4.8), due to the HCl present in the SIOX-5TO and acting as catalyst of the sol-gel process of the commercially available polysiloxane. Therefore, in view of a possible future application of the treatment on historical burnt paper artifacts, the pH of the dispersion composed of nanocelluloses in SIOX-5TO was raised, in order to avoid the risk of exposing the treated cellulose and the nanocelluloses from the treatment itself to acid-catalyzed degradation reactions.

The pH of the nanocomposite dispersion was raised to 7, 8 and 9. The choice of a slightly alkaline pH is explained by the increased polymerisation rate expected at basic pH due to basic catalysis. The strengthening efficiency of the three combined formulations at different pH was tested.

For each unsized and sized RPM samples different applications were carried out: part of each sample was treated with a dispersion of CNC (0.3% w/v) and MFC (0.06% w/v) in ethyl alcohol and part with the nanocomposite at the three pH values (7, 8 and 9). Fold resistance tests were performed using the tailor-made apparatus to measure the critical folding angle (CFA) and showed the efficiency of the different nanocomposite formulations in improving the paper resistance to folding. This efficiency was best for both the unsized and sized samples treated with the new formulation of nanocellulose combined with the polysiloxane than with the nanocellulose mix alone. Only in one case, for the SP samples treated with the combination nanocellulose/polysiloxane at pH 9, the performance as reinforcing agent was not successful. The best results in enhancing paper flexibility and strength in all the treated unsized and sized samples were achieved by the formulation composed of nanocellulose and SIOX-5TO at pH 8. The increase in paper mechanical performance was the most remarkable so far achieved in the very large number of folding tests performed: +22.3% for the unsized (UP) samples and +15.0% for the sized

(SP) samples. It is also important to underline the fact that the uptakes inducing these results were in a low range (1-3%) and perfectly comparable with those in other treatments. This is all the more interesting that adding too much weight to paper with a treatment can be a problem in conservation. For the same samples, for instance, the improvement in fold resistance achieved by the nanocellulose dispersion was +13.7% and +10.0% for the sized one.

The physico-chemical modifications induced by the combined treatment in the burnt paper were investigated with ATR-FTIR and with SEM/EDS analysis.

ATR-IR spectra did not track differences in the samples before and after treatment,
while the observation of the samples by SEM/EDS before and after the treatments revealed the presence of the main element of the TEOS-based polysiloxane SIOX-5TO, silicon, in the entire cross section of the treated samples, both unsized and sized. On the contrary, silicon is usually absent or present in trace in the untreated samples. This confirmed the ability of the nanocomposite combined formulation to penetrate the paper and permeate the fragile paper matrix with a network of stabilizing and strengthening nanocomposite.

Chapter 7 | References

Brinker, C. J. (1988). «Hydrolysis and condensation of silicates: effects on structure». *Journal of Non-Crystalline Solids*, 100, 31-50; https://doi.org/10.1016/0022-3093(88)90005-1

General conclusions and perspectives

This research was dedicated to develop an innovative solution for a recurrent problem in the preservation of our written cultural heritage, namely the large number of books and documents damaged by fire in libraries and archives, and left unattended in extremely fragile and dire conservation conditions.

Such historical papers are much more than a text to be read. Being part of our cultural heritage, their material evidence reflects the knowledge and the progress of the society that manufactured them, and conservation actions make sense only when considered in a historical perspectives, with all due respect for the original physicochemical features of the artifacts.

The conservator is expected to integrate historical and scientific knowledge in order to tailor the most appropriate treatment, as least invasive as possible, and altering the object to a lesser extent while effectively counteracting its decay.

On the basis of these premises, the present research took its first steps from the morphological and physicochemical characterization of some historical papers: a blank sheet belonging to a manuscript held at the Médiathèque l'Apostrophe in Chartres (dated to the 1830s) and some *bifolia* from an incunabulum (15th century) of the Library of the Episcopal Seminary in Padua, both victims of fire during bombings in 1944.

The cross-referencing and interpretation of data resulting from the different investigation techniques (spectroscopic, microscopic and chemical) applied to areas of unburned paper and to those of paper at different degrees in the combustion process, made it possible to assess the composition of the paper (fibrous matter, gelatin sizing, mineral elements), and the progressive changes induced in the fibres by thermal degradation. This was a crucial step for two reasons. The first one was to produce paper samples, to be used in the subsequent experimental part, in which the macro- and microstructural and physico-chemical characteristics were comparable to those of real historical papers. The other reason was to identify if some cellulose was still persisting and detectable even inside the severely charred fibres, and if gelatin had a role in partially protecting the paper during burning.

This information could be verified and on this basis, unsized samples and samples sized with gelatine were specifically prepared with a handmade rag paper, reproducing the basic composition of the historical one. The carbonization process was artificially reproduced to closely match the real carbonization, by hot plate burning. In this process, the plate temperature and heating time were standardized to obtain a quite uniform heat-induced degradation. This was assessed by spectroscopic, microscopic and physicochemical analyses, same as those performed on the burnt paper from the Chartres manuscript and from the Padua incunabulum. The detection of persisting cellulose in the burnt paper material was a crucial piece of information for tailoring the conservation treatment aimed at reinforcing the damage paper matrix using nanomaterials.

Nanomaterials great development and spread in the field of cultural heritage in recent decades are a sign of the contribution they can give to issues that cannot be approached otherwise in a more traditional way, as for instance for a reinforcing treatment for burnt paper.

In the present research, the application of nanocomposites based on nanocellulose dispersed in polymer polysilicates was expected to form a composite network able to establish physical and chemical interactions with the charred cellulose, while filling the voids created in the paper matrix by the effects of extreme heat degradation, which partially destroyed the cellulose fibres. To better understand if and to what extent nanocelluloses and polysiloxanes could participate in restoring the cohesion and mechanical resistance of the damaged cellulose, they were firstly tested separately on the laboratory burnt paper samples.

Microfibrillated cellulose (MFC), composed of thin and flexible micro-fibrils, and cellulose nanocrystals (CNC), with shorter rigid and fully crystalline whiskers, were applied individually, dispersed in alcohol at different concentrations, which allowed to assess their effectiveness in reinforcing the burnt paper. As the fragility of the burnt paper did not allow the use of standardized mechanical testing procedures, a folding endurance test was specifically developed to this purpose by employing a tailor-made simple apparatus. This allowed assessing the influence of the nanocellulose dispersions on the mechanical resistance of the paper by measuring a critical folding angle before breaking (CFA). This folding test proved very useful in distinguishing the degree of reinforcement and flexural improvement, and was used throughout this research.

The ethanol dispersion of MFC resulted the most suitable in improving the mechanical properties of the sized papers. The opposite situation was observed with respect to CNC, which was more

suitable for the unsized papers, suggesting that a treatment combining both MFC and CNC would be effective for unsized as well as for sized paper. The optimal reinforcing treatment was in fact achieved with a mixture composed of 0.3%CNC and 0.06%MFC dispersed in ethanol. This nanodispersion was applied by spraying with an airbrush on the charred paper areas. Its ability to enter the porous paper matrix, granting the nanocellulose penetratration within the samples was confirmed by SEM/EDS, and led to a remarkable improvement in the flexibility of the treated paper as well as to an increase of its resistance to mechanical stress, as measured by the CFA improvement.

Polysiloxanes are polymers already used in the conservation field, especially tailored as protective coatings due to the elasticity, resistance to chemical degradation and good ageing properties of the silica film that is formed when they polymerize *in situ*. Starting from previous studies and experimental works, in this research various formulations of polysiloxanes based on tetraethoxysilane (TEOS) and on aminoalkylalkoxysilanes were experimented for the first time on burnt paper. Their ability to permeate the paper matrix, and to enhance its physico-mechanical performances was compared. Although long investigated in previous studies and optimized to counteract the acidification phenomena that occur during paper aging, and reinforcing fragile papers by simultaneously bringing strength and flexibility, the application of the aminoalkylalkoxysilanes on the burnt charred paper in this research was unsuccessful. They led to an increase of the paper stiffness, as shown by flexometer measurements, and a decrease of their fold endurance. On the other hand, a polysiloxane formulation composed of TEOS and octyltriethoxysilane, OTES (5% in water and isopropanol), SIOX-5C, systematically enhanced the mechanical properties of the damaged paper in all the tests, allowing a decrease in its rigidity and an improvement of its fold resistance. This contrasted effect, which is the opposite as what had been observed in the literature on *normally* degraded paper (unburnt) – where polysilicate such as TEOS enhance the degraded paper brittleness – could tentatively be explained by the very nature of the material to be reinforced, where burnt paper has become highly carbonized. The fibre-fibre bonding and the hydrogen bonding that is the characteristic of paper is greatly affected and may no longer remain. Hence it is the remaining fibres structure skeletons that need to be stabilized and the firmer network brought by TEOS was thus more adequate.

In the final step, a newly formulated nanocomposite, based on the mixture of nanocelluloses directly dispersed in the polysiloxane SIOX-5TO water/isopropanol solution, was developed to

achieve the structural strengthening and the consolidating coating of the fragile burnt paper areas in a single treatment application.

The results of the folding endurance test confirmed that this combined treatment was more efficient than the nanocelluloses mixture (MFC/CNC) alone, when applied in small amount, such as to achieve uptakes in the paper of about 2%.

Even though the infrared spectroscopic analysis (ATR-FTIR) could not detect differences before and after treatment in the samples – in thus confirming a very limited alteration of the paper material – SEM/EDS examination confirmed the presence of silicon from the TEOS-based polysiloxane SIOX-5TO, and of the nanocellulose in the entire cross section of the treated samples, both unsized and sized. Finally, it is worthy to note that the new combined nanocomposite strengthening formulation is based in water and isopropanol, the latter is considered of low toxicity, suitable for *in loco* applications, directly in the libraries and archives holding written cultural heritage.

On the basis of the positive results gained from the experimentation, a preliminary test application of the nanocomposite combined treatment was carried out on the historic paper that had been dedicated to this study. As opposed to the samples employed in the experiments, these papers are written and even if the naked eye failed to detect the text in the charred blackened areas, the latter could be detected by multispectral survey techniques. It was then crucial that the reinforcing treatment developed in this research would facilitate the handling of the sheets, by increasing their mechanical resistance to stress, but would not compromise the textual information that could be gathered by spectroscopic multispectral imaging at a later state.

As preliminary step, a sheet from an account book dated from the first decades of the 19th century – bought from the antique market and free from the constraint of institutional cultural heritage – was treated according to the methodology developed. The formulation was sprayed on a selected area including the charred paper and some millimeters of the adjacent unburnt areas, masking the parts not intended to be treated (Fig. 1).

Figure 1. Distribution of the reinforcing formulation MFC/CNC/TEOS by airbrush on the charred area of the manuscript from the 19th century.

Multispectral investigation was carried out at the CIBA, Interdepartmental Centre for the Study of Cultural Heritage of the University of Padua, which led to images before and after treatment in visible light, in the ultraviolet and infrared spectral ranges. The comparison of multispectral images (Fig. 2) of the selected area pre-treatment (a, b, c) and post-treatment (a1, b1, c1), showed no negative alterations in the readability of the iron gall ink writing, and the text was fully revealed by the IR images pre (c) as well as post the application of the formulation.

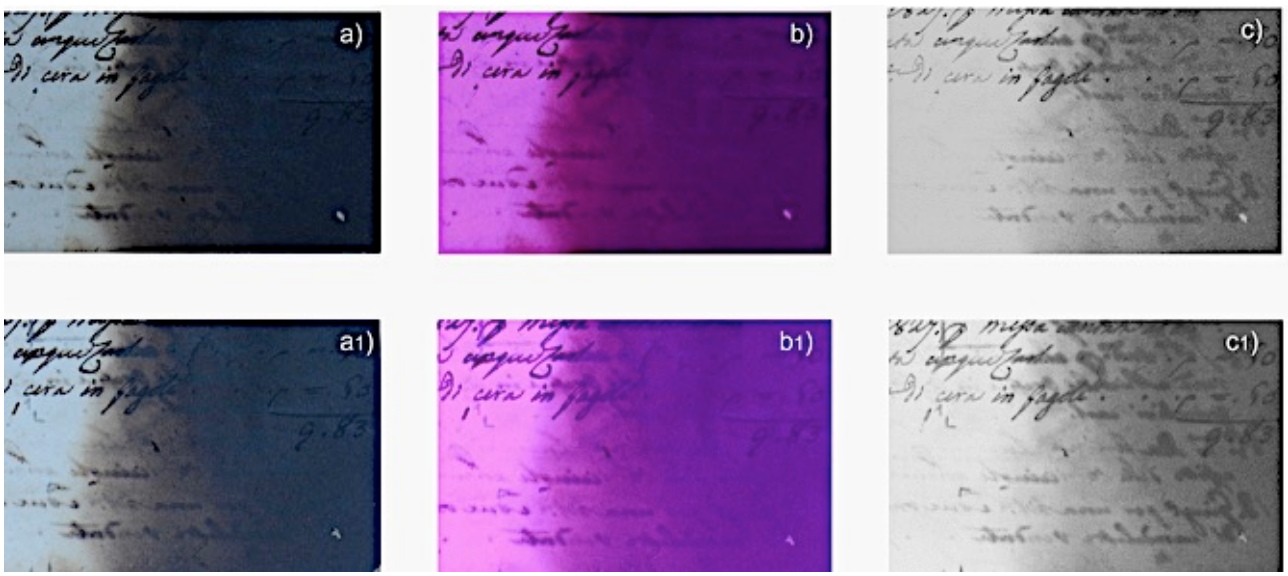

Figure 2. Multispectral images of the fragment from the Padua incunabulum before (a, b, c) and after (a1, b1, c1) reatment at visible light (a and a1), in the UV (b and b1) and IR (c and c1) band. Multispectral investigation and images: Rita Deiana, CIBA.

Some printed fragments completely burnt and free of the incunabulum *Lectio super secundo Decretalium* from the Library of the Episcopal Seminary of Padua, involved from the very beginning in this research, underwent also the treatment.

According to the multispectral images (Fig. 3), the print is fully readable in the IR spectral bands in the severely burnt area, to a similar extent before (c) and after the treatment, which does not interfere with any imaging investigation and reproduction of the text.

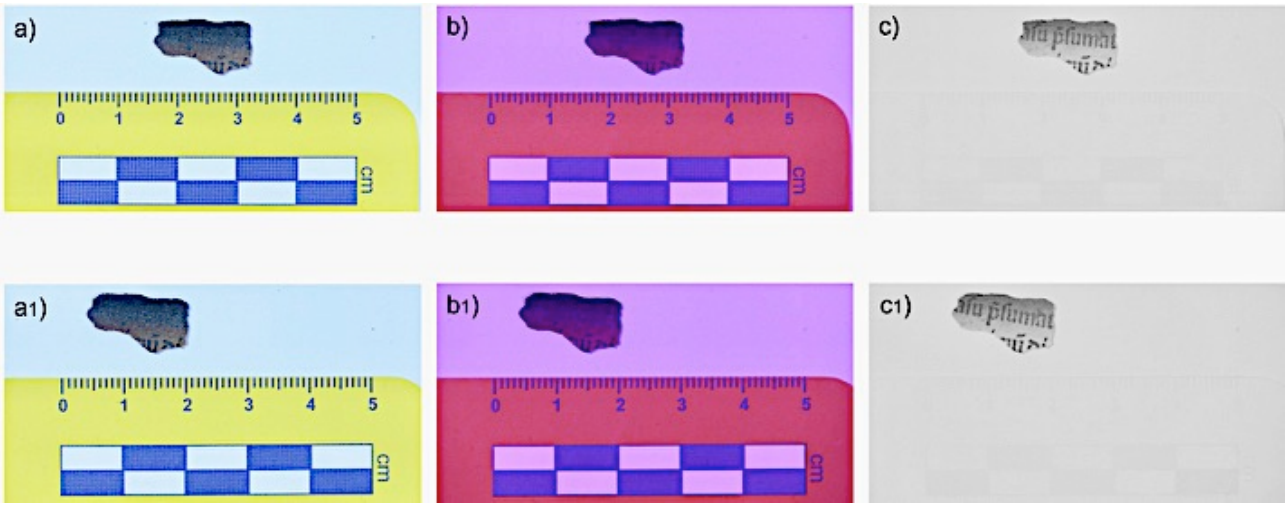

Figure 3. Multispectral images of the fragment from the Padua incunabulum before (a, b, c) and after (a1, b1, c1) treatment, taken at visible light (a and a1), in the UV (b and b1) and IR (c and c1) band. Multispectral investigation and images: Rita Deiana, CIBA.

Finally, this work culminated with a new perspective by carrying out the conservation treatment *in situ* in a library, on two leaves from a burnt manuscript held at the Médiathèque L'Apostrophe in Chartres, kindly offered for testing. The treatment was performed directly in the library study room (closed to the public on the treatment day) and involved the participation of the library staff to test the suitability of the *in loco* application of the methodology developed in the present research.

Two leaves from the ms. 1171 (*Catalogue de la Bibliothèque du Chapitre de Chartres*, 1752) were selected, one blank and the other handwritten with iron gall ink. Several location points of the burnt areas were analyzed with FORS (Fiber Optics Reflectance Spectroscopy) before spraying the reinforcing formulation all along the margins of the sheets (Fig 4), keeping a limited area on both the sheets untreated, as control.

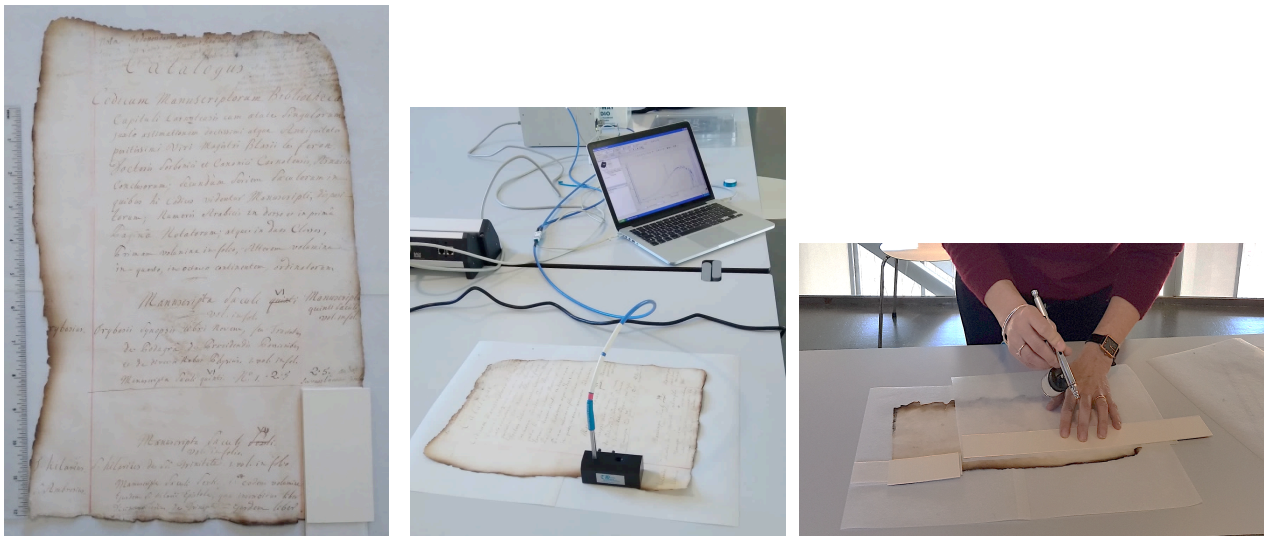

Figure 4. Ms 1171. Left: the handwritten sheet with the covered area kept untreated; centre: FORS analyses; right: reinforcing treatment of the charred paper margins.

Since the polymerization of the polysiloxan requires some time, analyses after applications could not be conducted on the same day and are planned to take place in the near future. Data collected before and after treatment will be compared to verify possible variations in paper and ink.

Such a treatment at the Médiathèque in Chartres represents, in the present work, the most complete moment of interaction between the different skills, both humanistic and natural sciences, that will increasingly have to be brought into play at the service of access and conservation of our cultural heritage.

Publications

Zanetti, M., Rossi, C., Bertoncello, R., Dupont, A.-L., Zoleo, A., Bougard, F. (2020). «La restauration des livres et documents endommagés par le feu : nouveaux matériaux et nouvelles méthodes: le projet CREMIB». *La Revue de la BNU*, 21, pp. 52-59

Zanetti, M., Zoleo, A. (2018). «Les documents en papier brûlés à Chartres. Perspective de restauration à l'aide des nanomatériaux». In: Société archéologique d'Eure-et-Loir (ed.) *Les rescapés du feu. L'imagerie scientifique au service des manuscrits de Chartres.* Société archéologique d'Eure-et-Loir, pp. 137-143.

Appendix Chapter 2

SEM/EDS investigation of the paper from the manuscript Chartres BM ms 1047

and from the Padua incunabulum.

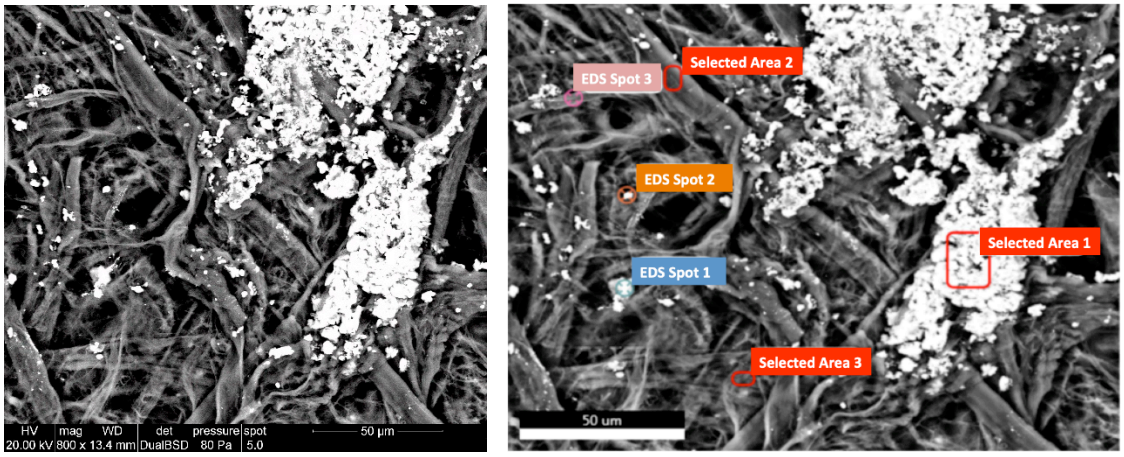

Chartres BM ms 1047, surface. SEM image (left) and areas investigated (right).

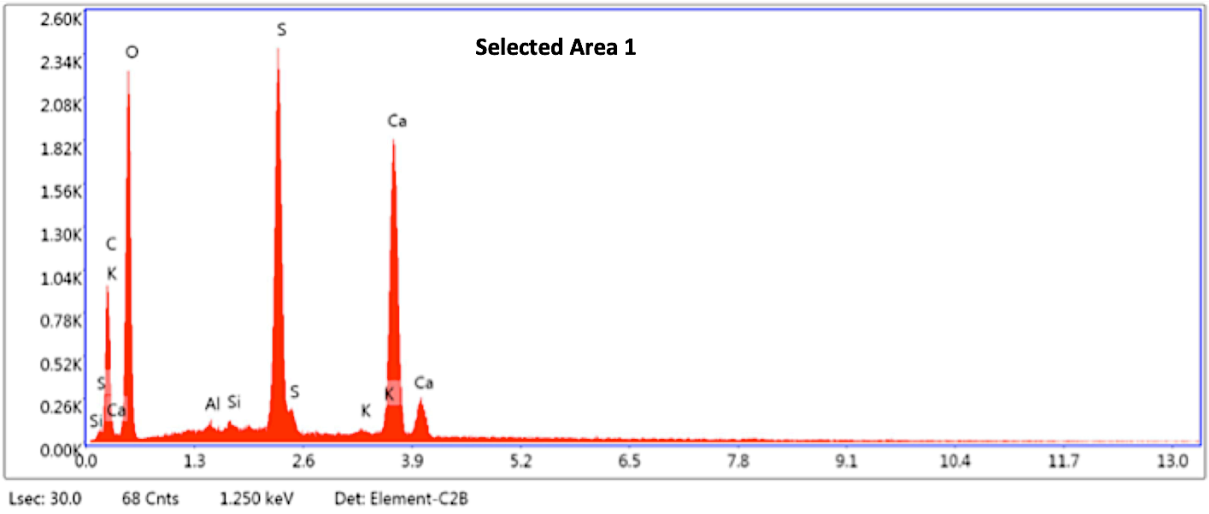

Selected Area 1 **eZAF Smart Quant Results**

Element	Weight %	Atomic %	Net Int.	Error %	Kratio	Z	A	F
C K	**19.04**	29.58	166.63	11.06	0.0451	1.0800	0.2195	1.0000
O K	**44.22**	51.56	497.73	10.31	0.0781	1.0347	0.1707	1.0000
AlK	0.13	0.09	6.44	63.63	0.0008	0.9219	0.6946	1.0055
SiK	0.16	0.10	9.25	37.83	0.0012	0.9423	0.8077	1.0093
S K	**14.53**	8.46	752.40	2.47	0.1276	0.9231	0.9409	1.0111
K K	0.39	0.18	14.62	26.19	0.0034	0.8742	0.9554	1.0416
CaK	**21.54**	10.02	684.82	2.37	0.1879	0.8903	0.9743	1.0057

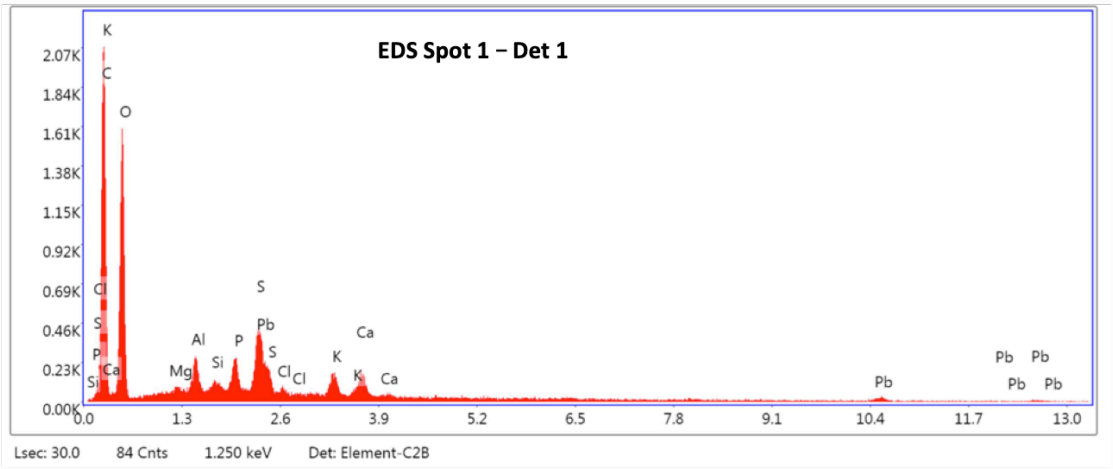

Element	Weight %	Atomic %	Net Int.	Error %	Kratio	Z	A	F
C K	**39.75**	**52.34**	**370.97**	**8.38**	**0.1677**	**1.0635**	**0.3966**	**1.0000**
O K	**42.31**	**41.83**	**345.38**	**10.12**	**0.0904**	**1.0186**	**0.2098**	**1.0000**
MgK	0.17	0.11	4.39	68.04	0.0009	0.9421	0.5735	1.0006
AlK	1.67	0.98	50.30	10.10	0.0109	0.9074	0.7153	1.0011
SiK	0.27	0.15	9.23	36.12	0.0020	0.9276	0.8084	1.0020
P K	1.92	0.98	56.05	8.28	0.0152	0.8911	0.8849	1.0032
S K	1.95	0.96	58.11	10.06	0.0164	0.9088	0.9241	1.0045
PbM	**6.60**	**0.50**	**78.09**	**11.94**	**0.0524**	**0.5987**	**1.2956**	**1.0243**
ClK	0.10	0.04	2.53	78.04	0.0008	0.8647	0.9066	0.9988
K K	2.32	0.94	49.87	11.51	0.0191	0.8608	0.9574	0.9987
CaK	2.94	1.16	54.20	11.00	0.0248	0.8767	0.9658	0.9976

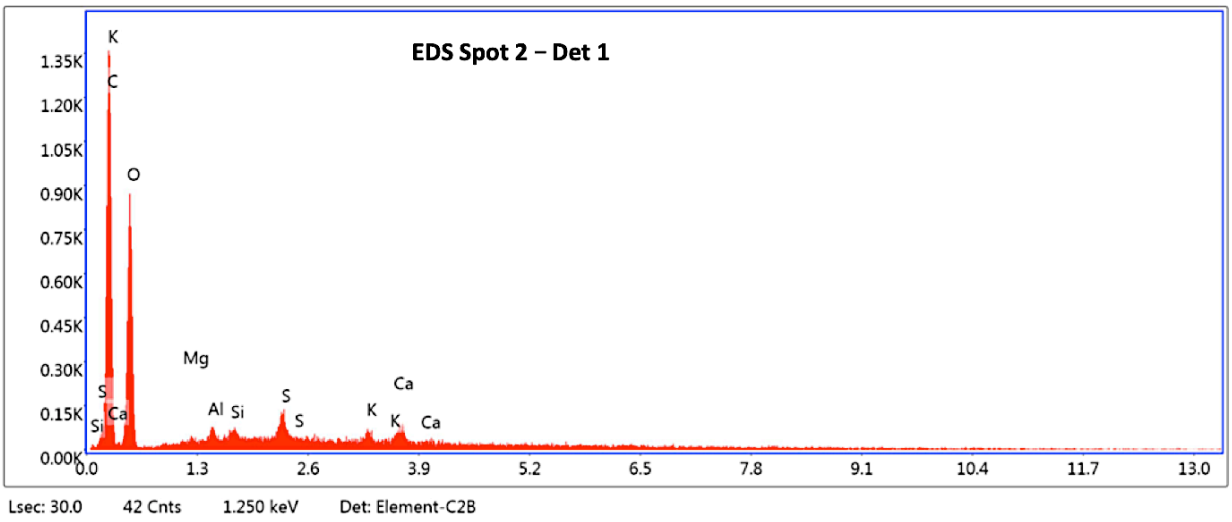

EDS Spot 2 – Det 1 eZAF Smart Quant Results

Element	Weight %	Atomic %	Net Int.	Error %	Kratio	Z	A	F
C K	47.65	56.55	264.75	7.99	0.2342	1.0304	0.4768	1.0000
O K	45.51	40.55	184.23	10.53	0.0944	0.9849	0.2105	1.0000
MgK	0.34	0.20	4.40	47.30	0.0019	0.9086	0.5935	1.0026
AlK	0.67	0.35	10.21	22.11	0.0043	0.8747	0.7383	1.0044
SiK	0.61	0.31	10.80	21.50	0.0046	0.8936	0.8406	1.0068
S K	1.90	0.84	29.07	14.15	0.0161	0.8748	0.9588	1.0128
K K	1.08	0.39	12.52	23.69	0.0094	0.8277	1.0099	1.0351
CaK	2.25	0.80	22.02	19.05	0.0197	0.8427	1.0129	1.0254

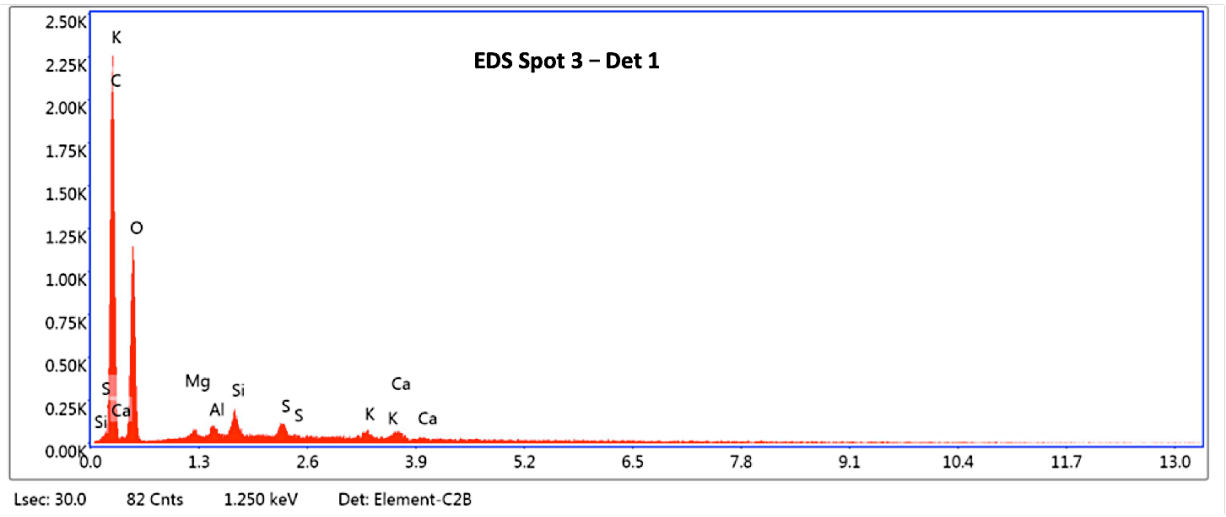

EDS Spot 3 eZAF Smart Quant Results

Element	Weight %	Atomic %	Net Int.	Error %	Kratio	Z	A	F
C K	51.43	60.00	436.55	7.33	0.2631	1.0273	0.4981	1.0000
O K	42.75	37.45	245.93	10.41	0.0859	0.9818	0.2046	1.0000
MgK	0.38	0.22	7.35	39.15	0.0021	0.9055	0.6050	1.0027
AlK	0.63	0.33	14.35	18.60	0.0041	0.8717	0.7481	1.0045
SiK	1.40	0.70	36.79	10.58	0.0106	0.8906	0.8488	1.0060
S K	1.13	0.49	25.31	14.44	0.0096	0.8718	0.9576	1.0124
K K	0.96	0.34	16.21	19.91	0.0083	0.8249	1.0124	1.0332
CaK	1.32	0.46	18.93	20.23	0.0116	0.8398	1.0153	1.0298

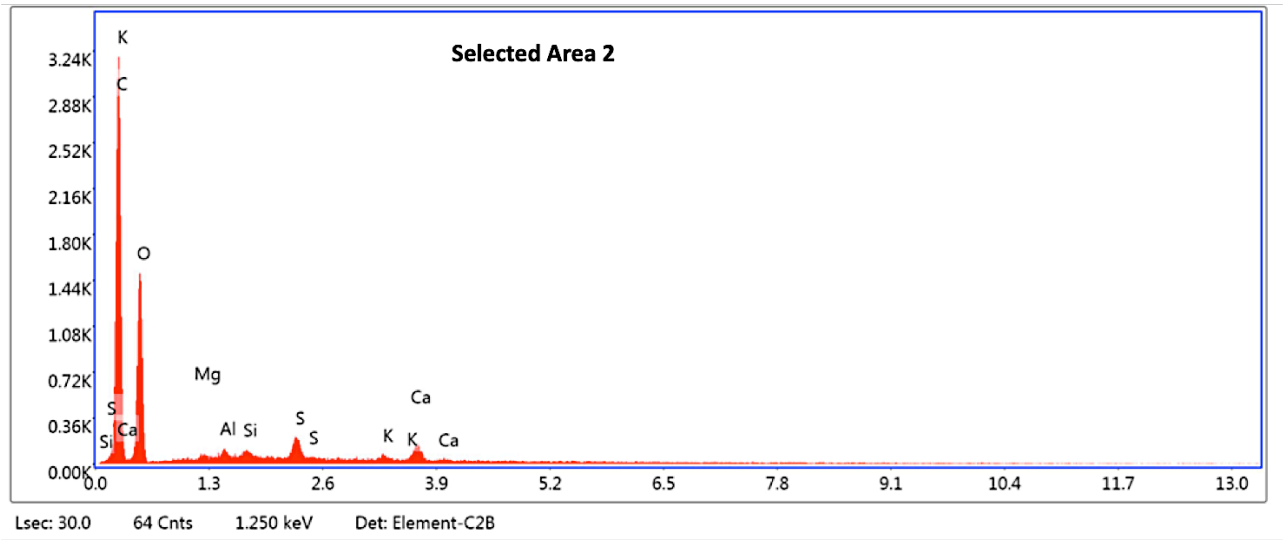

Selected Area 2 **eZAF Smart Quant Results**

Element	Weight %	Atomic %	Net Int.	Error %	Kratio	Z	A	F
C K	52.01	60.75	623.71	7.02	0.2668	1.0275	0.4991	1.0000
O K	41.86	36.70	328.56	10.37	0.0814	0.9821	0.1980	1.0000
MgK	0.32	0.18	8.56	28.69	0.0017	0.9058	0.6044	1.0026
AlK	0.55	0.29	17.75	18.84	0.0036	0.8720	0.7483	1.0044
SiK	0.51	0.25	18.86	20.00	0.0039	0.8909	0.8496	1.0069
S K	1.82	0.80	57.80	9.20	0.0155	0.8721	0.9645	1.0128
K K	0.61	0.22	14.70	19.96	0.0053	0.8252	1.0124	1.0385
CaK	2.32	0.81	46.90	11.00	0.0203	0.8401	1.0166	1.0270

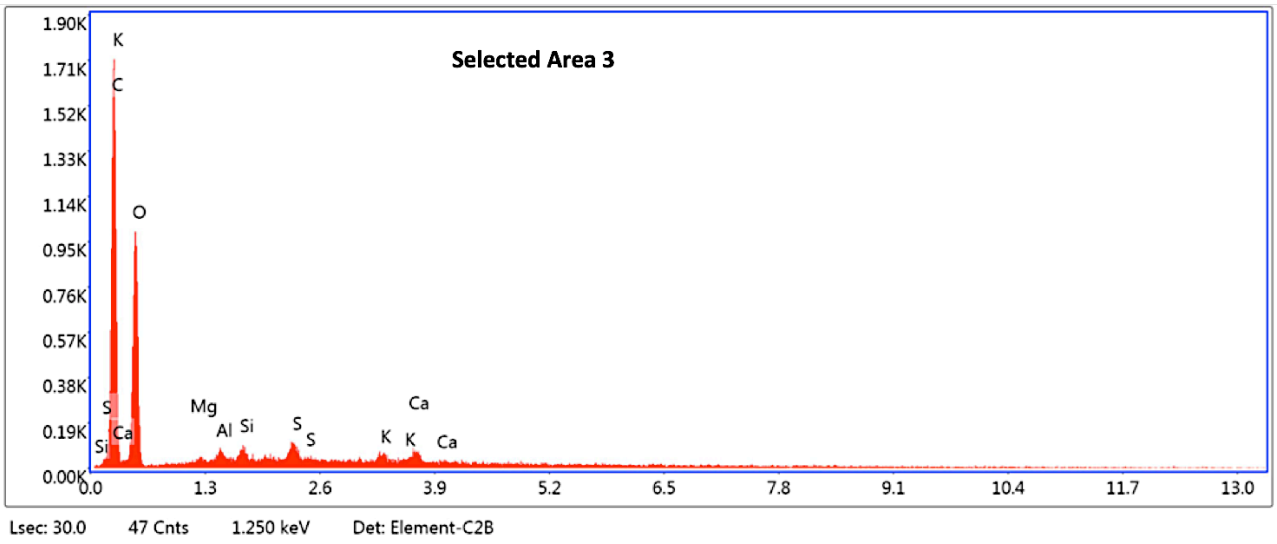

Selected Area 3 eZAF Smart Quant Results

C K	48.90	57.52	326.34	7.51	0.2505	1.0287	0.4981	1.0000
O K	45.27	39.99	211.80	10.43	0.0942	0.9833	0.2116	1.0000
MgK	0.35	0.20	5.16	40.51	0.0019	0.9069	0.5960	1.0026
AlK	0.71	0.37	12.55	19.38	0.0046	0.8731	0.7406	1.0043
SiK	0.68	0.34	13.90	19.31	0.0051	0.8920	0.8421	1.0064
S K	1.38	0.61	24.40	14.83	0.0117	0.8731	0.9592	1.0128
K K	1.04	0.38	13.87	22.53	0.0090	0.8261	1.0121	1.0343
CaK	1.67	0.59	18.87	20.77	0.0147	0.8411	1.0147	1.0282

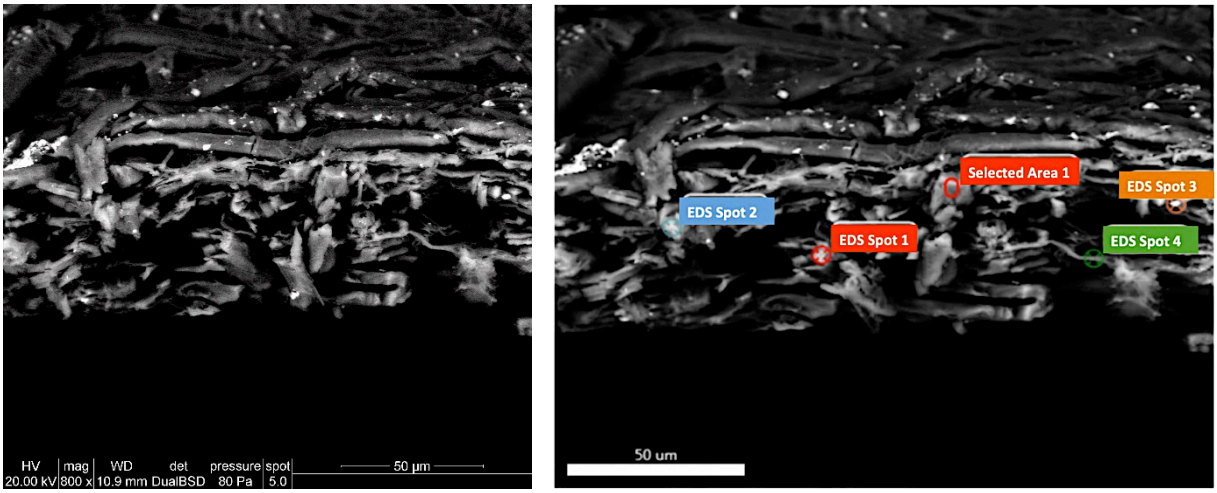

Chartres BM ms 1047, cross section. SEM image (left) and investigated areas (right).

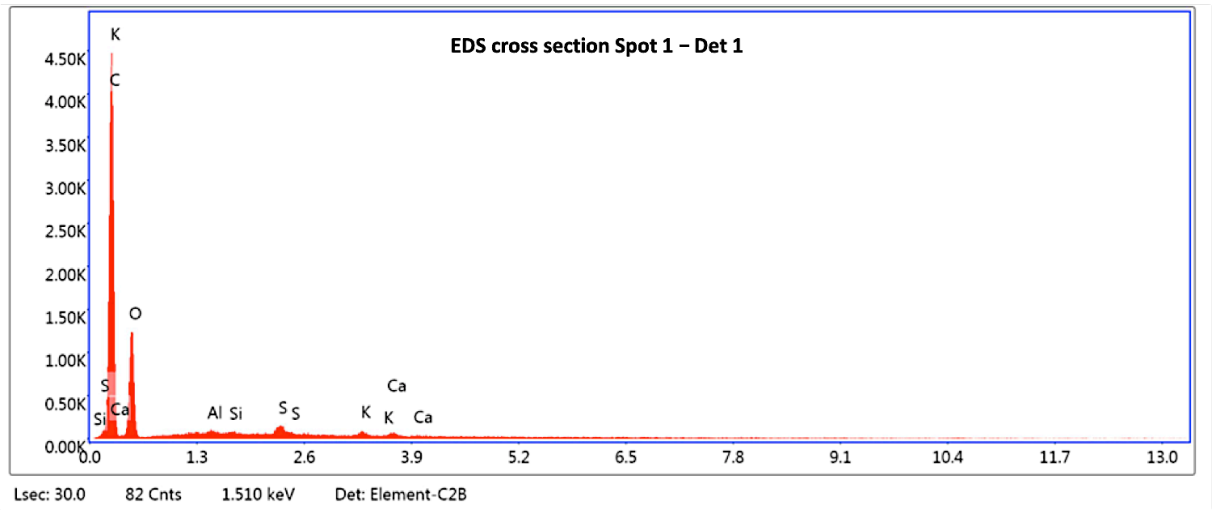

EDS cross section Spot 1 - Det 1 eZAF Smart Quant Results

Element	Weight %	Atomic %	Net Int.	Error %	Kratio	Z	A	F
C K	61.25	68.61	933.60	6.05	0.3632	1.0198	0.5815	1.0000
O K	36.07	30.33	272.39	11.24	0.0584	0.9744	0.1663	1.0000
AlK	0.31	0.15	11.79	25.71	0.0020	0.8648	0.7446	1.0042
SiK	0.12	0.06	5.37	66.24	0.0009	0.8835	0.8536	1.0067
S K	1.05	0.44	41.16	9.80	0.0090	0.8648	0.9760	1.0132
K K	0.63	0.22	18.72	16.56	0.0055	0.8181	1.0242	1.0355
CaK	0.58	0.19	14.61	26.24	0.0051	0.8329	1.0264	1.0388

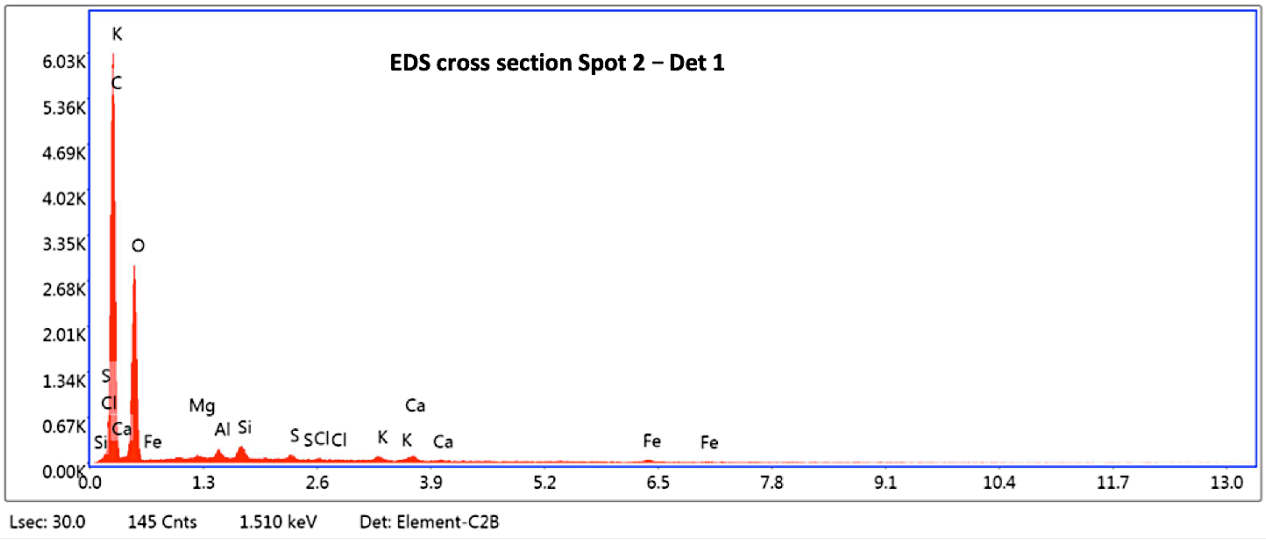

EDS Spot 2 - Det 1 eZAF Smart Quant Results

Element	Weight %	Atomic %	Net Int.	Error %	Kratio	Z	A	F
C K	53.07	61.08	1245.96	6.22	0.2958	1.0248	0.5437	1.0000
O K	43.36	37.46	617.05	10.10	0.0808	0.9793	0.1902	1.0000
MgK	0.24	0.14	11.82	28.05	0.0012	0.9030	0.5646	1.0022
AlK	0.50	0.26	30.42	12.77	0.0031	0.8693	0.7178	1.0038
SiK	0.72	0.36	52.19	9.24	0.0053	0.8881	0.8297	1.0054
S K	0.28	0.12	17.95	17.86	0.0024	0.8693	0.9575	1.0128
ClK	0.09	0.04	5.36	61.12	0.0008	0.8268	0.9884	1.0197
K K	0.50	0.18	24.37	15.25	0.0044	0.8225	1.0200	1.0362
CaK	0.70	0.24	29.30	18.18	0.0063	0.8374	1.0240	1.0394
FeK	0.53	0.13	12.94	26.06	0.0048	0.7458	1.0220	1.1797

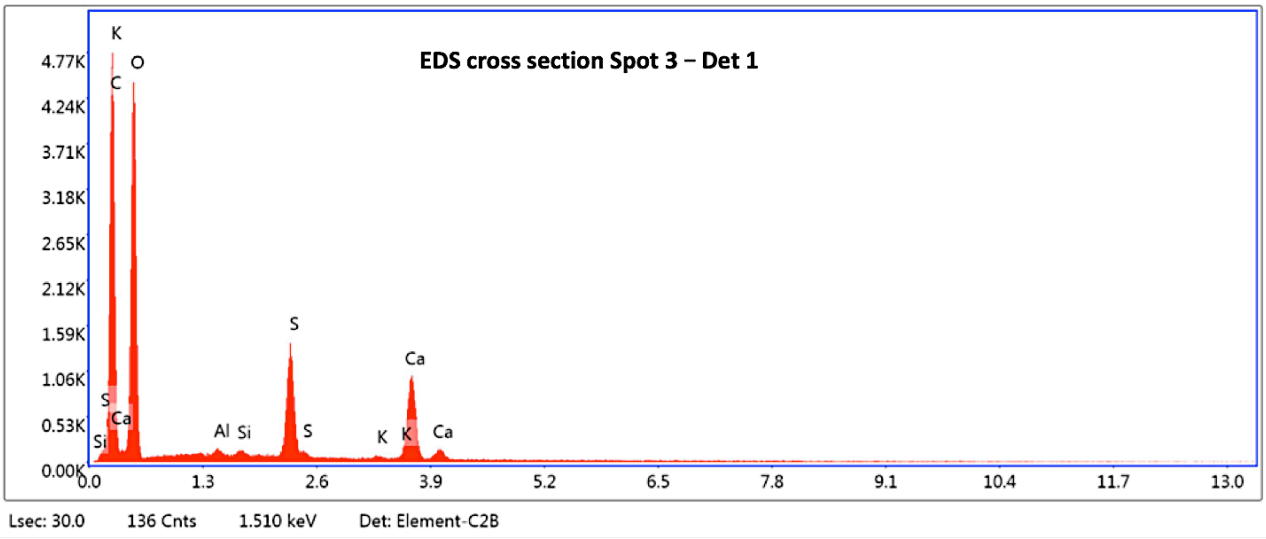

EDS Spot 3 - Det 1 eZAF Smart Quant Results

Element	Weight %	Atomic %	Net Int.	Error %	Kratio	Z	A	F
C K	40.65	50.61	948.46	8.07	0.1596	1.0392	0.3778	1.0000
O K	47.63	44.51	965.90	9.77	0.0896	0.9938	0.1894	1.0000
AlK	0.25	0.14	21.11	17.82	0.0015	0.8831	0.6949	1.0048
SiK	0.16	0.09	16.46	21.91	0.0012	0.9023	0.8128	1.0080
S K	4.59	2.14	414.56	2.87	0.0391	0.8834	0.9519	1.0124
K K	0.22	0.08	14.81	23.51	0.0019	0.8360	0.9990	1.0432
CaK	6.50	2.43	375.30	2.80	0.0568	0.8512	1.0096	1.0163

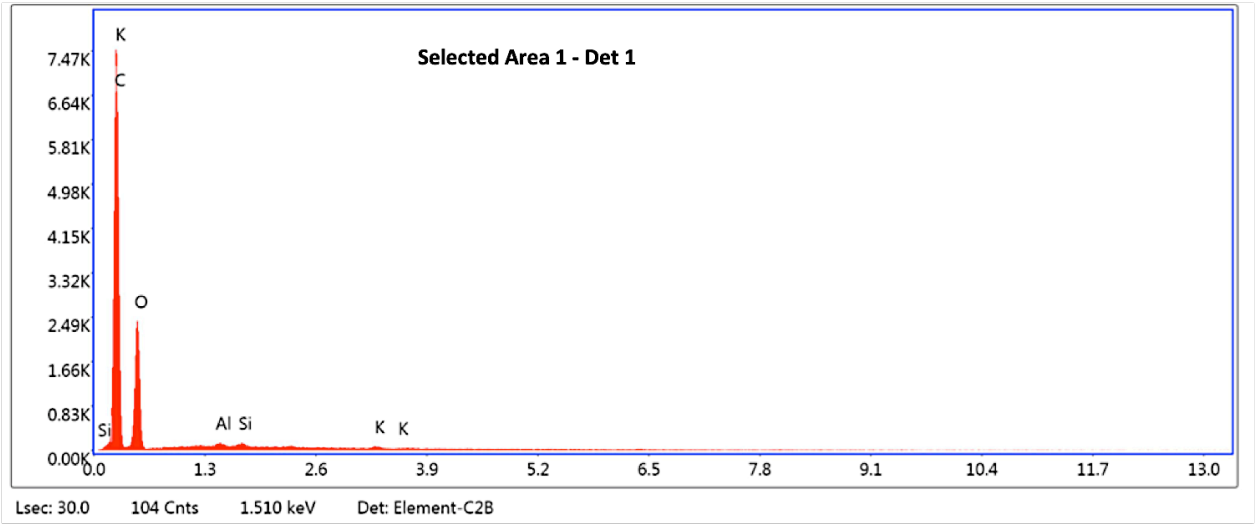

Selected Area 1 - Det 1 eZAF Smart Quant Results

Element	Weight %	Atomic %	Net Int.	Error %	Kratio	Z	A	F
C K	59.84	66.73	1618.00	5.28	0.3851	1.0186	0.6317	1.0000
O K	39.28	32.88	514.25	10.55	0.0675	0.9731	0.1766	1.0000
AlK	0.34	0.17	21.07	15.36	0.0022	0.8635	0.7390	1.0034
SiK	0.26	0.12	18.85	19.09	0.0019	0.8821	0.8489	1.0052
K K	0.29	0.10	13.95	29.54	0.0025	0.8168	1.0277	1.0366

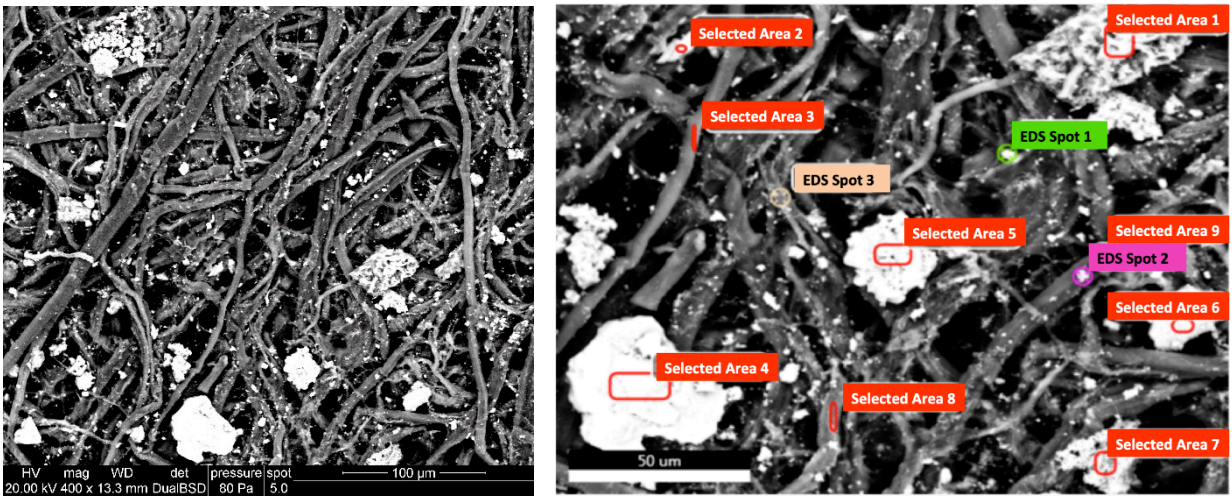

Padua incunabulum, surface. SEM image (left) and investigated areas (right).

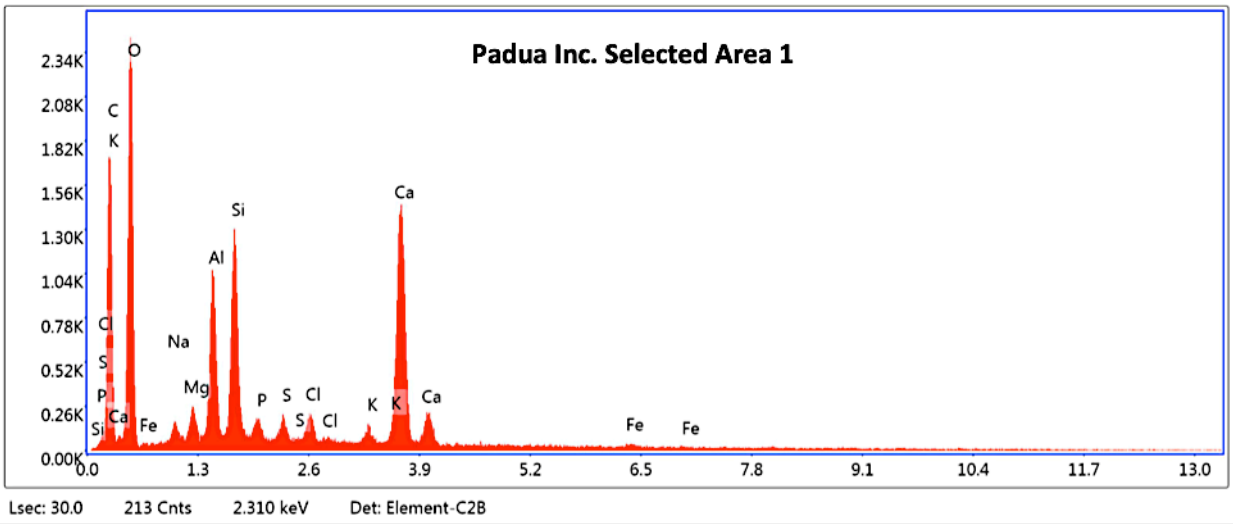

Selected Area 1 - Det 1 eZAF Smart Quant Results

Element	Weight %	Atomic %	Net Int.	Error %	Kratio	Z	A	F
C K	27.48	39.62	340.42	9.61	0.0821	1.0695	0.2796	1.0000
O K	40.10	43.40	541.63	10.12	0.0756	1.0241	0.1841	1.0000
NaK	1.01	0.76	27.81	16.61	0.0039	0.9306	0.4082	1.0018
MgK	1.18	0.84	55.52	10.22	0.0064	0.9466	0.5693	1.0032
AlK	5.13	3.29	286.89	5.59	0.0331	0.9116	0.7042	1.0045
SiK	5.75	3.54	360.13	4.86	0.0415	0.9317	0.7715	1.0053
P K	0.60	0.34	30.60	18.09	0.0044	0.8950	0.8118	1.0088
S K	0.71	0.38	38.15	14.26	0.0057	0.9126	0.8771	1.0134
ClK	1.15	0.56	57.10	11.19	0.0094	0.8682	0.9225	1.0198
K K	0.67	0.30	29.13	16.57	0.0059	0.8640	0.9753	1.0433
CaK	15.76	6.81	567.58	2.42	0.1383	0.8798	0.9885	1.0087
FeK	0.46	0.14	8.94	40.04	0.0038	0.7845	0.9984	1.0567

Selected Area 2 - Det 1

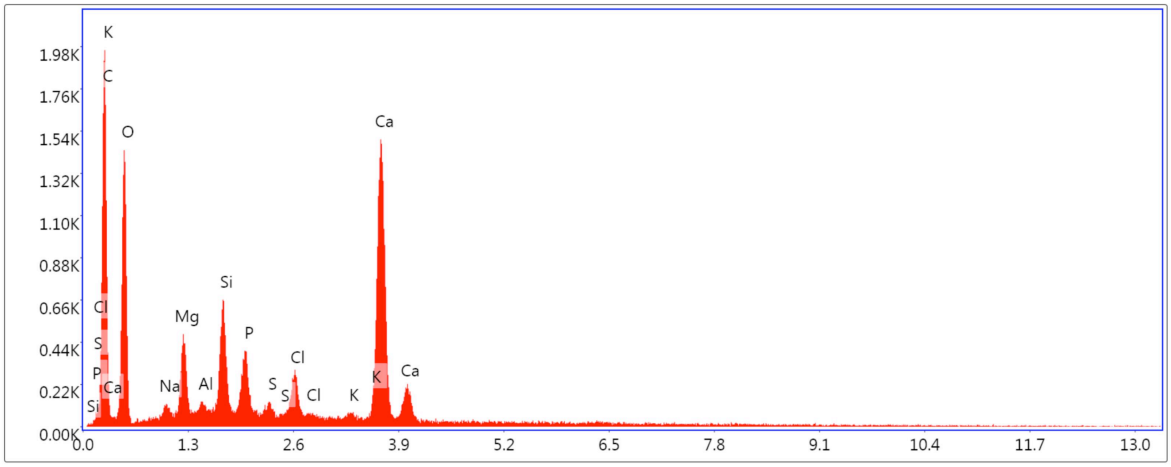

Selected Area 2 - Det 1 eZAF Smart Quant Results

Element	Weight %	Atomic %	Net Int.	Error %	Kratio	Z	A	F
C K	33.83	47.88	388.19	9.37	0.1123	1.0663	0.3113	1.0000
O K	34.24	36.38	328.55	10.69	0.0550	1.0210	0.1572	1.0000
NaK	0.80	0.59	18.47	18.37	0.0031	0.9278	0.4129	1.0017
MgK	2.95	2.07	117.10	8.04	0.0161	0.9438	0.5762	1.0028
AlK	0.39	0.24	17.73	20.75	0.0024	0.9089	0.6930	1.0050
SiK	3.27	1.98	178.16	5.52	0.0246	0.9290	0.8037	1.0070
P K	2.44	1.34	109.14	7.60	0.0189	0.8923	0.8573	1.0101
S K	0.43	0.23	19.63	20.64	0.0035	0.9099	0.9004	1.0156
ClK	1.97	0.94	82.88	8.76	0.0164	0.8657	0.9413	1.0218
K K	0.36	0.16	13.17	25.07	0.0032	0.8615	0.9820	1.0490
CaK	19.31	8.19	581.12	2.28	0.1697	0.8773	0.9947	1.0070

Selected Area 3 - Det 1

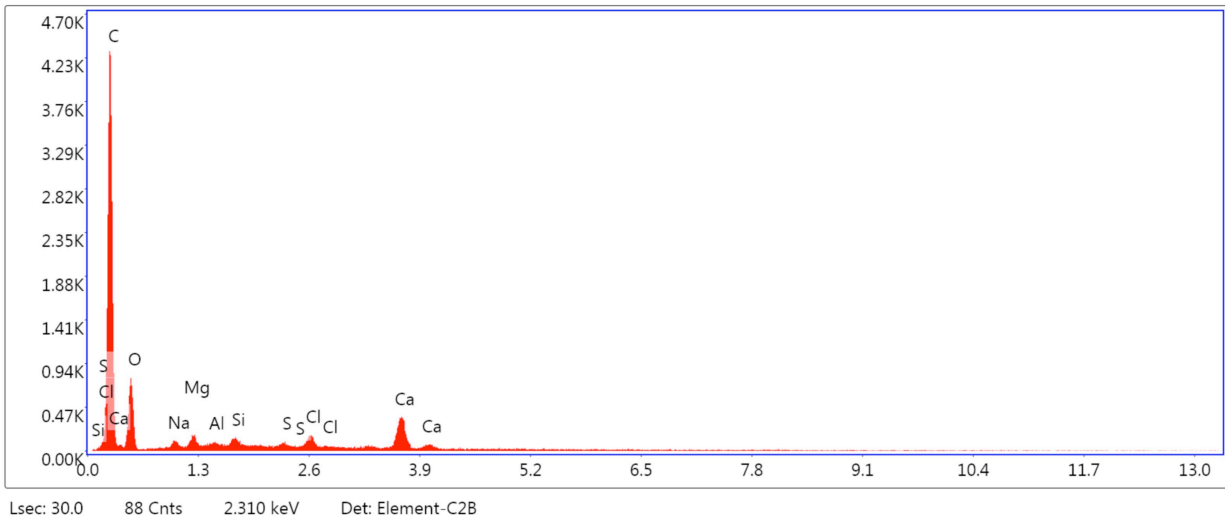

Selected Area 3 - Det 1 **eZAF Smart Quant Results**

Element	Weight %	Atomic %	Net Int.	Error %	Kratio	Z	A	F
C K	66.18	75.75	929.66	6.33	0.3597	1.0260	0.5297	1.0000
O K	23.10	19.85	148.28	13.27	0.0332	0.9808	0.1464	1.0000
NaK	0.98	0.58	18.57	17.31	0.0041	0.8898	0.4746	1.0016
MgK	1.00	0.57	31.70	12.37	0.0058	0.9048	0.6409	1.0027
AlK	0.34	0.17	12.29	27.75	0.0023	0.8710	0.7707	1.0048
SiK	0.67	0.33	28.21	13.24	0.0052	0.8899	0.8686	1.0073
S K	0.36	0.15	12.77	21.47	0.0031	0.8712	0.9731	1.0182
ClK	1.29	0.50	41.20	9.27	0.0109	0.8287	0.9965	1.0237
CaK	6.09	2.09	136.15	4.86	0.0532	0.8394	1.0212	1.0188

Selected Area 4 - Det 1

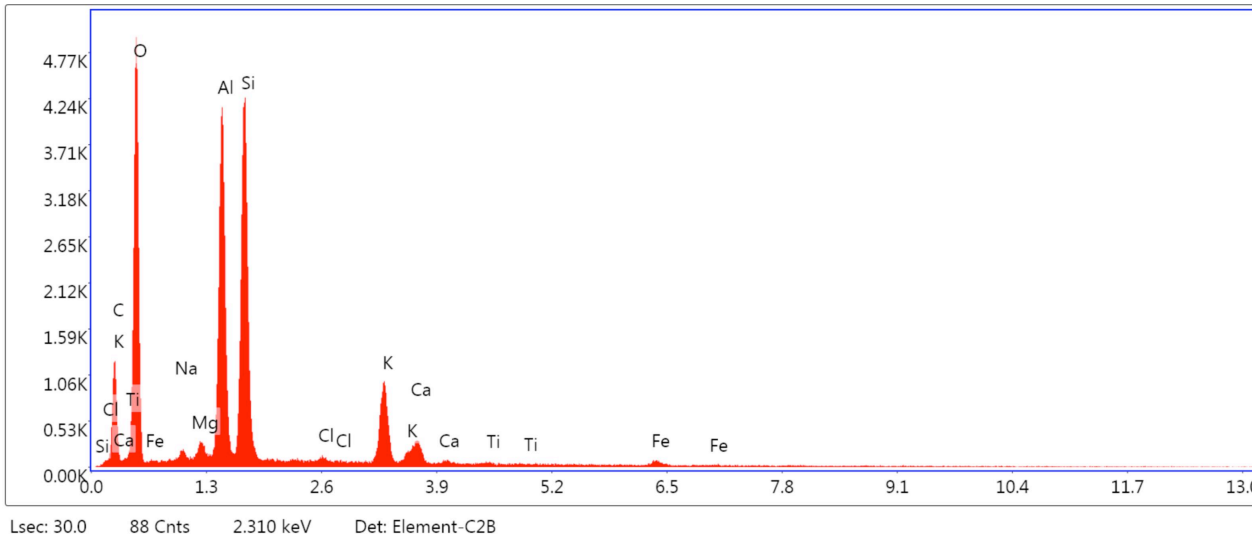

Selected Area 4 - Det 1 eZAF Smart Quant Results

Element	Weight %	Atomic %	Net Int.	Error %	Kratio	Z	A	F
C K	16.90	25.90	187.85	11.09	0.0337	1.0824	0.1842	1.0000
O K	42.37	48.76	1080.47	8.97	0.1121	1.0365	0.2552	1.0000
NaK	0.62	0.50	25.10	18.89	0.0026	0.9419	0.4425	1.0026
MgK	0.88	0.67	60.42	9.68	0.0052	0.9581	0.6070	1.0049
AlK	14.16	9.66	1133.75	4.25	0.0971	0.9227	0.7395	1.0049
SiK	15.46	10.14	1232.64	4.43	0.1056	0.9430	0.7222	1.0028
ClK	0.34	0.18	21.38	22.44	0.0026	0.8787	0.8607	1.0131
K K	6.06	2.86	335.52	3.59	0.0507	0.8744	0.9438	1.0142
CaK	2.11	0.97	99.20	6.90	0.0180	0.8904	0.9445	1.0133
TiK	0.21	0.08	9.01	42.58	0.0017	0.8071	0.9744	1.0274
FeK	0.88	0.29	23.96	21.01	0.0075	0.7938	1.0020	1.0698

Selected Area 5 - Det 1

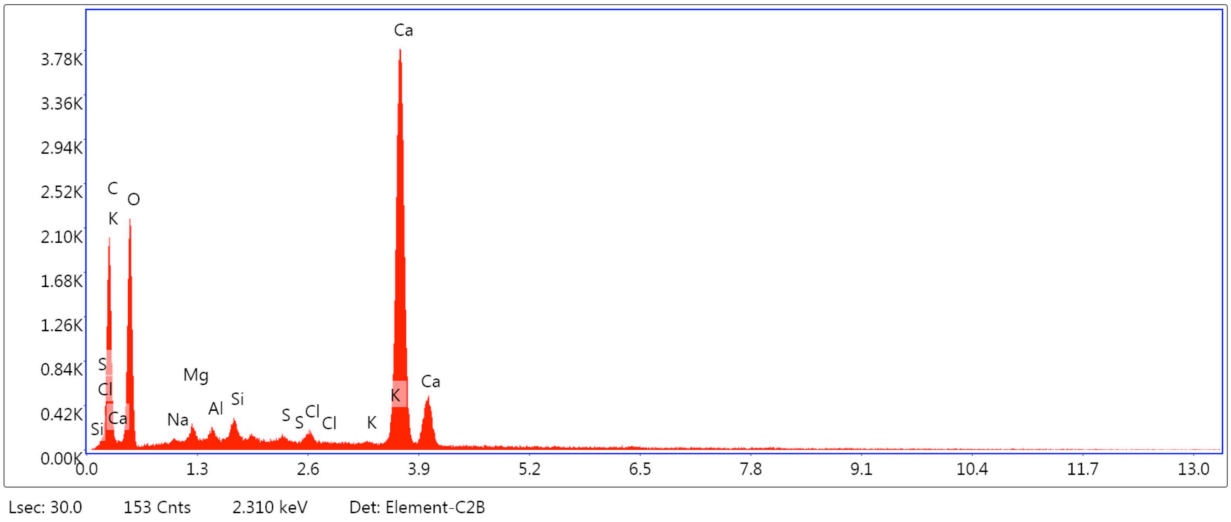

Selected Area 5 - Det 1e ZAF Smart Quant Results

Element	Weight %	Atomic %	Net Int.	Error %	Kratio	Z	A	F
C K	17.75	28.74	370.46	7.98	0.0838	1.0886	0.4336	1.0000
O K	42.04	51.10	474.78	10.55	0.0621	1.0435	0.1416	1.0000
NaK	0.20	0.17	5.29	73.10	0.0007	0.9492	0.3551	1.0013
MgK	0.72	0.58	33.51	14.15	0.0036	0.9658	0.5165	1.0025
AlK	0.45	0.32	25.70	15.08	0.0028	0.9303	0.6597	1.0045
SiK	0.80	0.56	55.16	11.32	0.0060	0.9510	0.7754	1.0073
S K	0.27	0.16	16.76	21.26	0.0024	0.9319	0.9173	1.0191
ClK	0.65	0.36	36.59	13.09	0.0057	0.8867	0.9552	1.0293
K K	0.11	0.05	5.34	62.99	0.0010	0.8827	0.9951	1.0659
CaK	37.01	17.96	1470.89	1.75	0.3359	0.8990	1.0055	1.0037

Selected Area 6 - Det 1

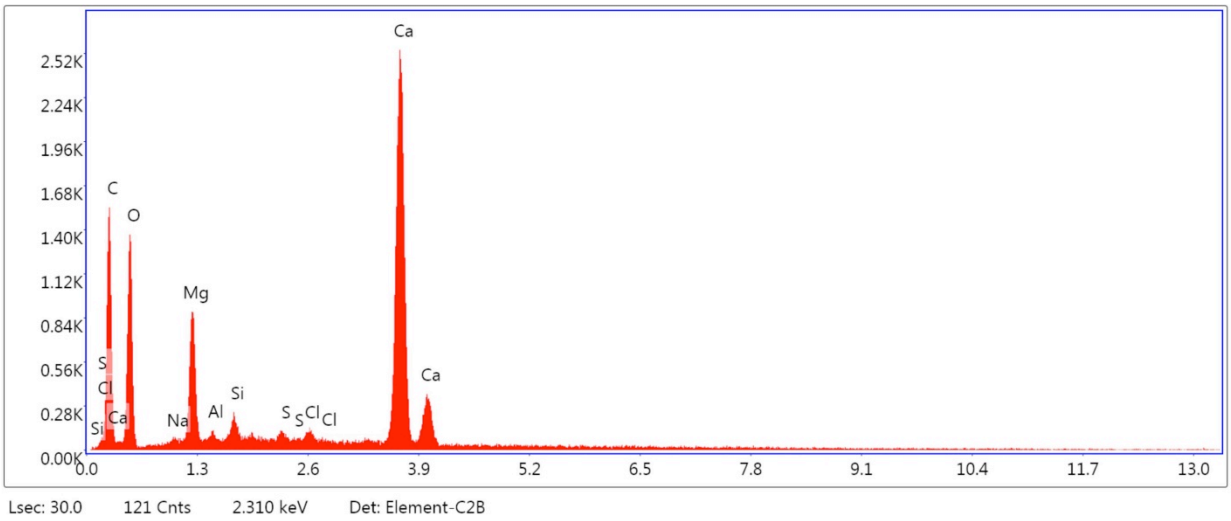

Selected Area 6 - Det 1 eZAF Smart Quant Results

Element	Weight %	Atomic %	Net Int.	Error %	Kratio	Z	A	F
C K	22.16	35.17	300.05	8.41	0.0919	1.0858	0.3821	1.0000
O K	35.50	42.28	296.23	10.82	0.0525	1.0406	0.1421	1.0000
NaK	0.38	0.32	7.86	35.87	0.0014	0.9464	0.3820	1.0016
MgK	6.29	4.93	226.81	7.17	0.0331	0.9629	0.5449	1.0022
AlK	0.30	0.21	12.33	27.92	0.0018	0.9276	0.6364	1.0041
SiK	0.88	0.60	43.30	11.06	0.0063	0.9482	0.7556	1.0067
S K	0.48	0.29	21.49	20.01	0.0041	0.9290	0.9048	1.0176
ClK	0.63	0.34	25.64	18.26	0.0054	0.8839	0.9444	1.0271
CaK	33.38	15.87	972.37	1.88	0.3007	0.8961	1.0014	1.0042

Selected Area 7 - Det 1

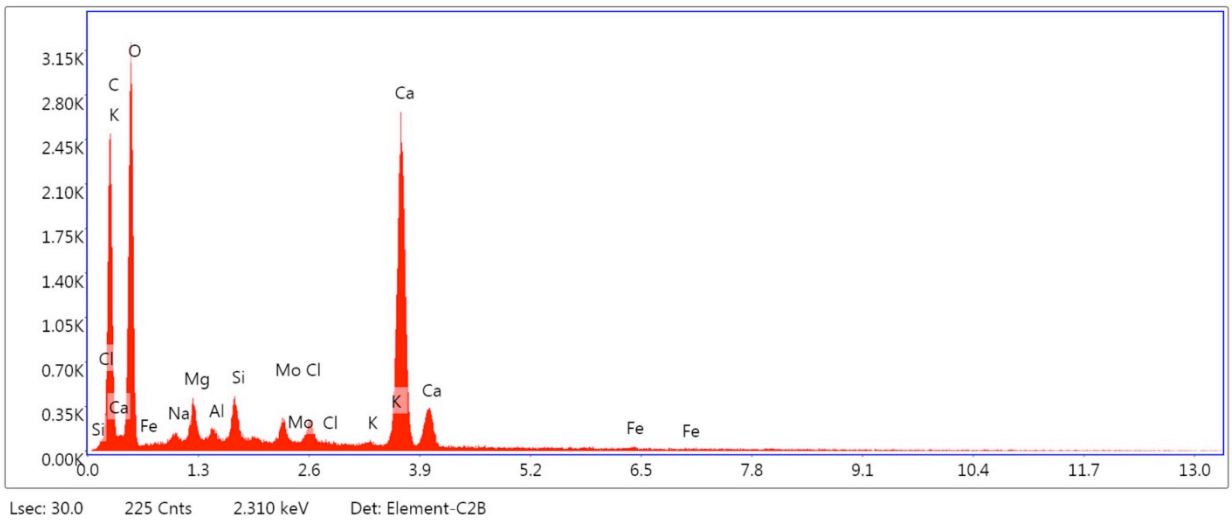

Selected Area 7 - Det 1e ZAF Smart Quant Results

Element	Weight %	Atomic %	Net Int.	Error %	Kratio	Z	A	F
C K	23.84	35.10	490.22	8.23	0.1031	1.0730	0.4029	1.0000
O K	46.11	50.96	669.36	10.03	0.0814	1.0278	0.1718	1.0000
NaK	0.64	0.50	18.40	20.73	0.0022	0.9343	0.3696	1.0014
MgK	1.71	1.24	86.24	8.82	0.0086	0.9505	0.5304	1.0024
AlK	0.39	0.26	23.91	15.89	0.0024	0.9155	0.6644	1.0043
SiK	1.27	0.80	92.87	7.50	0.0093	0.9357	0.7802	1.0068
MoL	1.45	0.27	47.59	13.72	0.0114	0.7158	1.0894	1.0061
ClK	0.98	0.49	57.96	10.74	0.0083	0.8721	0.9500	1.0230
K K	0.13	0.06	6.83	62.54	0.0012	0.8681	0.9880	1.0524
CaK	23.23	10.25	973.46	1.92	0.2066	0.8840	1.0001	1.0064
FeK	0.23	0.07	5.21	63.43	0.0019	0.7885	0.9933	1.0478

EDS Spot 1 - Det 1

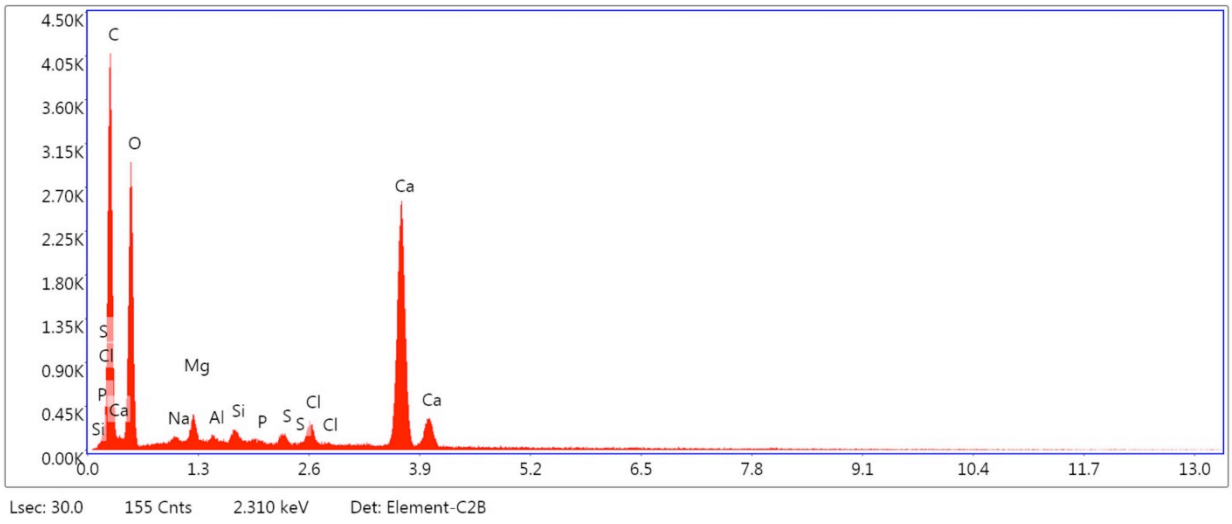

EDS Spot 1 - Det 1 eZAF Smart Quant Results

Element	Weight %	Atomic %	Net Int.	Error %	Kratio	Z	A	F
C K	33.57	46.14	821.35	7.27	0.1573	1.0594	0.4421	1.0000
O K	41.49	42.82	619.94	10.32	0.0687	1.0142	0.1631	1.0000
NaK	0.58	0.42	18.78	19.52	0.0021	0.9214	0.3871	1.0014
MgK	1.29	0.88	73.63	9.46	0.0067	0.9372	0.5514	1.0024
AlK	0.20	0.12	13.32	27.48	0.0012	0.9026	0.6882	1.0044
SiK	0.45	0.27	37.06	12.41	0.0034	0.9224	0.8025	1.0072
P K	0.11	0.06	7.65	69.29	0.0009	0.8860	0.8814	1.0121
S K	0.43	0.22	31.00	13.43	0.0037	0.9035	0.9362	1.0185
ClK	1.12	0.52	73.10	7.85	0.0096	0.8595	0.9687	1.0269
CaK	20.76	8.55	952.23	2.08	0.1840	0.8710	1.0104	1.0072

EDS Spot 2 - Det 1

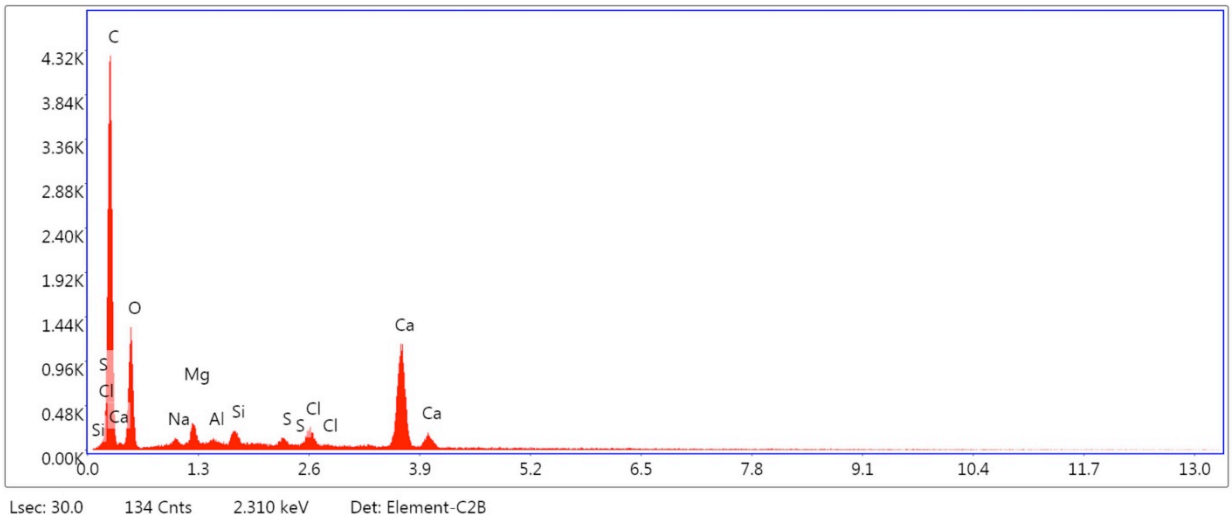

EDS Spot 2 - Det 1 e ZAF Smart Quant Results

Element	Weight %	Atomic %	Net Int.	Error %	Kratio	Z	A	F
C K	52.04	64.94	887.97	6.95	0.2525	1.0424	0.4655	1.0000
O K	28.93	27.10	258.82	11.23	0.0426	0.9973	0.1476	1.0000
NaK	0.74	0.48	17.82	17.46	0.0029	0.9055	0.4348	1.0015
MgK	1.43	0.88	58.76	10.05	0.0080	0.9209	0.6016	1.0026
AlK	0.28	0.15	13.25	26.88	0.0018	0.8867	0.7315	1.0047
SiK	0.78	0.42	43.77	10.30	0.0059	0.9061	0.8374	1.0074
S K	0.48	0.22	23.35	15.59	0.0041	0.8873	0.9546	1.0186
ClK	1.48	0.63	64.88	7.20	0.0126	0.8440	0.9820	1.0255
CaK	13.84	5.17	422.47	2.77	0.1213	0.8551	1.0146	1.0102

Selected Area 9 - Det 1

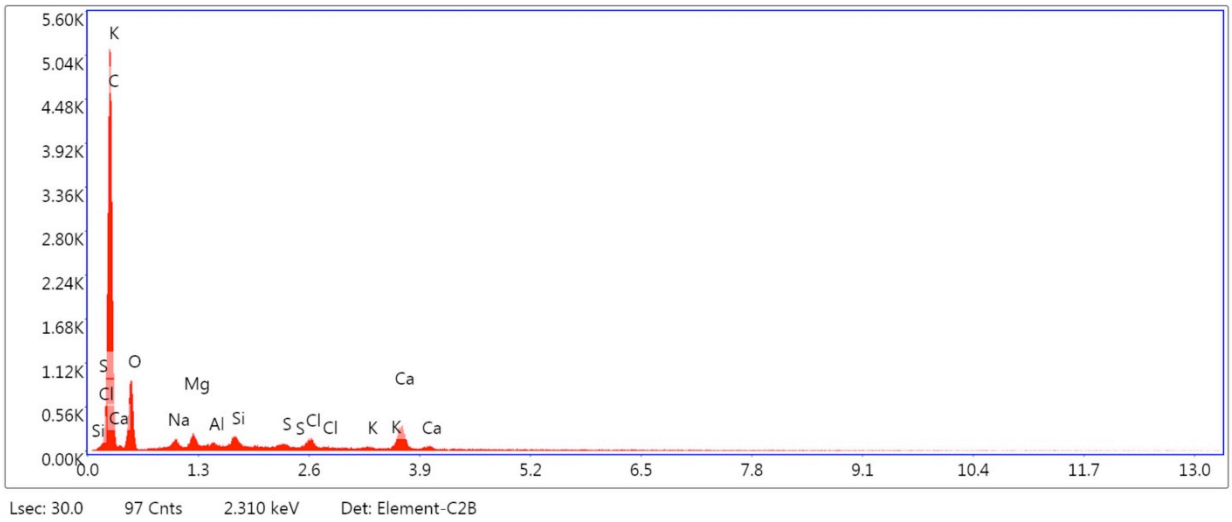

Selected Area 9 - Det 1 eZAF Smart Quant Results

Element	Weight %	Atomic %	Net Int.	Error %	Kratio	Z	A	F
C K	67.29	76.18	1099.57	6.46	0.3669	1.0238	0.5324	1.0000
O K	23.33	19.82	177.48	12.47	0.0343	0.9785	0.1501	1.0000
NaK	1.24	0.73	27.55	14.54	0.0053	0.8876	0.4806	1.0016
MgK	1.10	0.62	40.50	10.63	0.0064	0.9025	0.6444	1.0027
AlK	0.30	0.15	12.77	26.58	0.0020	0.8688	0.7726	1.0047
SiK	0.84	0.41	40.94	10.13	0.0065	0.8876	0.8705	1.0070
S K	0.42	0.18	17.27	17.18	0.0036	0.8689	0.9730	1.0172
ClK	1.10	0.42	40.44	9.82	0.0092	0.8265	0.9961	1.0224
K K	0.17	0.06	5.17	64.60	0.0015	0.8222	1.0160	1.0478
CaK	4.22	1.43	109.56	6.06	0.0369	0.8371	1.0210	1.0226

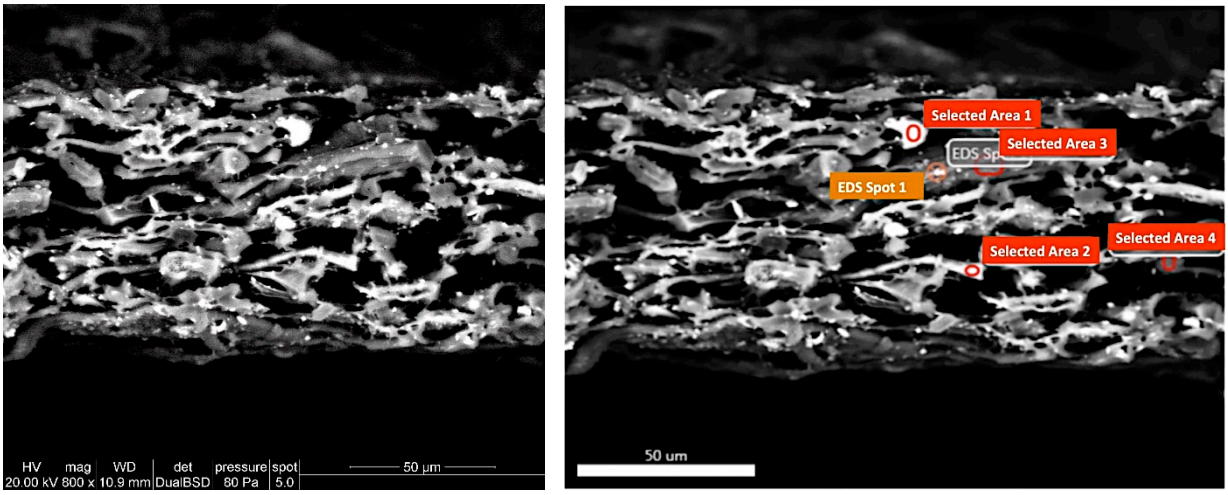

Padua incunabulum, cross section. SEM image (left) and investigated areas (right).

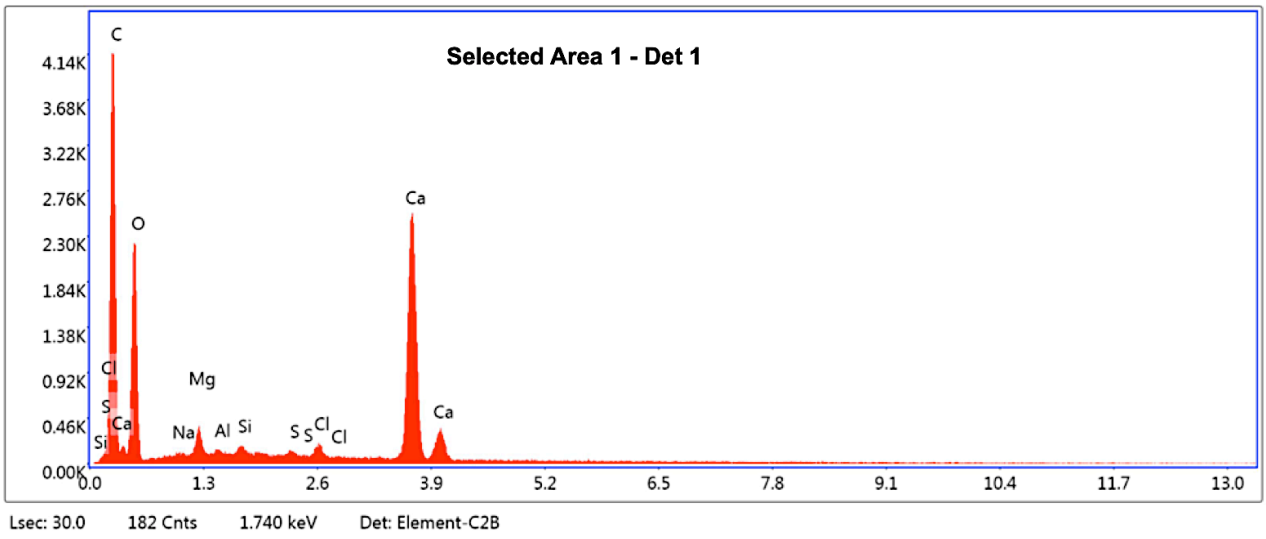

Selected Area 1 - Det 1 **eZAF Smart Quant Results**

Element	Weight %	Atomic %	Net Int.	Error %	Kratio	Z	A	F
C K	36.75	49.77	850.73	6.99	0.1821	1.0567	0.4688	1.0000
O K	39.22	39.88	482.50	10.66	0.0570	1.0115	0.1435	1.0000
NaK	0.34	0.24	9.77	35.78	0.0011	0.9190	0.3564	1.0014
MgK	1.32	0.88	69.25	10.50	0.0064	0.9347	0.5216	1.0024
AlK	0.15	0.09	9.73	41.68	0.0009	0.9002	0.6629	1.0044
SiK	0.29	0.17	23.00	20.26	0.0021	0.9200	0.7851	1.0073
S K	0.25	0.12	17.57	23.08	0.0021	0.9010	0.9332	1.0189
ClK	0.70	0.32	45.60	11.08	0.0060	0.8571	0.9699	1.0284
CaK	20.99	8.52	969.43	2.12	0.1866	0.8686	1.0158	1.0072

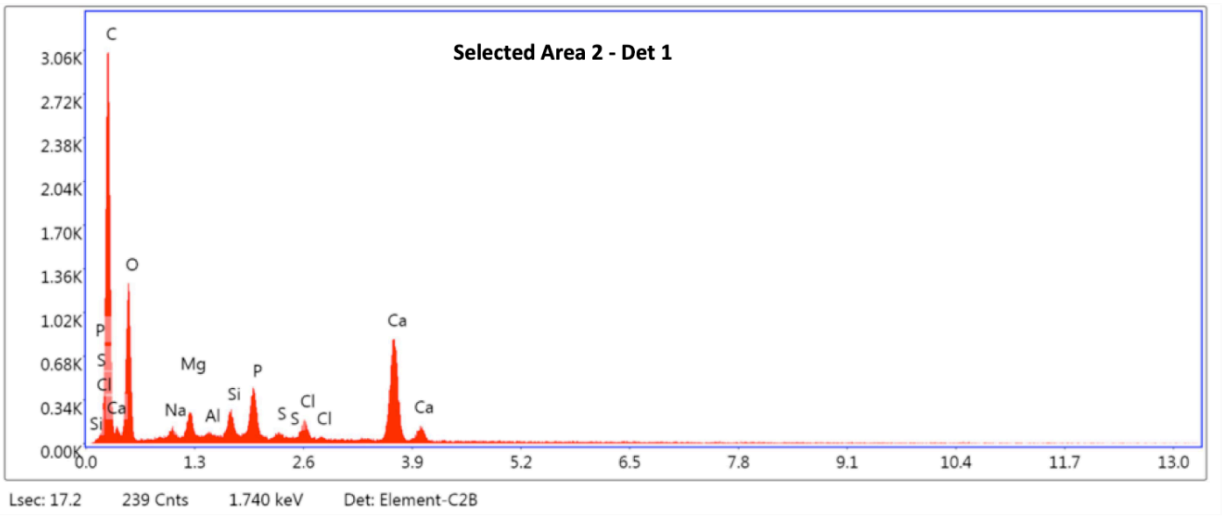

Selected Area 2 - Det 1 **eZAF Smart Quant Results**

Element	Weight %	Atomic %	Net Int.	Error %	Kratio	Z	A	F
C K	50.77	63.13	1086.24	7.93	0.2063	1.0419	0.3898	1.0000
O K	30.96	28.90	427.56	11.19	0.0448	0.9966	0.1451	1.0000
NaK	0.92	0.60	33.46	17.52	0.0034	0.9048	0.4038	1.0016
MgK	1.41	0.87	90.02	10.53	0.0074	0.9201	0.5702	1.0028
AlK	0.14	0.08	10.63	62.33	0.0009	0.8860	0.7065	1.0051
SiK	1.07	0.57	97.61	9.04	0.0080	0.9053	0.8222	1.0078
P K	2.74	1.32	210.09	5.65	0.0215	0.8695	0.8934	1.0102
S K	0.24	0.11	18.93	32.48	0.0020	0.8865	0.9262	1.0157
ClK	1.14	0.48	81.78	10.87	0.0095	0.8432	0.9641	1.0222
CaK	10.61	3.96	543.72	2.98	0.0929	0.8543	1.0116	1.0121

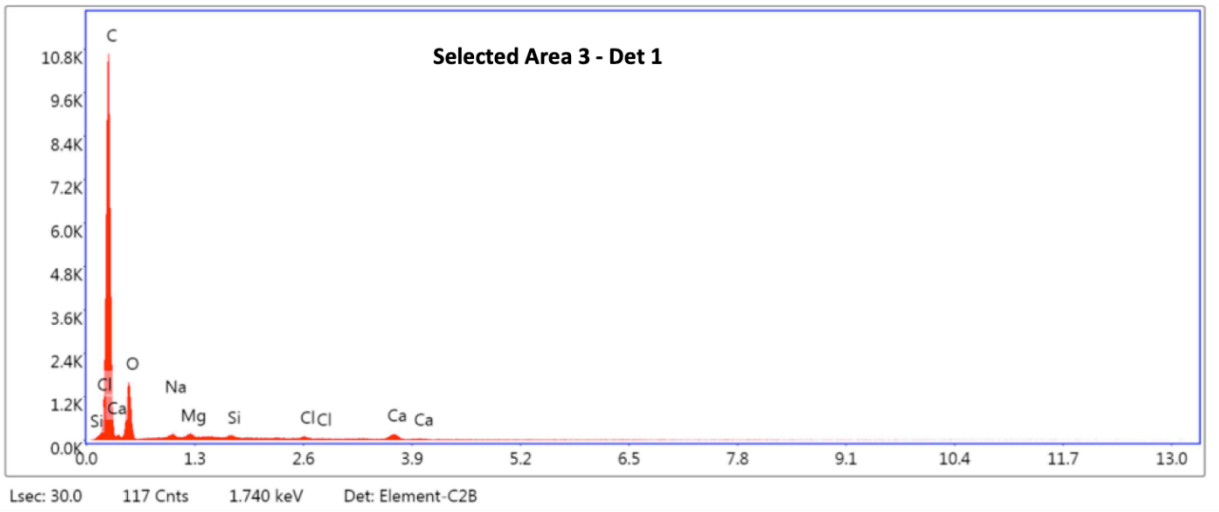

Selected Area 3 - Det 1 **eZAF Smart Quant Results**

Element	Weight %	Atomic %	Net Int.	Error %	Kratio	Z	A	F
C K	72.01	78.31	2257.32	4.64	0.4902	1.0151	0.6707	1.0000
O K	24.91	20.34	287.28	12.33	0.0344	0.9698	0.1424	1.0000
NaK	0.85	0.48	29.23	14.73	0.0034	0.8793	0.4472	1.0013
MgK	0.48	0.26	28.54	14.00	0.0027	0.8940	0.6194	1.0022
SiK	0.20	0.09	16.45	20.31	0.0015	0.8791	0.8718	1.0063
ClK	0.28	0.10	17.65	20.63	0.0023	0.8183	1.0106	1.0231
CaK	1.27	0.41	57.81	9.60	0.0113	0.8287	1.0341	1.0412

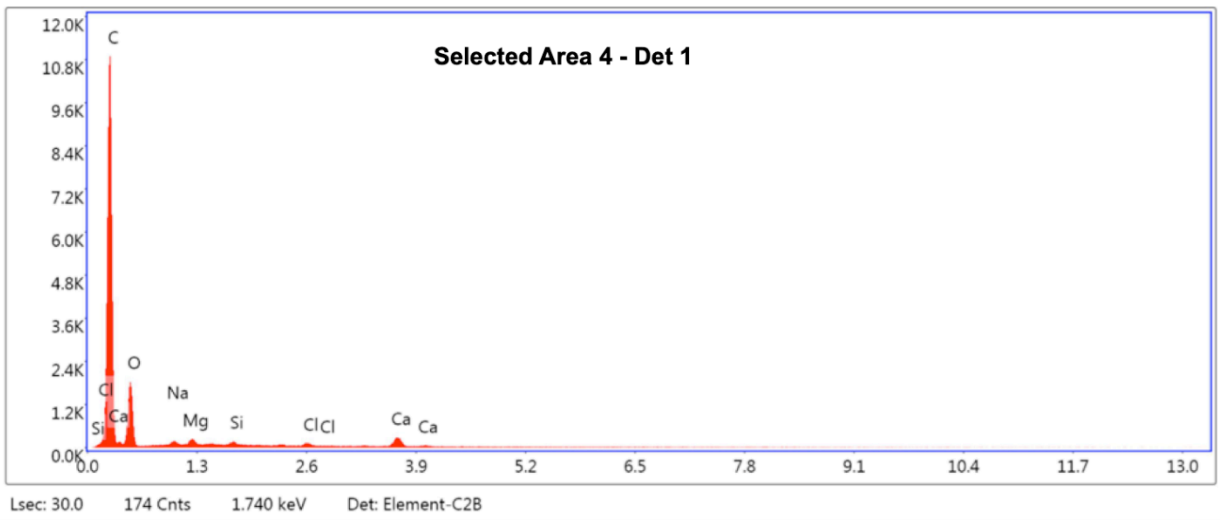

Selected Area 4 - Det 1 eZAF Smart Quant Results

Element	Weight %	Atomic %	Net Int.	Error %	Kratio	Z	A	F
C K	70.15	77.04	2334.32	4.95	0.4566	1.0171	0.6399	1.0000
O K	25.63	21.13	331.19	12.40	0.0357	0.9717	0.1434	1.0000
NaK	0.95	0.54	35.90	12.95	0.0037	0.8812	0.4434	1.0014
MgK	0.70	0.38	45.61	11.54	0.0039	0.8959	0.6142	1.0023
SiK	0.30	0.14	27.34	14.70	0.0023	0.8810	0.8655	1.0064
ClK	0.38	0.14	26.71	14.39	0.0032	0.8202	1.0074	1.0234
CaK	1.89	0.62	95.36	6.47	0.0168	0.8306	1.0325	1.0358

Materials and methods

1. Papers

1.2 Historical papers

The leaf from the Médiatheque L'Apostrophe in Chartres involved in physico-chemical investigations belongs to the manuscript Chartres BM ms 1047, *Histoire de l'ancienne cité des Carnute,* by Honoré-Félix-André Lejeune, 1830s.

The incunabulum held in the Episcopal Seminary Library of Padua is *Lectio super secundo Decretalium. Pars prima*, by Nicolaus de Tudeschis (Panormitanus), printed by Bernardino Stagnino in Venice, 1487.

The two leaves treated in situ at the Médiatheque L'Apostrophe in Chartres are from the manuscript Chartres BM ms. 1171, *Catalogue de la bibliothèque du chapitre de Chartres*, 1752.

The manuscript treated in Padua is an account book dated to the 19th century from the antique market.

1.3 Paper samples

Paper samples were obtained from a paper specifically produced by the Ruscombe Paper Mill, a traditional mill established in Margaux (http://ruscombepaper.com). This paper reproduces the basic features of the historical (13th -19th century) paper manufacture as it is made from rags, composed of hemp (70%) and linen fibres (30%), buffered with calcium carbonate, grammage 100 g/m^2. The sheets supplied by Ruscombe Paper Mill were 50 x 70 cm^2.

1.3.1 Sample name

Samples were prepared in several size (4x10 cm^2, 5x10 cm^2, 6x10 cm^2, 6x15 cm^2) according to the test they were prepared for. Samples are named UP (unsized paper) or SP (sized paper) followed by a number, which indicates the progression in the sample production.

Each UP and SP sample is cut in several substrips (1x10 cm^2 or 1x15 cm^2) according to the text, each strip treated with different products (Fig. 1) ; one strip per sample was always kept untreated as control.

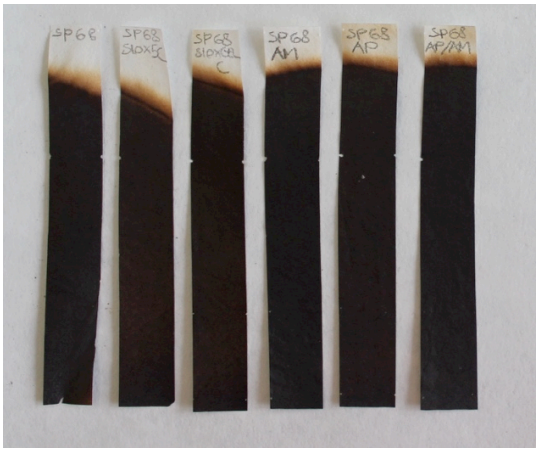

Figure 1. Sample SP68 prepared cut in substrips for testing.

Sample set was intended as the set of samples involved in the same test, i.e. sample set SP68-70 consisted of the sample SP68, SP69 and SP70.

2. Chemical products

2.1 Nanocellulose

Microfibrillated cellulose Exilva P 01-L was supplied by Borregaard in a 2% gel-like aqueous dispersion, surface pH 6 measured in laboratory; fibrous width 10-100 nm, length 0,5-50 microns.
Nanocrystalline cellulose was supplied by Melodea Ltd in a 3% aqueous suspension; according to the producer, pH 5.1, also verified by pH surface measure in laboratory; crystals width 5-20 nm, length 150-400 nm.

Films of nanocellulose (Chapter 4, Fig. 4.4 and 4.6) were prepared by disperding 0.2% w/v of MFC and 0.3% w/v of NCC in deionized water and stirring 5 minutes at 10000 rpm. 20 ml of both dilutions were separately poured in Petri dishes until complete casting evaporation.

Nanocellulose dispersions in water, ethyl alcohol and isopropyl alcohol were obtained by weighing the wanted quantity of MFC and of NCC and bringing to volume with the solvent.

Uniform dispersions were achieved by stirring for 5 minutes at 10 000 rpm.

2.2. Polysiloxanes

2.2.1 TEOS based alkoxysilanes (AS)

TEOS-based polysiloxane formulations were supplied by Siltea s.r.l. (Padua), composed of tetraethylorthosilicate functionalized with other silica precursors: octyltriethoxysilane, OTES, was in the formulations SIOX-5TO and SN1, while diethoxydimethylsilane, DDMES, was in SIOX-5S, SN1/DDMES and SIOX-5TD. All the formulations were in water/isopropyl alcohol mixture (water 52%/2-isopropyl alcohol 43%). Precursors were present in the formulations in different amounts: SIOX-5TO (5%), SIOX-5TD (5%), SN1 (9%), SN1d (9%), SIOX-5 S (30%).
All the products were ready-to-use.

2.2.2 Aminoalkylalkoxysilanes (AAAS)

Aminoalkylalkoxysilanes 3-aminopropylmethyldiethoxysilane (AMDES, 98%) and 3-aminopropyltriethoxysilane (APTES, 97%) were supplied commercially by ABCR (Gelest) and tested separately and in the mixture APTES/AMDES 1:1.
Aminoalkylalkoxysilanes were applied both pure and in a 5% v/v dilution in isopropanol

2.3 Other chemical products

Ethyl alcohol (96%) supplied by Sigma Aldrich

Isopropyl alcohol (98%) supplied by Sigma Aldrich

Sodium hydroxide solution (0.1 M) supplied by Sigma Aldrich

Sulfuric acid (99.99%), supplied by Sigma Aldrich

Nanorestore paper supplied by CSGI-Consorzio per lo sviluppo dei sistemi a grande interfase, Firenze. The formulation consists of Calcium hydroxide nanoparticles dispersed in 2-propanol (3 g/L)

3. Tools

Airbrush Belkits BEL-AIR 005, compressor piston type Typhoon by the Kaiser Trading Srl.

4. Sample morphological analyses

4.1 Optical microscope examination

An upright reflected-light Zeiss Axiotech HAL 100 microscope, equipped with camera, was employed using different techniques (reflected-light brightfield, reflected-light darkfield and reflected-light interference contrast).

4.2 Scanning electronic microscopy (SEM/EDS) investigation

FEI Quanta 200 microscope equipped with a tungsten source, with an associated EDAX energy dispersive spectroscopy (EDS) system and under low vacuum conditions, as required to reduce electron beam scatter; it was not necessary to treat samples by surface coating with a conductive material (Fig. 2)

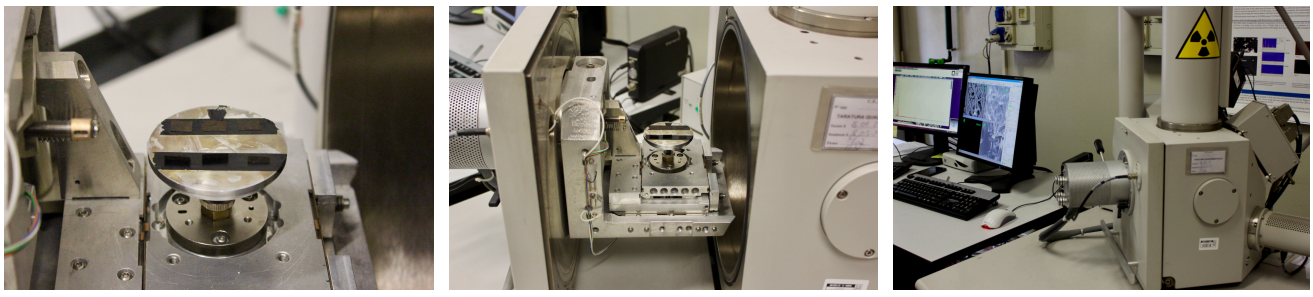

Figure 2. FEI Quanta 200 microscope. Samples preparation (left); entering the SEM (middle); collecting data (right).

Qualitative interpretation of EDS spectra and semi-quantitative estimation of oxide weight percentages were performed using the dedicated EDAX TEAM software, revealing the elemental composition of – and by inference the chemical compounds in – the samples. There is a direct relationship between the amount of X-rays emitted by each element present in a sample and the

concentration of that element in the sample, so that EDS allows one to convert measures in spectra and to assess the concentrations of the different chemicals present in the analyzed material.

5. Physico-chemical analyses

5.1 Infrared spectroscopic analyses (ATR-FTIR)

ATR spettrofotometer FT-IR Nexus 870 Nicolet, equipped with an ATR module with ZnSe crystal, was employed; 64 scans were adopted to analyse points with different degree of burning (Fig. 3)

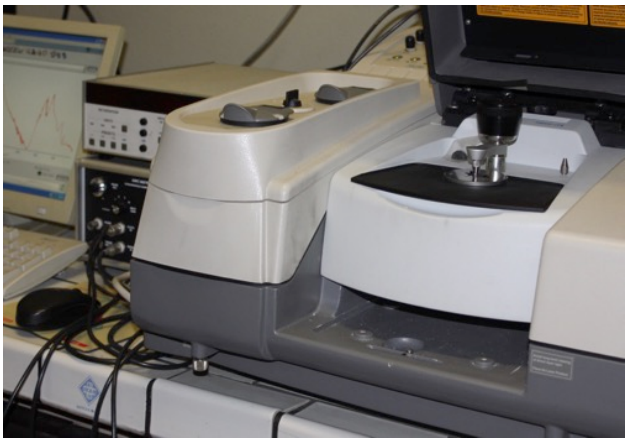

Figure 3. FT-IR Nexus 870 Nicolet, equipped with an ATR module with ZnSe crystal.

5.2 UV-VIS spectroscopic analyses (FORS)

An Ocean Optics HR2000+ UV-visible Spectrophotometer, equipped with a Reflection Probe RS200-7 to carry the light to the samples was used. The probe configuration was set at 90° with respect to the sample surface.

5.3 Raman spectroscopic analysis

A Renishaw inVia microRaman equipped with a Leica DM-LM microscope was employed, using a 10x objective, 0,5-1% laser power, a 10s scan time and line at 785 nm.

The technique was not informative for burnt paper due to the excessive fluorescence, which is a typical response of degraded paper and covers the Raman signals.

The influence of the SERS (Surface-Enhanced Raman Scattering) with the deposition of gold nanoparticles on the paper material to amplify the signal, provided just a little improvement: broad and weak signals of carbon black were observed in the burnt areas.

5.4 x-ray Powder Diffraction (XRPD)

Samples were mounted without any kind of preparation on zero-background Si sample holders, and data were collected using a Bragg–Brentano θ-θ diffractometer (PANalytical X'Pert PRO, Co Kα radiation, 40 kV and 40 mA) equipped with a real-time multiple strip (RTMS) detector (X'Celerator by Panalytical). Data acquisition was performed by operating a continuous scan in the range 3-85 [°2θ], with a virtual step scan of 0.02 [°2θ]. Diffraction patterns were interpreted using the X'Pert HighScore Plus 3.0 software by PANalytical, qualitatively reconstructing mineral profiles of the compounds by comparison with PDF databases from the International Centre for Diffraction Data (ICDD).

5.5 Dynamic bending stiffness

The determination of rigidity of a paper sample was made by resonance with a rigidimetre Adamel Lhomargy.

The measuring principle of the dynamic flexural rigidity, under normalized conditions, is calculated using the vibrating resonance length of a sample attached to an extremity (Fig. 4). The equipment makes the paper strip (sample) vibrate at a stable frequency (dynamic bending) and the rigidity is determined through the following formula, with the free length of the sample when it reaches its greatest amplitude of vibration and with the grammage of the paper tested:

$$R\left(\frac{N}{m}\right) = 3.19 \cdot F \cdot N^2 \cdot L^4$$

in which *F* is the sample mass per surface unit, *N* is the vibration frequency set to 25 Hz, *L* is the free length of the sample at resonance (m), *R* is the stiffness of the test material per unit width.

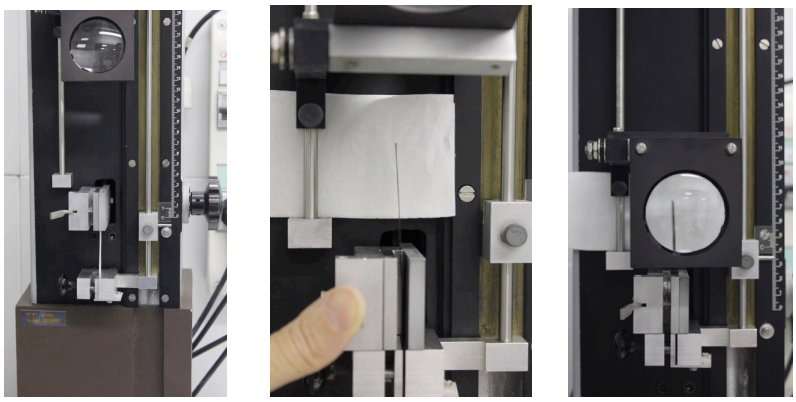

Figure 4. Rigidimetre (left), sample positioning (centre), sample in vibration (right).

Acknowledgements

This doctoral research was developed within the framework of the project denominated CREMIB - Conservation et REstauration des Manuscrits et des Incunables Brûlés, supported by the Domain d'intérêt majeur (DIM) Matériaux anciens et patrimoniaux of the Île-de-France region. I am especially grateful to DIM for bolstering and financing this work and, above all, for the development of research projects that enhance knowledge, preservation and conservation strategies aimed at safeguarding our precious cultural heritage.

I would particularly like to thank Nathalie Marlin and Giovanna Poggi for having served as rapporteurs of this work, and likewise Pierre Chastang for being part of my jury as examinateur.

To François Bougard, co-supervisor of this work, I extend immense gratitude for being the chief driver of the project, in tandem with Flavia De Rubeis. I am immeasurably grateful to Anne-Laurence Dupont and Alfonso Zoleo, my thesis supervisors, for having guided me on the path taken by this research, and for favouring me with the great competence and dedication that they invest in all their work, not to mention their unstinting friendliness.

I also wish to express my thanks to them and to François for having agreed, from the outset, on the relevance of involving historical papers in this research, so as to accelerate the development of a conservation methodology suitable for application to our written heritage. Given that laboratory samples can never fully replicate the complexity of real historical materials in their natural state, I am expecially grateful to Clotilde Périgault, director of the Médiathèque L'Apostrophe in Chartres, for having participated in the research, thereby enabling me to test some historical fire-damaged papers drawn from the library's collections, and to Myriam Vallot, vice-director, Michele Neveau, head of the manuscripts and the heritage collection, and Caroline Vannier, in charge of iconographic collections, for their valuable collaboration. For similar reasons, I am indebted with Claudia Rabel and Joanna Fronska from the Institute de recherche et d'histoire des textes (IRHT) for their attentive assistance and help at various times during this long work.

I cannot but express gratitude to the former and to the current director of the Library of the Episcopal Seminary in Padua, don Riccardo Battocchio and Giovanna Bergantino, both of whom I hold in the highest esteem and whose friendship is greatly valued by me.

I would also like to extend my thanks to Claudia Bortolussi and Michele Cecchin from Siltea Srl for their willingness to exchange ideas, for their valuable assistance, and for tailoring their formulations in order to make them more suitable for the purposes of this research.

This research work was partly conducted at the Department of Chemical Sciences of the University of Padua and partly at the CRC-Centre de Recherche sur la Conservation (MNHN) in Paris, where I benefited from the input of many people. Among them, I would like to thank Moreno Meneghetti, Renzo Bertoncello and Bertrand Lavédrine for their invaluable advice. For the great quantity of analyses carried out as a fundamental part of this research, I am indebted to Sabrina Paris and to Oulfa Belhadj from the CRC, and to Michele Secco and Federico Zorzi at Padua University. In the final phase of this work, the contribution of Rita Deiana from CIBA – University of Padua, added value by opening up future study perspectives. Accordingly, I warmly thank her as well.

In the course of this research, I have often cast a thankful thought to the memory of Paolo Calvini for the fascinating discussions we had on the complexity of paper materials: I would have liked him to have had more time and to have been able to play a role in this project.

I have accrued a considerable debt of gratitude to the people who are closest to me and who have played a substantial role in the development of this thesis. First of all, my personal and very special editor, Myriam, who was hugely generous with her friendship, time and skills and to my husband Carlo, an ever attentive reader and “error hunter” in the multiple drafts of this work. I would also like to thank Mark, whose suitable revision of my English contributed to the effectiveness of the exposition presented in the first chapter.

The role of Carlo was not only crucial for the ultimate revisions to the text: he anticipated and shared with me the basic concept underpinning this research – some years ago now – and has subsequently followed it step by step. To him I extend a loving embrace. He is the mainstay of my life and the indefatigable driving force behind the many professional experiences we are involved in together, and which sometimes overwhelm us, but which we always share with great enthusiasm.

This work demanded my unwavering dedication and all the patience my family could muster. Pietro and Martina have shared with Carlo and me the many sojourns in Paris that have contributed to the evolution of this work and have always offered me their support and 'pats on

the back', even in the last few months, when I have been completely immersed in the thesis. All my love to them, too.

I would also like to acknowledge my sincere friendship with Michela and Luigi, with Maria Speranza and Mauro : their unfailing encouragment has always been important to me.

Needless to say, I never forget my roots: my wonderful parents Isabella and Giuliano and my precious brother Emilio, the family from which I sprang and which certainly endowed me with my original “imprint”.

To you all, thank you for being who you are.

Abstract

Books and documents on paper harmed by fire in libraries and archives have often been left in very poor condition as conservation interventions with traditional materials and techniques have so far given unsatisfactory results. As a consequence, a large number of these documents are excluded from access and even from simple handling because they are prone to immediate fragmentation.

The research is dedicated to developing an innovative conservation treatment for strengthening burnt paper, with a specific focus on traditional handmade rag paper which was the support for writing and printing from the 13th to the 19th century in the Western Latin world. The main goal of this mechanical reinforcement is to allow cautious and safe future access to the text, including for the purpose of their reproduction for the benefit of the larger scholar community.

The study and physicochemical characterization of two burnt historical papers was carried out using pH measurements, morphological investigation by optical and scanning electronic microscope (SEM/EDS), spectroscopic techniques (ATR-FTIR, FORS) and X-ray Powder Diffraction (XRPD). This allowed a better understanding of the condition of paper materials harmed by fire, an essential step for producing burnt paper samples in the laboratory to be used experimentally, in which thermal degradation and burning effects (macro-and microstructure, physico-chemical characteristics) were comparable to those of the real historic ones.

The methodology developed is based on the use of nanocelluloses and polysiloxanes known to increase the strength of polymeric materials such as paper. Cellulose nanocrystals and microfibrillated cellulose were used together with various polysiloxanes formulations based on tetraethoxysilane (TEOS) and aminoalkylalkoxysilanes. These products were tested individually and combined, to form a biopolymer based reinforcing nanocomposite, which can be applied on the paper by spraying.

The nanocomposite formulations developed were compatible with the paper matrix. When applied on the charred areas of a burnt paper, they limited the tendency to fragmentation and material loss. The efficiency of the products was evaluated using SEM/EDS, ATR-FTIR and mechanical testing of the burnt paper samples. Considering the extreme fragility of the carbonised paper, which did not allow to use standardized mechanical strength measurements, a simple fold

to break resistance test was developed. The formulation based on nanocrystals and microfibrillated nanocellulose dispersed in a TEOS-based alkoxysilane penetrated into the paper and provided an increase in its mechanical resistance, while not changing the optical properties of paper and not leading to unwanted effects such as surface deposits, tidelines and deformation.

Preliminary test applications on a manuscript and a printed historical paper from the Médiathèque L'Apostrophe in Chartres and from the Library of the Episcopal Seminary of Padua, damaged in a blaze during the Second World War, were carried out.

Résumé

Les ouvrages et documents sur papier des fonds de bibliothèques et d'Archives endommagés par le feu sont le plus souvent laissés dans leur état d'altération extrême du fait du manque de méthodologies adéquates d'intervention, les méthodes traditionnelles étant inadaptées. Par voie de conséquence, un très grand nombre de ces documents sont incommunicables, voire même non manipulables, de par leur tendance à se fragmenter au moindre mouvement.

La recherche a permis de développer une méthodologie innovatrice de traitement de conservation-restauration, dans le but de renforcer le papier ayant subi un sinistre par le feu, avec une attention particulière portée aux papiers artisanaux de pâte chiffon, supports de l'écriture et de l'imprimerie du XIIIe au XIXe siècles dans le monde occidental de tradition latine.

L'objectif principal de ce renforcement mécanique est de permettre un accès futur, prudent et sécuritaire aux textes, y compris dans le but de pouvoir les reproduire afin de permettre leur étude par les chercheurs, notamment en sciences humaines.

La caractérisation physicochimique et morphologique fine de deux papiers brulés historiques originaux, a été faite grâce à des mesures de pH, de diffraction des rayons X par les poudres (XRPD), de microscopie électronique à balayage associée à la microanalyse par énergie dispersive de rayons X (SEM-EDX) et par des techniques spectroscopiques comme l'infra-rouge en réflectance totale atténuée (ATR-FTIR) et la réflectance de fibre optique (FORS). Cela a permis de mieux comprendre l'état d'un papier brulé, étape essentielle afin de reproduire des éprouvettes de

laboratoire dans lesquelles la dégradation thermique et les caractéristiques physicochimiques, de macro et de microstructure sont comparables à celles des originaux historiques endommagés.

La méthodologie développée se base sur l'utilisation de nanocellulose et de polysiloxanes, connus pour augmenter la résistance de matériaux polymères comme le papier. Des formulations combinant nanocristaux (CN) de cellulose et/ou cellulose micofibrillée (MFC) ont été utilisés avec diverses formulations à base de tetraethoxysilanes et d'aminoalkylalcoxysilanes. Ces produits ont été appliqués individuellement et en combinaison, par pulvérisation directement sur les parties brûlées.

Les formulations nanocomposites développées sont parfaitement compatibles avec la matrice papier. Après traitement, les portions brûlées ont une meilleure résistance à la fragmentation et à la perte de matière par manipulation. L'efficacité des produits a été évaluée par SEM-EDX, ATR-FTIR et par des essais mécaniques sur les éprouvettes. Pour ce faire, un moyen simple de mesurer la résistance au pliage a été conçu, aucun essai mécanique normalisé ne convenant étant donnée l'extrême fragilité du papier carbonisé.

Une formulation basée sur un mélange de CN et de MFC dispersé dans des alcoxysilanes à base de TEOS en solution alcoolique a permis une bonne pénétration dans le papier, une augmentation de la résistance au pliage, tout en conservant l'apparence visuelle du papier, et ce, sans effets indésirables tels que des dépôts de surface, des auréoles ou de la déformation.

Lors d'essais préliminaires cette formulation a été appliquée à un manuscrit conservé à la Médiathèque L'Apostrophe de Chartres et à un document historique imprimé de la bibliothèque du Séminaire épiscopal de Padoue, tous deux ayant été endommagés par des incendies lors de la seconde guerre mondiale.